UNIVERSITY OF SOUTH CAROLINA

Behavior of Pile to Bent Cap Connections Subjected to Seismic Forces

Dr. Paul H. Ziehl
Dr. Juan M. Caicedo
Dr. Dimitris Rizos
Dr. Timothy Mays
Aaron Larosche
Mohamed K. ElBatanouny
Brad Mustain

submitted to:

Federal Highway Administration

and

South Carolina Department of Transportation

June, 2012

SCDOT Research Project No. 672

Federal Project No. FHWA-SC-12-03

Department of Civil and Environmental Engineering
300 Main Street
Columbia, SC 29208
(803) 777 3614
cee@cec.sc.edu

This research was sponsored by the Federal Highway Administration and the South Carolina Department of Transportation. The opinions, findings and conclusions expressed in this report are those of the authors and not necessarily those of the FHWA or SCDOT. This report does not comprise a standard, specification or regulation.

Technical Report Documentation Page

1. Report No.	2. Government Accession No.	3. Recipient's Catalog No.
FHWA-SC-12-03		

4. Title and Subtitle	5. Report Date
Behavior of Pile to Bent Cap Connections Subjected to Seismic Forces	June 2012
	6. Performing Organization Code

7. Author(s)	8. Performing Organization Report No.
P. Ziehl, J. Caicedo, D. Rizos, T. Mays, A. Larosche, M. ElBatanouny, and B. Mustain	USC-SCDOT-672-1

9. Performing Organization Name and Address	10. Work Unit No. (TRAIS)
University of South Carolina Department of Civil and Environmental Engineering 300 Main Street Columbia, SC 29208	11. Contract or Grant No. SPR 672

12. Sponsoring Agency Name and Address	13. Type of Report and Period Covered
South Carolina Department of Transportation 955 Park St. P.O. Box 191 Columbia, SC 29202	Final Report January 2008 – June 2012
	14. Sponsoring Agency Code

15. Supplementary Notes

Prepared for the SCDOT in cooperation with the Federal Highway Administration

16. Abstract

Currently the South Carolina Department of Transportation employs a detail of a plain pile embedment for the connection between precast prestressed piles and cast-in-place bent caps. This connection has proved beneficial in terms of time and cost associated with construction, and has been previously investigated albeit in a limited capacity. As such an improved understanding of the behavior of the connection is warranted. The University of South Carolina has concluded a research program focusing on the behavior and design of this specific connection detail.

South Carolina contains the highest level of seismicity along the east coast of the United States. The state relies heavily on the transportation infrastructure and a high level of confidence in bridge design practices is essential. This research began with a focus on the evaluation and understanding of the current detail employed in the connection between precast prestressed piles and cast-in-place bent caps. The work continues with the investigation of parameters that affect this connection detail and proceeds with potential improvements to the detail. The connections are evaluated in terms of moment capacity, ductility, and damage mechanisms. Findings indicate that when constructed with an appropriate embedment length the connection at interior portions of a bent cap is able to achieve desirable response. Connections at exterior portions of bent caps are also shown to respond desirably given sufficient pile embedment depth along with appropriate detailing of the bent cap.

17. Key Words	18. Distribution Statement
Prestressed, bridge, seismic, pile, bent cap	No restrictions.

19. Security Classif. (of this report)	20. Security Classif. (of this page)	21. No. of Pages	22. Price
Unclassified	Unclassified	293	

PRINTING

This report was printed as follows:

Cost: $ 317.65

Total number of documents: 25

Cost per unit: $ 12.71

Disclaimer

The contents of this report do not necessarily reflect the views of the Federal Highway Administration or the South Carolina Department of Transportation. This report does not constitute a standard, specification, or regulation.

Acknowledgements

The authors thank the FHWA and SCDOT for sponsorship of this research project (SCDOT Project 672) and helpful input of Lucero Mesa, Barry Bowers, and Ken Johnson. The input and advice from the Steering Committee including Lucero Mesa, Barry Bowers, Ken Johnson (FHWA), Hongfen Li, Merrill Zwanka, Bill Mattison, and Ted Gettis is very much appreciated, as is the expertise provided by Collins Engineering. In addition to their work as primary chapter authors, thanks are extended to Drs. David Sanders of the University of Nevada-Reno and Jeff Mulliken of LPA Group for input and oversight throughout the project.

Additional appreciation is extended to David Meggs, Steve Nanney, Jesse Creel, and Kari Morrison from the SCDOT and to Dr. Jose Restrepo for helpful technical input.

The authors thank all companies contributing to this project in terms of materials and time. These contributors include Florence Concrete Products of Sumter, South Carolina, Holcim Cement Company, Hardaway Concrete, Steel Specialties of Mississippi, Glasscock Sand, and CMC Rebar. The authors wish to recognize the technical input provided by Eddie Deaver of Holcim Cement Company and JR Parimuha of Florence Concrete Products. Darryl Peterson of Vishay Micro-Measurements is also thanked for his contributions.

The authors thank their associates Avery Fox, William McIntosh, Shawn Sweigart, Jesè Mangual, and all other members of the project staff for their hard work and help throughout the duration of this project.

Abstract

Currently the South Carolina Department of Transportation employs a detail of a plain pile embedment for the connection between precast prestressed piles and cast-in-place bent caps. This connection has proved beneficial in terms of time and cost associated with construction, and has been previously investigated albeit in a limited capacity. As such an improved understanding of the behavior of the connection is warranted. The University of South Carolina has concluded a research program focusing on the behavior and design of this specific connection detail.

South Carolina contains the highest level of seismicity along the east coast of the United States. The state relies heavily on the transportation infrastructure and a high level of confidence in bridge design practices is essential. This research began with a focus on the evaluation and understanding of the current detail employed in the connection between precast prestressed piles and cast-in-place bent caps. The work continues with the investigation of parameters that affect this connection detail and proceeds with potential improvements to the detail. The connections are evaluated in terms of moment capacity, ductility, and damage mechanisms. Findings indicate that when constructed with an appropriate embedment length the connection at interior portions of a bent cap is able to achieve desirable response. Connections at exterior portions of bent caps are also shown to respond desirably given sufficient pile embedment depth along with appropriate detailing of the bent cap.

Table of Contents

List of Tables and Figures

Chapter 1 - Introduction

This report details the findings of an investigation performed by the University of South Carolina (U.SC) in cooperation with the University of Nevada-Reno (UNR), the Citadel and the LPA Group. This investigation was designed to better understand the behavior of the connection between Cast-In-Place (CIP) bent caps and precast prestressed concrete piles typical of construction practices within the state of South Carolina.

Although several tasks have been completed following the project proposal "Behavior of Pile to Pile-Cap connections Subjected to Seismic Forces" this report will concentrate on the findings based on laboratory testing and finite element modeling. Other works contributing to these findings will be referenced but have been previously submitted.

1.1 Background

The South Carolina Department of Transportation (SCDOT) employs the use of a standardized connection between precast prestressed piles and CIP bent caps in bridge substructure construction. This connection is made by embedding piles into CIP bent caps to a depth of a single pile diameter or cross sectional dimension with a construction tolerance of ± 6.0 inches. While similar connections are used in many areas, the connection utilized by the SCDOT is unique in that no special detailing is required. Typical piles used in the state are square with cross sectional dimensions varying between 18 and 24 inches. The simplicity of the connection results in construction that is efficient in both time and cost. Maintaining the benefits of the current connection was a desired result of this study.

Due to the potential of a large seismic event within the state of South Carolina the development of connections that provide sufficient moment capacity and adequate ductility is necessary. Because the state of South Carolina relies heavily on its transportation system, maintaining the operational status of bridges following a large seismic event is critical. The bent caps of these systems are designed to remain elastic through a design earthquake. Therefore energy dissipation must occur at or below the connection to the piles. The reliance on this method of energy dissipation requires an improved understanding of the connection region so that the desired response to the system will be achieved when subjected to a design earthquake.

Connections similar in manner to the connections in question have recently been classified by ASCE's Seismic Design of Piers and Wharfs according to their response characteristics. This document, which is reviewed in the second chapter of this report, has classified connections as either 'Type A' or 'Type B' based on the inelastic response of the system. The significant difference between the two connection types is the area in which the inelastic response occurs. In Type A connections, the response is focused in the pile below the connection. In Type B connections, the response is focused in doweling action that occurs within the connection. Given the design method employed by the SCDOT where bent caps are intended to remain elastic the connection type desired is Type A.

Although these connections are currently being used throughout the state, the behavior of the connections when subjected to seismic activity is not well understood. Several studies have been completed involving connections similar to those in question, including work performed at the University of South Carolina (Harries and Petrou, 2002). Though important to this study, the preceding work has not adequately described the behavior of the connection.

1.2 Scope of work

The work completed and presented in this report is a result of several completed tasks. A review of available literature, discussions with members of local industry, and a parametric study of South Carolina bridges were conducted prior to initiating the laboratory investigations.

Nine full-scale specimens were fabricated and tested. Eight of these specimens were created with a single pile and a representative portion of a typical CIP bent cap. Based on the findings of the first eight specimens a three-pile specimen was designed, fabricated, and tested. These specimens were evaluated according to their behavior with emphasis on moment and displacement capacity, ductility, development of a plastic hinge mechanism, and cap performance. In addition to the physical specimens tested, finite element models were created and used to simulate the effects of varying pile sizes and embedment depths that could not be tested in the laboratory due to the constraints of the project.

The report also includes a design guide containing a detailed design example related to typical bridge construction in the state. The design example, seen in chapter nine of this report, incorporates the conclusions supported by the laboratory testing and finite element analyses.

1.3 Objectives and approach

The objective of this work is to evaluate the seismic performance of the current connection detail between CIP bent caps and prestressed concrete piles. The approach includes experimental, analytical, and numerical work as described within the report. Based on the results of the evaluation, the connection is to be optimized for ease of construction while maintaining appropriate response characteristics with regard to potential seismic events. Conclusions will provide the SCDOT with information satisfactory for the design of these connections intended to behave in accordance with SCDOT specifications.

1.4 Organization

This report details the investigation conducted by the University of South Carolina in cooperation with the University of Nevada-Reno, the Citadel, and the LPA Group. The extensive work in this study has included communication with industry leaders, a parametric study of typical South Carolina bridges incorporating the connection investigated, laboratory testing of eight full-scale single pile specimens, laboratory testing of a three pile full-scale specimen, a parametric study of the connection based on finite element models, and detailed design examples of the connections based on project findings.

This report is focused on the laboratory work conducted at the University of South Carolina and the University of Nevada-Reno and the finite element models developed in conjunction with this work. The report consists of the ten chapters listed below:

- Chapter 1 - Introduction
- Chapter 2 - Literature Review
- Chapter 3 - Fabrication and Instrumentation of Single Pile Specimens
- Chapter 4 - Experimental Setup and Loading Procedure
- Chapter 5 - Finite Element Modeling
- Chapter 6 - Interior Specimens
- Chapter 7 - Exterior Specimens
- Chapter 8 - Three Pile Specimen
- Chapter 9 - Design Guide and Example
- Chapter 10 - Recommendations and Conclusions

Chapter 2 - Literature Review

2.1 Introduction

A number of studies have been conducted on the topic of the connection between precast prestressed piles and cast in place bent caps. This chapter provides a brief review of relevant work with emphasis on recent work related to representative seismic loading. This chapter also provides a review of work related to the confining stress of prestressed strands because this is essential to the connection behavior.

2.2 Sheppard, 1983

In 1983, Sheppard (Sheppard, 1983) compiled a review of work completed by several authors regarding the connection behavior of prestressed concrete piles. Sheppard began with a review of published reports documenting damage as a result of earthquakes along with the findings of multiple Japanese laboratory investigations focused on the seismic performance of concrete members. In addition to this material, Sheppard reviewed tests conducted at Santa Pomeroy which investigated the behavior of prestressed piles when subjected to both a constant axial load and a flexural load. Along with the flexural load cases, these studies investigated the effects that spiral confinement had on the ductility of the piles. Sheppard provided several observations including:

- Batter piles can damage connected pile caps
- Potential plastic hinge areas are located at the pile cap and at a point of fixity
- Piles move and fail with soil which may lead to structural failure
- The confinement provided by spiral wire leads to increased specimen ductility, though that provided by a standard W 3.5 wire is insufficient
- Additional testing is needed both for determining demands of plastic hinge regions and to evaluate the potential differences between curvature and axial based design

With these observations Sheppard recommended seven different connections which may be used between prestressed piles and CIP bent caps. One such connection is that of a plain pile embedment. This recommendation is one of the first to recognize plain pile embedment.

2.3 Joen and Park, 1990

Joen and Park published a two part study investigating the performance of octagonal prestressed piles connected to bent caps. In the first part of the study, the authors compared the results of six specimens to five additional specimens of similar nature. The primary variables investigated were the amount and strength of steel within the piles. The second study investigated the connection between piles and CIP bent caps, which is related to the current study. Six specimens named PC 1 through PC 6 were included. Specimens PC1 and PC2 were plainly embedded into a bent cap. Specimens PC3, PC4, and PC5 were embedded with exposed prestressing strands. The final specimen, PC6, utilized dowel bars to make the connection. In addition to the prestressing strands, specimens PC2 and PC4 also contained passive reinforcement.

Specimens were subjected to constant axial loads with cyclic bending applied at the end of the pile. Pile deflections were increased in magnitude through displacement ductility factors of at least 8.0. Experimental results were compared with four methods of determining pile flexural strength. The authors recommended that dowel bars such as those in specimen PC6 not be used as they may lead to premature failure. The authors recommended the use of the connection type used in specimens PC1 and PC2, a plain pile embedment. The authors further recommended the use of spiral steel at the embedment region within the bent cap noting that this steel improved the bond between prestressed strands and the surrounding concrete.

2.4 Shahawy and Issa, 1992

The authors tested nineteen piles embedded in a simulated cap with variable embedment lengths. The piles were subjected to lateral loads of increasing magnitude at a rate of 3 kips per cycle up to an applied value of 18 kips. At this point load increments were decreased to 1 kip per cycle until it was determined that the specimen had failed. A simulated cap was used in testing so that a confining stress could be imparted to the pile specimens. The effect of this confinement as a result of cap shrinkage may have a significant impact on the specimen's performance. Before the nineteen specimens were tested, the authors first embedded a pile fit with vibrating wire strain gages into a cast in place bent cap. This test was conducted to determine a reasonable value of confining stress which was found to be 525 psi at 28 days. This value was then used as an upper limit of clamping stress applied to the remaining specimens. By applying a constant 200 kip compressive load to the end region of the pile, the values of confining stress were varied with pile embedment length. Embedment lengths used were 36, 42, 48 and 60 inches resulting in confining stresses of 379, 340, 298 and 238 psi respectively. Shahawy and Issa were able to demonstrate that in cases where confining stress is present the current ACI Equation 12-4 for development length of prestressed strands is overly conservative. The authors then proposed a modification to the ACI equation.

2.5 Harries and Petrou, 2001

In 2001 Harries and Petrou published "Behavior of Precast, Prestressed Concrete Pile to Cast-in-Place (CIP) Pile Cap Connections". The objective of the study was to determine if the use of

plainly embedded piles to cast in place bent caps could be used by the South Carolina Department of Transportation.

The authors determined the connection to be viable assuming the connection was intended to develop the full capacity of the pile. Models introduced by Mattock and Gaafar (Mattock and Gaafar, 1982) and Marakis and Mitchell (Marakis and Mitchell, 1980) were used to predict the behavior of two test specimens used in the research.

Test specimens were created with 18 inch square prestressed piles 18 feet in length plainly embedded into CIP bent caps. Caps were cast 7 feet in length with a 3 foot square cross section. In the two specimens tested, piles were embedded to depths of 18 and 24 inches. Cyclic loading was applied at a distance of 146 inches from the face of the connection while a 200 kip axial load was constantly applied to the end of the pile. Each of the two specimens reached the full nominal capacity leading the authors to conclude that the 18 inch embedment depth was adequate. A minimum embedment of 12 inches was specified. An additional pullout test was conducted on one of the specimens to determine if the connection was susceptible to pullout failure. Without any significant pullout after achieving a load of 75 kips it was determined that the connection could withstand ratcheting due to a seismic event.

It has been determined that typical service loads of South Carolina bridges result in pile axial loads lower than the 200 kips used in the study. This reduction in axial load combined with interest in exterior connections presents a need for additional evaluation of connection behavior.

2.6 Xiao, 2003

This study focused on the behavior of cast in place caps connected to prestressed piles with shallow embedment (as described by the authors). The aim was to determine the moment capacity of the connection, thereby accounting for this moment capacity as opposed to assuming the connection behaved as a hinge.

The study consisted of four pile-to-bent cap specimens, though the results of only three were presented. The piles were 14 inches square with a length of 67 inches. Six ½ inch diameter prestressing strands were encased with a W11 spiral spaced at a 2 inch pitch. Each pile also contained four No. 6 dowel bars spanning the length of the pile with an additional 34 inches exposed at one end. Each pile was embedded into a cap to a depth of 29.5 inches.

Of the three specimens, two were subjected to a combination of axial load and cyclic displacement. The third test specimen was tested under variable axial load. The two specimens tested with cyclic pile displacements were subjected to displacements corresponding to drift ratios of 1, 1.5, 2, 3, 4, and 6 percent. The third specimen was tested with axial loading in increments of ± 50 kips beginning with an initial axial load of 200 kips. Ultimately, axial loads of 500 kips in compression and 100 kips in tension were reached before the testing procedure was shifted to displacement control.

The results of these tests were used to develop a method in which the moment capacity of the connection could be determined. The methodology incorporated both the flexural capacity of the pile as well as the ‘embedment mechanism’. The embedment mechanism considered the methodology presented by Mattack and Gaafar, 1982, and the PCI handbook. It was determined

that by considering the flexural capacity as well as the methodology of Mattock and Gaafar, a prediction of the behavior could be obtained with reasonable accuracy while maintaining a conservative approach. The combination of the flexural capacity with the methodology presented by PCI compared well with the observed experimental behavior.

Xiao concluded that specimens such as those tested may develop sufficient moment capacity given the embedment of the dowel bars. Additionally, relatively simple calculations considering both flexural and embedment mechanisms could safely predict the moment capacity and the dowel bars could adequately resist tensile forces.

2.7 Roeder et al., 2001

In this study eight single pile to bent caps specimens were tested. In addition to the physical tests finite element models were created for each specimen. The results of the models were compared with the experimental results.

Each of the eight test specimens were created with a series of dowel bars which made the connection to the bent caps. An example of a bar configuration from this study can be seen in Figure 2.1. Additionally, the bar configuration of each specimen is shown in Table 2.1.

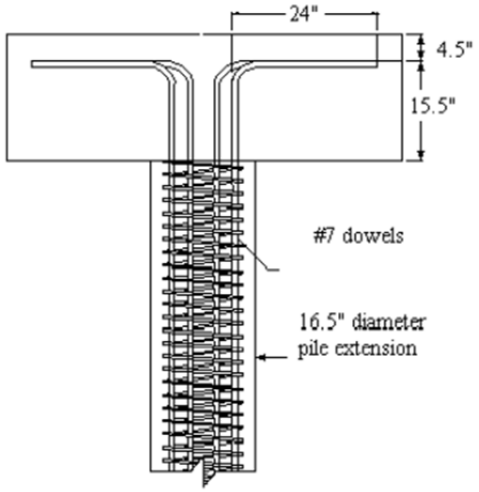

Figure 2.1 Dowel Configuration (Roeder, 2001)

Table 2.1 Test Specimens (Roeder, 2001)

Specimen Number	Dowel Configuration	Axial Load
1	Bent, Extended Outward	No Axial Load Applied
2	Bent, Extended Outward With Spiral	No Axial Load Applied
3	Bent Outward	No Axial Load Applied
4	Bent Outward	Axial Load Applied
5	Bent Inward	Axial Load Applied
6	T-Headed Dowel	Axial Load Applied
7	Bonded Bars	Axial Load Applied
8	Bent Outward, Light Deck Reinforcement	Axial Load Applied

The finite element models constructed for each specimen were created using RUAMOKO. The models were subjected to a time history analysis as taken from records of the Kobe, Newhall, and El Centro earthquakes.

Conclusions of the study were gathered from the comparisons between the finite element models and the experimental behavior of the physical test specimens. It was concluded that all specimens performed adequately. Damage was seen to increase with higher levels of axial load. Confinement of the dowels within the caps had little effect on specimen performance. The connections made through T-headed bars performed well in comparison with other specimens and was recommended as a simple connection type, especially in areas of limited space. Ductility was also found to decrease with decreases in pile length and increases in pile diameter.

2.8 Teguh et al., 2006

In 2006, a finite element modeling study was conducted based on the results of the tests performed by Harries and Petrou in 2001. The goal was to improve the design of bent caps while developing a moment capacity of the connection. The study was conducted by comparing results gathered through analytical approaches presented by Mattock and Gafar, 1982, Marcakis and Mitchell, 1980, and the experimental results of Harries and Petrou, 2001.

The finite element portion of the work was completed in several phases. Using SAP 2000 the linear elastic range of the units was predicted. A time history analysis using a record of the 1995 Kobe earthquake was performed using RUAUMOKO, and DIANA 9.0 was used to perform a nonlinear cyclic analysis.

The study showed general agreement between modeled specimens and the experimental work of Harris and Petrou. From this study it was determined that SAP 2000 was able to reasonably predict the load versus displacement response.

2.9 ASCE, 2008

Several methods have been developed to connect piles to bent caps across the United States. A number of these connection types are shown Figure 2.2. Recently ASCE's Seismic Design of Piers and Wharfs also adopted a method which defines the behavior of these connections. This document defines connections as either 'Type A' or 'Type B' according to the expected behavior of the connection.

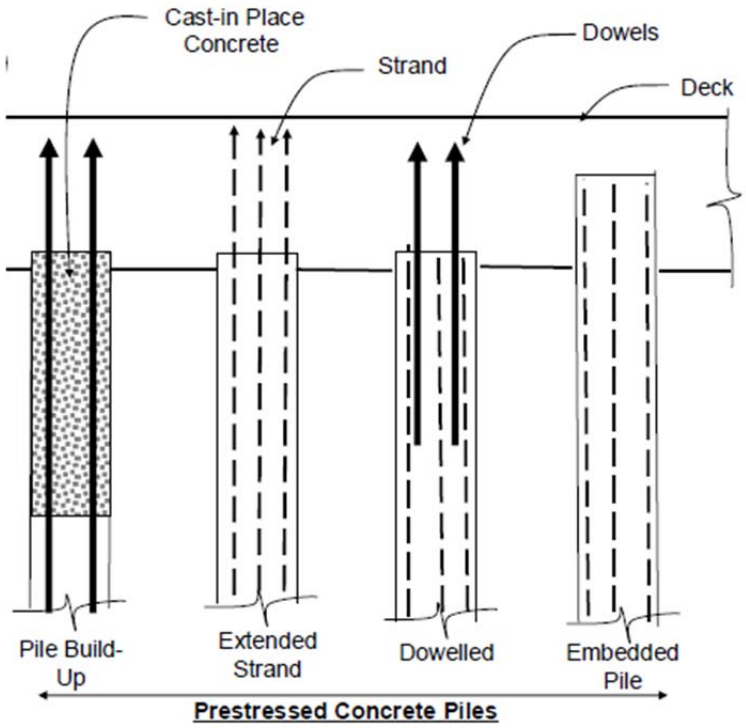

Figure 2.2 Typical Connections between Prestressed Piles and CIP Bent Caps

Details of the classification system are supported by the visual aid presented in Figure 2.3. Type A connections are designed to localize damage to areas within the pile below the interface of the pile and cap. This area is subject to the development of a plastic hinge over a given length of the pile. Rotations should then be limited to the area of plastic hinging and should not occur within the bent cap itself. Localizing damage is achieved by designing the interface and cap portion to be as strong if not stronger than the pile below. By limiting rotations to the pile the bent cap is protected from damage. The location of the localized damage is beneficial for inspections or repairs that may be needed through the life of the structure. This connection type has been shown to be achievable through a deep embedment of a pile or through the use of dowels extending from the pile into the cap.

Type B connections are more common than type A connections. These connections are typically constructed so that the interface between the two elements used is weaker than that of the pile below. Any inelastic response of the connection is usually achieved through dowels between the two elements at the connection.

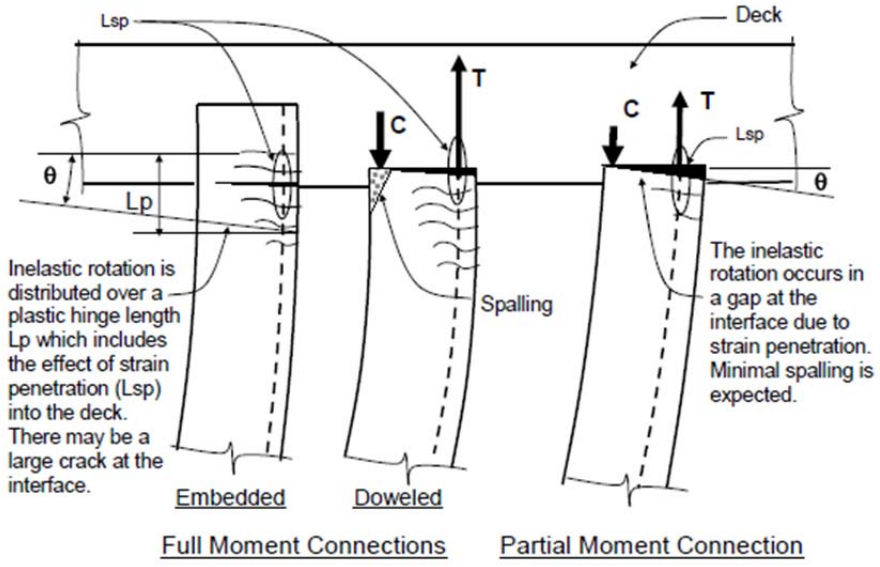

Figure 2.3 ASCE Classification

In the reviewed cases studying the behavior of connections between precast piles and cast in place bent caps the majority of the connections were made with special detailing, separating these cases from the proposed connection of a plain pile embedment.

Chapter 3 - Fabrication and Instrumentation of Single Pile Specimens

3.1 Introduction

The focus of this study is to assess and improve upon the current construction practices employed by the state of South Carolina regarding plainly embedded precast prestressed piles into cast-in-place bent caps. Although the connection is both time and cost efficient the behavior of the connection is not well understood. To evaluate the connection eight full-scale single pile specimens were fabricated and tested at the University of South Carolina structures laboratory. These specimens were designed and fabricated in accordance with the SCDOT Bridge Design Manual, SCDOT Seismic Design Specifications, and the AASHTO Guide Specifications for LRFD Seismic Bridge Design (AASHTO, 2007). All piles used in specimen fabrication were cast at Florence Concrete Products of Sumter, South Carolina. The cast-in-place bent caps were fabricated and cast at the University of South Carolina (U.SC). All instrumentation was performed by members of the project staff at U.SC. Test specimens were cast over a time period of 20 months beginning with the first set of piles being cast January 23, 2009.

3.2 Bent cap fabrication

Bent caps were designed by U.SC in consultation with members of local industry and input from the SCDOT. Bent cap portions of test specimens were designed to represent both interior and exterior portions of a typical bent cap. Caps were designed with a reinforcement scheme intended to represent a realistic worst case scenario. All reinforcement within bent caps was type ASTM A706. All longitudinal reinforcement was terminated with standard hooks. With the exception of two specimens standard 90° hooks were used. Two specimens utilized a reduced cap depth as later described. In those specimens standard 180° hooks were used for termination of the longitudinal reinforcement.

Reinforcing cages and formwork for each specimen were constructed by members of the project staff at U.SC. Each of the eight caps was cast in the U.SC Structures laboratory with concrete provided by Hardaway Concrete of Columbia, South Carolina. Following casting, caps were kept in formwork for a period of one week with the exposed surface treated with a curing compound and covered in plastic sheeting. A photograph showing casting of two specimens is shown in Figure 3.1.

Figure 3.1 Casting of Bent Caps - Specimens IB-18-1 and EB-18-1

Interior specimens

Four single pile specimens were fabricated to represent an interior portion of a typical bent cap. Each of these specimens was cast with a length of six feet 11.5 inches. Piles were embedded in the center of this length. The length of the specimen was taken from the results of a parametric study completed as a part of this investigation (Mays and Mulliken, 2008). The study indicated a seven foot center to center spacing between piles is generally representative of construction in South Carolina. Specimen lengths were reduced from the seven feet found in the parametric study by ½ inch to accommodate boundary conditions of the test setup. Of the four interior specimens, three were cast with a three foot square cross section. The fourth specimen retained the three foot width, but the depth was changed to two feet six inches. The reduced depth was intended to represent shallower caps sometimes constructed in the coastal regions of South Carolina. In these regions caps are cast with a reduced depth to minimize surface water interaction.

Each of the interior specimens was constructed with similar reinforcing designs, with the exception of the specimen having reduced cap depth. The reinforcement of this specimen was modified first by reducing the height of the shear reinforcement and also by terminating longitudinal reinforcement with 180° hooks as opposed to 90° hooks used in the other three specimens. Reinforcement for both designs is shown in Figure 3.2.

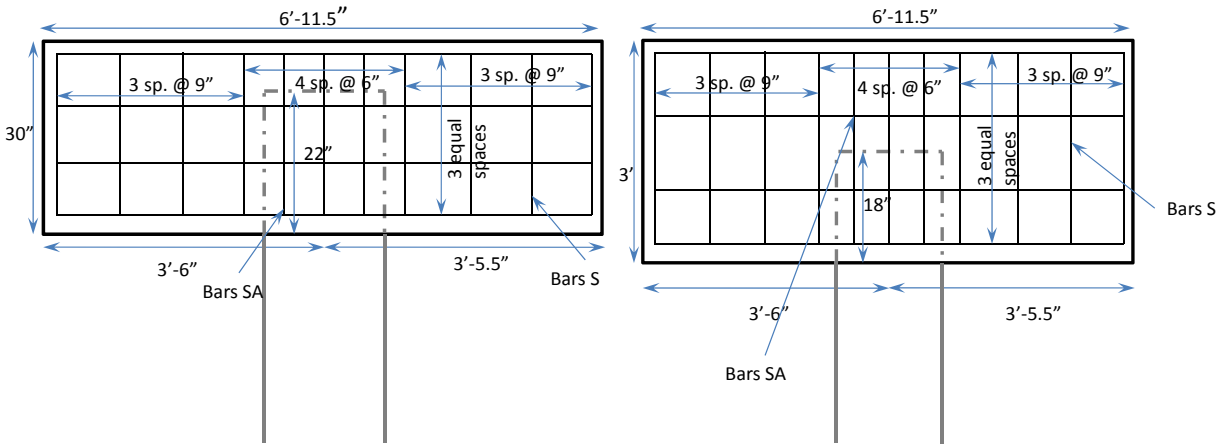

Figure 3.2 Bent Cap Reinforcement - Interior Specimens

The primary variable investigated in the interior test specimens was the depth of pile embedment. The first two interior specimens were created with standard dimensions, and with an embedment depth of 18 inches. These specimens are named IB-18-1 and IB-18-2 (Interior Bent - Embedment Depth - Specimen Number). The final specimen having a square cross section of three feet, named IB-26-1, was created with a pile embedment of 26 inches. The fourth interior specimen (cast with a reduced depth) had a pile embedment of 22 inches, named IB-22-1.

Each of the interior specimens was instrumented with five weldable uniaxial strain gages produced by Vishay Mirco-Measurements. These gages were affixed to longitudinal reinforcement at the center of the embedment region. A diagram and photo of the gage placement is shown in Figure 3.3. Gages were placed at three points along the reinforcement at the top of the bent while two additional gages were placed at the bottom of the cap.

Interior bent cap specimens were cast with two inch diameter PVC pipes fit through the cap at four locations. These pipes created voids that were used to fit each specimen to a steel loading frame.

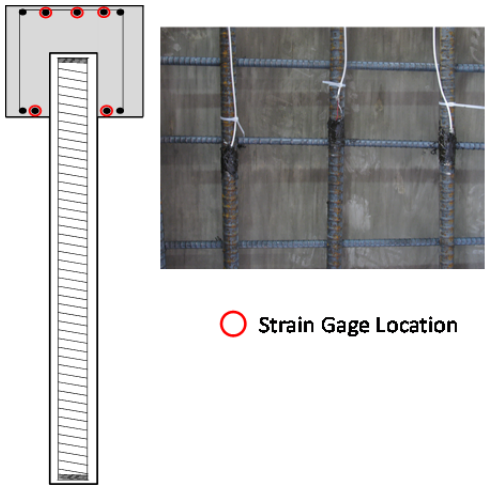

Figure 3.3 Strain Gage Locations in Bent Cap - Interior Specimens

Exterior specimens

Four specimens that were representative of an exterior portion of a bent cap were also fabricated. Three of the four external specimens had a three foot square cross section similar to most of the interior specimens. The length of these specimens was five feet four inches. Similar to the interior specimens, this length was determined based on results of the parametric study and in consultation with the SCDOT. Unlike the interior specimens, the piles in the exterior specimens were not embedded into the center of the bent cap length. The pile was located at a distance of three feet six inches from the centerline between adjacent piles. The exterior end of these specimens refers to the termination end of the bent cap. The distance from the center of the pile to the exterior end of the cap measured one foot 10 inches. The fourth exterior specimen was cast with a width of three feet as for the other three specimens; however both the depth and length of the specimen were changed. The depth of this specimen was reduced to a depth of two feet six inches, similar to specimen IB-22-1. In addition to the depth change, the length of this specimen was increased to a length of six feet. While the length from the center of the pile to the interior face of the bent cap remained constant, the length to the exterior face was increased by eight inches.

The reinforcement design was modified slightly from the interior specimens to take into account the reduced length at the exterior end of the bent cap. In addition to the reduced length the standard SCDOT end reinforcement detail was used in each of the four specimens (Figure 3.4).

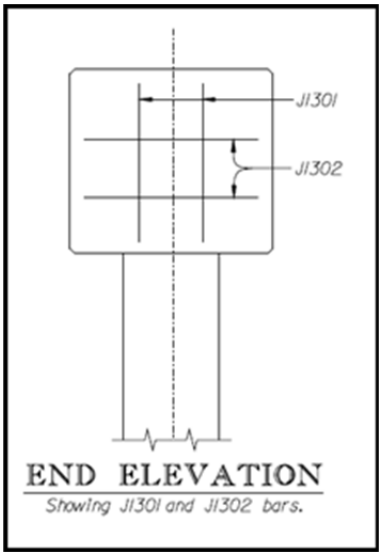

Figure 3.4 Reinforcement in End Region - Exterior Specimens

Each exterior bent cap was instrumented with five strain gages. Similar to the interior specimens, gages were fixed to longitudinal reinforcement at the center of the pile embedment.

Test results related to specimen EB-18-1 indicated that the standard reinforcement design did not provide adequate confinement at exterior ends of the bent cap. The lack of confinement in this specimen led to undesired damage in the cap (discussed in Chapter 7). As a result, three methods of improving performance were proposed. The proposed methods were a) to construct exterior connections as a hinge; (b) to increase reinforcement within the bent cap, effectively increasing

stiffness of the cap and connection while providing confinement to the connection; and (c) to increase the length of the cap at the exterior end allowing the additional concrete to provide confinement to the connection. These connection schemes are described in more detail below.

Standard connection:

EB-18-1 was constructed with a reinforcing design similar to that of each of the interior specimens. The design of the reinforcing scheme was modified slightly from the interior specimen due to the reduced length at the exterior end of the cap. In addition to a reduced length a standard SCDOT end cap detail, Figure 3.4, was used. This specimen was tested with an embedment depth of 18 inches which is equal to the default value currently used by the SCDOT for this pile size.

Hinge connection:

This exterior specimen was designed with a connection such that an idealized hinge is created at the connection. Unlike the plain pile embedment of the other test specimens, the connection was constructed with four No. 6 reinforcing bars extending from the pile into the bent cap. Each of these bars was grouted into the pile to a depth of 24 inches. From the end of the pile each bar extended 12 inches and was terminated with a 90° hook. A photograph and schematic of the bar configuration is shown in Figure 3.5.

The piles were drilled to a depth slightly greater than the required 24 inches. Each hole was filled with a grout (Five Star Products) designed to reach a 28-day compressive strength of 5,000 psi. Each bar was then embedded with the hooks placed in the orientation shown in Figure 3.5. Each of the embedded bars was instrumented with two strain gages of the same model used in the bent caps. These gages were placed at locations of 12 and 30 inches from the end of each embedded bar.

In addition to the dowel bars, the pile was embedded into the cap to a depth of two inches. At the point of embedment the pile was wrapped with Styrofoam sheeting. The compressibility of the sheeting facilitated the hinge behavior. This specimen is named EB-2-1, reflecting the two inch embedment.

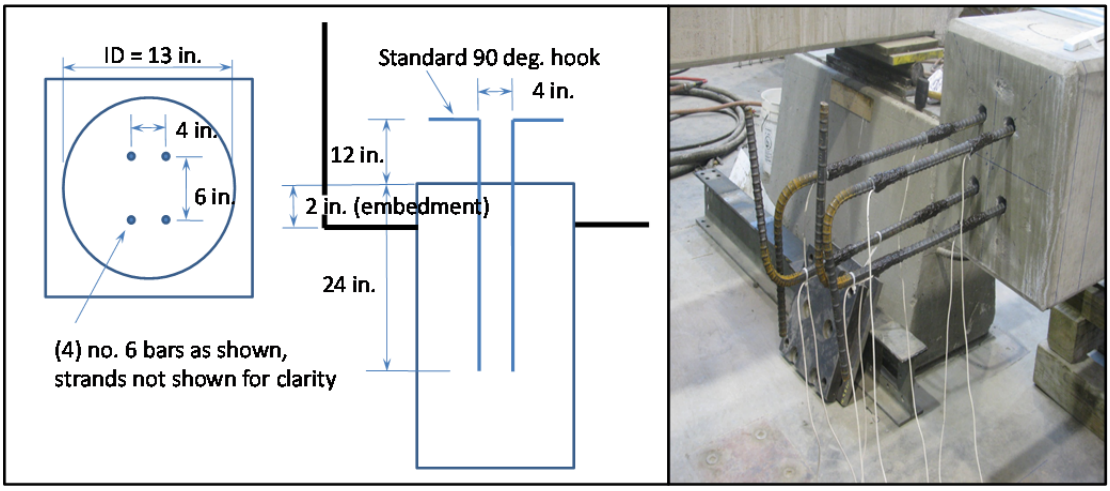

Figure 3.5 Hinge Connection - Specimen EB-2-1

Additional bent cap reinforcement:

This specimen was heavily reinforced with respect to the other specimens. The additional reinforcement added additional confinement to the connection while stiffening the bent cap. The reinforcement scheme of this specimen was designed through a strut and tie analysis. The design began with a reinforcement plan used in the bent cap of specimen EB-18-1, the standard connection. From the results of the strut and tie analysis additional reinforcement was added to the design. At the pile embedment region a No. 3 square spiral was added. This spiral was spaced two inches from the pile at each face. At a maximum pitch of three inches, the spiral extended from the bottom layer of longitudinal reinforcement to a distance of three inches above the pile. Two four leg stirrups were added on either side of the pile embedment region. These stirrups were placed at a spacing of three and 7/8 inches center to center with the first spacing measured from the center of the No. 3 spiral. To accommodate tensile stresses extending through the width of the bent cap at the interior side four cross ties were added to the reinforcement cage. These bars were constructed of No. 6 reinforcement and spaced evenly through the bottom half of the cap depth at a distance of eight inches from the center of the spiral. An additional No. 9 U-bar was bundled with existing longitudinal reinforcement at the bottom of the bent cap. The closed end of this bar was placed at the exterior end of the bent cap. A schematic of this reinforcing scheme and a photograph of the constructed cage are shown in Figures 3.6 and 3.7.

Along with the modifications to the reinforcement the embedment depth was also increased. This specimen was constructed with a pile embedment of 26 inches and named EB-26-1. Similar to the interior specimen with the same embedment, this depth represents an embedment slightly greater than that currently allowed by SCDOT construction tolerances.

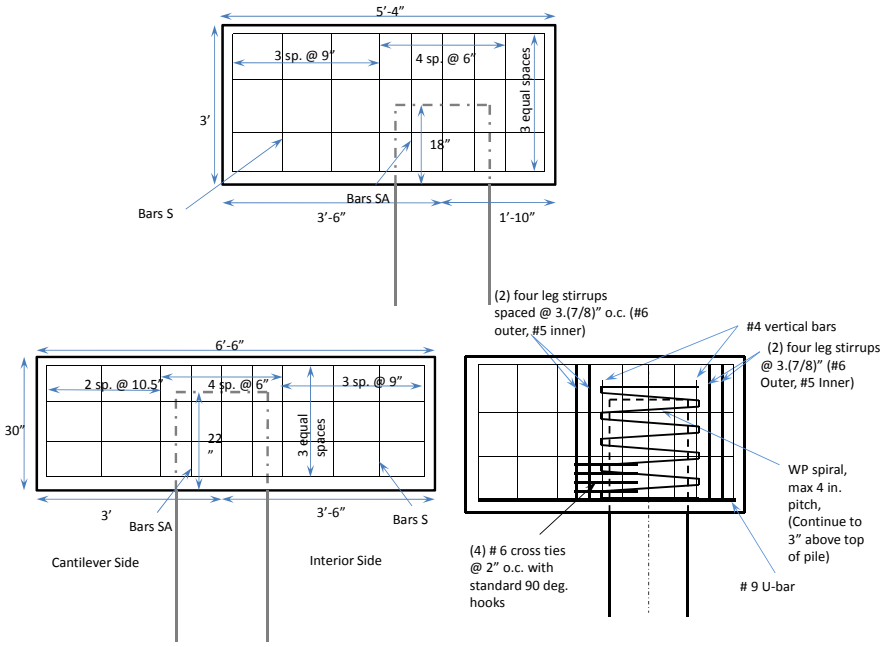

Figure 3.6 Bent Cap Reinforcement - Exterior Specimens

Figure 3.7 Reinforcement Cage - Specimen EB-26-1

Additional bent cap length:

The third method for improving the performance of the exterior specimens was to increase the length of the overhang (from one foot 10 inches to three feet, measured from the center of the pile to the end of the overhang), resulting in improved confinement (Figure 3.6, lower left). The bent cap depth of this specimen was also altered. The bent cap was reduced to the two foot six inch dimension used for specimen IB-22-1. The reinforcement design of this specimen was altered as required by the geometric changes. The embedment depth of this specimen was 22 inches, similar to that of the interior specimen with a reduced cap depth. The specimen is therefore named EB-22-1.

3.3 Pile fabrication

Piles were cast in two sets at Florence Concrete Products of Sumter, South Carolina. Although the length of the piles changed between the two sets all other aspects of the piles remained constant. All piles were cast with a square cross section of 18 inches. A ¾ inch chamfer was added to each corner and extended through the length of each pile. Piles were prestressed with a nine strand pattern as shown in Figure 3.8. The strands used were ½ inch diameter, 270 ksi low relaxation. A W6 spiral encased the strands within a 13 inch inner diameter. This spiral was pitched at one inch for five turns at either end of the pile and at three inches through the remaining length. Figures 3.9 and 3.10 show a schematic and a photograph during fabrication. Strands were initially stressed to 75% of their ultimate tensile strength corresponding to a load of 31,000 pounds. The concrete used to cast the piles was provided by Florence Concrete Products and designed to achieve 28-day compressive strength of 5,000 psi.

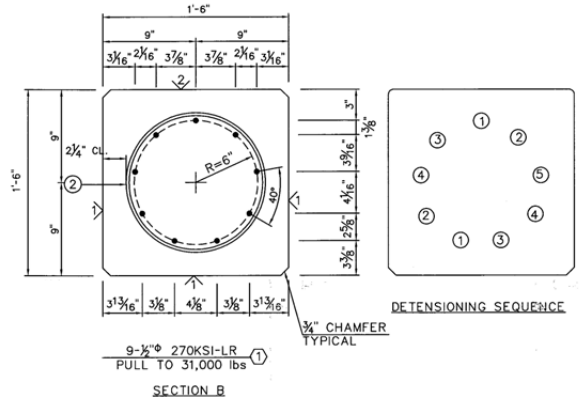

Figure 3.8 Strand Pattern and De-tensioning Sequence

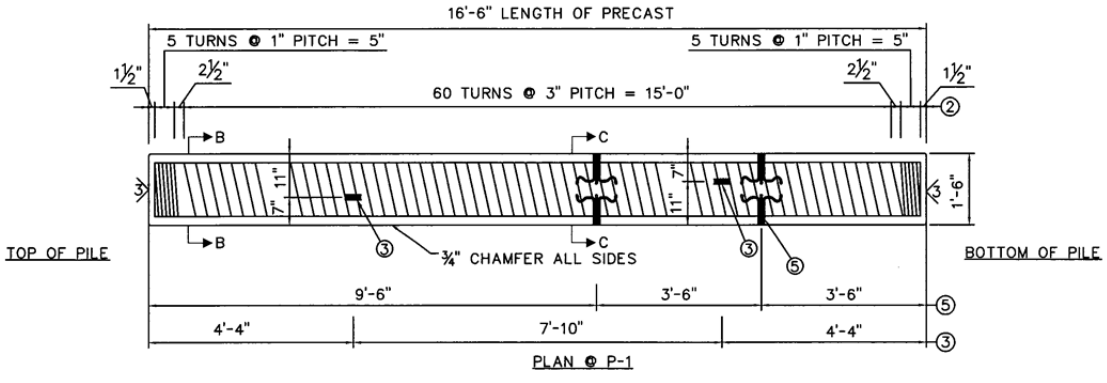

Figure 3.9 Pile Reinforcement

Figure 3.10 Pile Fabrication

The first set of piles was cast January 23, 2009. This set contained seven piles with a length of 18 feet. Piles from this set were used for all specimens with the exception of specimens IB-22-1 and EB-22-1. The measured 28-day strength was 8,300 psi.

Pile set two was cast June 6, 2010. The piles in this set were cast at a length of 16 feet 6 inches and were used in the fabrication of specimens IB-22-1 and EB-22-1. Piles cast in this set reached 28-day compressive strength of 8,230 psi. These piles were internally instrumented, as shown in Figure 3.11. The instrumentation included seven CEA-250-120 strain gages manufactured by Vishay Micro Measurements and two Geokon model 4200 Vibrating Wire Strain Gages (VWSG). Three strain gages were epoxied to strands at locations of 13 inches and 29 inches from the embedded end of the pile. At a distance of 29 inches the remaining strain gage was placed on the W6 spiral. Strain gages were used to measure strain in the strand and spiral as well to monitor strand slipping. The two VWSG were placed at 11 inches from the embedded end of the piles, corresponding to the center of the pile embedment region. Gages were placed both parallel and perpendicular to the planes of pile displacement. VWSG were used to measure the strain due to shrinkage of the bent cap concrete.

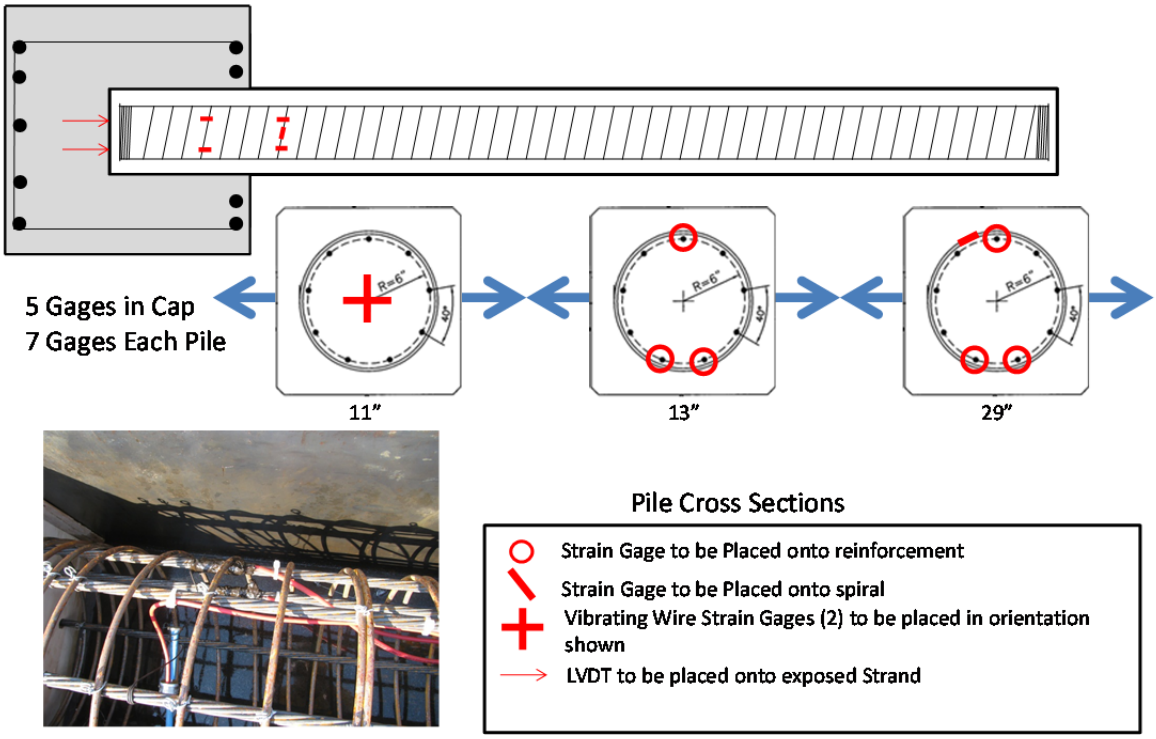

Figure 3.11 Pile Instrumentation - Specimens IB-22-1 and EB-22-1

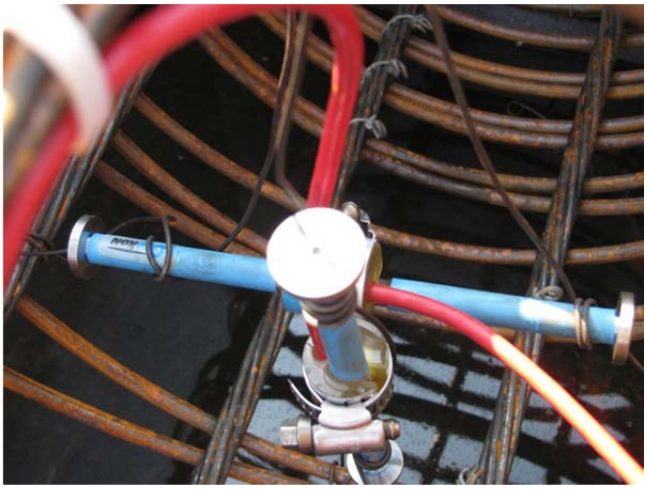

Figure 3.12 Placement of Vibrating Wire Strain Gages

3.4 Additional instrumentation

In addition to the instrumentation described above, a number of specimens were also instrumented with two Linear Variable Differential Transducers (LVDT's) fit onto the embedded end of the piles. The LVDTs were model 9615 manufactured by BEI Duncan. These LVDTs were fit onto two exposed prestressing strands located nearest to the planes of displacement to

detect strand slip. The gages and their location are shown in Figure 3.13. The LVDTs were used in all specimens with the exception of specimens IB-18-1 and EB-18-1.

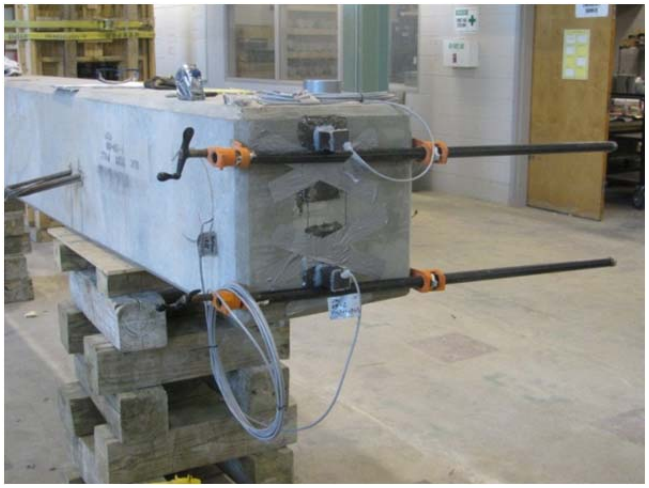

Figure 3.13 Strand Slip Gages

Chapter 4 - Experimental Setup and Loading Procedure

4.1 Introduction

Nine full-scale test specimens were included in this investigation. Eight specimens were constructed as single pile specimens representative of typical South Carolina bent caps. The final specimen was constructed with three piles and a single bent cap. This specimen was designed based on the results of the single pile specimens. This chapter details the experimental setup for the single pile specimens and addresses the external instrumentation and loading procedures. Information specific to the three-pile specimen is addressed later.

Four of the single pile specimens were representative of an interior pile to bent cap connection, and four were representative of exterior connections. The instrumentation and loading procedure was similar for both specimen types. However, the experimental setup was altered between each specimen type.

4.2 Experimental setup - Interior specimens

The experimental setup for the interior specimens is shown in Figures 4.1 and 4.2. Each interior specimen was tested in the orientation of casting. Four steel rods of two inch diameter were placed through voids cast into the caps. These rods were then bolted to a specially designed reaction frame. The reaction frame was constructed with arms at either side of the bent cap. These arms were equal in length to the standard three foot bent cap depth.

Interior specimens were tested with a constant axial load applied to the end of each pile. Load was applied through a deep steel member designed for these tests. Threaded steel rods placed at either side of the specimen were pin-connected to the reaction frame. These rods spanned the length of the pile and fit through the steel member. A 50 kip capacity hollow core hydraulic ram (Enerpac) was then fit to each rod. During testing, the hydraulic rams were controlled with a single small hydraulic pump ensuring equal pressure was constantly provided to each ram. Photographs of this assembly are shown in Figures 4.2 and 4.3. The pin connection between the reaction frame and threaded steel rods allowed the applied load to remain in plane with the pile through a full range of displacements during testing. The 50 kip magnitude of the constant axial load was determined through the parametric study previously described.

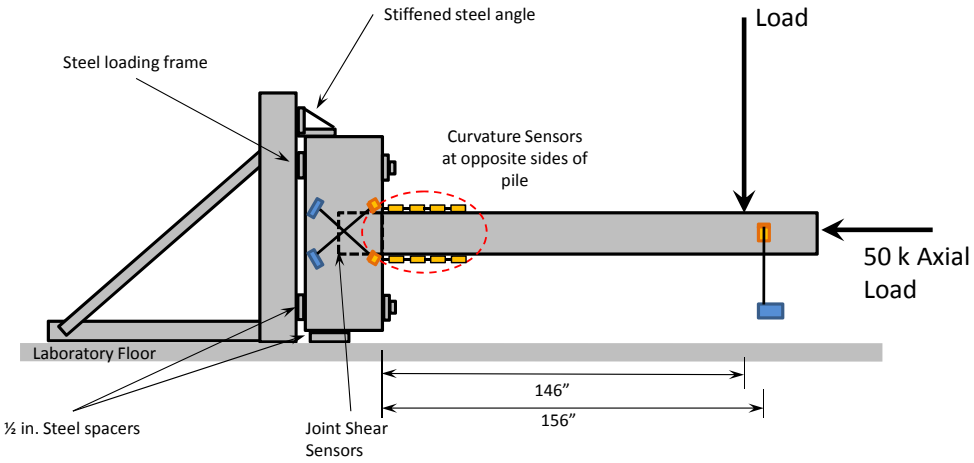

Figure 4.1 Experimental Setup - Interior Specimens

Figure 4.2 Photograph of Experimental Setup - Interior Specimen

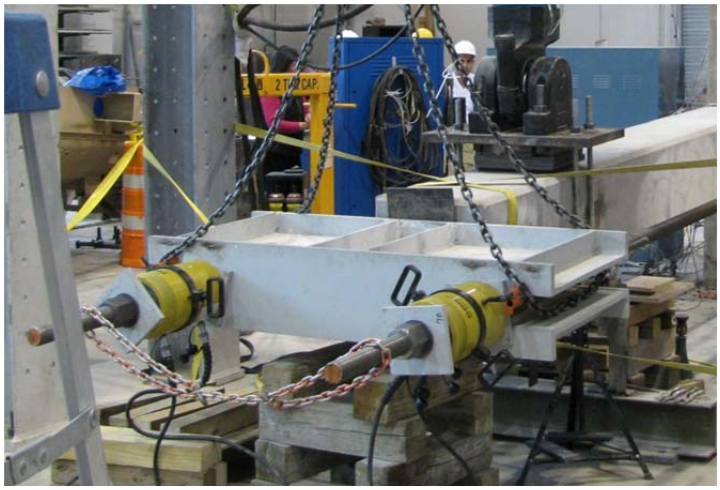

Figure 4.3 Axial Load Assembly - Interior Specimen

Load was applied transversely to the pile at a distance of 146 inches from the face of the connection with a 235 kip capacity hydraulic actuator (Shorewestern) as shown in Figure 4.4. The distance of the transverse load was determined based on an average distance to the point of contra-flexure, as determined through the parametric study.

Figure 4.4 Hydraulic Actuator

To achieve the desired boundary conditions, a ½ inch thick steel washer was inserted between the reaction frame and bent cap at each of the four steel rods. An additional ½ inch thick steel plate with an approximate area of one square foot was placed between the specimen cap and the strong floor. These boundary conditions served to minimize confinement of the bent cap joint region.

4.3 Instrumentation - Interior specimens

Specimens were monitored using a number of sensors. Two string potentiometers (Vishay CDS-20) with a range of ± 10 inches measured pile displacements at a distance of 156 inches from the bent cap soffit. Additional string potentiometers were used to monitor joint shear by mounting two sensors to the cap in an X orientation in the embedment region. This configuration is shown in Figure 4.5. Four plunger type linear transducers (Vishay HS-50) with a range of ± 1 inch were mounted to the top and bottom faces of the pile in series extending away from the soffit to calculate pile curvature (Figure 4.6). This type of sensor was also used to monitor rotation of the cap, with sensors mounted between the cap and the reaction frame one foot above and below each end of the cap. The LVDT within the hydraulic actuator served as an additional measure of pile displacement. The load cell within the actuator was used to record applied load. These measurements were recorded by the data acquisition system within the controller. All other data was recorded by supplemental data acquisition systems (Vishay). Table 4.1 provides a listing of the instrumentation devices.

Table 4.1 Instrumentation - Interior Specimens

Gage Type	Gage Purpose/Measurement	Location	Model
String Potentiometer	Joint Shear	Embedment Region on Cap	CDS-20
String Potentiometer	Joint Shear	Embedment Region on Cap	CDS-20
String Potentiometer	Displacement	Pile 156 inches from Soffit	CDS-20
String Potentiometer	Displacement	Pile 156 inches from Soffit	CDS-20
Linear Transducer	Displacement	Pile 156 inches from Soffit	HS-100
LVDT	Displacement	Pile 146 inches from Soffit	Shorewestern Actuator
Load Cell	Load	Pile 146 inches from Soffit	Shorewestern Actuator
Linear Transducer	Pile Curvature	(4) In Series from Soffit Pile's Top Face	HS-50
Linear Transducer	Pile Curvature	(4) In Series from Soffit Pile's Bottom Face	HS-50
Linear Transducer	Cap Rotation	* 1foot From Top and Bottom of Cap Between Cap and Reaction Frame	HS-50
Uniaxial Strain Gage	Cap Rotation	**(3) at Prestressing Strand 13 inches from Embedded end	C2A-06-062LW-120
Uniaxial Strain Gage	Strand Slippage	**(3) at Prestressing Strand 29 inches from Embedded end	C2A-06-062LW-120
Linear Transducer	Strand Slippage	(2) At Exposed Strands Embedded end of Pile	BEI 9615
Uniaxial Strain Gage	Spiral Strain	**Pile Spiral 29 inches from Embedded end	C2A-06-062LW-120
Uniaxial Strain Gage	Reinforcement Strain	(5) Longitudinal Reinforcement within Cap	CEA-06-W250A-120
Vibrating Wire Strain Gage	Confining Strain	**Center of Pile 9 inches from Embedded end	Geokon M4200

* Refers to Gage Location while in a Testing Position
**Refers only to Specimen IB-22-1

Figure 4.5 String Potentiometers for Joint Shear

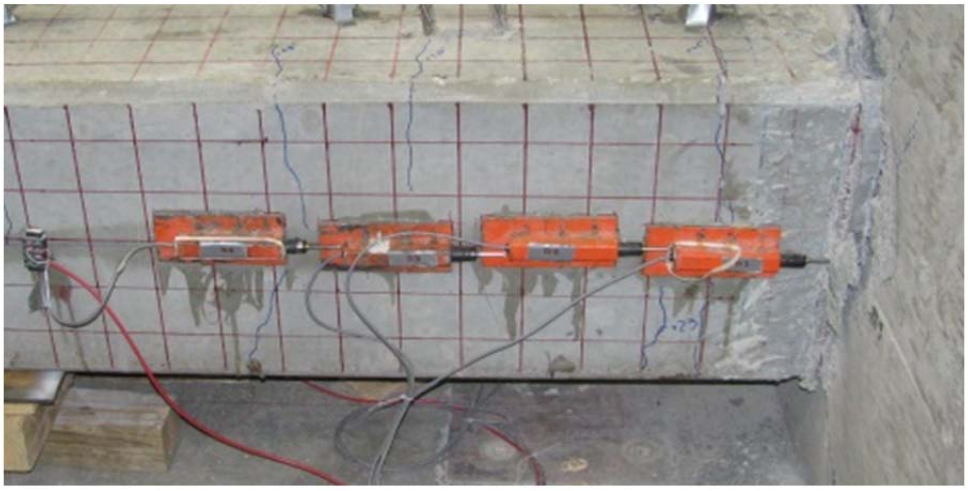

Figure 4.6 Curvature Sensors

4.4 Loading procedure - Interior specimens

Positive and negative displacements were applied to the piles in a reverse cyclic pattern. Vertical displacements away from the laboratory strong floor were considered positive. Displacements

were provided by the hydraulic actuator in all tests with the exception of IB-18-1. A typical displacement versus time representation of the loading protocol is shown in Figure 4.7.

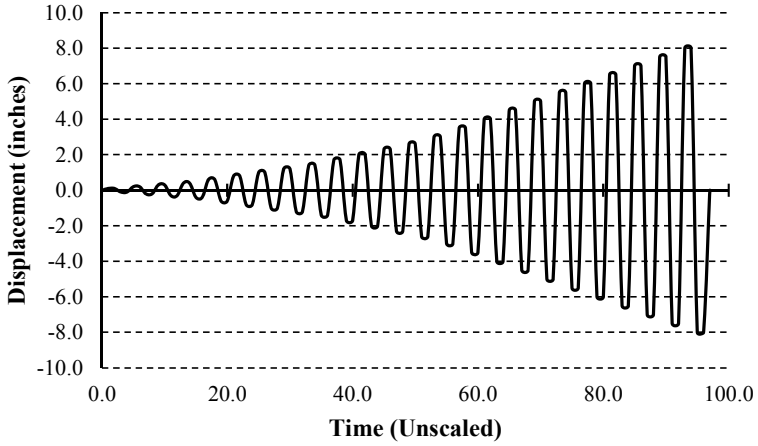

Figure 4.7 General Displacement Protocol

Displacements for IB-18-1 were applied through a combination of a 55 kip capacity hydraulic actuator (MTS) used for displacements up to ± 3.0 inches and two Enerpac 50 kip capacity hydraulic cylinders used for displacements between ± 3.0 and ± 8.0 inches. Testing of this specimen began 42 days after casting. Initial displacement cycles from ± 0.1 inches through ± 0.8 inches were increased in magnitude by 0.1 inch per cycle. Following these cycles, displacement increments between cycles were increased to 0.2 inches through displacements of ± 1.4 inches at which point increments were again increased to 0.3 inches up to ± 2.6 inches. A final displacement cycle of ± 3.0 inches was achieved before the hydraulic actuator was replaced with the hydraulic cylinders. The hydraulic cylinders displaced the pile in increments of 1.0 inch until a final displacement cycle of ± 8.0 inches was achieved.

Displacements of specimens IB-18-2, IB-26-1, and IB-22-1 were achieved with the large stroke hydraulic actuator shown in Figure 4.4. Displacement cycles between ± 0.1 inches and ± 0.6 inches were achieved with 0.1 inch increments. This increment was increased to 0.2 inches for cycles of ± 0.8 inches through ± 1.4 inches. Increments were increased to 0.3 inches through cycles of ± 2.6 inches. From this point through a final cycle of ± 8.0 inches increments of 0.5 inches were applied.

4.5 Experimental setup - Exterior specimens

Specimens were tested with both the longitudinal axis of the bent cap and pile parallel to the strong floor. A self-reacting test setup was used for all exterior specimens so that both axial compressive and axial tensile loads could be applied. While the interior specimens were effectively tested with constant axial loading, axial tensile loads in the opening direction were needed to simulate seismic loading for the exterior specimens (Figures 4.8 and 4.9).

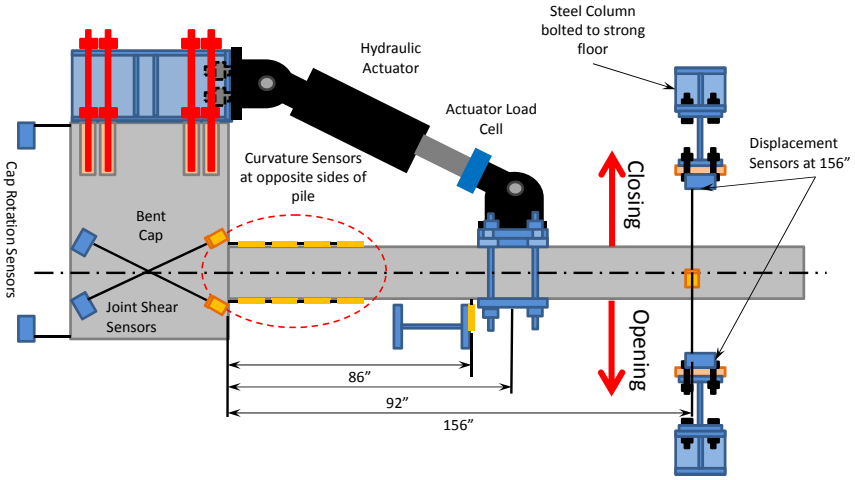

Figure 4.8 Experimental Setup - Exterior Specimens

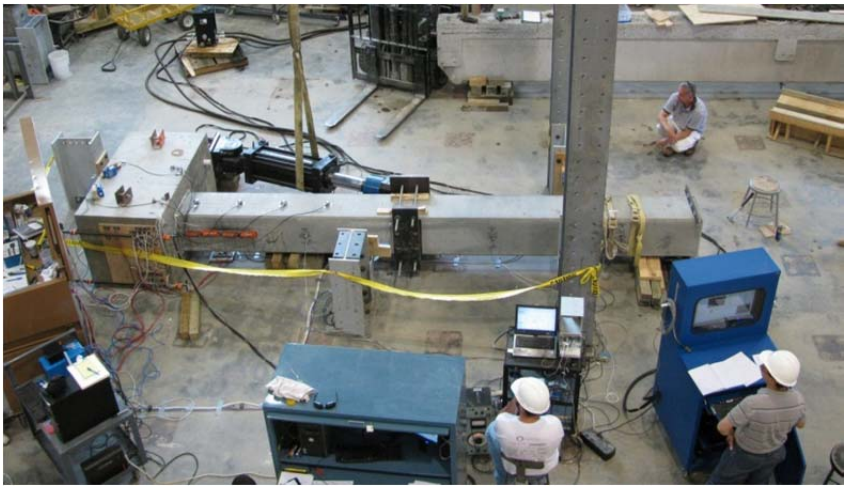

Figure 4.9 Photograph of Experimental Setup - Exterior Specimens

During these tests the actuator was connected to the interior end of the bent cap portion of the specimen as well as to the pile itself at a distance of 92 inches from the soffit. With this positioning pile displacements and desired axial load levels were achieved. 'Closing' the actuator resulted in axial compressive loading along with what will be referred to as negative pile lateral displacement. 'Opening' the actuator resulted in axial tensile loading and positive pile displacement.

At the bent cap the actuator was connected to a stiffened W-member. This member was bolted to the cap by embedding twelve one and 1/4 inch diameter threaded rods to a distance of 18 inches into the cap. The rods were placed by first drilling holes into the bent cap at the desired locations. Holes were drilled with a diameter of one and 3/8 inches and a depth of 18 and 3/4 inches. The additional diameter and depth allowed for proper epoxy set as recommended by the manufacturer (Hilti, 150-max high strength epoxy). This connection assembly is shown in Figure 4.10.

At the actuator connection to the pile four steel angles of dimensions four inches x three inches x ¾ inches were placed at either side of the actuator to minimize slipping. Each plate was fastened to the pile with four ¾ inch diameter anchors (Hilti) embedded to a depth of eight inches. This connection was monitored for any gaps developing between the steel angles and the actuator head. In the few instances that gaps did occur they were very small and promptly filled with aluminum shims. A photograph of the actuator connection to the pile is shown in Figure 4.11.

Figure 4.10 Actuator Connection at Bent Cap - Exterior Specimens

Figure 4.11 Actuator Connection at Pile - Exterior Specimens

Pile ends were supported by a roller system. This support was employed to prevent damage to the connection which may have otherwise resulted from the self-weight of the pile. For EB-18-1 and EB-2-1 this support was constructed with a Hillman roller. For EB-22-1 and EB-26-1 the end of the pile was supported by an 18 inch square plate to which four rollers were attached. This assembly rested on top of a lubricated steel plate. Photographs of both systems are shown in Figures 4.12 and 4.13.

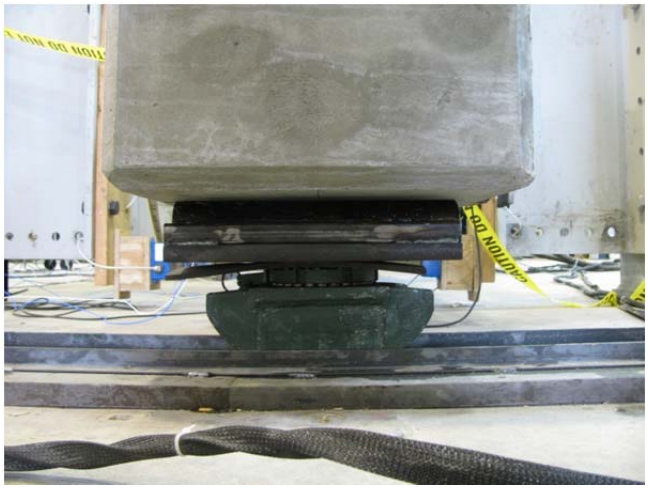

Figure 4.12 Hillman Roller End Pile Support - Exterior Specimens

Figure 4.13 Four Roller End Support - Exterior Specimens

4.6 Instrumentation - Exterior specimens

Instrumentation for these specimens was similar to the interior specimens. Pile displacements were measured with four string potentiometers (Vishay CDS-20) having a range of ± 10.0 inches. This measurement was taken at a distance of 156 inches from the face of the connection. This sensor was also used to monitor joint stresses using a setup identical to that used in the testing of the interior specimens. Two additional sensors were used to monitor any rotation of the cap. Rotation measurements were captured by mounting a gage at either side of the bent cap to both the cap and a steel frame with a distance of 10 inches separating the two. Eight plunger type linear transducers were used to monitor curvature of the pile. Four of these sensors were placed in series extending away from the joint at either side of the pile. Exterior specimen instrumentation is shown in Figure 4.8 and is presented in tabular form in Table 4.2.

Table 4.2 Instrumentation - Exterior Specimens

Gage Type	Gage Purpose/Measurement	Location	Model
String Potentiometer	Joint Shear	Embedment Region on Cap	CDS-20
String Potentiometer	Joint Shear	Embedment Region on Cap	CDS-20
String Potentiometer	Displacement	Pile 156 inches from Soffit	CDS-20
String Potentiometer	Displacement	Pile 156 inches from Soffit	CDS-20
String Potentiometer	Displacement	Pile 86 inches from Soffit	CDS-20
String Potentiometer	Displacement	Pile 86 inches from Soffit	CDS-20
LVDT	Displacement	Pile 92 inches from Soffit	Shorewestern Actuator
Load Cell	Load	Pile 92 inches from Soffit	Shorewestern Actuator
Linear Transducer	Pile Curvature	(4) In Series from Soffit Each side of Pile	HS-50
String Potentiometer	Cap Rotation	* (2) Back of Cap 1 foot from each end	CDS-20
Uniaxial Strain Gage	Strand Slippage	**(3) at Prestressing Strand 13 inches from Embedded end	C2A-06-062LW-120
Uniaxial Strain Gage	Strand Slippage	**(3) at Prestressing Strand 29 inches from Embedded end	C2A-06-062LW-120
Linear Transducer	Strand Slippage	(2) At Exposed Strands Embedded end of Pile	BEI 9615
Uniaxial Strain Gage	Spiral Strain	**Pile Spiral 29 inches from Embedded end	C2A-06-062LW-120
Uniaxial Strain Gage	Reinforcement Strain	(5) Longitudinal Reinforcement within Cap	CEA-06-W250A-120
Vibrating Wire Strain Gage	Confining Strain	**Center of Pile 9 inches from Embedded end	Geokon M4200
* Refers to Gage Location while in a Testing Position ** Refers only to Specimen EB-22-1			

4.7 Loading procedure - Exterior specimens

Specimen EB-18-1 was the first specimen tested. Displacements of ± 0.1, ± 0.2, ± 0.3, and ± 0.4 inches were first achieved. Displacement cycles continued to increase with 0.1 inch increments through cycles of ± 0.8 inches. Cycles were increased in magnitude to 0.2 inches through displacements of 2.8 inches. Some displacement cycles were repeated as a problem was encountered with one of the data acquisition systems. From this point, the magnitude of displacement cycles was increased to ± 0.4 inches through a final displacement cycle of ± 8.0 inches. The displacement history of this specimen is shown in Figure 4.14.

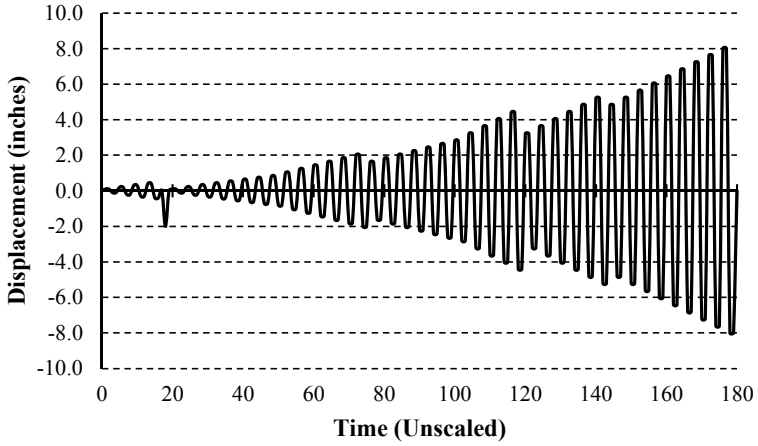

Figure 4.14 Displacement Protocol - Specimen EB-18-1

The three other specimens were tested with identical displacement cycles. Cycles of magnitude 0.1 inch were employed until displacements of ± 0.6 inches were achieved. Increments were increased to 0.2 inches through cycles of ± 1.4 inches. Cycles from ± 1.7 to ± 2.6 inches were completed with increments of 0.3 inches. From ± 3.0 inches through the remainder of the test, ± 8.0 inches, increments of 0.5 inches were used. The displacement history of these specimens is shown in Figure 4.7.

Chapter 5 - Finite Element Modeling

5.1 Introduction

A parametric study based on finite element analysis was conducted with ABAQUS FEA version 6.10 to supplement experimental investigations of the single pile specimens. Table 5.1 details the study matrix. This matrix is meant to include modeled specimens at the extremes of a number of variables. Both interior and exterior specimen models were created. Bridge construction in South Carolina typically employs square piles with variable cross sectional dimensions, generally ranging between 18 and 24 inches. The matrix shown in Table 5.1 incorporates extremes of pile dimensions. Also varied in the test matrix is the embedment depth, including a shallow as well as a deep embedment for each specimen type. The shallow and deep embedment depths were defined in conformance with the current construction tolerances prescribed in the South Carolina Bridge Design Manual. Piles are currently embedded into bent caps a distance equal to one pile cross sectional dimension with an allowable tolerance of ± 6.0 inches. The deep embedment for an 18 inch square pile was 22 inches as opposed to 24 inches which would equal a pile cross sectional dimension + 6.0 inches. Specimens modeled with 18 inch piles also incorporated a reduced cap depth to represent the coastal regions of the state.

Table 5.1 Description of Specimens Modeled

	Interior Specimens		**Exterior Specimens**	
Pile Dimension (inches)	**Embedment Depth (inches)**			
18	22	12	22	12
24	30	18	30	18

5.2 Modeling of the pile

Models were constructed by first creating the pile and then the bent cap. Both 18 and 24 inch square piles were created in ABAQUS according to typical pile designs used in the state. To begin the creation of these models a design for both piles and bent caps was established. Designs were first created for 18 and 24 inch piles. Following the pile designs, four bent cap designs were created. These four designs included an interior bent cap with an 18 inch square pile; an exterior bent cap with an 18 inch square pile; an interior bent cap with a 24 inch square pile; and an exterior bent cap with a 24 inch square pile.

Dimensions and reinforcement for each is shown in Figures 5.1 and 5.2. The models were given unique names. For example IB-18-22 is the name given to a model having an interior bent cap with an 18 inch square pile cross sectional dimension and 22 inch embedment.

Models of both 18 and 24 inch piles were created in a series of steps using the material models described later. Steps included creating the prestressing strands in the layout given by the individual pile designs and applying a material model to the strands, stressing the strands,

creating the concrete portion of the piles with the correct material model, and then releasing the strands.

Strands were laid out in the orientation and length dictated by the design. The geometry was created by constructing an orphan mesh with the same cross sectional properties as a typical prestressing strand. A 1/4 inch block length was used for the first four inches on either end of the strand and a two inch block length was used for the remainder. A nonlinear steel material model was applied based on the SCDOT Seismic Design Specifications as later described. Once the strand geometry was created three boundary conditions were applied to each strand. The center point on one end of each strand was fixed in all directions (x, y, and z) and the rest of the nodes on that end were fixed only in the z direction. On the opposite end of the strand the center point was then fixed in both the x and y directions. A pressure load of 164,000 and 165,000 psi was applied at the other end of the strands for the 18 inch and 24 inch square piles, respectively. This load corresponds to the effective stress in the strands after losses when applied to the pile. These loads were chosen so that after the strands are released the remaining stress in the strands will be approximately 160,000 psi.

Following pre-tensioning of the strands, spiral wire and concrete portions of the pile were created. The spiral wire was created using a 3-D solid revolved shape. This shape was revolved about the outside diameter of the strand geometry with the pitches shown in Figure 5.3. The concrete portion of the pile was created by building an orphan mesh in the same way the strands were created. Since the Mander confined concrete model was used, a circular section of the pile had to first be created separate from the rest for the confined concrete and then combined with the rest of the pile. One inch blocks were used for the entire length of the pile.

Upon the creation of the necessary pile portions the strands and spiral were coupled to the concrete using an embedded element constraint. A fixed boundary condition was then applied to the geometric center of the pile and the pile centerline was fixed in the x and y directions allowing compressive deformation in the pile with the release of the pretensioned strands. After the strands are released, the piles were coupled with the bent caps in the final model.

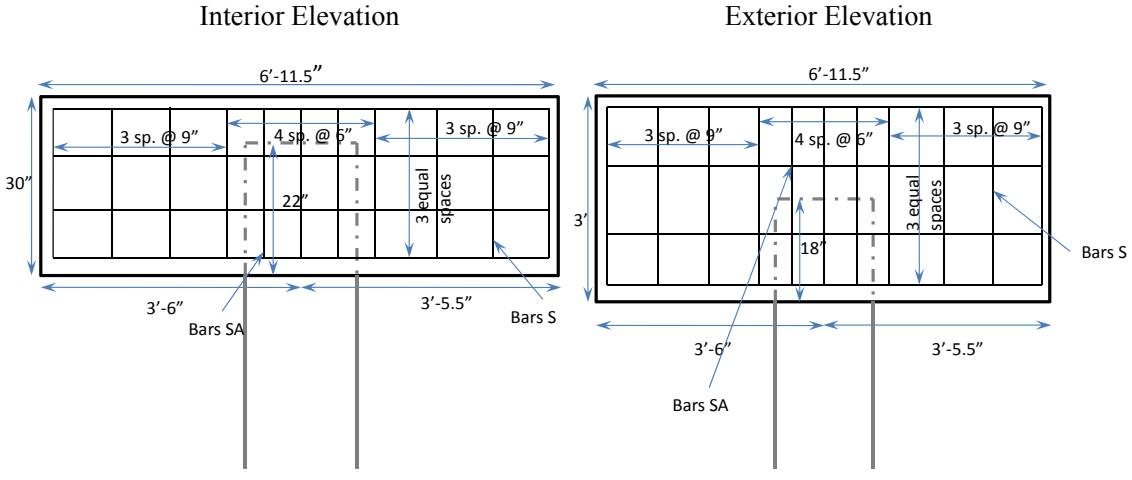

Figure 5.1 Reinforcement Pattern (18 inch Square Pile)

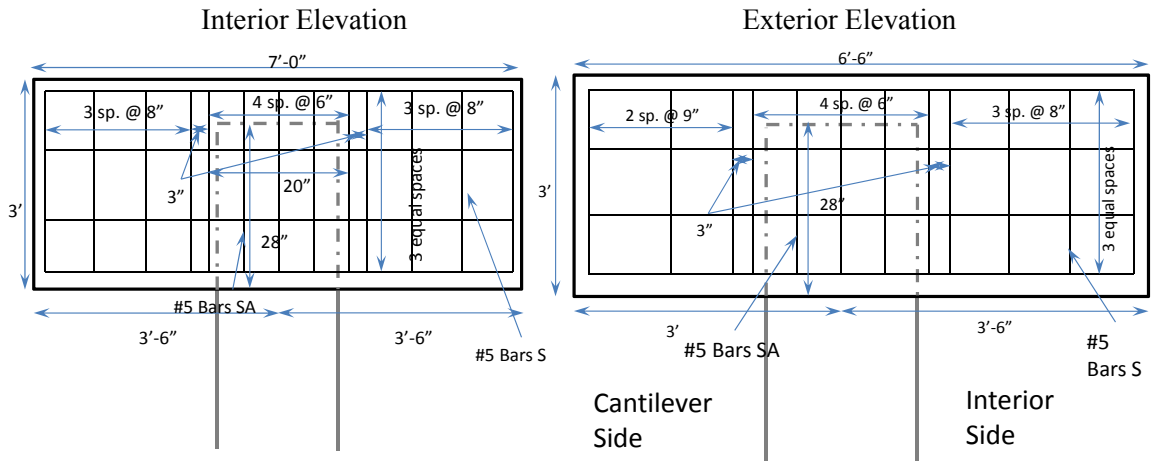

Figure 5.2 Reinforcement Pattern (24 inch Square Pile)

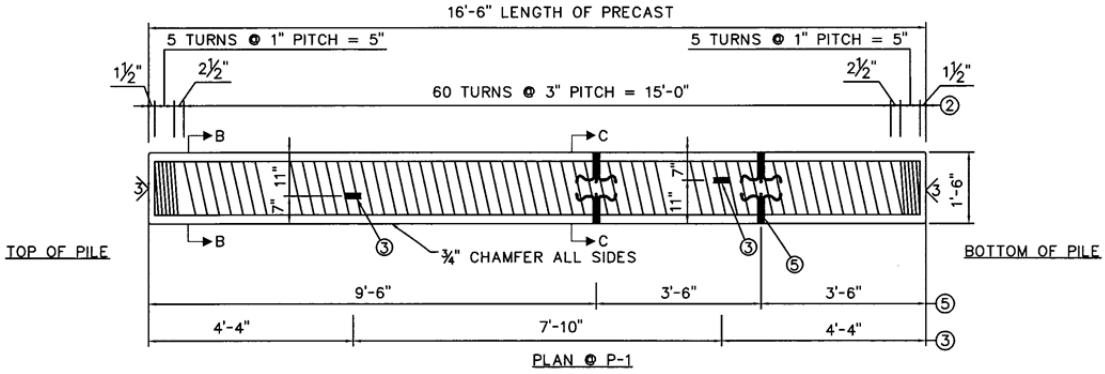

Figure 5.3 Modeled Pile Reinforcement

5.3 Modeling of the bent cap

Both interior and exterior portions of a typical bent cap were modeled. This included a variety of specimens (Table 5.1). Bent cap dimensioning is dependent upon pile sizing. Bent caps are most often designed with a three foot square cross section when constructed in conjunction with 18 inch square piles. Cap width is then modified based on the pile geometry. Caps are generally designed with a minimum width equal to two times the pile dimension. For example, a 20 inch square pile would require a 40 inch cap width. A cap fit with 24 inch square piles would be designed with a width of 48 inches. This study used bent cap widths of 36 inches and 48 inches in combination with 18 and 24 inch square piles.

Current practice is to embed piles to a depth of a single pile cross sectional dimension with a construction tolerance of ± 6.0 inches. With these constraints a cap depth of 36 inches is assumed to perform adequately with piles of cross sectional dimension up to 24 inches. A 36 inch cap depth was utilized in creation of the bent cap models to which 24 inch square piles were connected. Although this same cap depth may be used with piles of smaller dimensions, this study aimed to address a broad range of construction practices employed by the state of South

Carolina. One such construction practice is the use of a reduced cap depth. Caps are sometimes designed with a reduced depth to minimize surface water interaction. This is a common practice in the low country area of the state near the coastal regions. To address this, bent caps connected to 18 inch square piles were modeled with a reduced cap depth of 30 inches.

Unlike the cap depth and width, the cap length remained unchanged with changes in pile cross section. The length of interior bent caps as well as the length to the interior side of exterior specimens was determined based on the results of a parametric study as previously described. These lengths are based on a center to center spacing between piles of seven feet. Interior specimen bent cap length was a constant seven feet, while the length of exterior specimens was held constant at 6 feet 6 inches with the pile centered 3 feet 6 inches from the interior side of the specimen.

Four bent cap models were created including an interior cap for an 18 inch square pile; an exterior cap for an 18 inch square pile; an interior cap for a 24 inch square pile; and an exterior cap for a 24 inch square pile. Each cap was modeled with a reinforcement design specific to the cap. The reinforcement design was completed to represent a realistic but 'worst case' scenario similar to the physical test specimens. The designs are summarized in Figures 5.1 and 5.2.

With the appropriate material models the bent cap models were created in ABAQUS as a separate element from the previously created piles. The caps were created by first building the reinforcement cages. The reinforcement cages were created with 3-D deformable solid extrusions of each bar arranged in the proper locations, and a typical 1.0 inch mesh was applied.

5.4 Material models

The four material models used are described in this section. These were taken from the SCDOT Seismic Design Specifications (SCDOT SDS). One material model was used to describe the behavior of mild reinforcement within the caps and piles while a second model was used for the prestressing strand within the piles. All mild reinforcement within both bent caps and piles was modeled using the "Nonlinear Reinforcement Steel Model for Ductile Reinforced Concrete Members." This model is found in SCDOT SDS section 6.6.2. Figure 5.4 details the specific parameters of the model used in this study. Mild steel in South Carolina bridge construction is specified to be ASTM A706. The expected properties of this steel type are given in SCDOT SDS section 6.6.2.

Figure 5.5 shows the stress strain behavior of the prestressing strands within the piles as given by the "Nonlinear Prestressing Strand Model." This model is found in SCDOT SDS section 6.6.3. The model shown in Figure 5.5 shows the maximum stress model used for prestressing strands. Due to shrinkage of the bent cap concrete, the development length of prestressing strands is a function of the embedment depth. The material models for prestressing strands were modified to be specific to the embedment depth employed by the model. To account for the embedment depth modeled, the maximum stress of the prestressing strand material model was reduced to be equal to the calculated slipping stress corresponding to the modeled embedment depth. The values of slipping stress used in each of the models are shown in Table 5.2.

In addition to the material models for steel reinforcement, two material models were used to describe the behavior of concrete elements within the models. These two models are both

described as ‘Mander Models’, which incorporate both confined and unconfined concrete models. A confined concrete model was applied to all concrete elements for each at locations within the spiral reinforcement of the piles. All remaining concrete elements of the pile were given a material model of unconfined concrete. A ‘Mander’ material model was also used in the creation of the bent cap concrete elements. These elements were assigned as unconfined. Both confined and unconfined concrete material models are described in SCDOT SDS section 6.6.4. Figure 5.6 shows the stress-strain relationship of both confined and unconfined concrete assumed by the Mander material model. It should be noted that these material models are created using expected concrete properties given for typical design strengths of piles and bent caps. In the state of South Carolina piles and bent caps are designed to reach 28-day strength of 5,000 psi and 4,000 psi, respectively. Expected material properties are given by the SCDOT SDS in the material model section, Section 6.6.4.

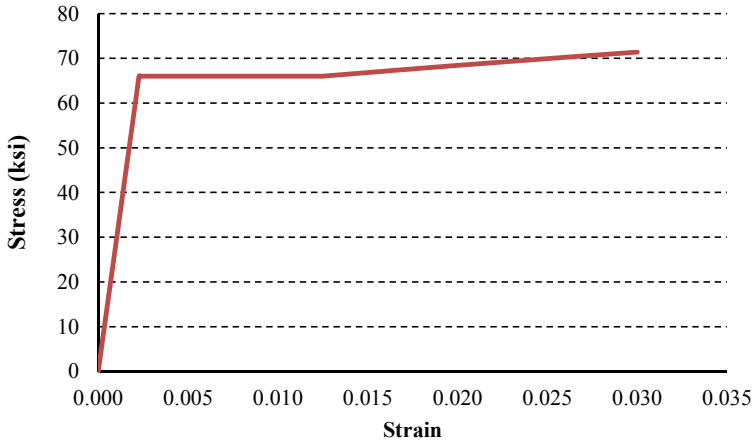

Figure 5.4 Material Model for Mild Steel Reinforcement

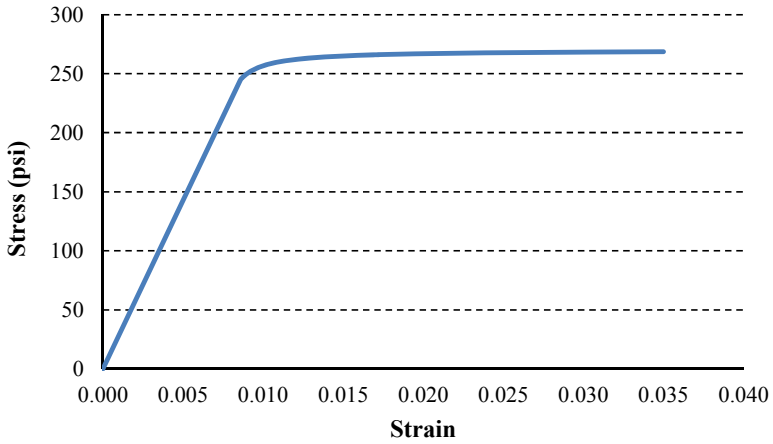

Figure 5.5 Material Model for Prestressing Strand

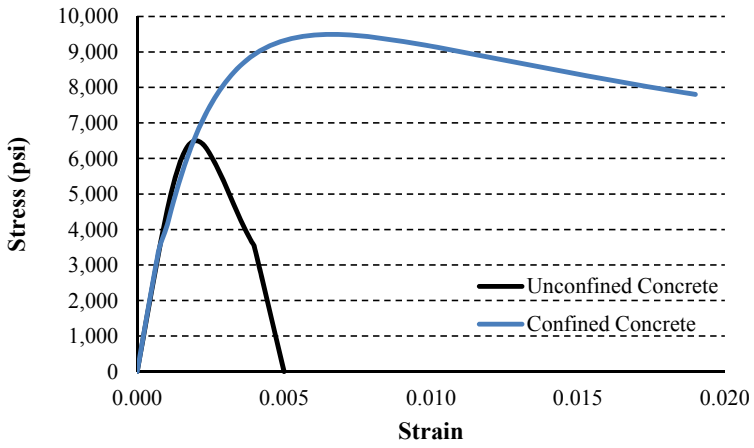

Figure 5.6 Material Models for Concrete in Precast Piles

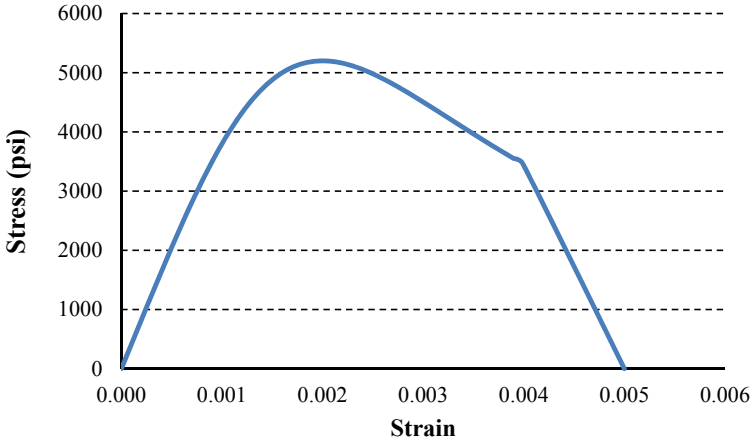

Figure 5.7 Material Model for Bent Cap Concrete

Table 5.2 Embedment Length and Modeled Slipping Stress

Embedment Depth (inches)	Calculated Slipping Stress (psi)
12	120,000
18	167,200
22	181,600
30	210,400

5.5 Boundary conditions and loading procedure

The simulations were run in a manner similar to that of the physical test specimens. A fixed boundary condition was applied over the top surface of the bent caps. Loading conditions varied between interior and exterior specimens.

Interior specimens were subject to a constant axial load of 50 kips applied at the end of the pile, over the surface of the pile end. Lateral loading was applied over a six inch by six inch square centered at 146 inches from the connection between the bent cap and the pile. Due to symmetry these models were displaced in a single direction to the point of maximum load.

The loading and load application of the exterior specimens was different from that of the interior specimens. To apply load a plate and arm assembly was connected to the pile centered at a distance of 92 inches from the connection. The plate was modeled as a six inch square of ¼ inch depth connected to an arm. The arm was set at an angle to the plate equal to that of the initial angle used in physical testing. Both the plate and the arm were assigned a material model with an artificially high modulus to simulate a rigid body. Loading was then applied through this plate and arm assembly resulting in both lateral and axial loading depending on the direction of the applied load. Figure 5.8 shows this plate and arm detail. Loading was applied to the modeled specimen in the same way that loading was applied in the laboratory test specimens.

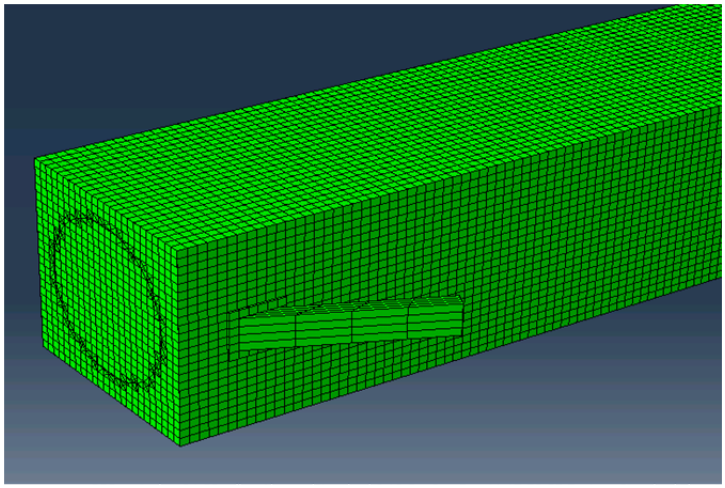

Figure 5.8 Loading Assembly for Exterior Specimens

5.6 Model validation

A convergence study was conducted to ensure that the correct element behavior was obtained while at the same time maintaining a reasonable level of computational time. A model was analyzed using four separate element sizes, three, one, ½, and ¼ inch. Convergence was determined by analyzing the stresses at a specific point on the bent cap at the connection to the pile (Figure 5.10). By plotting the stresses over this area the optimal element size was determined, as shown in Figure 5.9. From the plot it can be seen that convergence of the stresses

over the given area occurs with an element size of 1.0 inches, therefore this element size was utilized for all models.

Additional validation was performed through a comparison of measured response and simulated response using measured properties of a physical specimen. The comparison was performed with specimen IB-18-22. A comparison was made between the yield displacement and the corresponding moment. With a 2% offset method used for yield calculation the model shows yield of the specimen to occur at a displacement of 0.46 inches with a corresponding moment of 1,860 kip-inches. By comparison the yield during the physical test occurred at a displacement of 0.8 inches with a corresponding moment of 1,840 kip-inches.

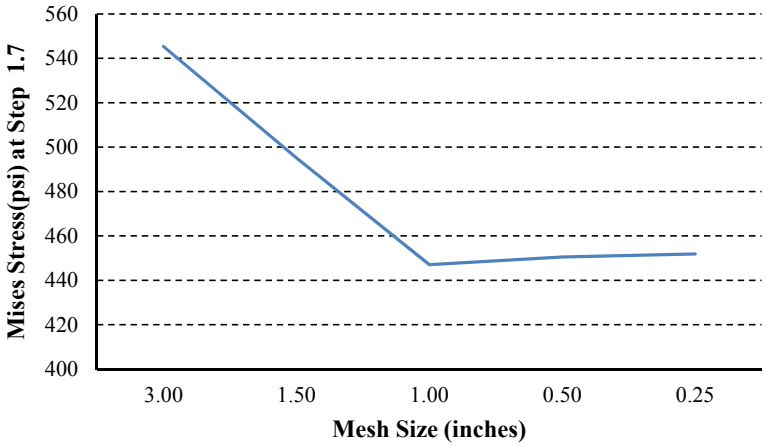

Figure 5.9 Results of Convergence Study

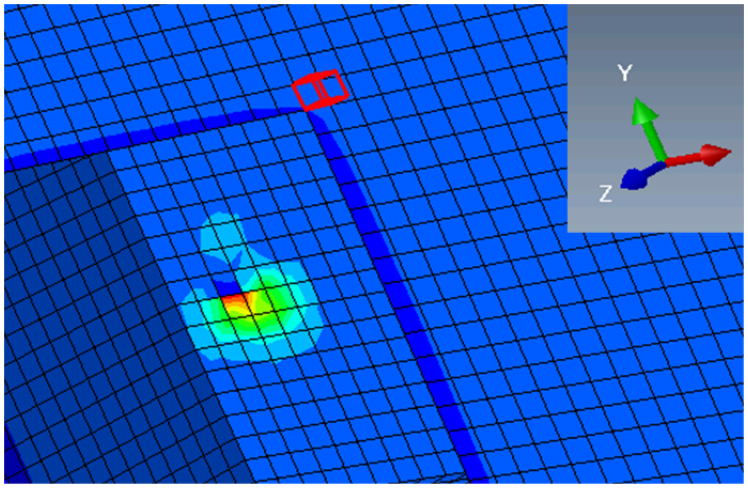

Figure 5.10 Element Reference Coordinate System

5.7 Interior specimen results

The behavior of the pile elements can be modeled with a less computationally expensive moment curvature analysis. The finite element analysis investigates the global behavior of the specimen and the localized behavior within the bent cap. Several aspects of the bent cap were also analyzed at the point at which global yielding occurs. These aspects include:

- The tensile stresses in the bent cap at the point of global yield
- The location of tensile cracking within the bent cap at this point
- The extent to which these cracks propagate into the bent cap
- The extent and location of compressive failure (crushing or spalling) within the cap at the point of global yield
- The stress within the bent cap reinforcement at the point of global yield

In the following sections behavior of individual elements within the bent cap are presented for both interior and exterior specimens. Figure 5.10 details the coordinate system used. The highlighted element in this figure is referred to as element (0, 0, 0). For brevity at times elements will be referred to with a single coordinate, in such cases this nomenclature will indicate an X coordinate with coordinates Y and Z equal to 0.

The results are presented with the following general outline:

1. Global yield
2. Maximum principle stress at global yield
3. Location of cracking at global yield
4. Crack propagation/penetration at global yield
5. Load step at crack initiation
6. Location of potential concrete crushing or spalling at global yield
7. Penetrations of potential concrete crushing or spalling at global yield
8. Strain in bent cap reinforcement cage at global yield
9. Crack propagation/penetration at maximum displacement

5.7.1 Specimen IB-18-22

The global yield of the specimen occurred at time step = 1.40. This time step corresponds to a displacement of 0.46 inches and a moment equal to 1,865 kip-inches. The global yield was estimated using a 2% offset as shown in Figure 5.11. It is clear that the specimen exhibited non-linear behavior at the point of global yield.

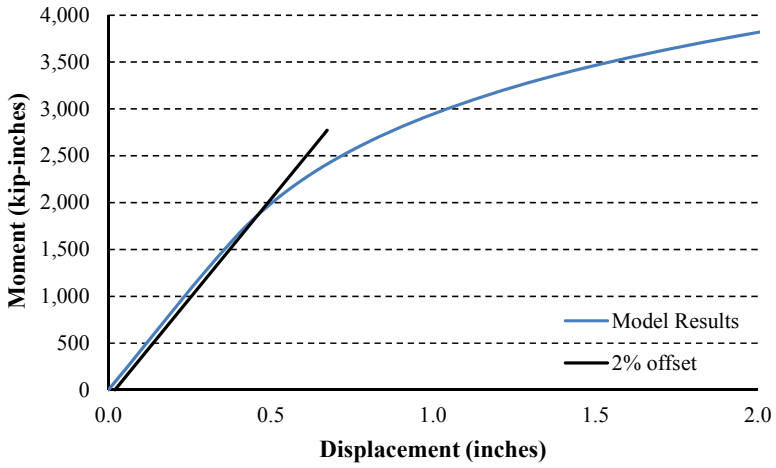

Figure 5.11 Moment versus Displacement - Specimen IB-18-22

Figure 5.12 shows the maximum principle stresses of the elements at the interaction surface between the pile and the bent cap at the point of global yield. Elements in this figure colored grey or bright red have reached the point of tensile cracking. This figure details the propagation of cracked elements into the bent cap. It can be seen that at the point of global yielding local elements have cracked to a depth of four inches from the face of the bent cap.

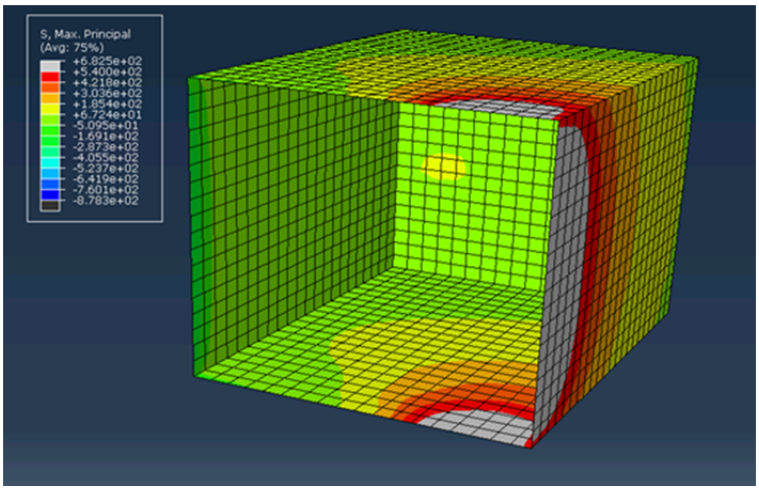

Figure 5.12 Maximum Principle Stresses on the Bent Cap Surface at Global Yield - Specimen IB-18-22

The propagation of cracking in the Y direction at the point of global yield is shown in Figure 5.13. The bent-cap is cut to show the top face of elements with y = 0. It can be observed that the stress level at the top of these elements is less than the maximum concrete tensile stress and therefore the propagation of cracking is limited to a value of less than one inch in the positive Y direction.

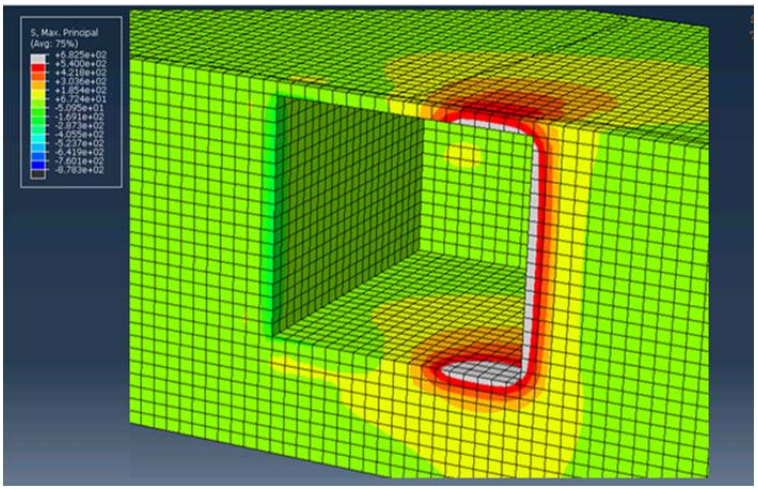

Figure 5.13 Maximum Principle Stress within the Bent Cap at Global Yield - Specimen IB-18-22

Crack initiation was determined as shown in Figure 5.14. The initiation of cracking occurred at displacement of 0.22 inches (time step 1.20). From this figure it can be seen that first tensile cracking along the pile occurs at element -1 and -2. The moment at which cracking occurred is equal to 945 kip-inches.

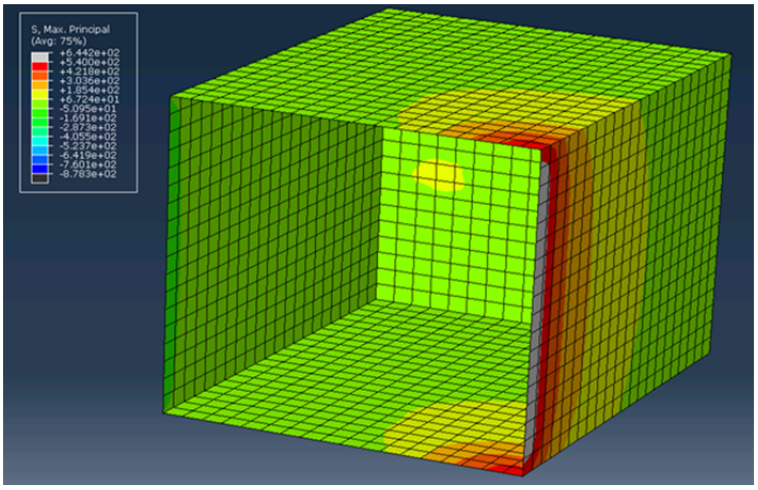

Figure 5.14 Crack Initiation - Specimen IB-18-22

Along with the location of tensile cracking within the bent cap at the point of global yield, the location of local compressive failure (concrete crushing or spalling) is also of interest. Figure 5.15 shows the minimum principle stress versus displacement at element -18. The highest compressive stress is seen to be 4,160 psi. This value is 64% of the maximum compressive stress of the concrete element.

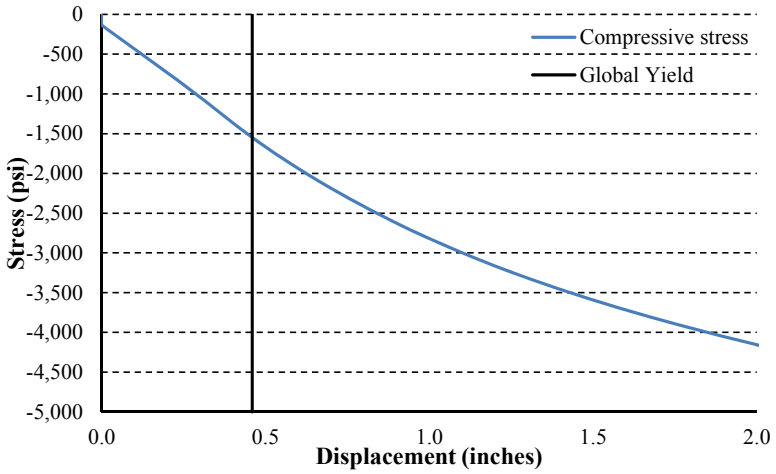

Figure 5.15 Minimum Principle Stress versus Displacement at Element (x = -18) - Specimen IB-18-22

The stress in the bent cap reinforcement was also determined at the point of global yielding. Figure 5.16 is a representation of the reinforcement cage at the global yield point. Where tensile cracking has occurred within the concrete elements the stress in the reinforcement is elevated. Checking the maximum principle stress it is seen that the value is below 1,520 psi which is well below the yield point (Figure 5.17).

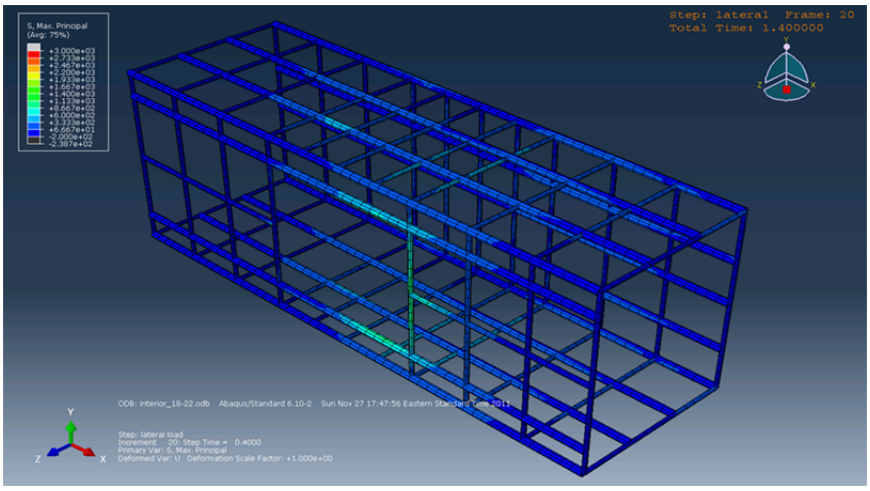

Figure 5.16 Maximum Principle Stress in Bent Cap Reinforcement at Global Yield - Specimen IB-18-22

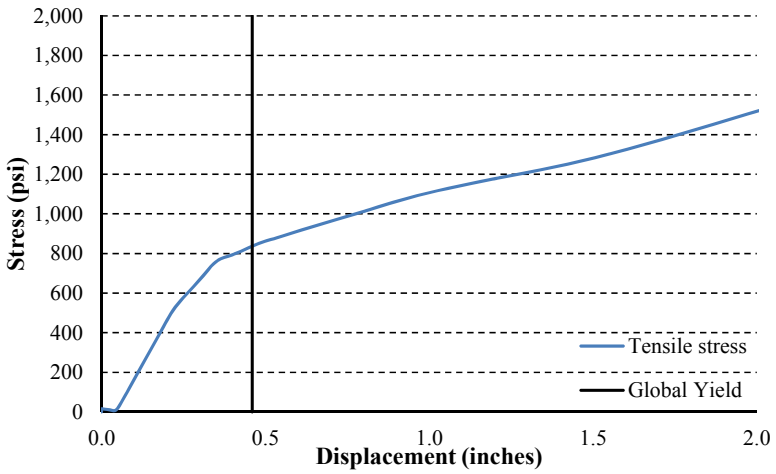

Figure 5.17 Maximum Reinforcement Stress versus Displacement - Specimen IB-18-22

The initiation of tensile cracking as well as crack propagation at the point of global specimen yield is reported above. These parameters are also of interest at the maximum displacement of the model. Figures 5.18 and 5.19 indicate the depth of tensile cracking within the bent cap at the ultimate time step, which corresponds to a displacement of two inches. It can be seen that the cracking penetrates the bent caps to distances of less than 12 inches in the negative X direction, 12 inches in the negative Z direction, and two inches in the positive Y direction.

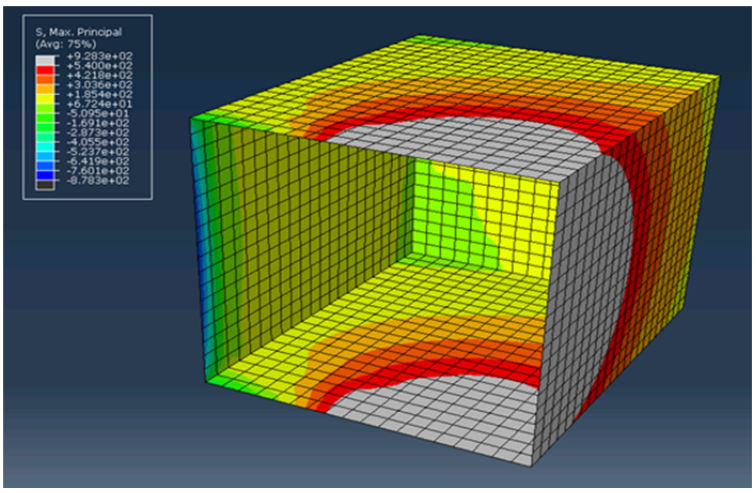

Figure 5.18 Crack Propagation (X and Z direction) at Displacement of 2 Inches - Specimen IB-18-22

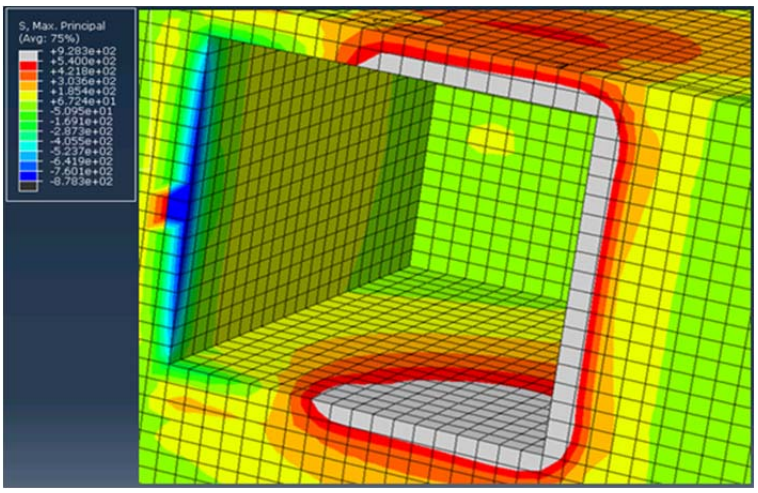

Figure 5.19 Crack Propagation (Y direction) at Displacement of 2 Inches - Specimen IB-18-22

5.7.2 Specimen IB-18-12

The global yield of the specimen occurred at time step = 1.34. This time step corresponds to a displacement of 0.40 inches and a moment of 1,520 kip-inches. The global yield was estimated using a 2% offset as shown in Figure 5.20. The specimen exhibited non-linear behavior at the point of global yield.

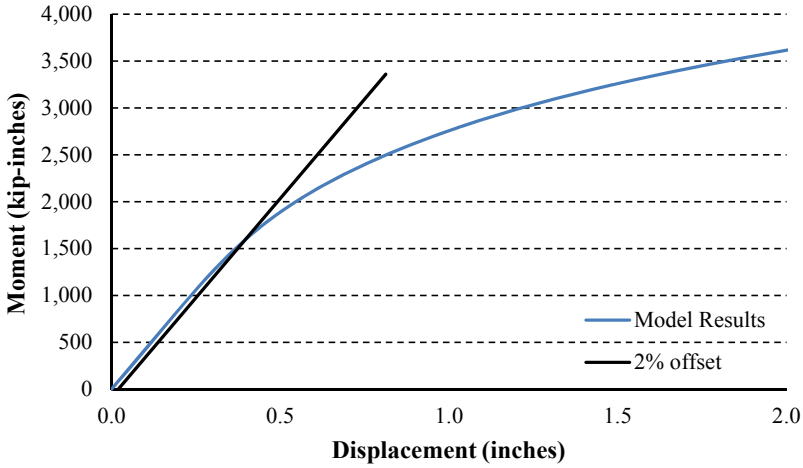

Figure 5.20 Moment versus Displacement - Specimen IB-18-12

Figure 5.21 shows the maximum principle stress of the elements at the interaction surface between the pile and the bent cap at the point of global yield. Elements colored grey or bright red have reached the point of tensile cracking. This figure details the propagation of cracked elements into the bent cap. At the point of global yield local elements have cracked to a depth of three inches from the face of the bent cap.

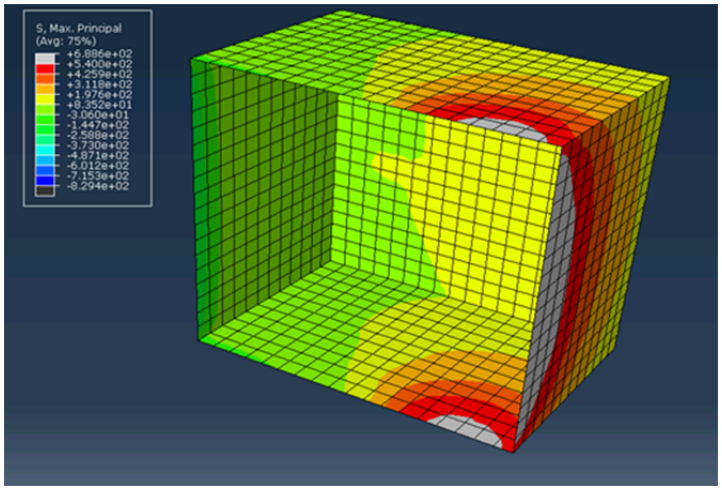

Figure 5.21 Maximum Principle Stress on the Bent Cap Surface at Global Yield - Specimen IB-18-12

The propagation of cracking in the Y direction at the point of global yield is shown in Figure 5.22. The bent cap is cut to show the top face of elements with y = 0. The stress level at the top of these elements is less than the maximum concrete tensile stress and therefore the propagation of cracking is limited to a value under one inch in the positive Y direction.

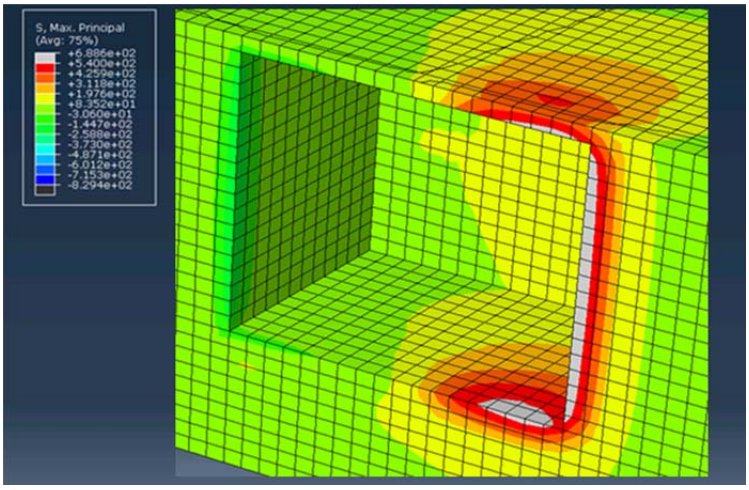

Figure 5.22 Maximum Principle Stress within the Bent Cap at Global Yield - Specimen IB-18-12

The point of crack initiation is shown in Figure 5.23. The initiation of cracking occurred at a displacement of 0.22 inches (time step 1.20). From this figure it can be seen that first tensile cracking along the pile occurs at element -1 and -2. The moment at which cracking occurred is equal to 855 kip-inches.

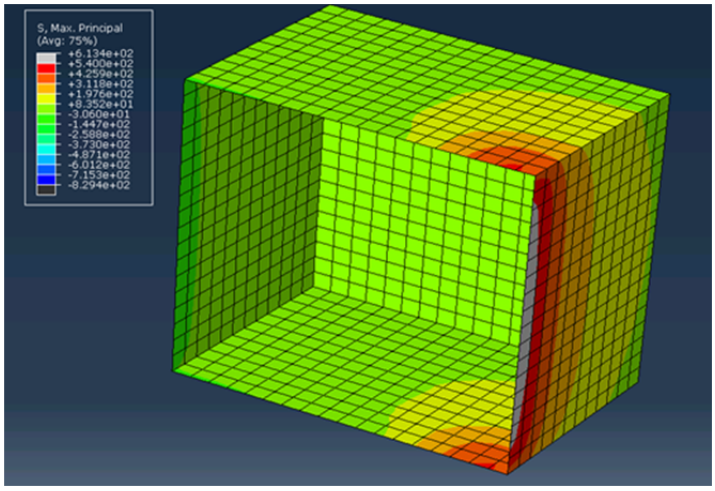

Figure 5.23 Crack Initiation - Specimen IB-18-12

Along with the location of tensile cracking within the bent cap at the point of global yield, the location of local compressive failure (crushing or spalling) is also of interest. Figure 5.24 shows the minimum principle stress versus displacement at element -18. The highest compressive stress is seen to be 4,200 psi. This value is 65% of the maximum compressive stress of the concrete. It is assumed that at the point of global yield local compressive failure does not occur.

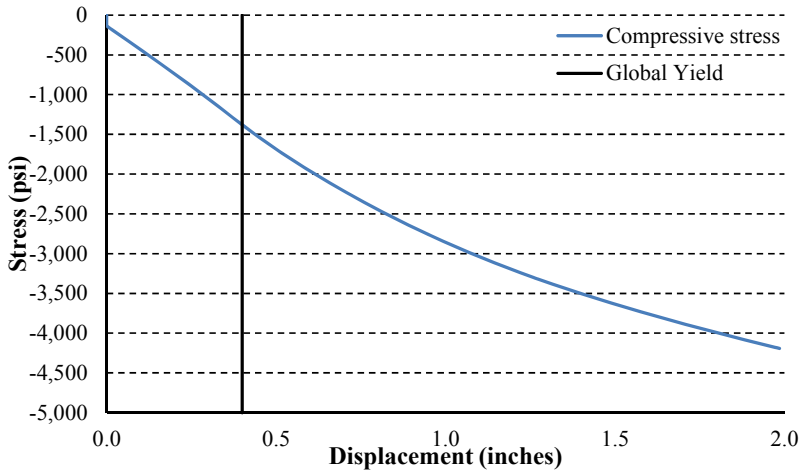

Figure 5.24 Minimum Principle Stress versus Displacement at Element (x = -18) - Specimen IB-18-12

The stress in the reinforcement of the bent cap was also determined at the point of global yield (Figure 5.25). As expected at the areas of tensile cracking the stress in the reinforcement is elevated. The maximum stress is below 1,000 psi which is well below the yield point (Figure 5.26).

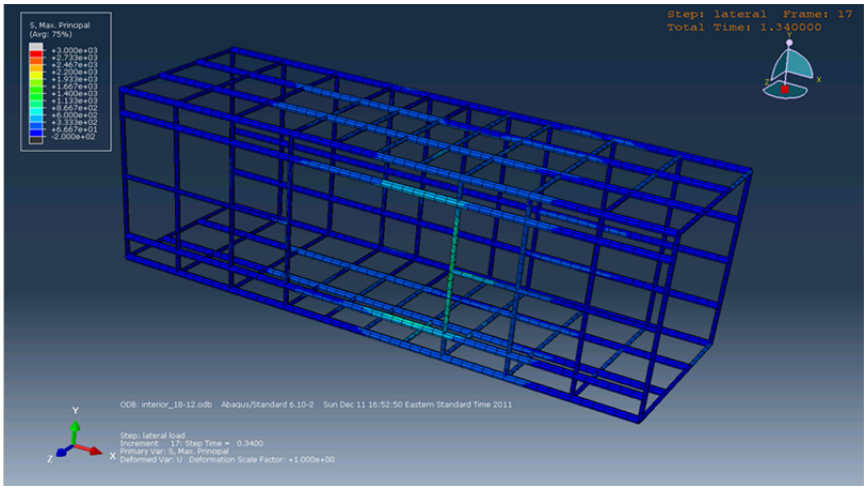

Figure 5.25 Maximum Principle Stress in Reinforcement Cage at Global Yield - Specimen IB-18-12

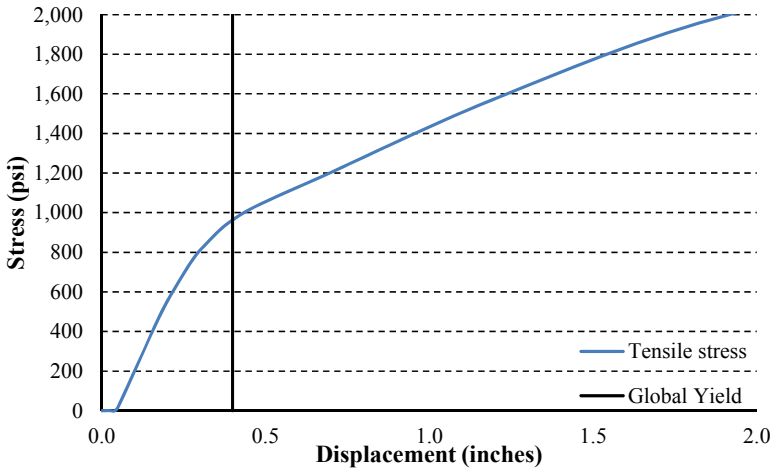

Figure 5.26 Maximum Reinforcement Stress versus Displacement - Specimen IB-18-12

The initiation of tensile cracking and its propagation at the point of global yield are reported above. These parameters are also of interest at the ultimate time step (maximum displacement). Figures 5.27 and 5.28 indicate the depth to which tensile cracking occurs within the bent cap corresponding to a displacement of 2.0 inches. The cracking at this time step penetrates the bent caps to distances of less than 12 inches in the negative X direction, nine inches in the negative Z direction, and two inches in the positive Y direction.

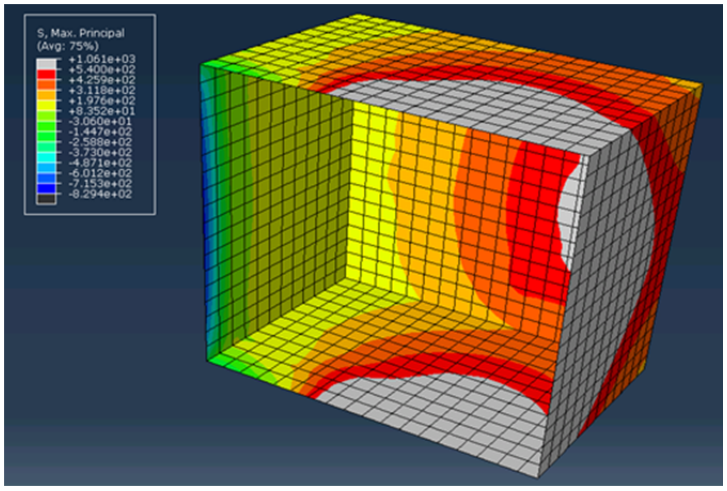

Figure 5.27 Crack Propagation (X and Z Direction) at Displacement of 2 Inches - Specimen IB-18-12

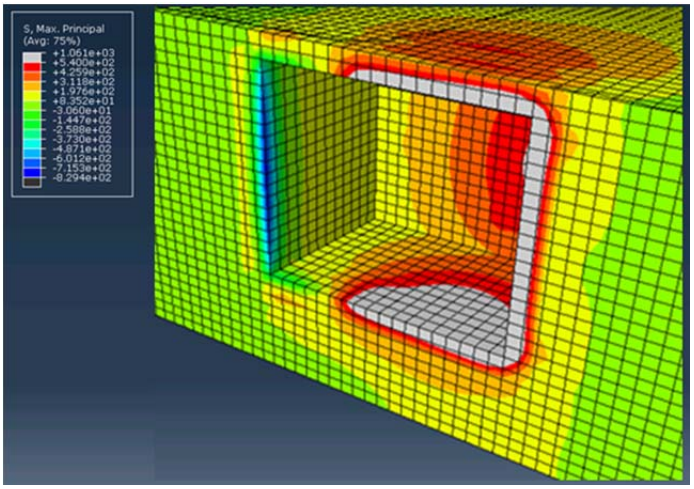

Figure 5.28 Crack Propagation (Y direction) at Displacement of 2 Inches - Specimen IB-18-12

5.7.3 Specimen IB-24-30

Global yield occurred at time step = 1.50, corresponding to a displacement of 0.41 inches and a moment equal to 4,910 kip-inches. Global yield was estimated using a 2% offset as shown in Figure 5.29. The specimen exhibited non-linear behavior at the point of global yield, similar to the previous specimens.

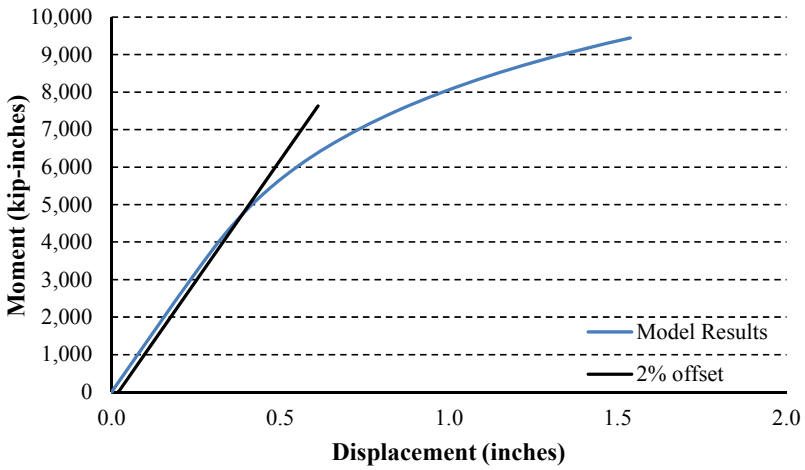

Figure 5.29 Moment versus Displacement - Specimen IB-24-30

Figure 5.30 shows the maximum principle stress of the elements at the interaction surface between the pile and the bent cap at the point of global yield. Dark grey elements and elements within the area encompassed by the dark grey have reached the point of tensile cracking. It can be seen that at the point of global yield local elements have cracked to a depth of seven inches from the face of the bent cap.

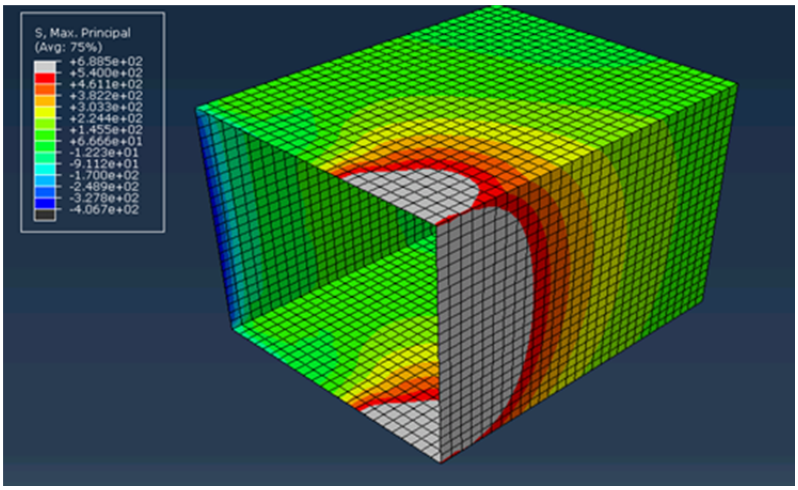

Figure 5.30 Maximum Principle Stress on the Bent Cap Surface at Global Yield - Specimen IB-24-30

The propagation of cracking in the Y direction at the point of global yield is shown in Figure 5.31. The bent cap is cut to show the top face of elements with y = 1. Cracking in the Y direction exceeds one inch and is less than two inches.

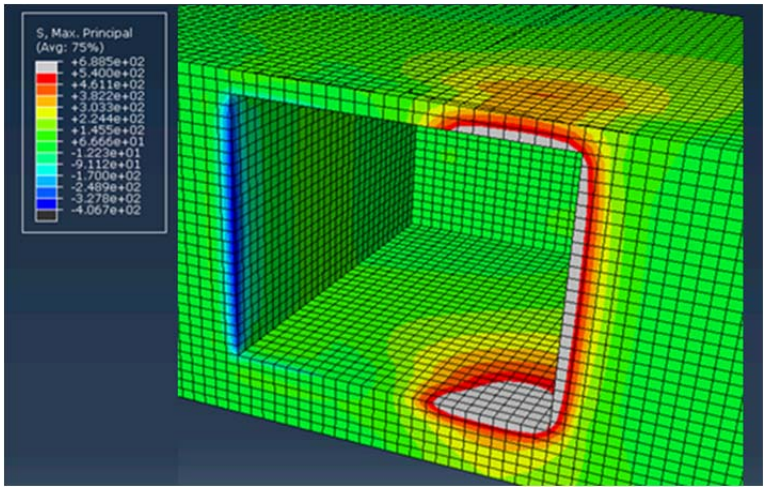

Figure 5.31 Maximum Principle Stress within the Bent Cap at Global Yield - Specimen IB-24-30

The point of crack initiation was determined as shown in Figure 5.32. The initiation of cracking occurred at a displacement of 0.13 inches (time step 1.18). From this figure it can be seen that first tensile cracking along the pile occurs at elements -1 and -2 at 1,700 kip-inches.

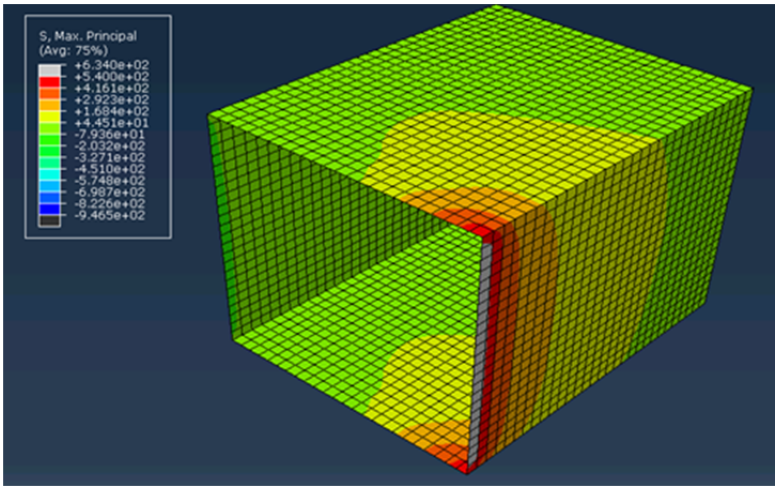

Figure 5.32 Crack Initiation - Specimen IB-24-30

The location of local compressive failure (crushing or spalling) is also of interest. Figure 5.33 shows the minimum principle stress versus displacement at element -24. The highest compressive stress at this element is 4,950 psi, which is 76% of the maximum compressive stress of the concrete.

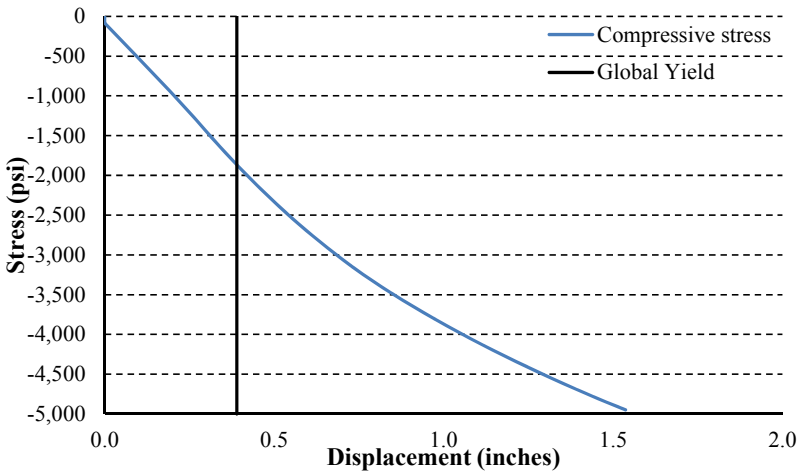

Figure 5.33 Minimum Principle Stress versus Displacement at Element (x = -24) - Specimen IB-24-30

Figure 5.34 shows the reinforcement cage at the global yield point. At the areas where tensile cracking has occurred, the stress in the reinforcement is elevated. The level of maximum tensile stress is below 1,250 psi (Figure 5.35).

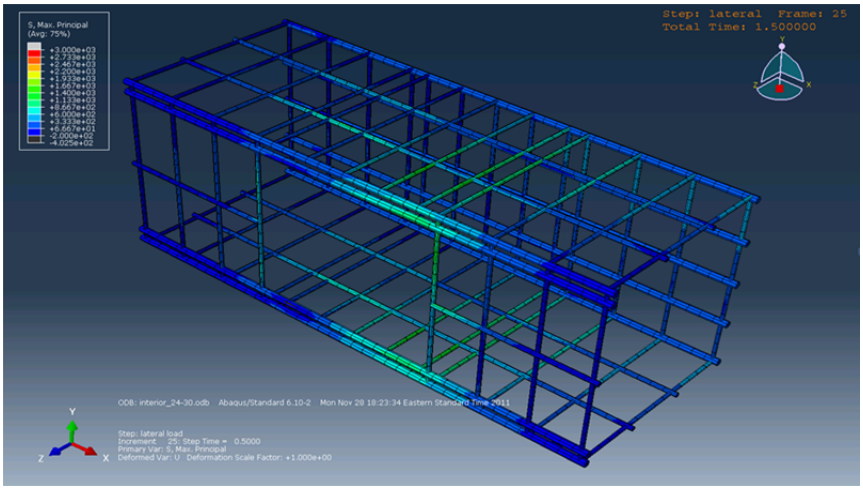

Figure 5.34 Maximum Principle Stress in Reinforcement Cage at Global Yield - Specimen IB-24-30

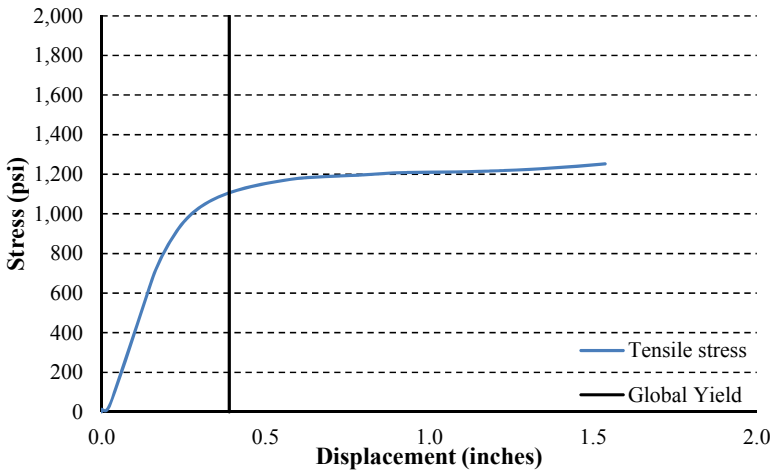

Figure 5.35 Maximum Reinforcement Stress versus Displacement - Specimen IB-24-30

Figures 5.36 and 5.37 indicate the depth to which tensile cracking occurs within the bent cap corresponding to a displacement of 1.53 inches. The cracking at this time step penetrates the bent cap to distances of less than 16 inches in the negative X direction, 17 inches in the negative Z direction and six inches in the positive Y direction.

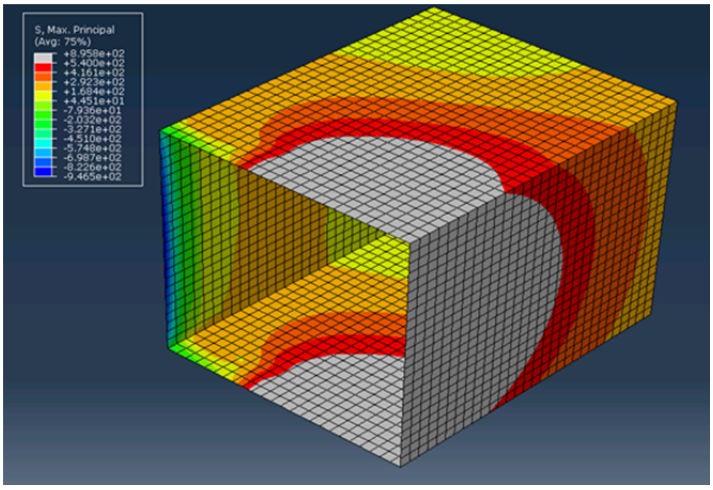

Figure 5.36 Crack Propagation (X and Z direction) at Displacement of 1.53 Inches - Specimen IB-24-30

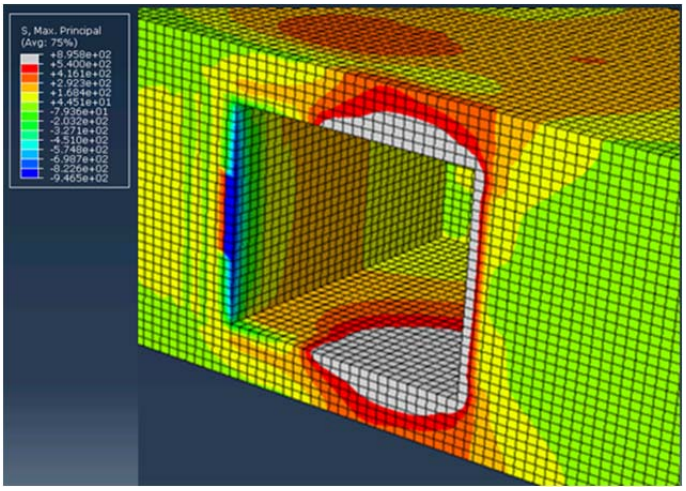

Figure 5.37 Crack Propagation (Y direction) at Displacement of 1.53 Inches - Specimen IB-24-30

5.7.4 Specimen IB-24-18

Global yield occurred at time step = 1.50, corresponding to a displacement of 0.40 inches and a moment of 4,795 kip-inches. Global yield was estimated using a 2% offset as shown in Figure 5.38.

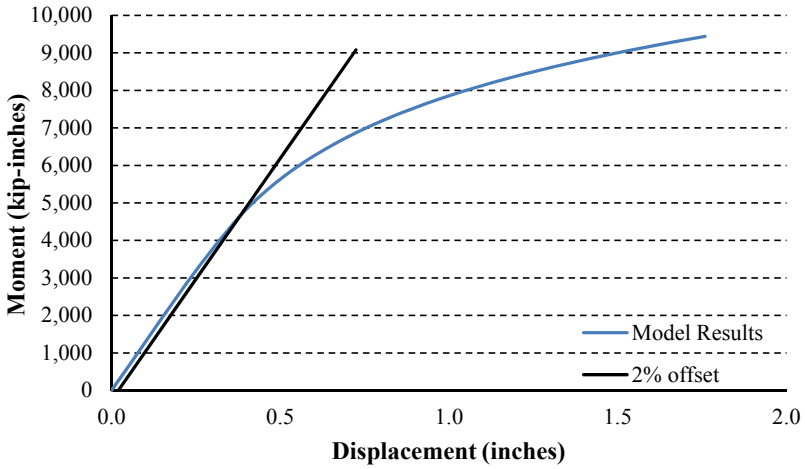

Figure 5.38 Moment versus Displacement - Specimen IB-24-18

Figure 5.39 shows the maximum principle stress of the elements at the interaction surface between the pile and the bent cap at the point of global yield. At the point of global yield local elements have cracked to a depth of eight inches from the face of the bent cap.

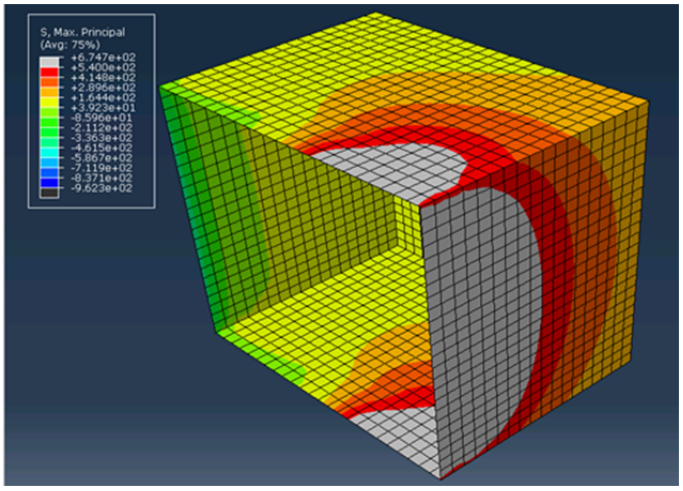

Figure 5.39 Maximum Principle Stress on the Bent Cap Surface at Global Yield - Specimen IB-24-18

The propagation of cracking in the Y direction at the point of global yield is shown in Figure 5.40. The bent cap is cut to show the top face of elements with y = 1. Cracking in the Y direction exceeds one inch and is less than two inches.

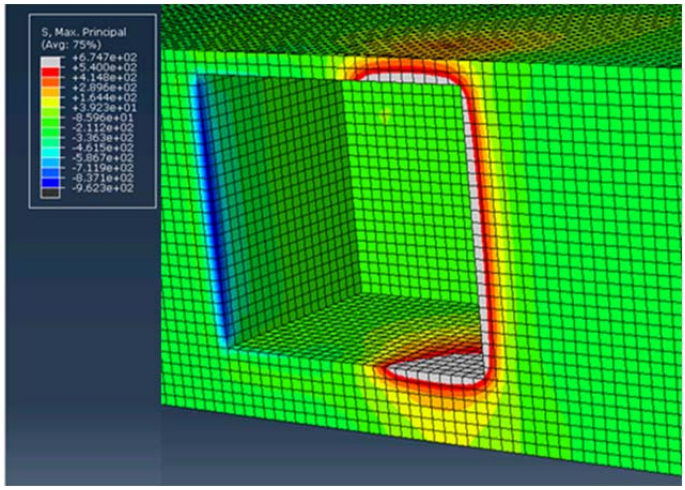

Figure 5.40 Maximum Principle Stress within the Bent Cap at Global Yield - Specimen IB-24-18

Crack initiation is shown in Figure 5.41. The initiation of cracking occurred at displacement of 0.13 inches (time step 1.18). First tensile cracking occurred at elements -1 and -2 at 1,725 kip-inches.

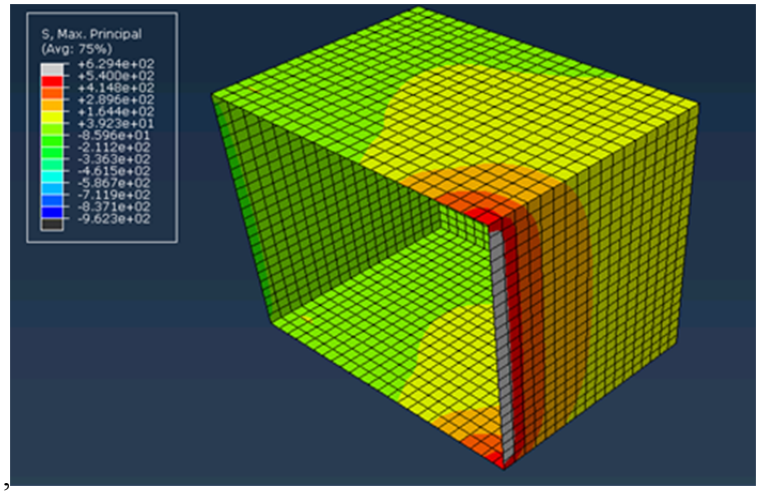

Figure 5.41 Crack Initiation - Specimen IB-24-18

Figure 5.42 shows the minimum principle stress versus displacement at element -24. The highest compressive stress at this element is 5,200 psi, corresponding to 80% of the maximum compressive stress.

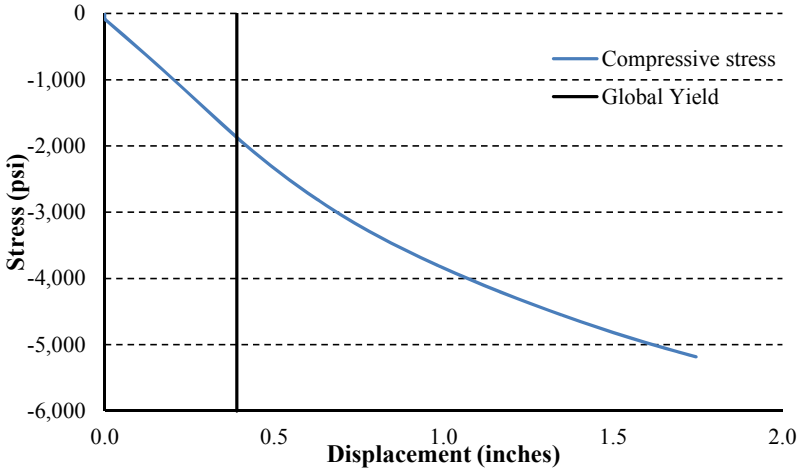

Figure 5.42 Minimum Principle Stress versus Displacement at Element (x = -24) - Specimen IB-24-18

Figure 5.43 shows the reinforcement cage at the global yield point. Where tensile cracking has occurred, the stress in the reinforcement is elevated. The stress in the reinforcement is below 1,270 psi (Figure 5.44).

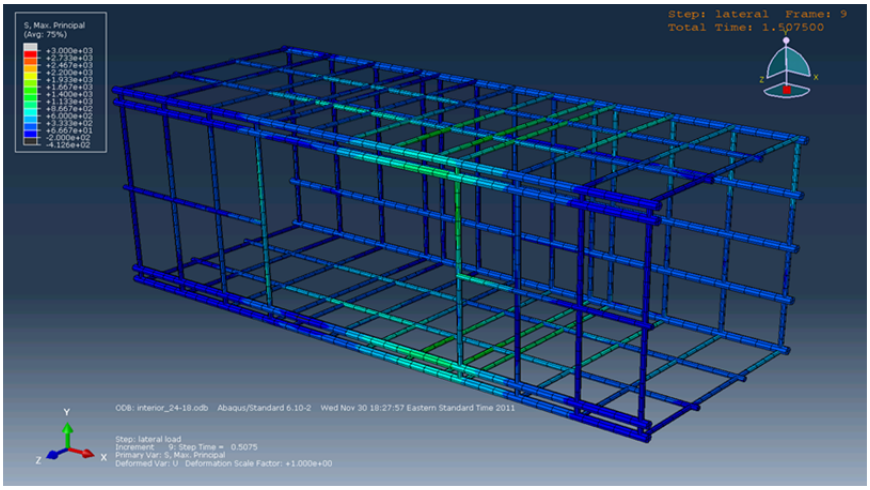

Figure 5.43 Maximum Principle Stress in Reinforcement Cage at Global Yield - Specimen IB-24-18

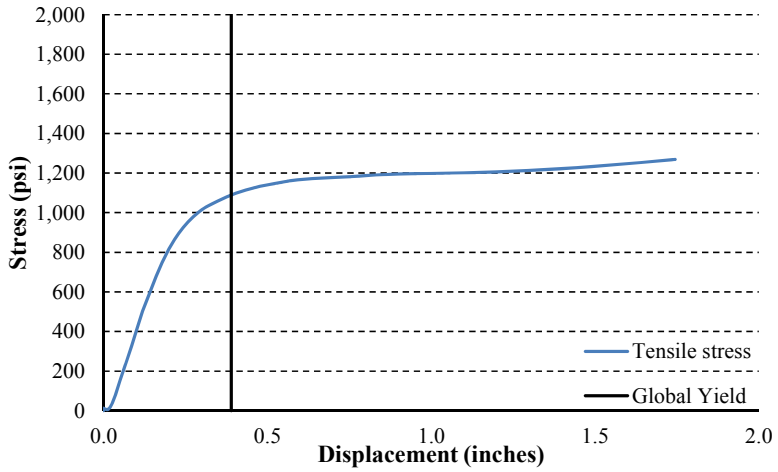

Figure 5.44 Maximum Reinforcement Stress versus Displacement - Specimen IB-24-18

Tensile cracking in the bent cap at a displacement of 1.76 inches is shown in Figures 5.45 and 5.46. Cracking penetrates the bent cap to distances of less than 17 inches in the negative X direction, 17 inches in the negative Z direction and five inches in the positive Y direction.

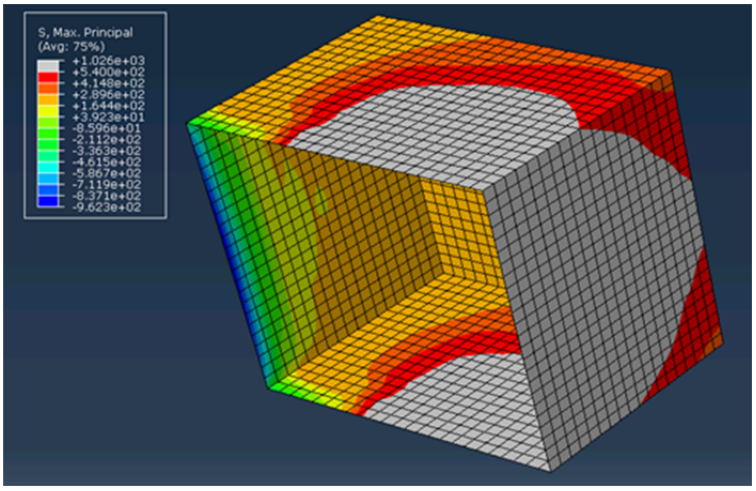

Figure 5.45 Crack Propagation (X and Z Direction) at Displacement of 1.76 Inches - Specimen IB-24-18

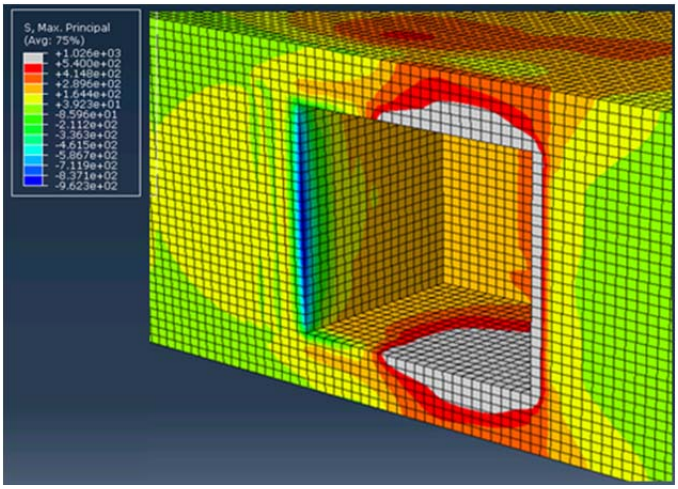

Figure 5.46 Crack Propagation (Y direction) at Displacement of 1.76 Inches - Specimen IB-24-18

5.8 Exterior specimen results

Similar methods to those used for the interior specimen models were also used for the exterior specimen models as described below.

5.8.1 Specimen EB-18-22

Global yield occurred at time step = 0.28, corresponding to a displacement of 0.35 inches and a moment equal to 1,125 kip-inches. Global yield was estimated using a 2% offset as shown in Figure 5.47.

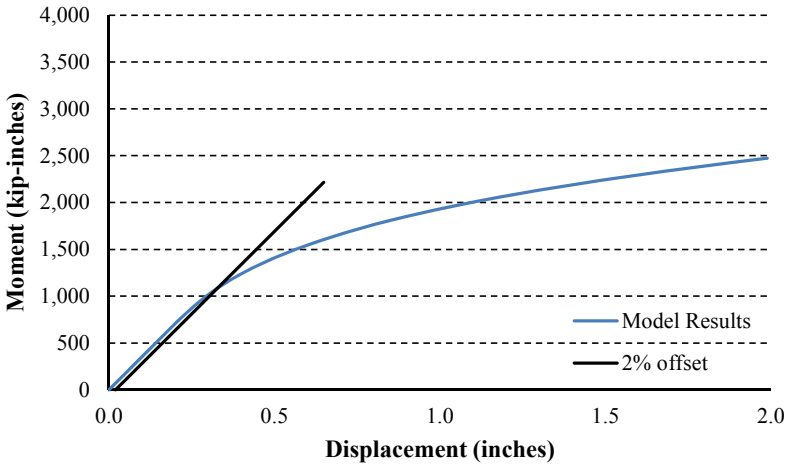

Figure 5.47 Moment versus Displacement - Specimen EB-18-22

Figure 5.48 shows the maximum principle stress of the elements at the interaction surface between the pile and the bent cap at the point of global yield. At the point of global yield local elements have cracked to a depth of four inches from the face of the bent cap.

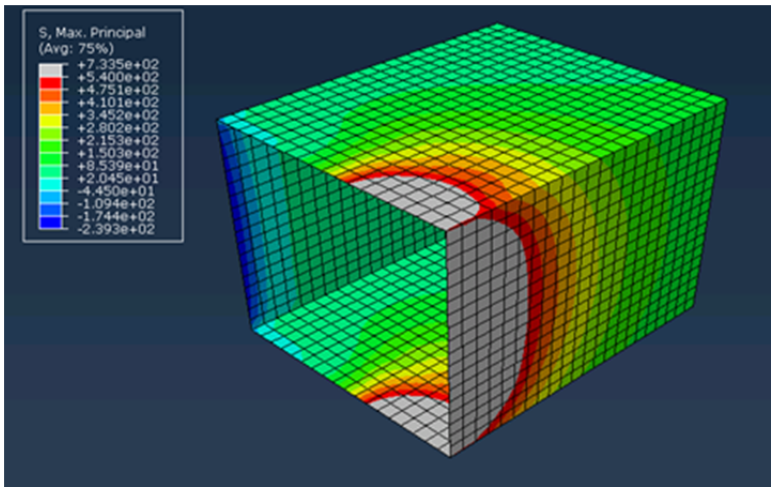

Figure 5.48 Maximum Principle Stress on the Bent Cap Surface at Global Yield - Specimen EB-18-22

The propagation of cracking in the Y direction at the point of global yield can be seen in Figure 5.49. The bent cap is cut to show the top face of elements with y = 1. Cracking in the Y direction exceeds one inch and is less than two inches.

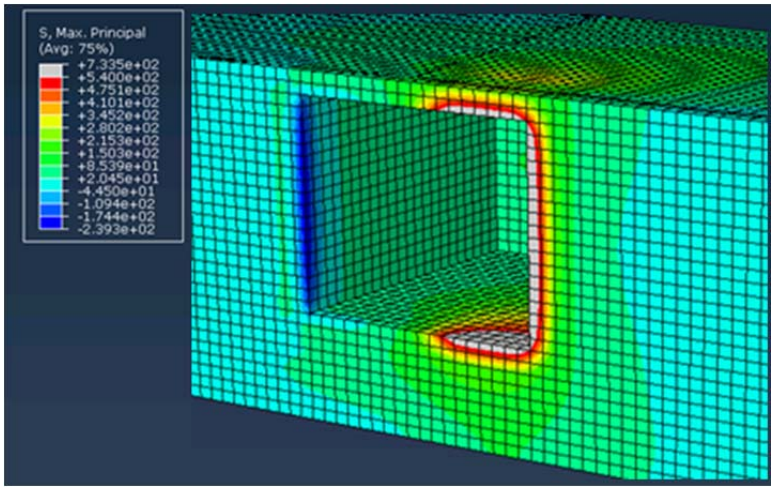

Figure 5.49 Maximum Principle Stress within the Bent Cap at Global Yield - Specimen EB-18-22

The point of crack initiation is shown in Figure 5.50. The initiation of cracking occurred at displacement of 0.14 inch (time step 0.12). First tensile cracking along the pile occurs at elements -1 and -2, corresponding to a moment of 490 kip-inches.

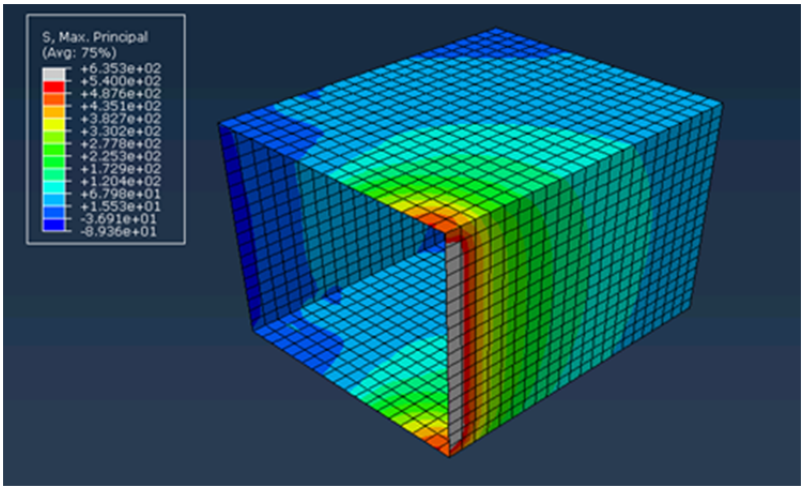

Figure 5.50 Crack Initiation - Specimen EB-18-22

Figure 5.56 shows the minimum principle stress versus displacement at element -18. The highest compressive stress is 4,100 psi, which is 63% of the maximum compressive stress.

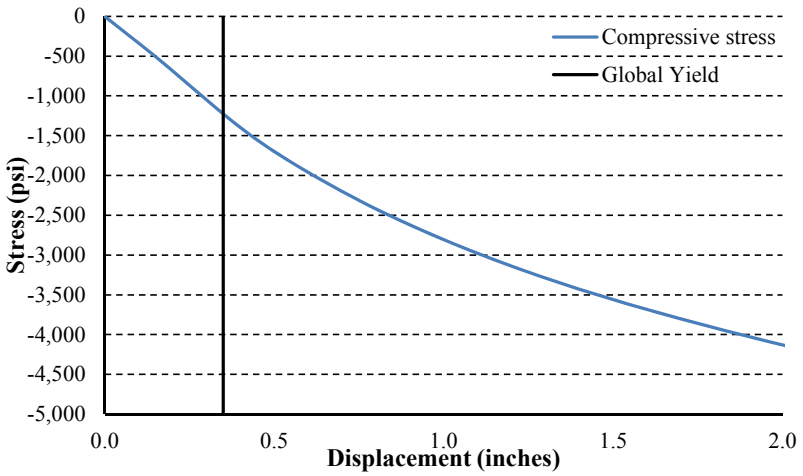

Figure 5.51 Minimum Principle Stress versus Displacement at Element (x = -18) - Specimen EB-18-22

Figure 5.52 shows the reinforcement cage at the global yield point. The stress is below 1,630 psi (Figure 5.53).

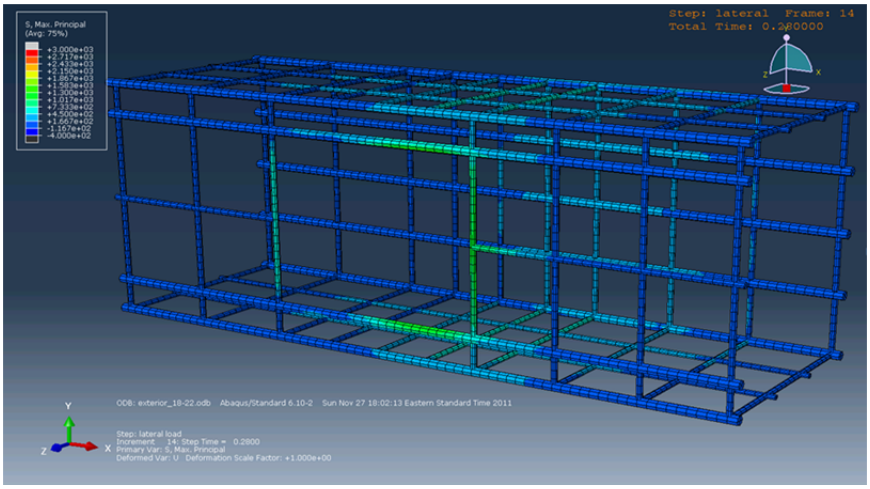

Figure 5.52 Maximum Principle Stress in Reinforcement Cage at Global Yield - Specimen EB-18-22

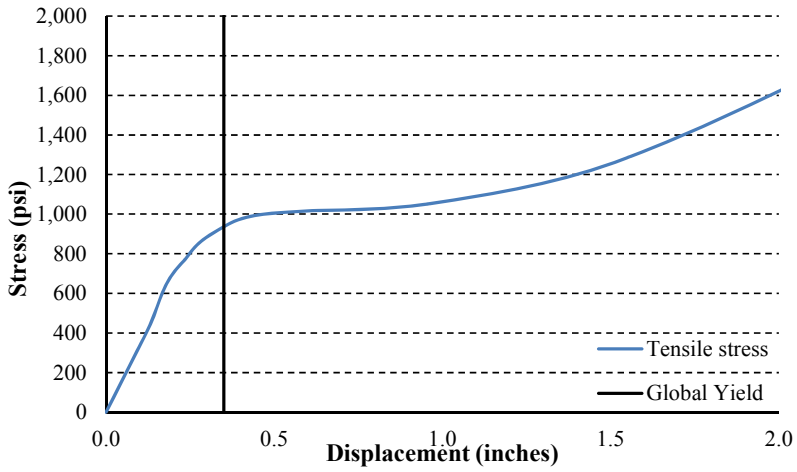

Figure 5.53 Maximum Reinforcement Stress versus Displacement - Specimen EB-18-22

Figure 5.54 and 5.55 indicate the depth to which tensile cracking occurs within the bent cap at the ultimate time step, corresponding to a displacement of two inches. Cracking at this time step penetrates the bent caps to distances of less than 13 inches in the negative X direction, 13 inches in the negative Z direction, and three inches in the positive Y direction.

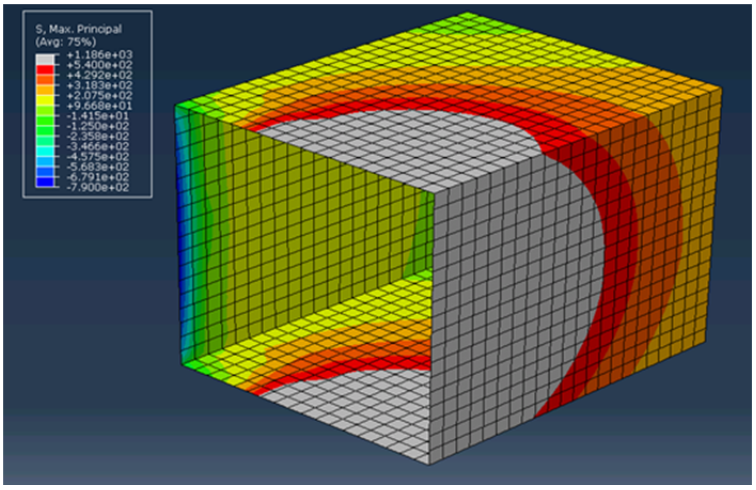

Figure 5.54 Crack Propagation (X and Z direction) at Displacement of 2 Inches - Specimen EB-18-22

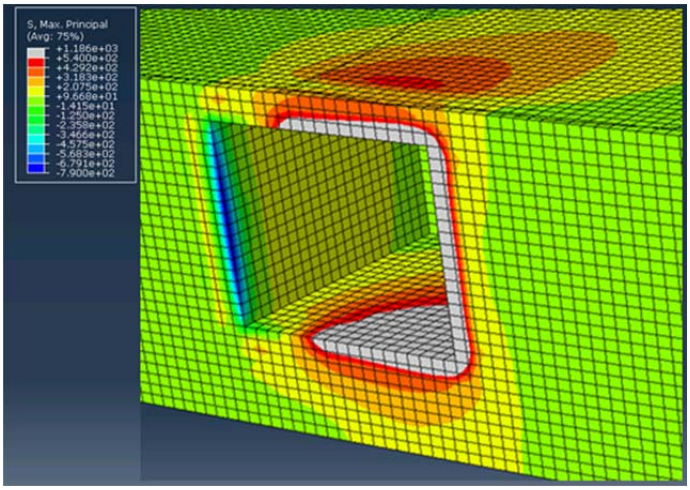

Figure 5.55 Crack Propagation (Y direction) at Displacement of 2 Inches - Specimen EB-18-22

5.8.2 Specimen EB-18-12

Global yield occurred at time step = 0.14, corresponding to a displacement of 0.33 inches and moment equal to 1,050 kip-inches. Global yield was estimated using a 2% offset as shown in Figure 5.56.

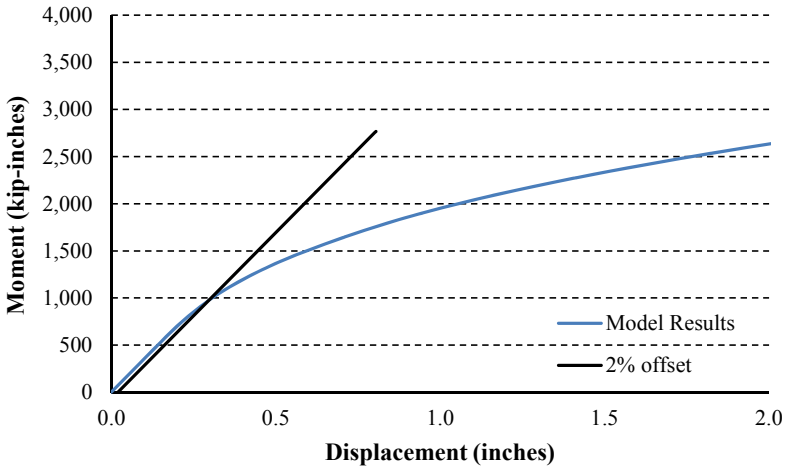

Figure 5.56 Moment versus Displacement - Specimen EB-18-12

Figure 5.57 shows the maximum principle stress of the elements at the interaction surface between the pile and the bent cap at the point of global yield. At the point of global yield local elements have cracked to a depth of four inches from the face of the bent cap.

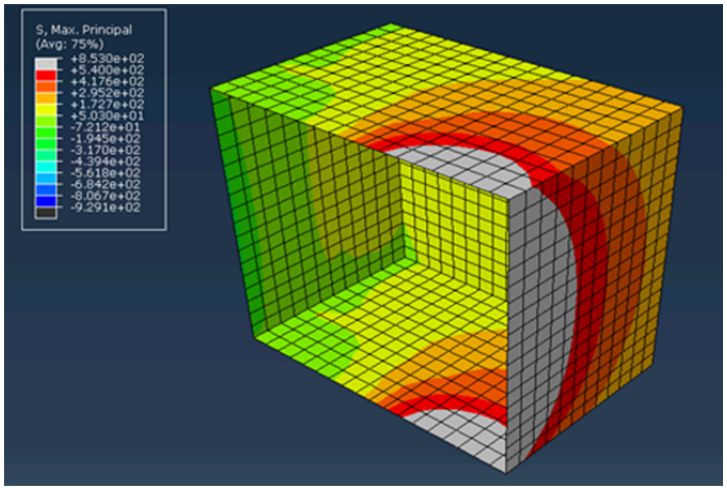

Figure 5.57 Maximum Principle Stress on the Bent Cap Surface at Global Yield - Specimen EB-18-12

The propagation of cracking in the Y direction at the point of global yield is shown in Figure 5.58. The bent-cap is cut to show the top face of elements with y = 1. Cracking in the Y direction exceeds one inch and is less than two inches.

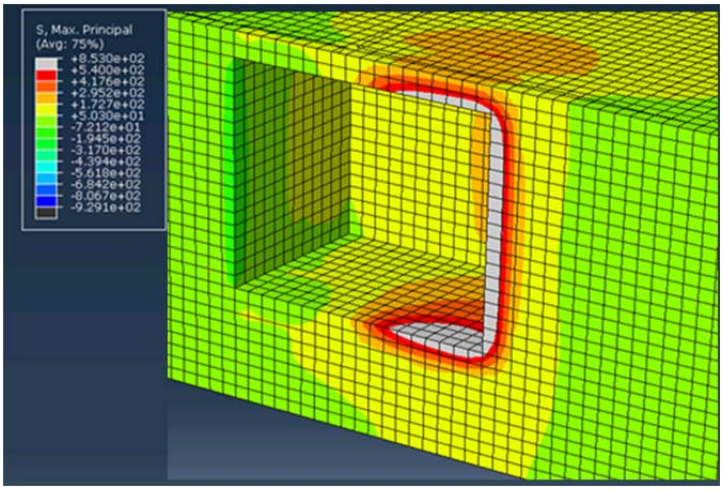

Figure 5.58 Maximum Principle Stress within the Bent Cap at Global Yield - Specimen EB-18-12

The initiation of cracking occurred at displacement of 0.13 inches (time step 0.06). First tensile cracking along the pile occurs at elements -1 and -2 at a moment of 455 kip-inches (Figure 5.59).

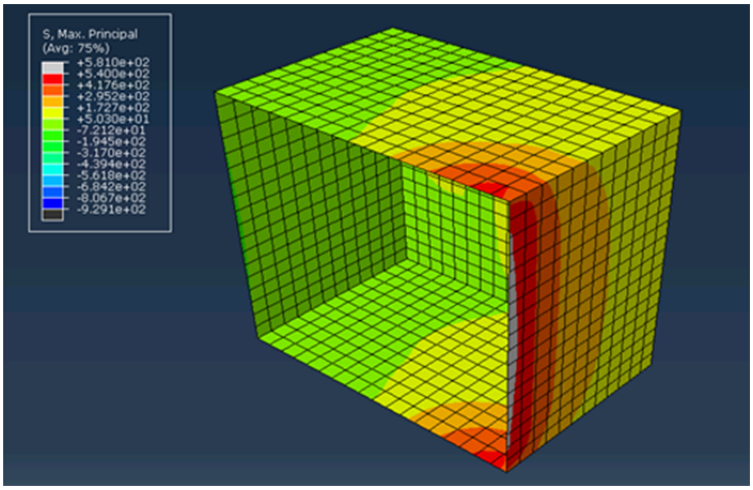

Figure 5.59 Crack Initiation - Specimen EB-18-12

Figure 5.60 shows the minimum principle stress versus displacement at element -18. The highest compressive stress is 4,335 psi, corresponding to 67% of the maximum compressive stress.

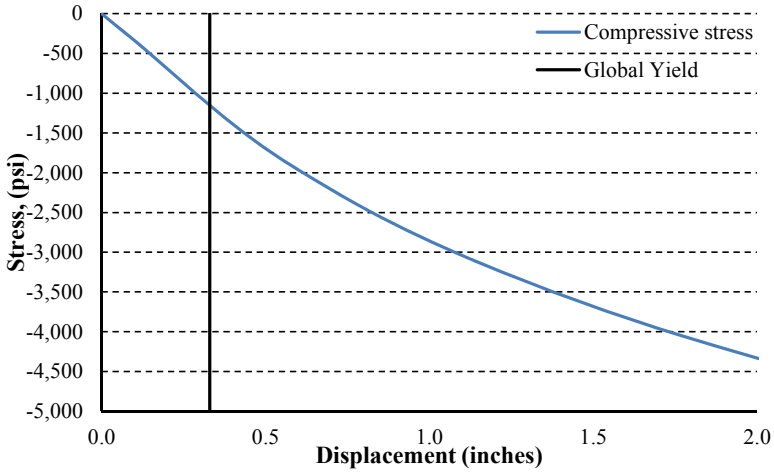

Figure 5.60 Minimum Principle Stress versus Displacement at Element (x = -18) - Specimen EB-18-12

Figure 5.61 shows the reinforcement cage at the global yield point. The maximum tensile stress in the reinforcement is below 2,765 psi (Figure 5.62).

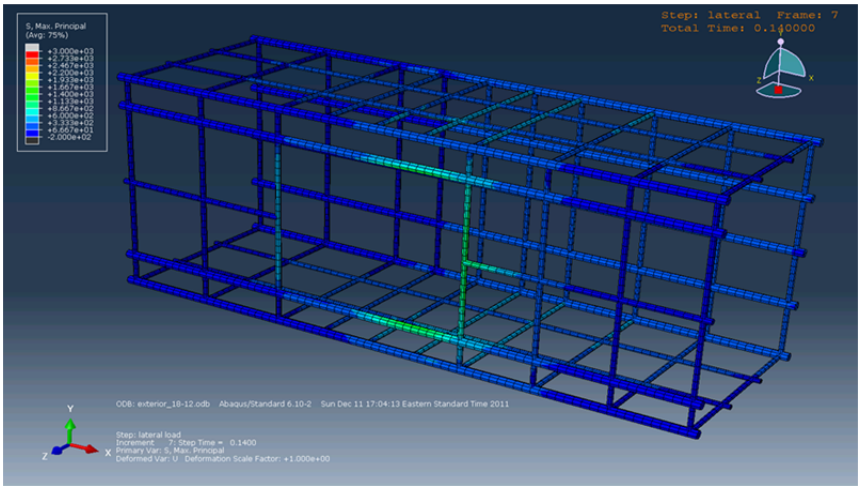

Figure 5.61 Maximum Principle Stress in Reinforcement Cage at Global Yield - Specimen EB-18-12

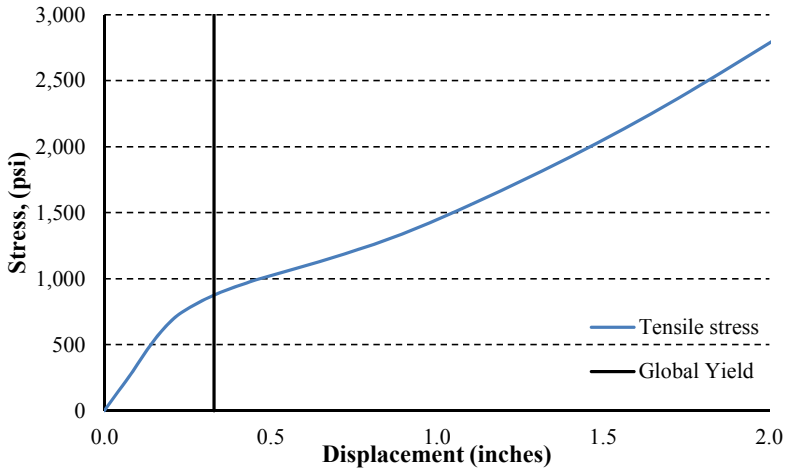

Figure 5.62 Maximum Reinforcement Stress versus Displacement - Specimen EB-18-12

Figures 5.63 and 5.74 indicate the depth to which tensile cracking occurs within the bent cap at the ultimate time step, corresponding to a displacement of 2.0 inches. The cracking at this time step penetrates the bent caps to distances of less than 13 inches in the negative X direction, 12 inches in the negative Z direction, and four inches in the positive Y direction.

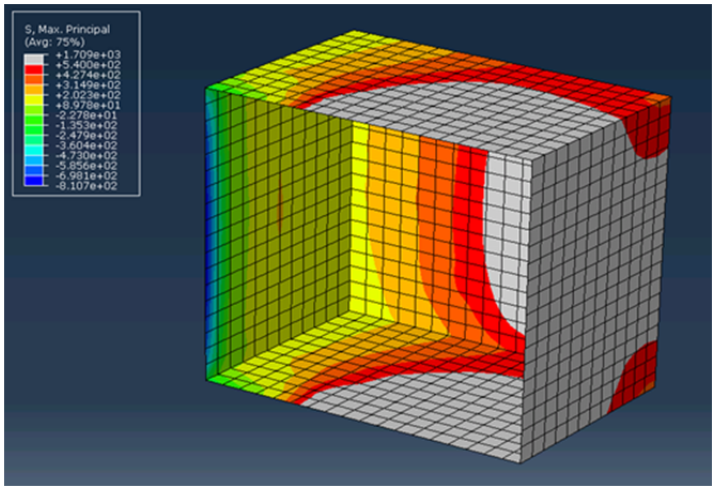

Figure 5.63 Crack Propagation (X and Z direction) at Displacement of 2 Inches - Specimen EB-18-12

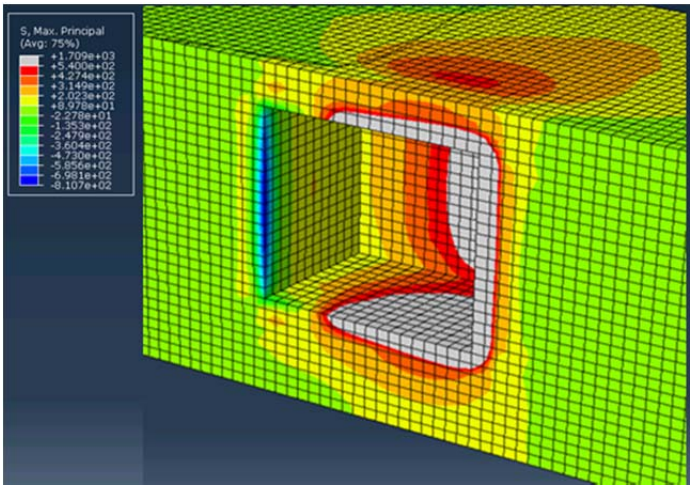

Figure 5.64 Crack Propagation (Y direction) at Displacement of 2 Inches - Specimen EB-18-12

35.8.3 Specimen EB-24-30

Global yield occurred at time step = 0.58, corresponding to a displacement of 0.28 inches and a moment equal to 2,515 kip-inches. Global yield was estimated using a 2% offset as shown in Figure 5.65.

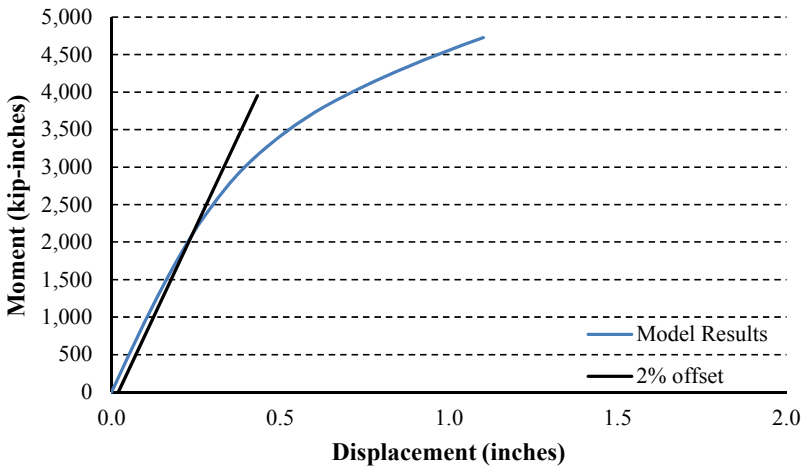

Figure 5.65 Moment versus Displacement - Specimen EB-24-30

Figure 5.66 shows the maximum principle stress of the elements at the interaction surface between the pile and the bent cap at the point of global yield. At the point of global yield local elements have cracked to a depth of 10 inches from the face of the bent cap.

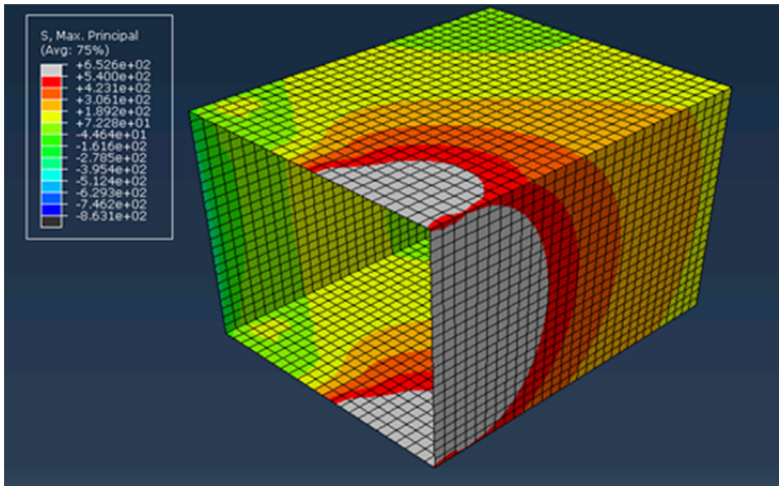

Figure 5.66 Maximum Principle Stress on the Cap Surface at Global Yield - Specimen EB-24-30

The propagation of cracking in the Y direction at the point of global yield is shown in Figure 5.67. The bent cap is cut to show the top face of elements with y = 2. Cracking in the Y direction is less than three inches.

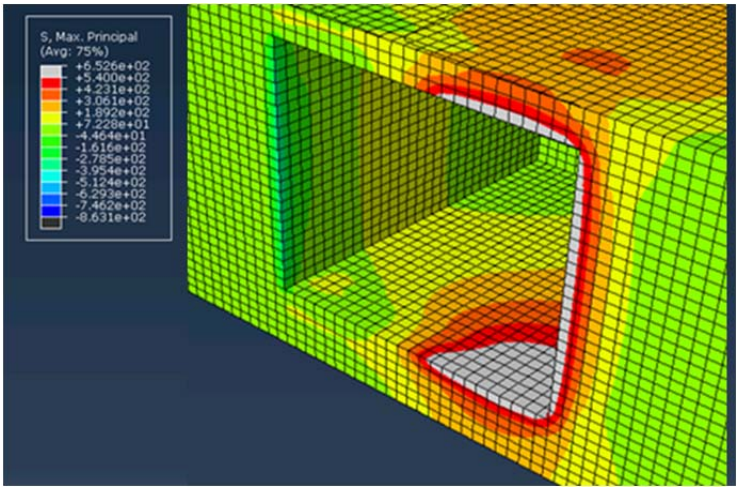

Figure 5.67 Maximum Principle Stress within the Cap at Global Yield - Specimen EB-24-30

The initiation of cracking occurred at displacement of 0.10 inches (time step 0.18). First tensile cracking along the pile occurs at element -1 and -2 at a moment of 910 kip-inches (Figure 5.68).

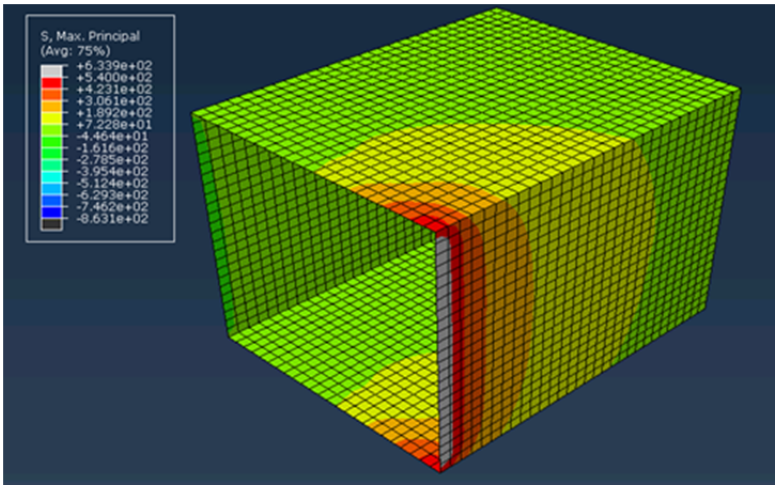

Figure 5.68 Crack Initiation - Specimen EB-24-30

Figure 5.69 shows the minimum principle stress versus displacement at element -24. The highest compressive stress is 3,920 psi, corresponding to 60% of the maximum compressive stress.

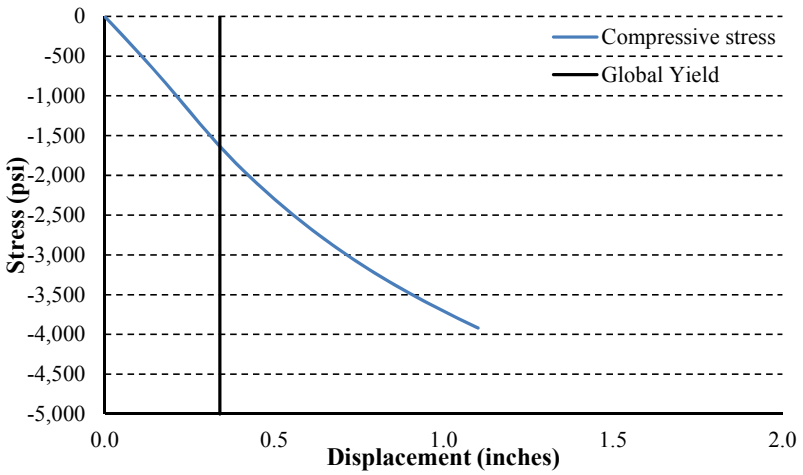

Figure 5.69 Minimum Principle Stress versus Displacement at Element (x = -24) - Specimen EB-24-30

Figure 5.70 shows the reinforcement cage at the global yield point. The level of stress in the reinforcement is below 1,250 psi (Figure 5.71).

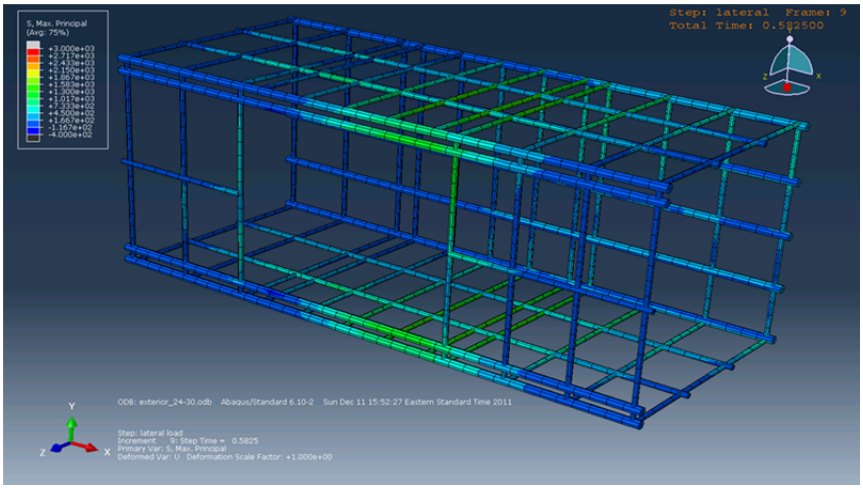

Figure 5.70 Maximum Principle Stress in Reinforcement Cage at Global Yield - Specimen EB-24-30

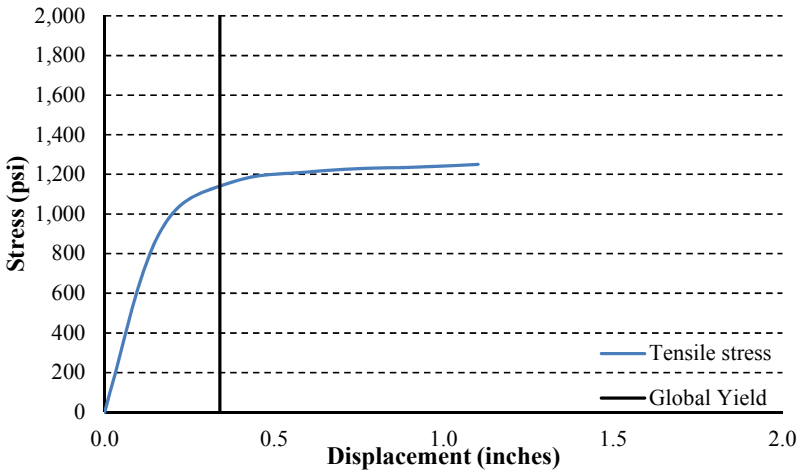

Figure 5.71 Maximum Reinforcement Stress versus Displacement - Specimen EB-24-30

Figures 5.72 and 5.73 indicate the depth to which tensile cracking occurs within the bent cap corresponding to a displacement of 1.10 inches. Cracking penetrates the bent caps to distances of less than 17 inches in the negative X direction, 19 inches in the negative Z direction, and five inches in the positive Y direction.

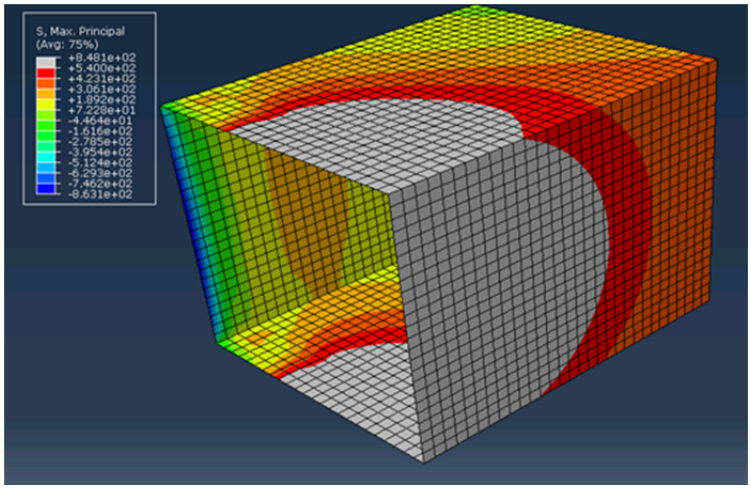

Figure 5.72 Crack Propagation (X and Z direction) at Displacement of 1.10 Inches - Specimen EB-24-30

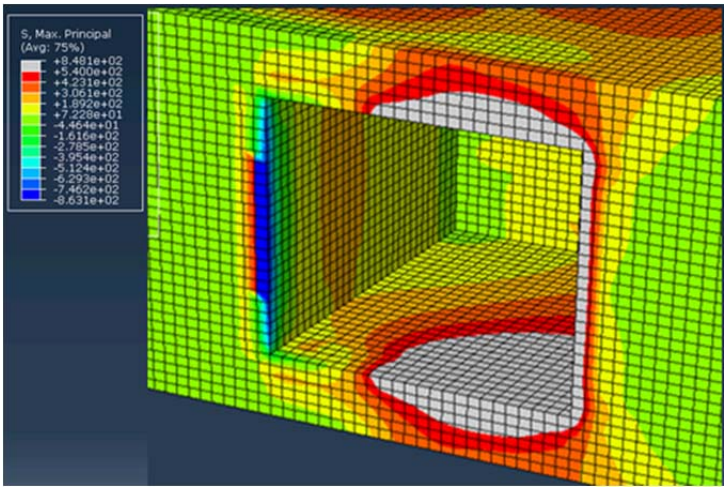

Figure 5.73 Crack Propagation (Y direction) at Displacement of 1.10 Inches - Specimen EB-24-30

5.8.4 Specimen EB-24-18

The global yield of the specimen occurred at time step = 0.28, corresponding to a displacement of 0.27 inches and a moment of 2,330 kip-inches. Global yield was estimated using a 2% offset as shown in Figure 5.74.

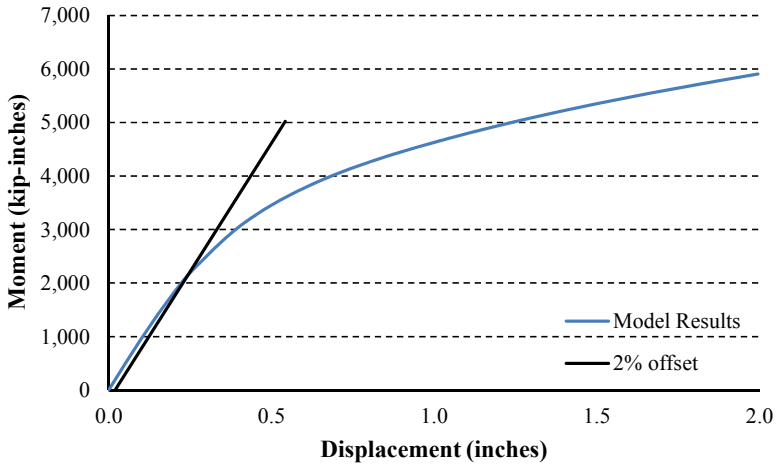

Figure 5.74 Moment versus Displacement - Specimen EB-24-18

Figure 5.75 shows the maximum principle stress of the elements at the interaction surface between the pile and the bent cap at the point of global yield. At the point of global yield local elements have cracked to a depth of seven inches from the face of the bent cap.

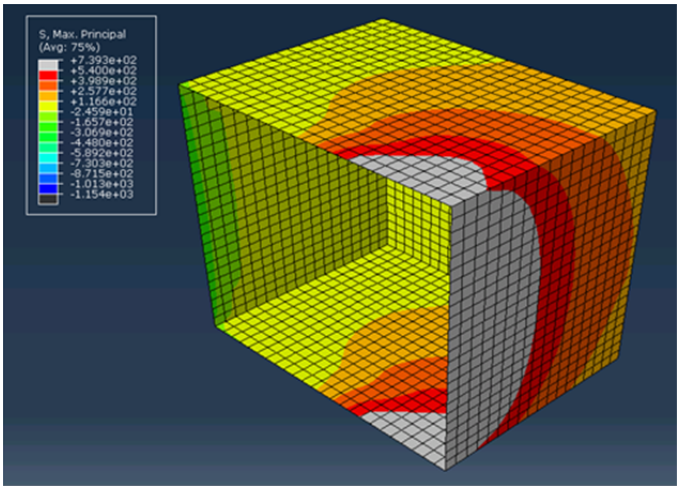

Figure 5.75 Maximum Principle Stress on the Bent Cap Surface at Global Yield - Specimen EB-24-18

The propagation of cracking in the Y direction at the point of global yield can be seen in Figure 5.76. The bent cap is cut to show the top face of elements with y = 1. Cracking in the Y direction is less than two inches.

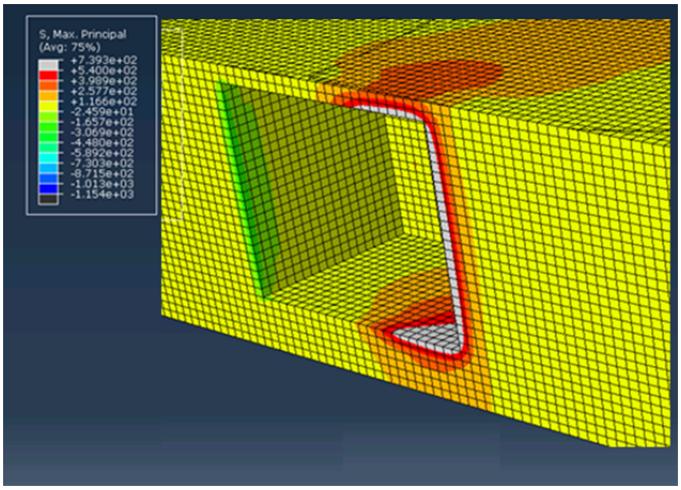

Figure 5.76 Maximum Principle Stress within the Bent Cap at Global Yield - Specimen EB-24-18

Crack initiation occurred at displacement of 0.10 inches (time step 0.11). First tensile cracking along the pile occurs at element -1 and -2 at a moment of 915 kip-inches (Figure 5.77).

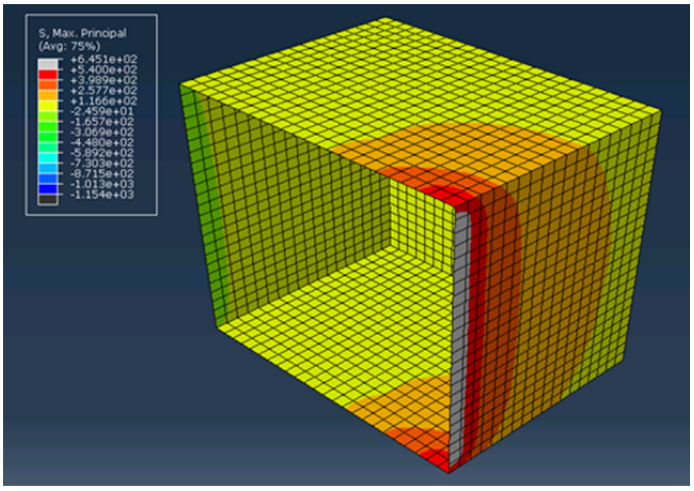

Figure 5.77 Crack Initiation - Specimen EB-24-18

Figure 5.78 shows the minimum principle stress versus displacement at element -24. The highest compressive stress at this element is 5,300 psi, corresponding to 81% of the maximum compressive stress.

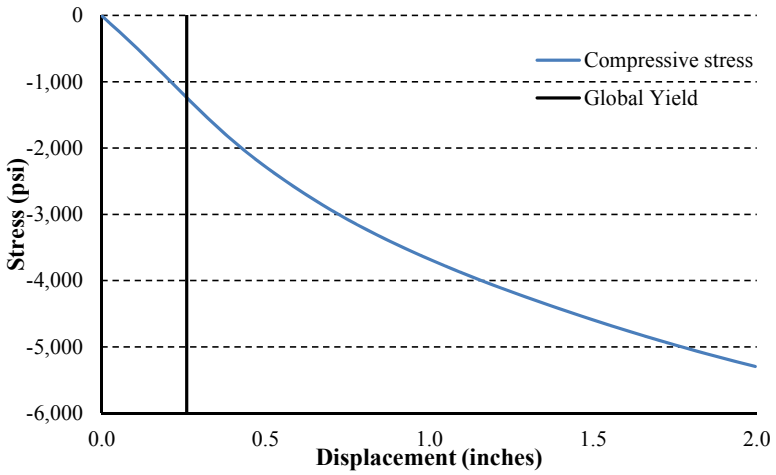

Figure 5.78 Minimum Principle Stress versus Displacement at Element (x = -24) - Specimen EB-24-18

Figure 5.79 shows the reinforcement cage at the global yield point. The maximum stress in the reinforcement is below 1,190 psi (Figure 5.80).

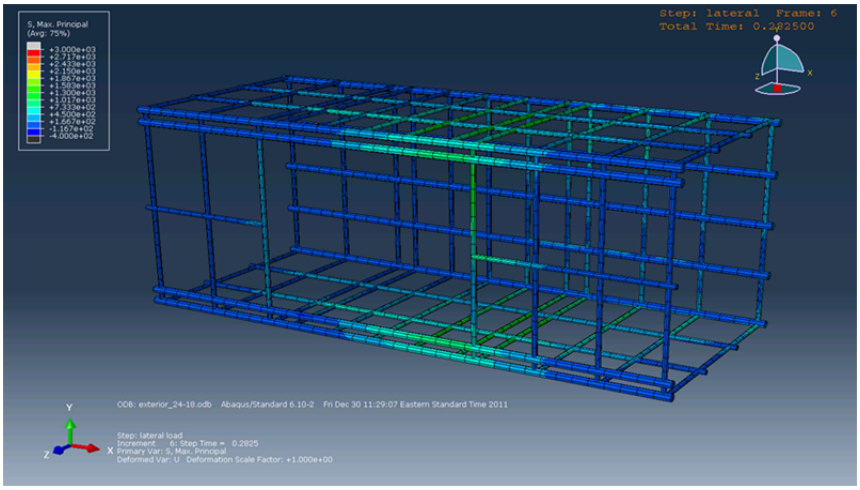

Figure 5.79 Maximum Principle Stress in Reinforcement Cage at Global Yield - Specimen EB-24-18

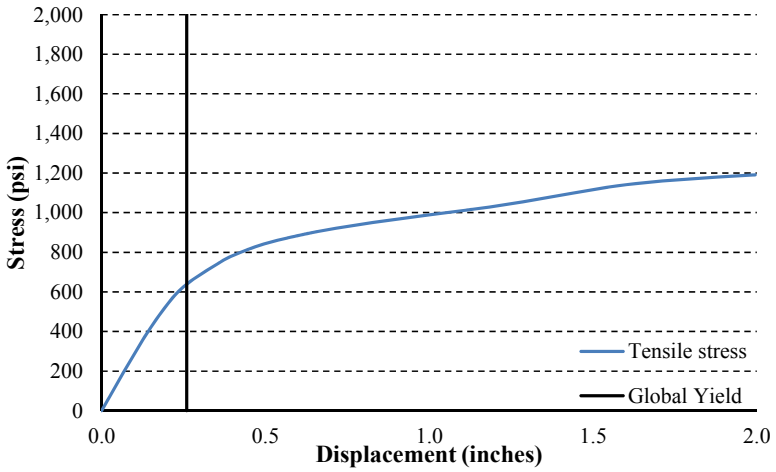

Figure 5.80 Maximum Reinforcement Stress versus Displacement - Specimen EB-24-18

Figures 5.81 and 5.82 indicate the depth to which tensile cracking occurs within the bent cap at a displacement of 2.0 inches. Cracking penetrates the bent cap to distances of 18 inches in the negative X direction, 18 inches in the negative Z direction, and six inches in the positive Y direction.

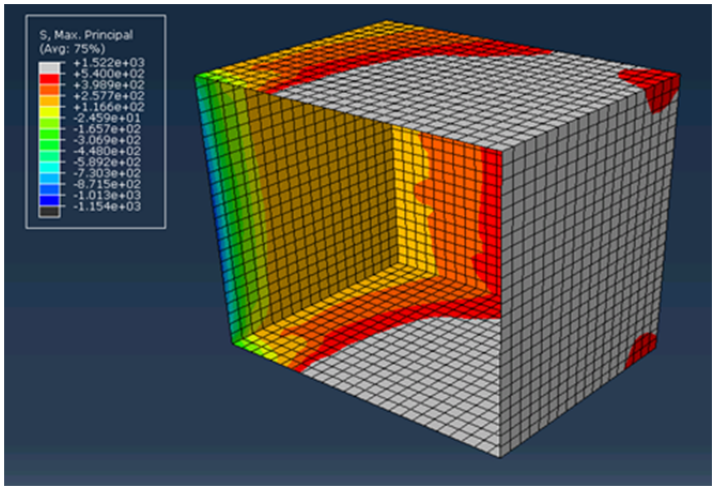

Figure 5.81 Crack Propagation (X and Z direction) at Displacement of 2 Inches - Specimen EB-24-18

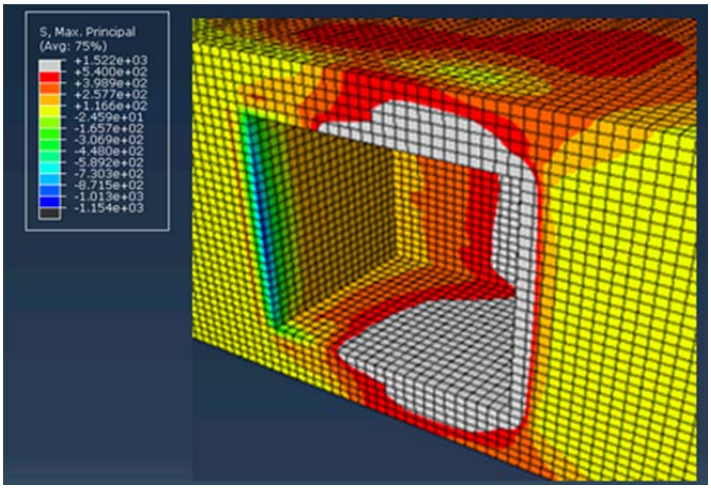

Figure 5.82 Crack Propagation (Y direction) at Displacement of 2 Inches - Specimen EB-24-18

5.9 Comparison of specimens

The following sections summarize the findings from the finite element modeling described above.

5.9.1 Interior Specimens

Table 5.3 summarizes the interior specimen results in terms of displacement and moment at crack initiation, global yield, and the ultimate model step. Piles with longer embedment depth, holding the diameter constant, achieved increased moment at the different stages. This is attributed to the fact that longer embedment depth leads to increased slipping stress, and consequently higher moment.

Table 5.3 Results - Interior Specimens

Pile Diameter (inches)	Embedment Depth (inches)	Crack initiation		Global yield		Ultimate model step	
		Displacement (inches)	Moment (kip-inches)	Displacement (inches)	Moment (kip-inches)	Displacement (inches)	Moment (kip-inches)
18	12	0.22	855	0.40	1,520	2.00	3,630
	22	0.22	945	046	1,865	2.00	3,820
24	18	0.13	1,725	0.40	4,795	1.73	9,440
	30	0.13	1,725	0.41	4,910	1.53	9,445

18 inch square piles: For the crack initiation stage, both embedment depths for the 18 inch square pile cracked at the same displacement while the moment for the 22 inch embedment specimen exceeded that of the 12 inch embedment specimen by 10%. This was not the case for global yielding as the specimen with 22 inch embedment yielded at a higher displacement and a higher moment than that of the 12 inch embedment specimen. The ratios between displacements and moments of IB-18-22 and IB-18-12 at global yield are 115% and 127%. At an ultimate displacement of two inches, IB-18-22 had a higher moment than that of IB-18-12 by 5%.

24 inch square piles: The crack initiation stage occurred at the same displacement and moment for both specimens. For global yield, IB-24-30 had a slightly higher displacement than IB-24-18. The moment at which yield occurred for specimen IB-24-30 is larger than that of IB-24-18 by 2%. At the ultimate model step, the moments achieved by both specimens were similar but the displacement at which the moment was achieved is higher in specimen IB-24-18 in comparison to IB-24-30 by 13%.

Comparison of pile sizes: As shown in Table 5.3, the moments achieved by the 24 inch square pile specimens are higher than those of the 18 inch square pile specimens at all stages, while displacements are less. Piles with larger cross-sectional area resulted in increased moment capacity but reduced ductility.

5.9.2 Exterior Specimens

Table 5.4 summarizes the exterior specimen results in terms of displacement and moment at crack initiation, global yield, and ultimate model step.

Table 5.4 Results - Exterior Specimens

Pile Diameter (inches)	Embedment Depth (inches)	Crack initiation		Global yield		Ultimate model step	
		Displacement (inches)	Moment (kip-inches)	Displacement (inches)	Moment (kip-inches)	Displacement (inches)	Moment (kip-inches)
18	12	0.13	455	0.33	1,050	2.00	2,625
	22	0.14	490	0.35	1,125	2.00	2,495
24	18	0.10	915	0.27	2,330	2.00	5,900
	30	0.10	910	0.28	2,515	1.10	4,725

18 inch square piles: The crack initiated at a slightly higher moment and displacement for the specimen with increased embedment. The trend was the same for global yielding as the specimen with 22 inch embedment yielded at a higher displacement and a higher moment in comparison to the specimen with 12 inch embedment. The ratios between displacements and moments for EB-18-22 and EB-18-12 at global yield are 106% and 107%.

24 inch square piles: Crack initiation occurred at the same displacement and moment for both specimens. For global yield, EB-24-30 had a slightly higher displacement than EB-24-18 with a ratio of 4%. The ratio between moments at which global yield occurred for specimens EB-24-30 and EB-24-18 is 108%. At a displacement of 1.10 inches both models achieved the same moment.

Comparison of pile sizes: Table 5.3 shows that the moments achieved by the 24 inch square pile are higher than those of the 18 inch square pile at crack initiation and global yield. Larger pile dimensions increase the moment capacity of the connection but reduce the ductility.

Chapter 6 - Interior Specimens

6.1 Introduction

This chapter presents test results of the four single pile specimens, which are representative of an interior portion of a typical South Carolina bent cap. The construction and testing methodology are described in previous chapters. Physical testing of the specimens began September 18, 2009 with specimen IB-18-1 and was concluded with specimen IB-22-1 on September 17, 2010. Specimen notation is repeated here for convenience. Interior specimens are described as IB-XX-X. IB is for Interior Bent, the first numbers following IB represent the pile embedment depth, and the final number is the specimen number (1st or 2nd specimen of this type). The results of specimen IB-18-1 are combined from the tests of two similar specimens. When results from these two specimens are presented individually the specimens are denoted IB-18-1.1 and IB-18-1.2.

6.2 Material performance

All piles were cast at Florence Concrete Products of Sumter, South Carolina. Two sets of piles were cast for the interior specimens. Strength required for form removal was achieved within the first 24 hours. The first set of piles used in the creation of specimens IB-18-1, IB-18-2 and IB-26-1 were cast on January 23, 2009. These piles reached average 28-day strength of 8,300 psi. The pile used for specimen IB-22-1 was cast on June 6, 2010, and reached 28-day strength of 7,200 psi. Piles were required to reach 28-day compressive strength of 5,000 psi.

Bent caps for each specimen were cast-in-place in the structures laboratory at the University of South Carolina. Caps for each specimen were cast individually at separate times over the span of the project. Table 6.1 details the date on which the bent caps of each specimen were cast in addition to the test date for each specimen.

Table 6.1 Specimen Casting and Testing Dates

Exterior Specimens			
Specimen	**Cast Date**	**Test Date**	**Time Difference (Days)**
IB-18-1.1	2/16/2009	3/31/2009	43
IB-18-1.2	5/21/2009	6/4/2010	14
IB-18-2	12/4/2009	4/19/10	136
IB-22-1	7/30/2010	9/17/2010	49
IB-26-1	10/19/2009	1/29/10	102

Concrete material tests were performed for all elements used to construct the test specimens. Tests were conducted for the determination of compressive strength, split tensile strength, and elastic modulus. Compressive testing was performed at 7, 14, 28, and 56 days after casting. Split tensile strength and elastic modulus testing was conducted at 28 and 56 days after casting. Table

6.2 details the results of material testing. Testing was not conducted on each pile but rather as a group.

Following the completion of testing, core samples were taken from the specimens. These were taken both from the pile and bent cap elements. Cores were taken with four inch diameter and were cut to a length of eight inches. The cores were used for evaluation of in-situ compressive strength near the time of testing (Table 6.2).

Table 6.2 Material Testing Results by Specimen

		Cylinder	Piles (1)	Piles (2)	IB-18-1.1	IB-18-1.2	IB-18-2	IB-26-1	IB-22-1
Compressive Strength, f'c (psi)	3 Day	Avg.	5,500	-	-	-	-	-	-
	7 Day	1	-	-	4,300	4,100	4,000	3,500	3,200
		2	-	-	4,300	4,200	3,600	3,700	3,600
		3	-	-	-	-	4,100	3,300	3,300
		Avg.	-	-	4,300	4,150	3,900	3,500	3,400
	14 Day	1	-	-	5,100	5,600	4,500	3,100	-
		2	-	-	4,500	5,200	4,500	4,000	-
		3	-	-	-	-	-	3,700	-
		Avg.	-	-	4,800	5,400	4,500	3,600	-
	28 Day	1	8,200	7,300	5,500	5,800	4,200	3,800	-
		2	8,400	7,300	5,500	5,600	5,200	4,800	-
		3	-	7,200	-	-	5,300	4,600	-
		Avg.	8,300	7,266	5,500	5,700	4,900	4,400	-
	56 Day	1	-	7,700	6,200	-	5,800	5,700	4,800
		2	-	8,700	6,600	-	5,700	5,700	5,800
		3	-	8,300	-	-	6,100	6,100	6,000
		Avg.	-	8,200	6,400	-	5,900	5,800	5,500
	Core Sample	Pile	-	-	-	-	10,900	6,300	9,400
		Cap 1	-	-	-	-	7,700	7,000	6,700
		Cap 2	-	-	-	-	7,200	6,200	5,500
Elastic Modulus, E (ksi)	Day:		60			28	28	28	
		1	2,700	-	-	2,020	3,200	2,500	-
		2	2,700	-	-	2,040	3,000	3,100	-
		3	3,100	-	-	2,200	-	-	-
		Avg.	2,830	-	-	2,090	3,100	2,800	

The pile of specimen IB-22-1 was fit with two Geokon model 4200 vibrating wire strain gages prior to casting. A photo of the placement of these gages is shown in a previous chapter. These

gages were installed into the pile at a distance of 11 inches from the embedded end, corresponding to the midpoint of the pile embedment. One gage was parallel to the displacement of the pile while the other was perpendicular.

These gages were used to calculate stresses resulting from shrinkage of the bent cap. With cast-in-place construction bent cap shrinkage results in a confining stress on the pile. The magnitude of this stress was calculated based on the gage strain readings (Table 6.3). This confining stress results in improved bond between prestressing strands and surrounding concrete, allowing pile embedment depths to be less than required for full development of prestressing strands as described in ACI 318-08 (ElBatanouny et al., 2012).

Table 6.3 Vibrating Wire Strain Gage Measurements

	Gage 1		Gage 2	
	Strain (10^{-6})	**Stress (psi)**	**Strain (10^{-6})**	**Stress (psi)**
Following Pile Casting	2,871	-	2,900	-
Prior to Testing	2,721	-	2,720	-
Difference	150	-727	180	-872
Avg. Stress (psi)	-800			

6.3 Moment curvature modeling

Moment-curvature models were created for each of the four interior specimens using XTRACT. Measured material properties were used as material property inputs. The material models were used as described by section six of the SCDOT SDS. These material models included both confined and unconfined concrete as well as prestressing and passive reinforcement. The Mander model as described in section 6.6.4 and 6.6.5 of the SCDOT SDS was used to model the confined concrete portion of the piles.

Piles were modeled with two separate numerical models. The first of these models was created by setting the maximum stress in the prestressing strands equal to the ultimate strand capacity. With the use of this maximum stress, the modeled output was that of a pile which is fully developed. The second model was created by limiting the maximum stress in prestressing strands to that of a calculated slipping stress. This stress was calculated with an equation developed to calculate the development length of prestressing strands in confined sections. The determination of slipping stress in prestressing strands is a function of the pile embedment length as well as the time between the casting of the bent cap and loading of the specimen (ElBatanouny et al., 2012). The output of the second model is the expected moment versus displacement behavior of each specimen. Table 6.4 details the maximum stress available to the prestressing strands in each model.

Table 6.4 Specimen Slipping Stresses

Specimen	Embedment depth (inches)	Experimental results		Slip Equation	
		Max. Moment (kip-inches)	Slipping stress* (ksi)	Max. Moment (kip-inches)	Slipping stress (ksi)
IB-18-1	18	2,350	185	2.320	184
IB-18-2	18	2,090	160	2,230	184
IB-22-1	22	2,950	270	2,400	196
IB-26-1	26	2,770	270	2,620	220

** = Experimental slipping stress was determined through the observation of maximum moment achieved.*

6.4 Specimen results

The results of the four interior specimens are presented in terms of the following parameters:

- General information
- Moment capacity
- Ductility capacity and percent drift
- Development of a plastic hinging mechanism
- Joint shear stress and cap performance

Several figures are presented displaying the behavior of each specimen.

Figure 6.1 details the method by which stresses in the joint region were calculated.

$$v_{jh} = \frac{M_p}{h_b D_c b_{je}} \quad (8\text{-}20)^{1}$$

v_{jh} : Average joint shear stress (ksi)
M_p : Maximum moment achieved (k-in)
h_b : Depth of the cap (in)
D_c : Maximum cross sectional dimension of pile (in)
b_{je} : Effective joint width (in)

Allowable Principal tensile stress (ksi)

$$P_t \leq 0.379\sqrt{f_c'} \quad (8\text{-}23)^{1}$$

Allowable Principal compressive stress (ksi)

$$P_c \leq 0.25\, f_c' \quad (8\text{-}24)$$

$$P_c, P_t = \frac{f_h+f_v}{2} \pm \sqrt{\left(\frac{f_h+f_v}{2}\right)^2+{v_{jh}}^2} \quad (8\text{-}16,8\text{-}17)^{1}$$

P_c: Principal compressive stress (ksi)
P_c: Principal tensile stress (ksi)
f_h: Average axial horizontal stress (ksi)
f_v: Average axial vertical stress (ksi)

$$f_v = \frac{P_{col}}{b_{je}(h_b+D_c)} \quad (8\text{-}21)^{1}$$

$$f_h = \frac{P_b}{b_b h_b} \quad (8\text{-}22)^{1}$$

$$b_{je} = D_c + h_c \quad (8\text{-}19)^{1}$$

b_b : Width of column (in)
h_c : Width of column (in)

[1] :SCDOT Seismic Design Specifications for Highway Bridges Version 2.0

Figure 6.1 Joint Stress Calculation Methodology

6.5 Specimen IB-18-1

General information

Specimen IB-18-1 was tested over a period of days beginning on September 18, 2009, 42 days after casting of the bent cap. The loading protocol differed slightly from that of the remaining interior specimens and is described in preceding chapters.

Hysteretic behavior and moment capacity

The hysteretic behavior is shown in Figures 6.2 through 6.4. Displacements correspond to pile displacements measured at a distance of 156 inches from the face of the connection between the pile and bent cap. Moment is calculated as the force applied to the pile multiplied by the application distance of 146 inches. Due to the nature of the experimental setup as described in Chapter 4, P-delta effects are not considered in the calculation of moment. Figure 6.2 shows the moment versus displacement behavior of this specimen. The results of the moment curvature models are also plotted. The solid line in Figure 6.2 represents results from the moment curvature model assuming that the full capacity of the pile is achieved. The dashed line is plotted from the results assuming that prestressing strands will slip at a given level of stress based on curing time and embedment length (see Table 6.4).

From Figure 6.2 it can be seen that specimen IB-18-1 reaches a maximum moment of approximately 2,350 kip-inches in the positive direction at a displacement of 2.8 inches. The maximum moment achieved in the negative direction is 2,330 kip-inches, also at a displacement of 2.8 inches. The ultimate moment capacity of the specimen is taken as the average of these two values. Thus specimen IB-18-1 achieved an ultimate moment capacity of 2,340 kip-inches at a displacement of approximately 2.8 inches.

Figure 6.2 provides a means of comparison between the desired behavior of the specimen and that gathered experimentally. The experimental results do not reach predicted values when strand slipping is not considered. Thus the specimen was not able to develop the full capacity of the pile. When slipping is considered, the predicted results correspond to the experimental results.

Figures 6.3 and 6.4 elaborate upon the experimental behavior. Figure 6.3 shows a load versus displacement plot from the test of this specimen. In this plot, load is applied laterally from the hydraulic actuator (or rams). Similar to Figure 6.2, displacement is taken as the measured value at 156 inches from the soffit. The specimen reached maximum applied lateral loads of approximately 16 kips in both the positive and negative directions. Figure 6.4 shows the moment versus rotation behavior of this specimen. In this plot rotation is calculated as the inverse tangent of displacement at 156 inches divided by the distance of 156 inches.

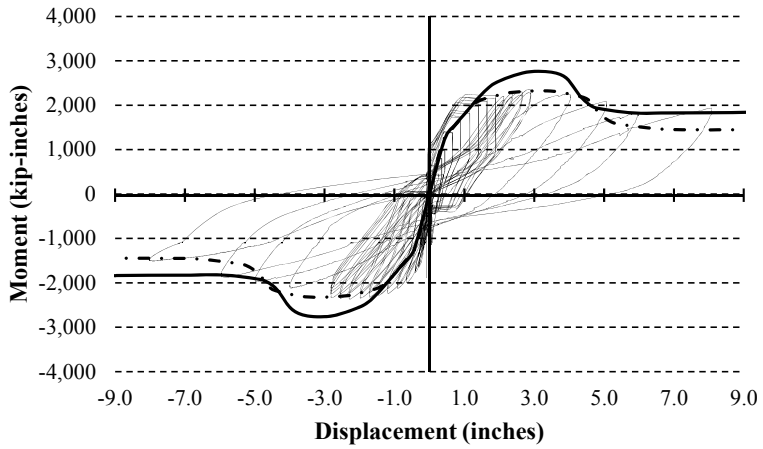

Figure 6.2 Moment versus Displacement - Specimen IB-18-1

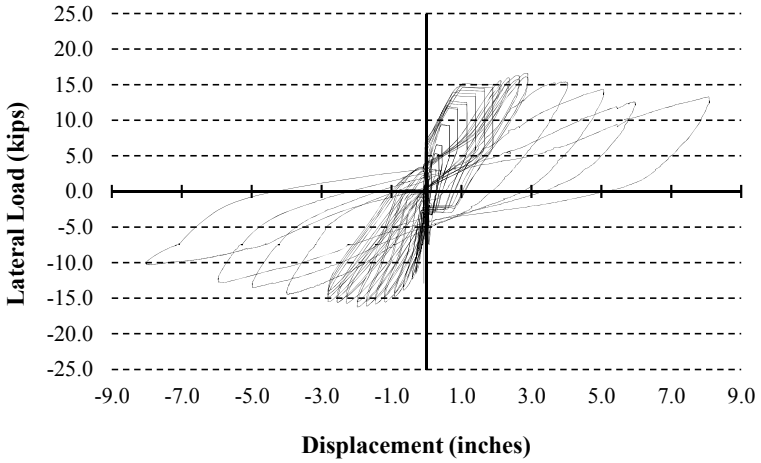

Figure 6.3 Lateral Force versus Displacement - Specimen IB-18-1

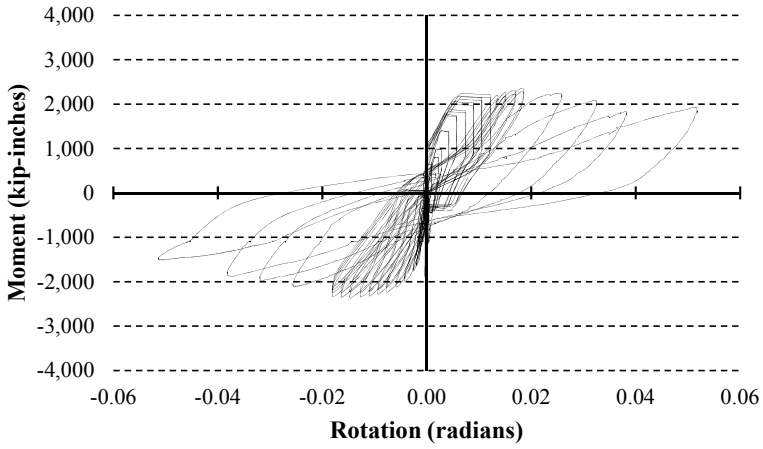

Figure 6.4 Moment versus Rotation - Specimen IB-18-1

Ductility capacity and % drift

Figure 6.5 shows the moment versus displacement results of specimen IB-18-1. This figure details aspects of the specimen behavior which relate to the percent drift and ductility capacity of the specimen. Ductility is identified as the axis labeled μ_c. Percent drift is an axis plotted above the experimental behavior and labeled Θ_r. The black outlined circles on the plot are the points at which the specimen is considered to yield in the positive and negative directions. The point at which the specimen yields is defined as the point at which the behavior of the specimen deviates from linearity. This is determined both graphically as well as calculated using the elastic portion of the response. A positive displacement is considered to be upward. The black circles on the plot represent the point at which the specimen reaches what is considered its displacement capacity. Displacement capacity is determined as the displacement corresponding to the point at which the moment capacity of the specimen degrades below 80 percent of its ultimate value. This value is based on convention and considered to be conservative.

The ductility capacity of the specimen may be calculated using the black outlined and black points shown in Figure 6.5. Ductility is calculated as the displacement capacity (inches) divided by the yield displacement (inches) and described in Equation 6.1.

$$\mu_c = \frac{\Delta_c}{\Delta_y} \qquad \text{(Eqn. 6.1)}$$

As seen from the black outlined circles in Figure 6.5, this specimen is determined to yield at 0.4 inches in both the positive and negative directions. The black circles are shown to correspond to displacements of approximately 5.9 inches in either the positive or negative directions. During this displacement cycle the maximum moment achieved is reduced to 80 percent of the ultimate moment. Using these values, the displacement ductility is calculated as 14.8. Per the SCDOT SDS, specimens should achieve a displacement ductility capacity of at least 3.0. Specimen IB-18-1 therefore exceeds this desired displacement ductility capacity.

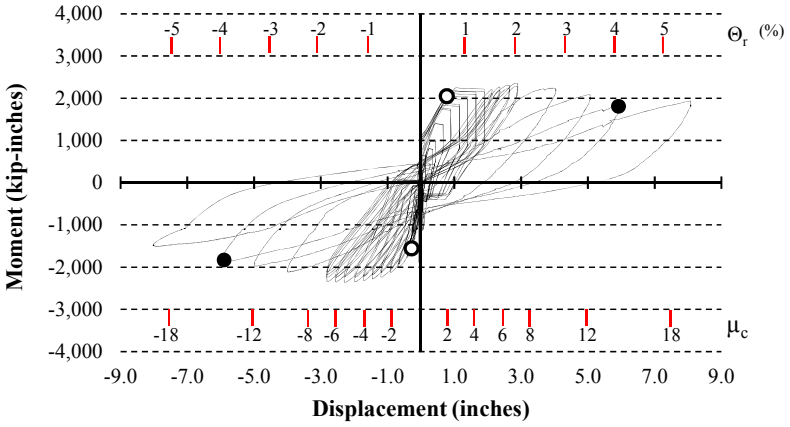

Figure 6.5 Displacement Ductility - Specimen IB-18-1

Plastic hinge mechanism and cracking pattern

The connection between piles and bent caps are designed such that damage as a result of a seismic event is limited to the pile. During such an event bent caps should remain elastic. With a plain embedment, damage in the pile should be distributed along the length of the pile away from and below the soffit. The pile should develop a plastic hinge in this region as a means to dissipate the energy resulting from a seismic event. To aid in design the SCDOT defines a plastic hinge length that should develop in the pile (Equation 6.2).

$$L_p = 0.08*L \geq D^* \qquad \text{(Eqn. 6.2)}$$

In Equation 6.2, L is given as the length of the pile between the soffit and the point of contra-flexure (inches). With the test setup used this length is 146 inches. D* is given as the pile diameter, or cross sectional dimension. In this case, the dimension D* is equal to the pile cross sectional dimension of 18 inches which governs the minimum plastic hinge length. The experimentally determined plastic hinge length is estimated based on the energy dissipation as determined through the curvature gages combined with the cracking pattern along the length of the pile.

The cracking pattern is shown in Figure 6.6. Cracking extends along the length of the pile to a distance of 30 inches from the soffit. Figure 6.7 shows photographs of damage in the pile throughout testing. From these photographs, it can be seen that a large crack developed about the perimeter of the pile at the interface between the pile and bent cap.

Figure 6.8 shows four plots of moment versus curvature along the length of the pile. The primary method of energy dissipation in the pile is through the development of large cracks extending approximately three inches outside of the interface. Based on these cracks and the data shown in Figure 6.8 a plastic hinge length of 15 inches is estimated for this specimen.

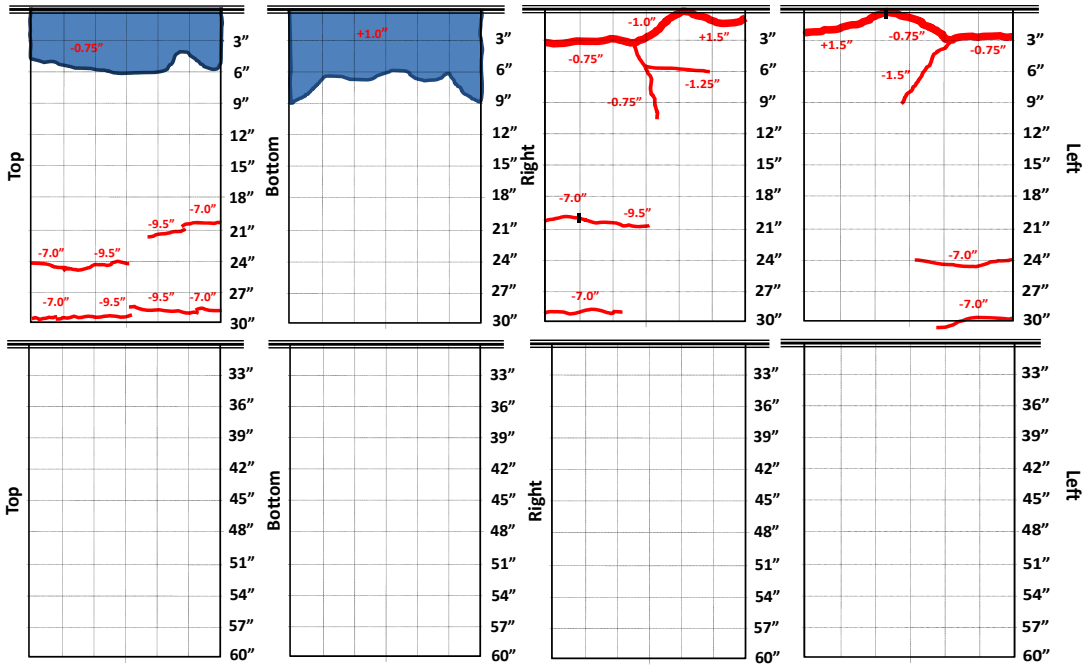

Figure 6.6 Crack Locations - Specimen IB-18-1

Figure 6.7 Damage Locations - Specimen IB-18-1

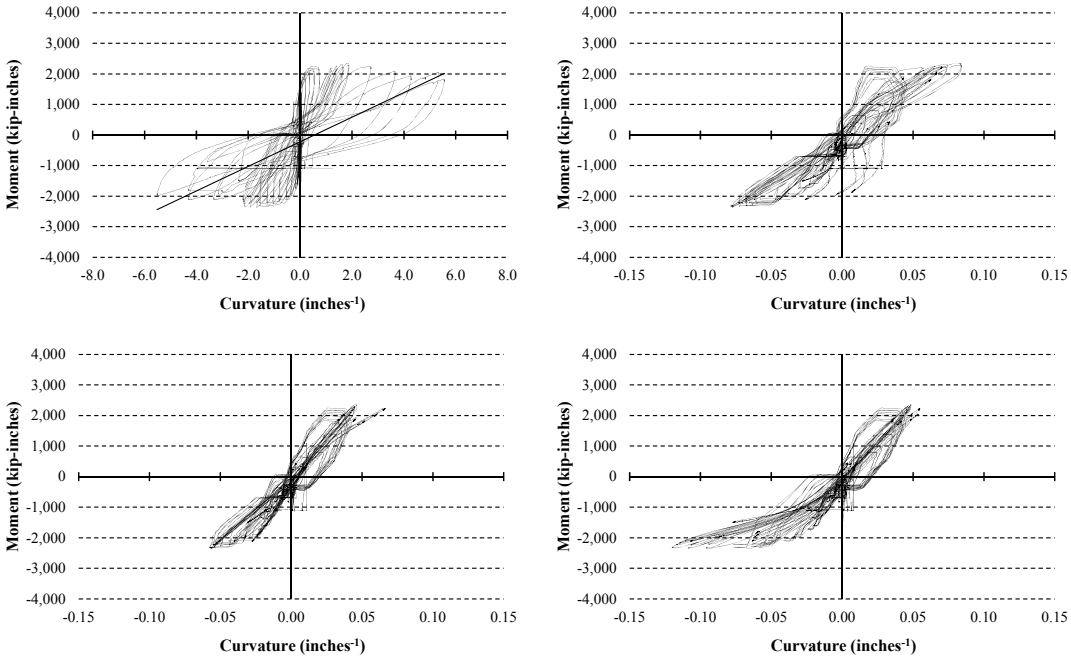

Figure 6.8 Moment versus Curvature - Specimen IB-18-1

Joint shear stress, cap performance, and additional damage observations

Figure 6.9 shows a photograph of the soffit region following testing. Spalling occurred about the perimeter of the pile embedment location. The majority of the test was completed without observation of spalling. Spalling about the soffit began to occur at displacements of ±5.0 inches corresponding to the displacement capacity of the specimen.

With the exception of spalling at later stages of testing, the bent cap did not exhibit any signs of cracking throughout the application of the testing protocol. This leads to the observation that tensile and shear stresses within the bent cap at the joint region were held to low levels through the test.

Joint shear stresses within the bent cap were calculated according to Section 8.7 of the SCDOT SDS (Table 6.5). In addition to the calculation of stresses this table also provides the allowable stresses in the element, and maximum principle stresses in the joint region. From Table 6.5 it is clear that the calculated values are within the tolerances provided by the SCDOT.

Figure 6.9 Joint Region Following Test Completion - Specimen IB-18-1

6.6 Specimen IB-18-2

General information

Specimen IB-18-2 was cast on December 4, 2009. The test of the specimen was conducted 113 days following the casting date, using the hydraulic actuator as opposed to the hydraulic ram/actuator combination used for specimen IB-18-1. The specimen was constructed with a pile from the first pile set. The concrete used in construction of the bent cap reached a compressive strength of 5,900 psi at 56 days. The 18 inch embedment used in the construction of this specimen represents the SCDOT recommended embedment depth.

Hysteretic behavior and moment capacity

The hysteretic behavior is shown in Figures 6.10 through 6.12. As with specimen IB-18-1 this behavior is presented with plots of moment versus displacement, lateral force versus displacement and moment versus rotation. Moment is again calculated by multiplying the lateral load as given by the hydraulic actuator by the distance at which the load was applied, 146 inches from the soffit. Displacement is taken from the measured displacement at 156 inches from the soffit and rotation is again found by the arctangent of displacement at 156 inches divided by the distance to the measured point of 156 inches. Figure 6.10 also presents the performance of the specimen as compared to the two moment curvature models. The results of the two models are shown with black lines. The full pile capacity model is given as a solid black line and the model based on strand slipping is shown as a dashed line.

From Figure 6.10, it can be seen that the specimen achieves maximum values of moment of 2,100 kip-inches and 2,050 kip-inches in the positive and negative directions, respectively. These maximum moments correspond to values of displacement of 1.7 inches in the positive direction and 1.0 inch in the negative direction. The moment capacity of the specimen is given as the average of these moment and displacement values. Thus the moment capacity of the specimen is 2,075 kip-inches with a corresponding displacement of 1.35 inches

From Figure 6.10, the specimen performance is compared with the predicted results. The numerical model which accounts for strand slipping, given by the dashed line, corresponds to the specimen behavior. Similar to specimen IB-18-1, specimen IB-18-2 does not develop the full capacity of the pile. This is seen by the gap between the first model in Figure 6.10 and the experimental results. With the close representation given by the second numerical model it is concluded that the prestressing strands within the piles did slip, resulting in the behavior shown.

Figure 6.11 provides behavior in terms of lateral load versus displacement. This plot shows levels of lateral force applied to the specimen reaching maximum values near 14.5 kips. These values of maximum load correspond to the displacements found at the points of maximum moment previously described. Figure 6.12 shows behavior in terms of moment versus rotation.

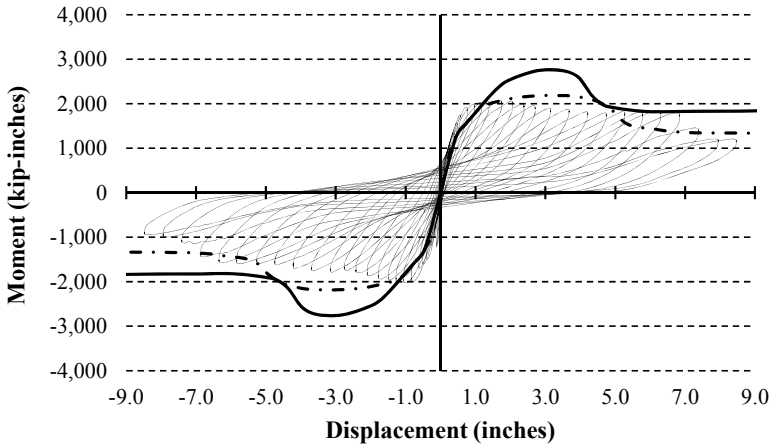

Figure 6.10 Moment versus Displacement - Specimen IB-18-2

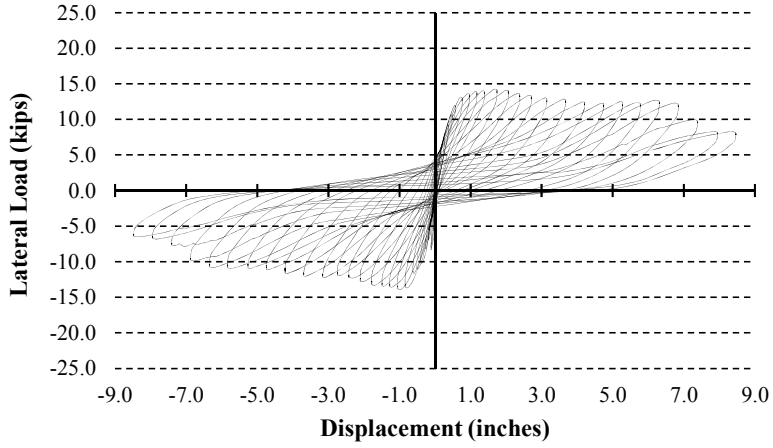

Figure 6.11 Lateral Force versus Displacement - Specimen IB-18-2

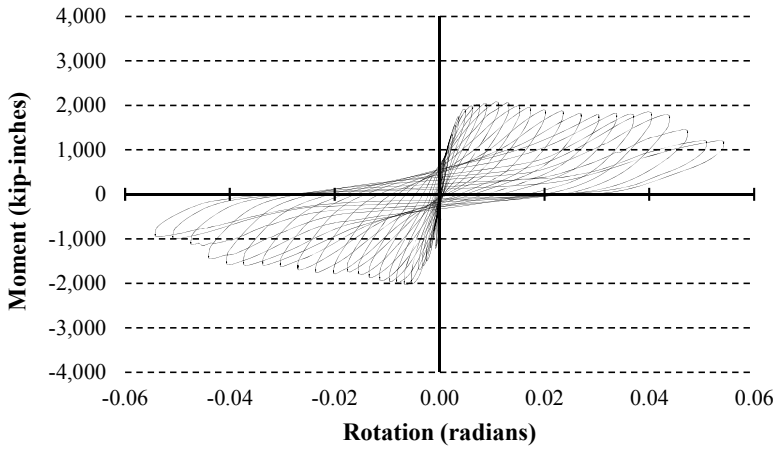

Figure 6.12 Moment versus Rotation - Specimen IB-18-2

Ductility capacity and % drift

In Figure 6.13, the results of the numerical models are removed from the plot and points corresponding to yield displacement and displacement capacity are inserted. The point at which the specimen is determined to yield is given by a black outlined circle and the displacement capacity is given with a black circle. The plot also shows displacement ductility and percent drift.

Figure 6.13 shows the specimen to have reached a point of yielding at a displacement of 0.53 inches in the positive direction corresponding to a yield moment of 1,720 kip-inches. In the negative direction, yielding occurred at a displacement of 0.56 inches with a moment value of 1,680 kip-inches. Values of displacement capacity were found to be 7.4 inches in the positive direction and 5.4 inches in the negative direction. Using these values, ductility capacity is calculated in each direction. Displacement ductility capacities are calculated as 14.0 and 10.0 in the positive and negative directions, respectively. Thus an average ductility capacity for the specimen is determined to be 12.0.

The specimen exceeds the values set by the SCDOT SDS. Further, the minimum displacement ductility capacity of 10.0 exceeds the value of 8.0 corresponding to an operational classification of 2 (SCDOT). As seen from the plots detailing the hysteretic behavior, degradation of the specimen was minimal through a wide range of displacements.

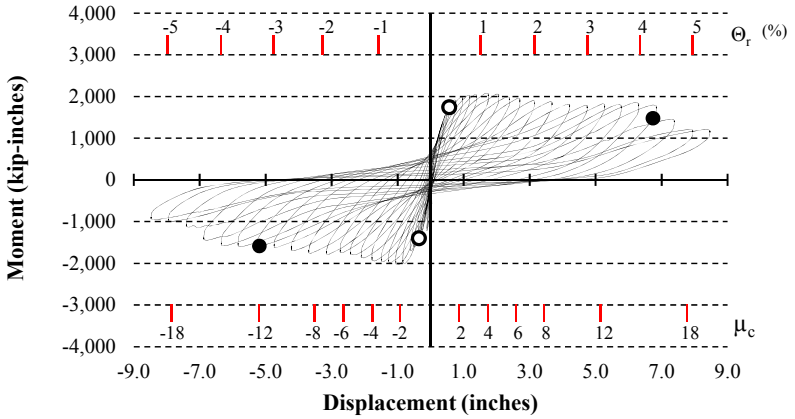

Figure 6.13 Displacement Ductility - Specimen IB-18-2

Plastic hinge mechanism and cracking pattern

The cracking pattern of this specimen is shown in Figure 6.14. Cracks are observed to have occurred to a distance of 36 inches from the face of the connection. Large cracks developed near the interface between the pile and bent cap, and these cracks dissipate the majority of the energy. However; unlike specimen IB-18-1, cracking in this specimen is seen to extend further along the length of the pile. Damage to the pile is also shown in the photographs of Figure 6.15. The extent of this damage along the length of the pile is used in conjunction with moment curvature data to estimate the length of the plastic hinge.

The moment curvature data is shown in Figure 6.16. This data is gathered from linear potentiometers placed in series along the length of the pile within the plastic hinge zone. From the plots in Figure 6.16 energy dissipation can be clearly seen through the first two points of measured curvature, seen through the areas under the hysteretic loops given in each of the plots. A reduction of this dissipation is seen in points of measurement three and four.

Using both the cracking pattern diagram of Figure 6.14 and the plots detailing the moment curvature behavior of the pile, the plastic hinge length is estimated to be 15 inches.

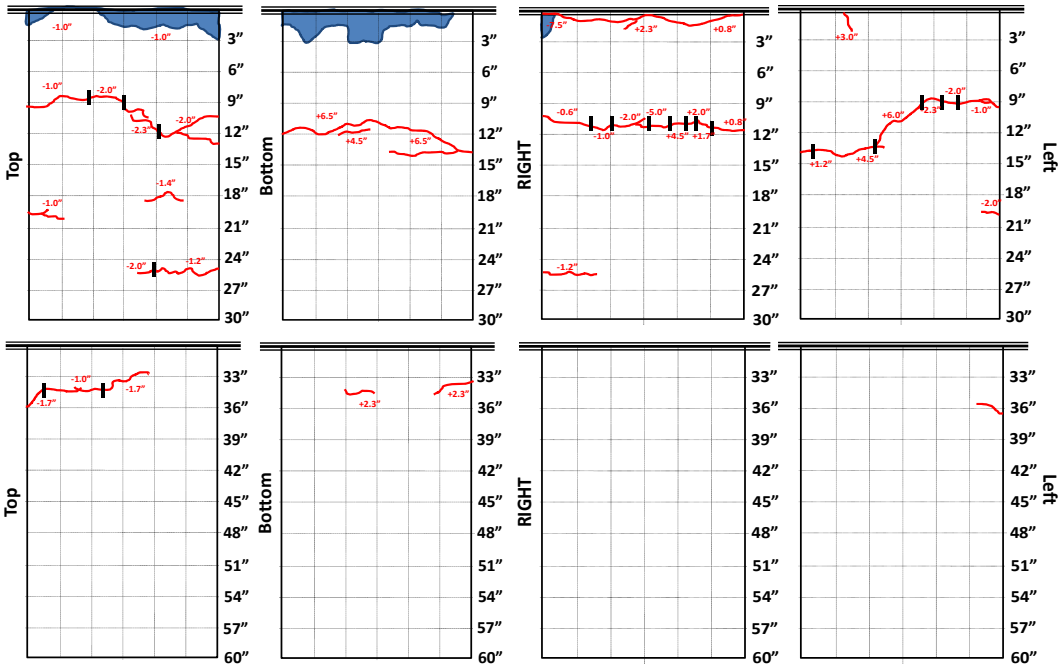

Figure 6.14 Crack Locations - Specimen IB-18-2

Figure 6.15 Damage Locations - Specimen IB-18-2

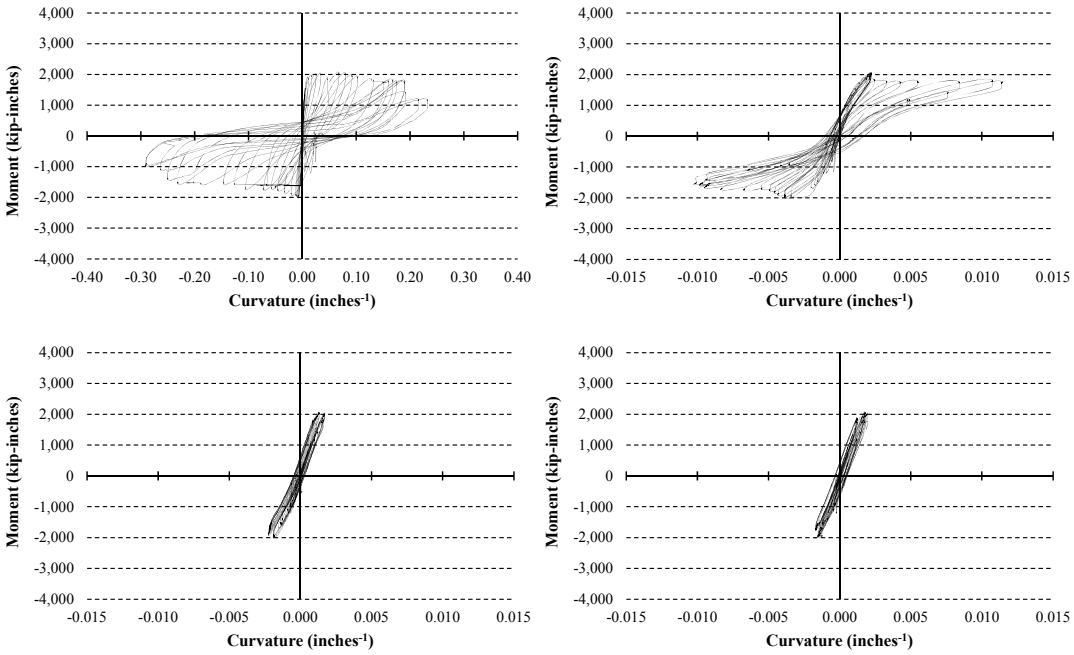

Figure 6.16 Moment versus Curvature - Specimen IB-18-2

Joint shear stress, cap performance, and additional damage observations

Minimization of damage to the bent cap is desirable. Figure 6.17 shows the bent cap of specimen IB-18-2 following testing of the specimen. This figure shows spalling to have occurred in the bent cap along the top surface of the connection to the pile. Similar to specimen IB-18-1, the spalling observed in this specimen occurred during the later stages of the test. In addition to the spalling, a single crack was observed to occur in the bent cap. This crack is shown in Figure 6.17, though at the time of this photo spalling occurred at the origin of the crack. Cracking in the bent cap was observed following the displacement cycle of ±2.5 inches. The crack extended outward from the top corner of the connection to approximately five inches. Additional cracking in the bent cap was not observed.

Stresses in the joint region were calculated using the methodology presented in Figure 6.1. The results of these calculations are shown in Table 6.5. All stresses calculated in this region were well below the allowable stresses set by the SCDOT SDS.

Figure 6.18 shows plots of the measured strain within the bent cap at two locations. Each bent cap element was instrumented with five uniaxial strain gages placed onto longitudinal reinforcement. Figure 3.3 details the location of each of these gages. During the casting of this specimen one of these gages was damaged. The results of the two gages in which the greatest strain values were recorded are presented in Figure 6.18. The data were recorded by the gages at positions one and four presented on the left and right respectively. Values of moment versus time are plotted in each graph for reference. From these plots a maximum value of strain is seen from strain gage 1, located on the longitudinal No. 9 reinforcing bar closest to the connection. The maximum value of strain recorded by these gages reached 85 micro-strain, corresponding to four percent of the yield stress.

Figure 6.17 Joint Region Following Test Completion - Specimen IB-18-2

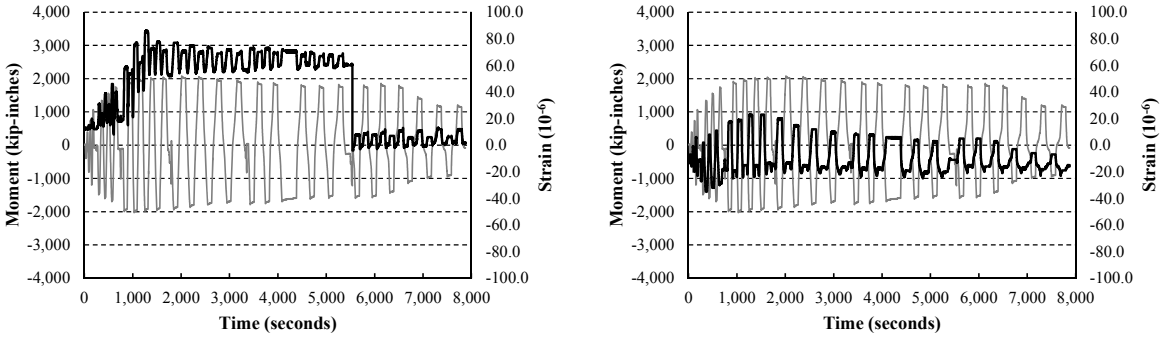

Figure 6.18 Bent Cap Strain - Specimen IB-18-2

6.7 Specimen IB-26-1

General information

Specimen IB-26-1 was created with the deepest pile embedment of the four interior specimens. This specimen was tested beginning on February 9, 2010, corresponding to 136 days following casting of the bent cap. The specimen was created with a pile from the first pile set. The bent cap reached a compressive strength of 5,800 psi at 56 days. The 26 inch embedment depth used was employed to test a maximum embedment. The embedment depth is 1.44 times the current embedment depth recommended by the SCDOT and is two inches greater than the upper end of the tolerance allowed by the same recommendation.

Hysteretic behavior and moment capacity

Figures 6.19 through 6.21 detail the hysteretic behavior presented in the same fashion as specimens IB-18-1 and IB-18-2. The three plots include moment versus displacement results in Figure 6.19, lateral force versus displacement in Figure 6.20, and moment versus rotation in

Figure 6.21. Figure 6.19 includes the results of the two moment curvature models. The results of these models are plotted using a solid and a dashed black line for the full capacity and strand slipping models, respectively.

The maximum moments achieved are shown in Figure 6.19. These moments were approximately 2,780 kip-inches in the positive direction and 2,640 kip-inches in the negative direction. In the positive direction the maximum moment was reached at a displacement of 3.5 inches. The maximum moment in the negative direction was reached at a displacement of 3.0 inches. Averaging the two values, a specimen moment capacity of 2,710 kip-inches is calculated.

In Figure 6.19 a drastic decline in moment capacity is evident during the displacement cycle of 7.0 inches. This decline is the result of a sudden rupture of a prestressing wire (or wires) within a strand. The effect of this rupture is clear through the remaining displacement cycles in the test.

Also of note in Figure 6.19 is the comparison between experimental results and the results from the two moment curvature models. In the positive direction the specimen is seen to behave similar to that predicted by the model based on the full development of the pile. In the negative direction the behavior is slightly less than that of this model, though this may be explained by the damage occurring to the pile during the positive displacements of the loading cycle. In all loading cycles conducted with the hydraulic actuator positive displacements are conducted prior to negative displacements. Given the behavior of the specimen it can be said that the 26 inch embedment of this specimen coupled with the time between the casting and testing date resulted in the specimen developing the full pile capacity.

Figures 6.20 and 6.21 also detail the hysteretic behavior of the specimen and are presented in terms of lateral load versus displacement and moment versus rotation, respectively. From Figure 6.20 displaying the lateral load versus displacement of this specimen, it may be seen that the specimen reaches levels of applied lateral load of approximately 19 and 18 kips in the positive and negative directions respectively. The rupture during the loading cycle of +7.0 inches is evident in these plots.

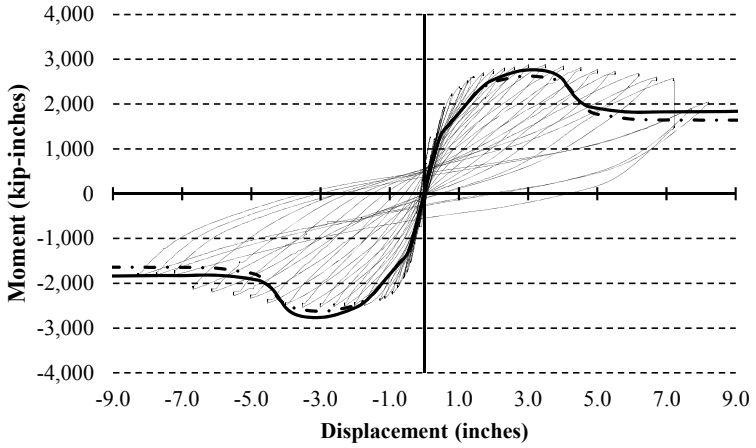

Figure 6.19 Moment versus Displacement - Specimen IB-26-1

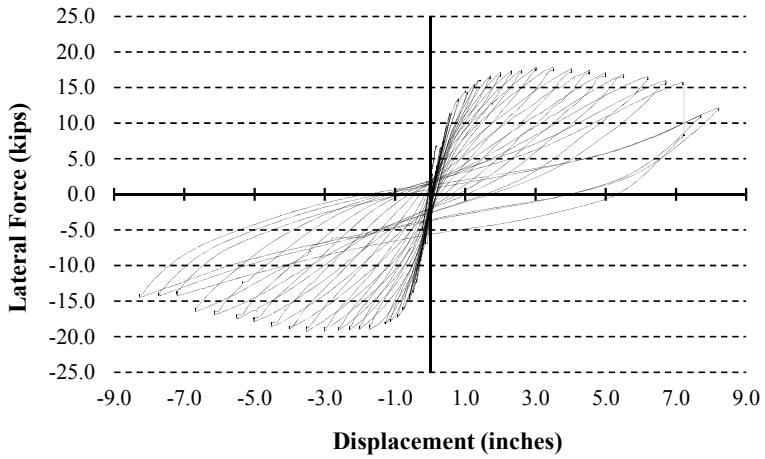

Figure 6.20 Lateral Force versus Displacement - Specimen IB-26-1

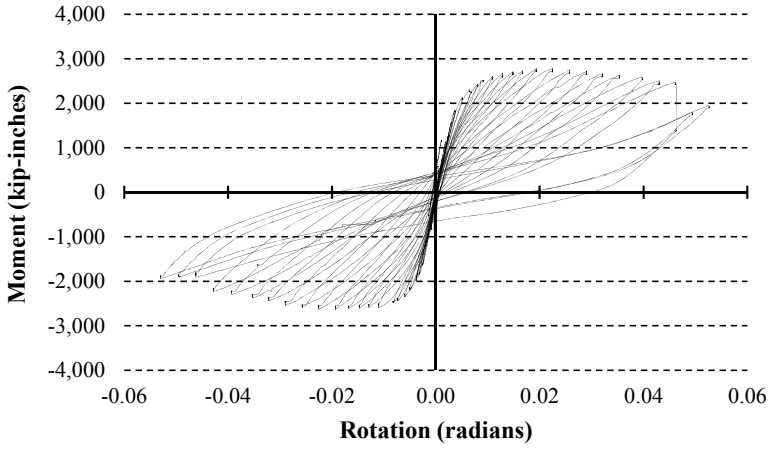

Figure 6.21 Moment versus Rotation - Specimen IB-26-1

Ductility capacity and % drift

Figure 6.19 is plotted in Figure 6.22 for detailing the points of calculation for specimen ductility and to show the percent drift. In Figure 6.22, percent drift is given as an additional axis shown above the experimental data (labeled as Θ_r).

Figure 6.22 details the yield displacement and displacement capacity of the specimens with black outlined and black circles, respectively. The yield points in both the positive and negative directions were 0.56 inches and 0.78 inches. The displacement capacities of the specimen were also determined as the displacement at which the moment capacity of the specimen has degraded below 80 percent of its ultimate value. Displacement capacities were determined to be 7.0 inches in both the positive and negative directions. In the positive direction, during the displacement cycle to +7.0 inches rupture caused a significant and immediate decrease in moment value. This point was taken as the displacement capacity. In the positive direction, the displacement ductility capacity was 12.5 and in the negative direction the value was 9.0. Thus the average ductility

capacity was 10.8. As with the previous two specimens presented, the specimen ductility capacity was greater than required by the SCDOT SDS.

The ductility capacity of the specimen was again reflective of the hysteretic behavior. The specimen displays desirable degradation behavior. Noticing again the comparison between experimental behavior and the numerical models as shown in Figure 6.19, it can be seen that the specimen behavior continues to show improvement compared to both models though cycles of 7.0 inches.

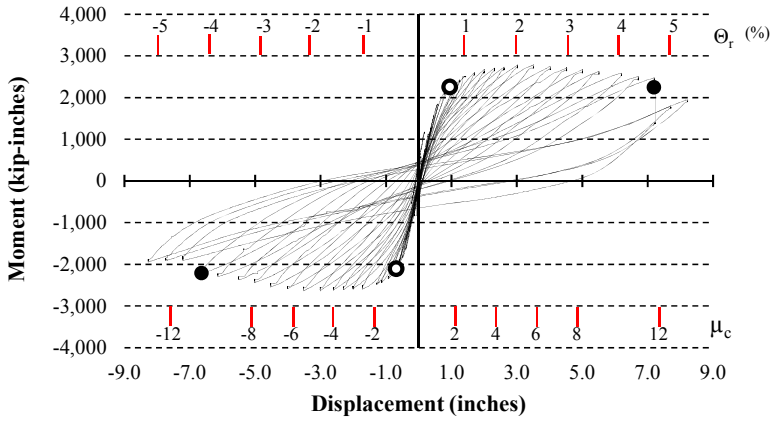

Figure 6.22 Displacement Ductility - Specimen IB-26-1

Plastic hinge mechanism and cracking pattern

The length of the plastic hinge mechanism was again estimated using the cracking distribution observed along the length of the pile as well as energy dissipation determined through moment curvature plots. Distribution of cracking along the length of the pile is shown in Figure 6.23. Additionally, plots of moment versus curvature are shown in Figure 6.24. Four plots are presented displaying the experimental moment versus curvature relationship. The four plots correspond to each of the measured points of curvature along the length of the pile.

As seen from the cracking distribution in Figure 6.23, the specimen exhibited extensive cracking extending away from the soffit. Cracking was observed to occur as far as 58 inches from the face of the connection. Cracking extended further than in any of the other interior specimens.

In Figure 6.24, plots of moment versus curvature are presented. A large amount of energy dissipation is seen at the first point of measurement. This is confirmed looking at Figure 6.25 which shows the development of a large crack about the perimeter of the pile near the interface of the connection. Although such a large amount of dissipation is seen at the first point of measure the remaining points of measure also show significant amounts of energy dissipation.

In addition to Figures 6.23 and 6.24, significant curvature of the pile beyond the points of measured curvature is shown in the photograph of Figure 6.26. With the information seen in each of these figures, a plastic hinge length of 25 inches is estimated.

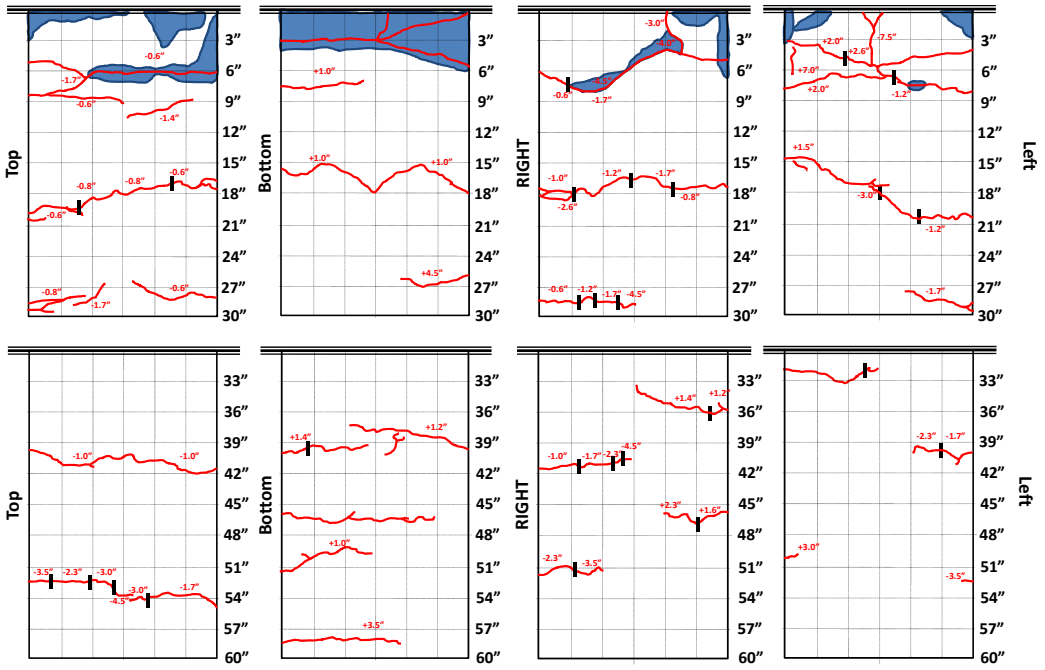

Figure 6.23 Crack Locations - Specimen IB-26-1

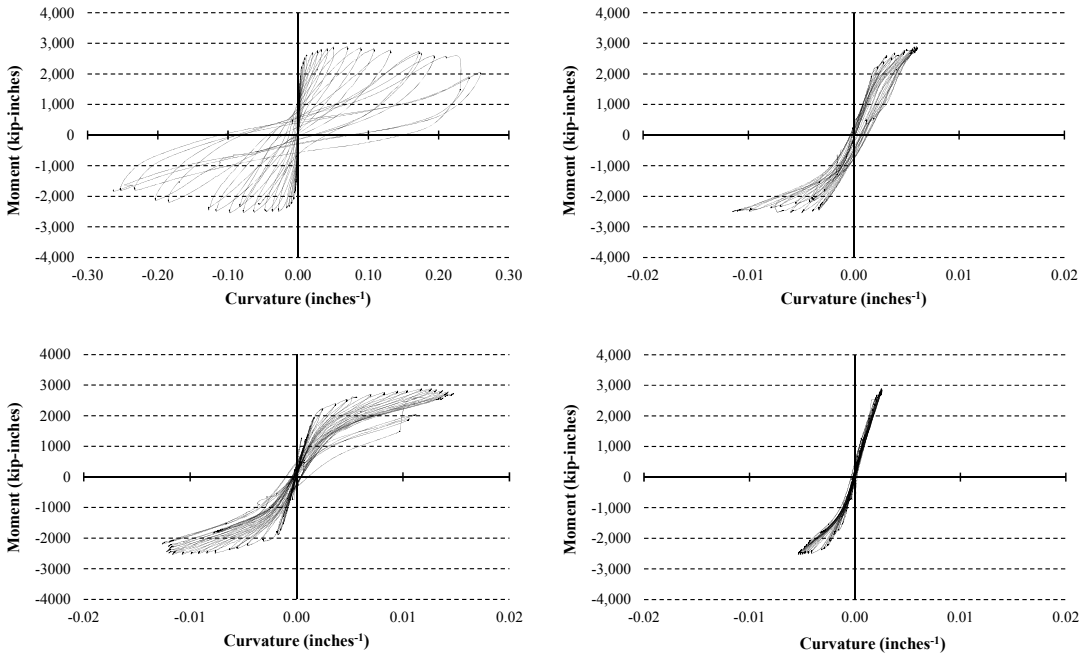

Figure 6.24 Moment versus Curvature - Specimen IB-26-1

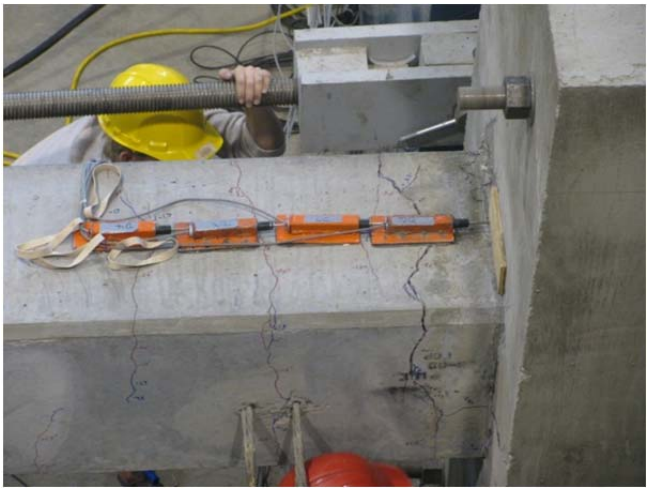

Figure 6.25 Observed Pile Damage - Specimen IB-26-1

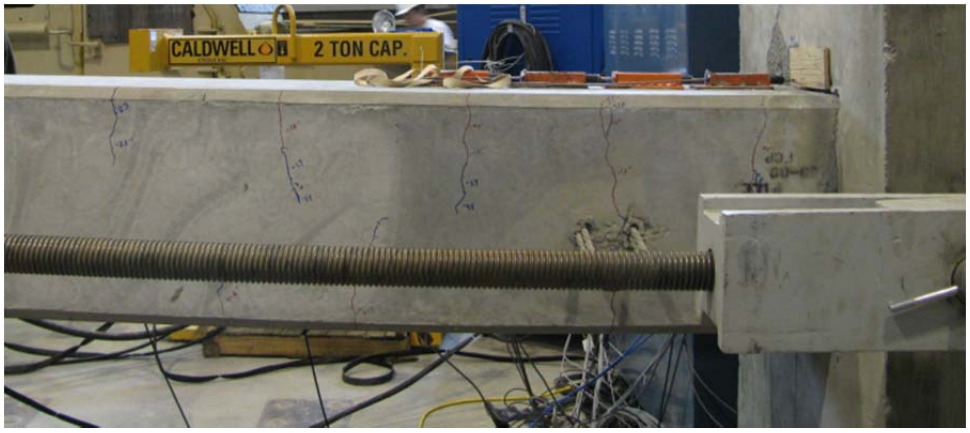

Figure 6.26 Observed Pile Curvature - Specimen IB-26-1

Joint shear stress, cap performance, and additional damage observations

Figure 6.27 shows photographs of the bent cap following testing. As seen in the photographs, the bent cap was more significantly damaged in comparison with the previous two specimens. This damage is seen in the photographs as spalling along the top face of the connection to the pile, as well as cracking extending away from the bottom corner of the connection. The spalling observed in this photo is not unusual compared with the two 18 inch embedded specimens, and occurs at approximately the same displacement (4.5 inches). The cracking behavior is not seen in either of the two specimens previously discussed. The cracks seen in the bent cap extend away from the lower half of the pile into the bent cap and in a single case extend around the front face and into the depth of the bent cap. These cracks were observed beginning at displacement of 4.5 inches.

Joint stresses were again calculated and are shown in Table 6.5. For this specimen the maximum joint shear stress was found to be 0.118 ksi while the principle tensile and compressive stresses were calculated as 0.106 and 0.132 ksi respectively. All values are within the allowable limits.

Results of strain (plotted in black and moment plotted grey) versus time are shown in Figure 6.28. Similar to specimen IB-18-2 four of the five gages placed in the bent cap were functional following casting of the bent cap. Results from each of these four gages are shown. A maximum absolute value of 95 micro-strain was recorded from gage 5, corresponding to five percent of the yield stress. This gage was placed on the longitudinal reinforcement closest to the cracking which occurred in the bent cap.

Figure 6.27 Joint Region Following Test Completion - Specimen IB-26-1

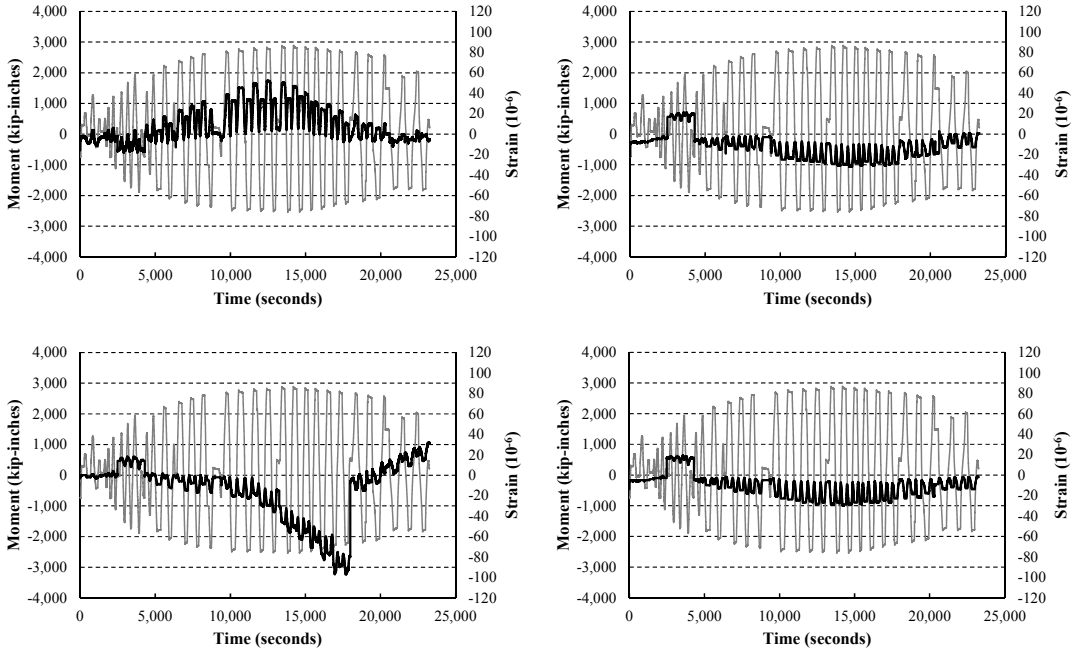

Figure 6.28 Bent Cap Strain - Specimen IB-26-1

This specimen was instrumented with two linear displacement gages placed on exposed strands at the embedded end of the pile. These gages were used to determine the point and magnitude of slipping of the prestressing strands. Figure 6.29 shows the displacement of each of these gages versus moment. From this figure it can be seen that each strand begins to slip at approximately

2,000 kip-inches. The figure also shows the top strand to slip to 0.41 inches by the conclusion of the test. The bottom strand reaches a value of 0.26 inches.

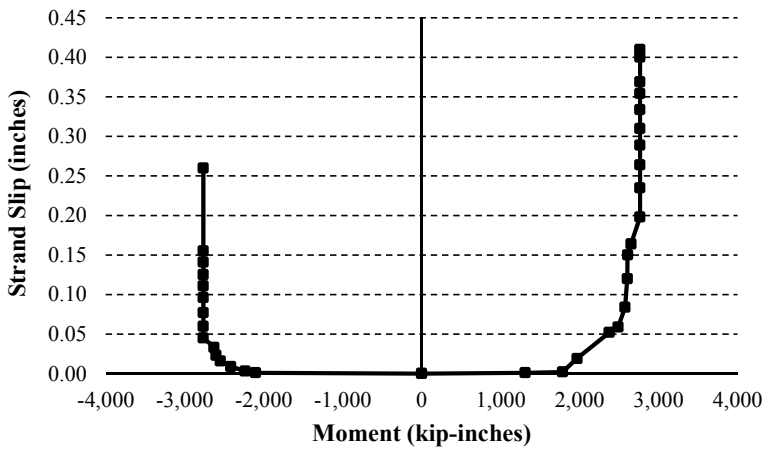

Figure 6.29 Strand Slip versus Moment - Specimen IB-26-1

6.8 Specimen IB-22-1

General information

Specimen IB-22-1 was created with a pile from the second casting group. The bent cap of this specimen was cast on July 30, 2009 and testing was completed on September 17, 2010, 49 days later. The bent cap reached a compressive strength of 5,500 psi at 56 days. The bent cap was cast with a reduced depth of two feet six inches, which is representative of bent caps constructed in the coastal areas of South Carolina. To accommodate this reduction in depth, longitudinal reinforcement was constructed with 180 degree hooks.

Hysteretic behavior and moment capacity

Plots detailing the hysteretic behavior are shown in Figures 6.30 through 6.32. These plots are presented in the same manner as for the previous specimens. Figure 6.30 shows specimen behavior in terms of moment versus displacement. From this figure, maximum moments in the positive and negative directions can be seen as 2,940 kip-inches and 2,920 kip-inches, respectively. These values occurred at displacement levels of 4.4 inches and 3.9 inches in the positive and negative directions. This specimen developed an average moment capacity of 2,930 kip-inches at an average displacement of 4.2 inches.

Figure 6.30 again details the results of the two moment curvature models developed for the specimen, and provides a comparison with experimental behavior. From Figure 6.30 it can be seen that specimen IB-22-1 compares well with the model developed assuming that full capacity of the pile is reached. In either direction the specimen develops an ultimate moment capacity that exceeds the value given by the full capacity model. Further, the ultimate moment in either direction occurs at a displacement greater in magnitude than that predicted by the model. In the

negative direction the specimen is seen to perform better than the prediction given by the model throughout the duration of testing. In the positive direction the specimen performs better than the model with the exception of displacement cycles between 1.2 and 2.6 inches. The specimen also performs favorably to the model developed which accounts for slipping of the prestressing strands. The specimen performed better than the predicted model throughout the test in both the positive and negative directions.

Figures 6.31 and 6.32 show the experimental behavior in terms of lateral force versus displacement and moment versus rotation, respectively. From Figure 6.31 the specimen is observed to reach values of load applied laterally to the pile of approximately 20 kips in either direction.

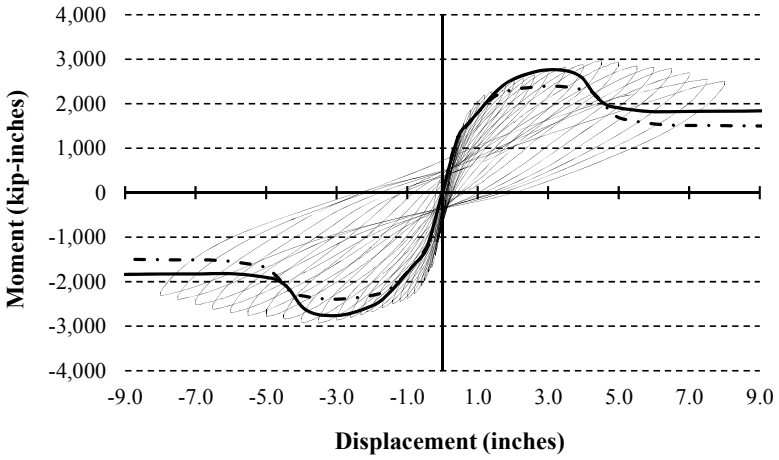

Figure 6.30 Moment versus Displacement - Specimen IB-22-1

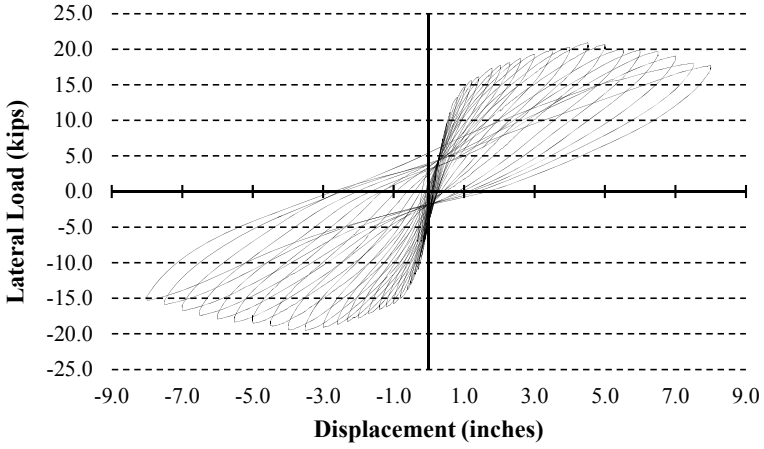

Figure 6.31 Lateral Force versus Displacement - Specimen IB-22-1

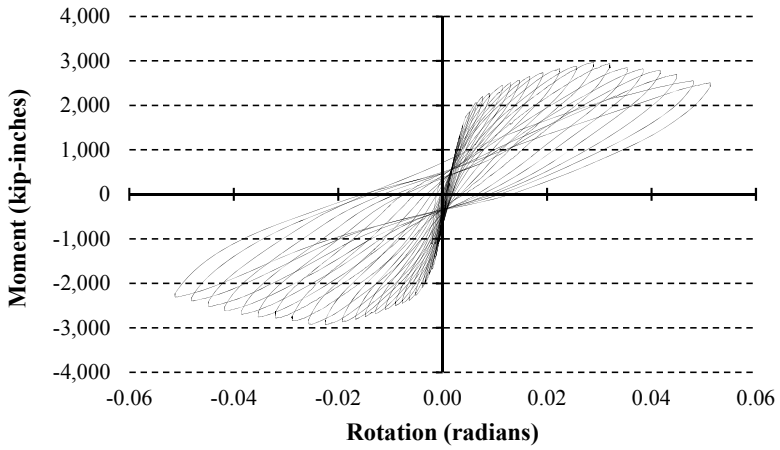

Figure 6.32 Moment versus Rotation - Specimen IB-22-1

Ductility capacity and % drift

Figure 6.30 detailing the moment versus displacement behavior of the specimen is plotted again in Figure 6.33. In this figure the predicted results of the numerical models are removed and replaced with horizontal axes detailing percent drift and ductility. Points displaying the estimated yield point of the specimen are shown along with points displaying the displacement capacity.

This specimen was determined to yield at a displacement of 0.8 inches in the positive direction and 0.6 inches in the negative direction. The displacement capacity is again taken to be the point at which the moment capacity degrades to 80% of the ultimate moment in either direction. Using this value, the displacement capacity of the specimen in the negative direction is found at the final displacement cycle tested of 8.0 inches. In the positive direction the moment value that the specimen achieved at the final displacement of 8.0 inches was equal to 2,500 kip-inches, nearly 150 kip-inches greater than the value of 0.8 times the ultimate moment in this direction. Therefore the displacement capacity is taken to be 8.0 inches.

With these values, ductility in either direction is calculated as 13.0 inches in the negative direction and 10.0 inches in the positive direction. The ductility capacity of the specimen as a whole is given as the average of these two values equal to 11.5. Similar to the previous three specimens discussed, the specimen ductility capacity as well as the minimum directional ductility capacity is greater than the maximum value as required by the SCDOT SDS.

The high displacement capacity again leads to commentary on performance following the ultimate moment capacity of the specimen in either direction. The specimen is seen to perform well in terms of degradation and thus energy dissipation following its ultimate moment capacity.

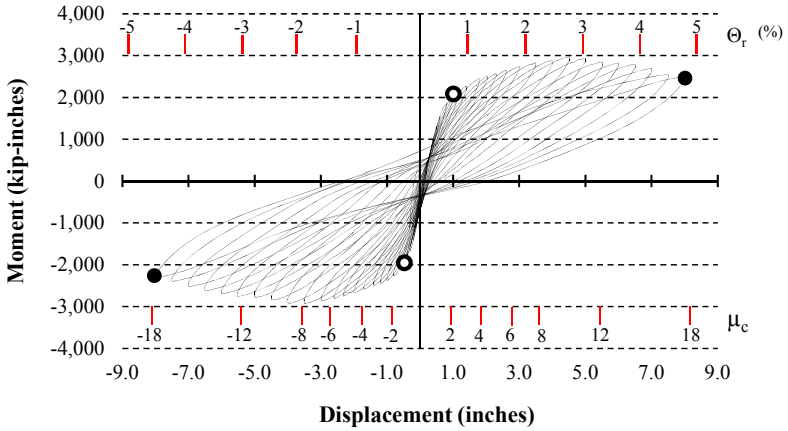

Figure 6.33 Displacement Ductility - Specimen IB-22-1

Plastic hinge mechanism and cracking pattern

The distribution of observed cracks along the length of the pile is shown in Figure 6.34. The figure details cracks occurring along the length of the pile on each of the four pile surfaces. Cracks are observed to occur as far as 56 inches from the soffit along the top of the pile. Noticing the cracking distributions along the top and bottom faces of the pile, it is seen that cracks forming as a result of a plastic hinge extend beyond the points of measured curvature within the expected plastic hinge zone. These cracking patterns along with other damage mechanisms along the length of the pile are also shown in Figure 6.35. This figure provides a series of photographs of the pile taken after testing. Along with the distribution of cracks some concrete crushing is seen at the top surface of the pile at the interface with the bent cap. Some spalling also occurs on the bottom surface of the pile.

Figure 6.36 shows the moment versus curvature relationships for each of the points of measured curvature. Significant hysteretic behavior is observed through the first three points of measured curvature corresponding to a distance of 15 inches from the face of the bent cap. The fourth point of measured curvature also displays energy dissipation though not to the extent of the previous three. The dominate point of energy dissipation is seen at the first point of measured curvature. This is a result of the largest crack in the pile developing about the perimeter just outside of the interface. This crack may be seen in the figures displaying the cracking pattern distribution and in the photographs of the pile following the specimen test.

In the case of this specimen the formation of the plastic hinge is estimated to be 25 inches. This is based on the energy dissipation through each point of measured curvature and the observation of cracking extending along the length of the pile beyond these points.

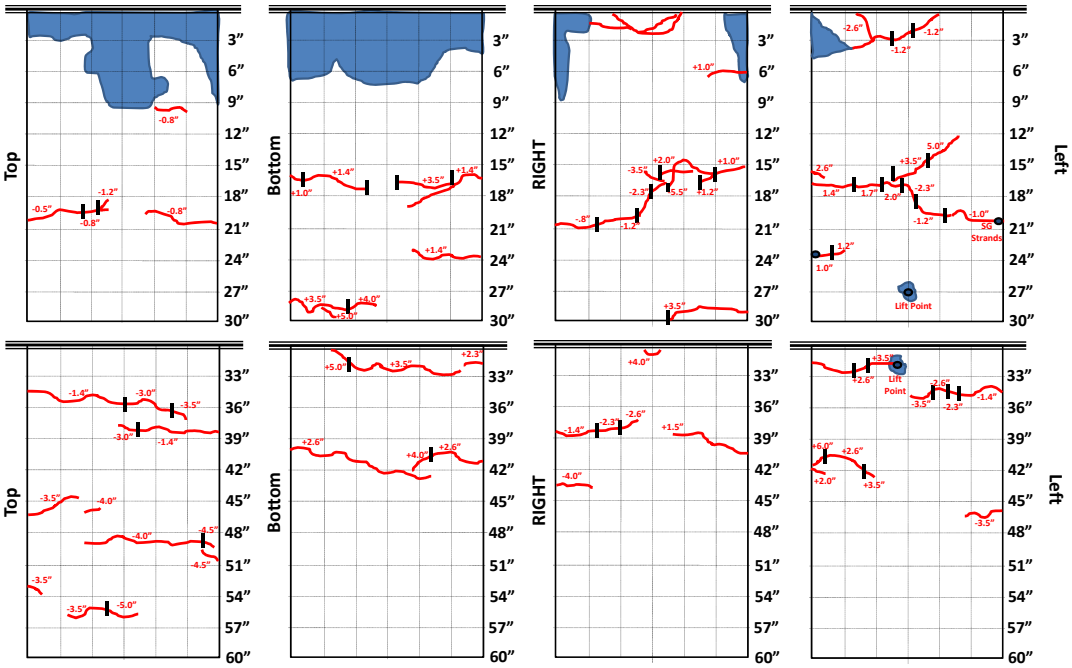

Figure 6.34 Crack Locations - Specimen IB-22-1

Figure 6.35 Damage Locations - Specimen IB-22-1

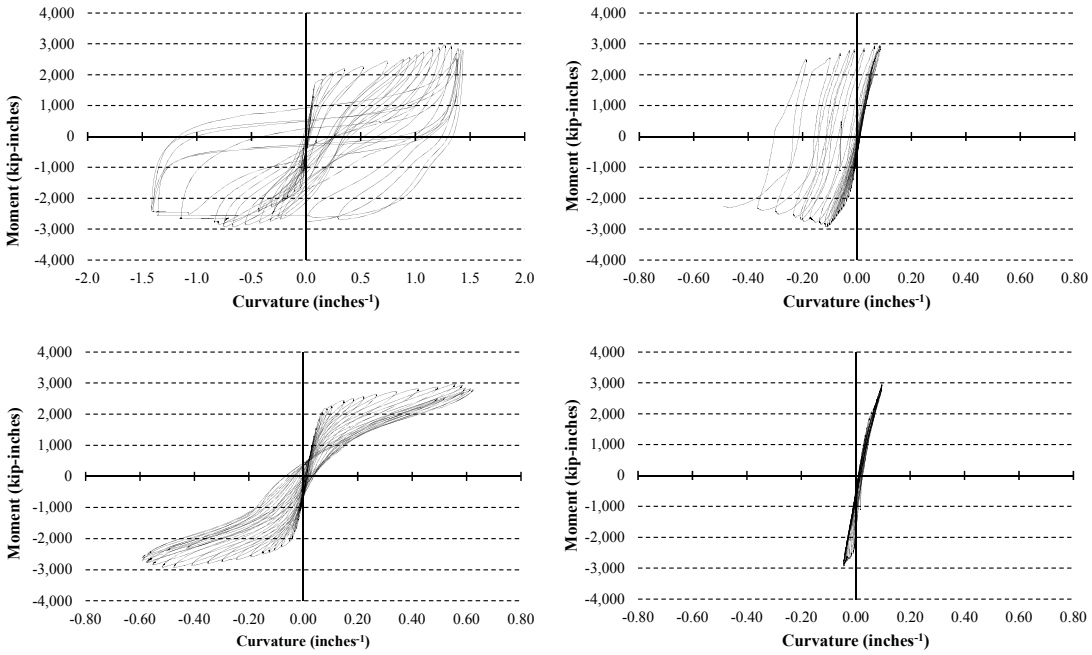

Figure 6.36 Moment versus Curvature - Specimen IB-22-1

Joint shear stress, cap performance, and additional damage observations

Figure 6.37 shows a photograph of the bent cap following testing. Only minor damage occurred in the bent cap. The bent cap spalled at the corners of the soffit with additional spalling along the top face of the connection to the pile. The spalling of the bent cap of this specimen is minor in comparison with the other specimens presented in this chapter.

Stresses in the joint region were calculated using the methodology presented in Figure 6.1. The results of these calculations are shown in Table 6.5. All stresses calculated in this region were well below the allowable stresses set by the SCDOT SDS. A maximum joint shear stress was calculated to be 0.152 ksi. Principle stresses were also computed as 0.138 and 0.167 ksi, corresponding to the maximum tensile and compressive stresses respectively.

Figure 6.37 Joint Region Following Test Completion - Specimen IB-22-1

This specimen was also instrumented with gages to record strand slipping. The gage instrumented to the top strand in the pile was damaged during the casting of the bent cap. The gage connected to the bottom strand was functional and results are shown in Figure 6.38. This plot, similar to Figure 6.29 provided for specimen IB-26-1, presents the strand slippage in terms of inches plotted against moment. The strand begins to slip initially at a moment of approximately -2,000 kip-inches and reaches a displacement of 0.35 inches at the conclusion of testing.

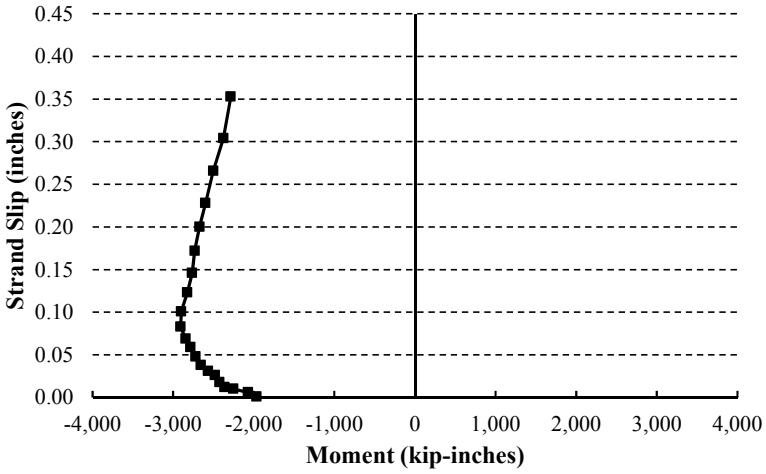

Figure 6.38 Strand Slip versus Moment - Specimen IB-22-1

Table 6.5 Joint Stress Calculation Results

Specimen	Principle Tensile Stress (ksi)	Principle Tensile Allowable (ksi)	Principle Compressive Stress (ksi)	Principle Compressive Allowable (ksi)	Shear Stress (ksi)
IB-18-1	0.088	0.257	0.114	1.35	0.100
IB-18-2	0.076	0.245	0.102	1.225	0.088
IB-26-1	0.106	0.228	0.132	1.064	0.118
IB-22-1	0.138	0.235	0.167	1.125	0.152

Chapter 7 - Exterior Specimens

In collaboration with Dr. David Sanders

7.1 Introduction

This chapter presents the results related to the four single pile exterior specimens. Testing of these specimens began with the test of specimen EB-18-1 on September 18, 2009. Specimens are notated by the pile embedment length and the specimen number tested. Each of the four specimens is described in Chapter 3. Different from the interior specimens, both embedment length and reinforcement design are considerations for results of the exterior specimens.

7.2 Material performance

Strands were de-tensioned 24 hours after casting. Compressive strength tests were performed on site at Florence Concrete Products. Specimens EB-18-1, EB-2-1 and EB-26-1 were created from the first set of piles cast. Specimen EB-22-1 was created with a pile from the second pile set cast. The material testing results are shown in Table 7.1.

Bent caps were cast-in-place as described previously. Table 7.2 details the date on which each cap was cast. In addition to the casting date, Table 7.2 also details the test date of each specimen as well as the number of days between the casting date and the testing date. Piles were oriented in the bent caps such that the "top bar" effect was minimized.

Material tests for specimen elements were performed at the Structures Laboratory at the University of South Carolina. Testing included concrete compressive strength, split tensile strength, and elastic modulus. Compression tests were performed on three cylinder samples at time periods of 7, 14, 28 and 56 days. Split tensile testing was conducted on three cylinder samples at periods of 28 and 56 days. Elastic modulus testing was performed at the same time intervals as the split tensile testing. Results of these tests are shown in Table 7.1. The results of testing performed on piles are shown in Table 7.1 as well as in Table 6.2.

Representatives from the University of South Carolina cast all cylinders used for the material tests. Test cylinders were kept in a controlled environment for proper curing. Core samples were taken from specimens EB-2-1, EB-26-1 and EB-22-1. Three core samples were taken from each of these specimens. A single core sample was taken from the pile of each specimen while two samples were taken from the bent caps. Samples were taken within one week of test completion. Core samples were taken for compression testing results near the time of testing. The results of the compression testing are shown in Table 7.1.

Table 7.1 Material Testing Results by Specimen

		Cylinder	Piles (1)	Piles (2)	EB-18-1	EB-2-1	EB-26-1	EB-22-1
Compressive Strength, f'c (psi)	3 Day	Avg.	5,500	-	-	-	-	-
	7 Day	1	-	-	4,300	3,800	3,300	3,200
		2	-	-	4,100	4,100	3,200	3,600
		3	-	-	-	4,000	3,500	3,300
		Avg.	-	-	4,200	4,000	3,300	3,400
	14 Day	1	-	-	5,100	3,700	3,600	-
		2	-	-	4,500	4,800	3,800	-
		3	-	-	-	4,000	3,400	-
		Avg.	-	-	4,800	4,200	3,600	-
	28 Day	1	8,200	7,300	5,500	5,500	-	-
		2	8,400	7,300	5,500	5,200	-	-
		3	-	7,200	-	4,500	-	-
		Avg.	8,300	7,266	5,500	5,100		-
	56 Day	1	-	7,700	6,200	-	5,900	4,800
		2	-	8,700	6,600	-	4,300	5,800
		3	-	8,300	-	-	-	6,000
		Avg.	-	8,200	6,400		5,100	5,500
	Core Sample	Pile	-	-	-	5,900	7,000	9,400
		Cap 1	-	-	-	5,800	4,500	6,700
		Cap 2	-	-	-	5,800	4,700	5,500
Elastic Modulus, E (ksi)	Day:		60			28		
		1	2,700	-	-	2,900	-	-
		2	2,700	-	-	3,200	-	-
		3	3,100	-	-	-	-	-
		Avg.	2,830	-	-	-	-	-

Table 7.2 Specimen Casting and Testing Dates

Exterior Specimens			
Specimen	**Cast Date**	**Test Date**	**Time Difference (Days)**
EB-18-1	2/16/2009	9/18/2009	214
EB-2-1	12/16/2009	6/2/2010	168
EB-22-1	7/30/2010	8/25/2010	26
EB-26-1	5/26/2010	7/7/2010	42

Similar to specimen IB-22-1, specimen EB-22-1 was instrumented with two vibrating wire strain gages. These gages were placed into the confined section of concrete within the pile at the center of the embedment length, as described in Chapter 3. The gages were used to determine the stress imparted onto the piles as a result of shrinkage of the cast-in-place bent cap. This shrinkage aids in the development of the prestressing strands within the pile and thus improves the overall behavior. The shrinkage imparts a confining stress onto the pile along the embedded length. As the frictional force is proportional to the normal force applied, the confining stress increases the frictional bond between the strand and concrete, thereby developing a higher moment capacity. The results of the vibrating wire strain gage measurements are shown in Table 7.3.

Table 7.3 Vibrating Wire Strain Gage Measurements

	Gage 1		**Gage 2**	
	Strain (10^{-6})	**Stress (psi)**	**Strain (10^{-6})**	**Stress (psi)**
Following Pile Casting	2,875	-	2,813	-
Prior to Testing	2,775	-	2,695	-
Difference	101	-520	118	-610
Avg. Stress (psi)	-565			

7.3 Moment curvature modeling

Two numerical models were created in XTRACT for comparison with the experimental results as previously described. This description is briefly repeated below for reference. The models were created using measured pile concrete material properties and assumed steel material properties. Material properties were input using the material models found in the SCDOT SDS.

Model 1 was created assuming that the strands are fully developed. This is accomplished by allowing the prestressing strands within the pile to reach their maximum tensile strength without slipping. The second model is created with a defined stress at which strand slipping will occur. The slipping stress is based on a number of parameters including the embedment length of the pile and time between the casting and testing dates. The slipping stress accounts for the shrinkage in the bent cap in terms of time and predicts the amount of clamping force that will result from this shrinkage. The clamping force affects the frictional bond between the strands and the surrounding concrete. The slipping stress may then be calculated as the stress which

overcomes the bond (ElBatanouny et al., 2012). Table 7.4 details the calculated slipping stress for each of the exterior specimens.

Table 7.4 Specimen Slipping Stresses

Specimen	Embedment Depth (inches)	Experimental results				Slip Equation			
		Max. Moment (kip-inches)		Slipping stress* (ksi)		Max. Moment (kip-inches)		Slipping stress (ksi)	
		opening	closing	opening	closing	opening	closing	opening	closing
EB-18-1	18	N/A	N/A	N/A	N/A	1,990	-2,130	190	190
EB-2-1	2	740	-970	N/A	N/A	1,030	-1,070	-	-
EB-26-1	26	1,790	-2,730	220	220	2,000	-2,300	201	201
EB-22-1	22	2,050	-2,830	215	215	1,860	-2,130	183	183

* = *Experimental slipping stress was determined through the observation of maximum moment achieved.*

7.4 Specimen results

Results for the exterior specimens are presented according to the following parameters:

- General information
- Moment capacity
- Ductility capacity and percent drift
- Development of a plastic hinging mechanism
- Joint shear stress and cap performance

Figure 7.1 details the methodology used to calculate stresses in the joint region of each cap. This figure may also be seen in Chapter 6. The methodologies given in Figure 7.1 are taken from the SCDOT SDS.

$$v_{jh} = \frac{M_p}{h_b D_c b_{je}} \quad (8\text{-}20)^{1}$$

v_{jh} : Average joint shear stress (ksi)
M_p : Maximum moment achieved (k-in)
h_b : Depth of the cap (in)
D_c : Maximum cross sectional dimension of pile (in)
b_{je} : Effective joint width (in)

Allowable Principal tensile stress (ksi)

$$P_t \leq 0.379\sqrt{f_c'} \quad (8\text{-}23)^{1}$$

Allowable Principal compressive stress (ksi)

$$P_c \leq 0.25\, f_c' \quad (8\text{-}24)$$

$$P_c, P_t = \frac{f_h + f_v}{2} \pm \sqrt{\left(\frac{f_h - f_v}{2}\right)^2 + v_{jh}^2} \quad (8\text{-}16, 8\text{-}17)^{1}$$

P_c: Principal compressive stress (ksi)
P_c: Principal tensile stress (ksi)
f_h: Average axial horizontal stress (ksi)
f_v: Average axial vertical stress (ksi)

$$f_v = \frac{P_{col}}{b_{je}(h_b + D_c)} \quad (8\text{-}21)^{1}$$

$$f_h = \frac{P_b}{b_b h_b} \quad (8\text{-}22)^{1}$$

$$b_{je} = D_c + h_c \quad (8\text{-}19)^{1}$$

b_b : Width of column (in)
h_c : Width of column (in)

[1]: SCDOT Seismic Design Specifications for Highway Bridges Version 2.0

Figure 7.1 Joint Stress Calculation Methodology

7.5 Specimen EB-18-1

General Information

The test of specimen EB-18-1 began on September 18, 2009. This specimen was constructed using a reinforcement design similar to that of the interior specimens (described in Chapter 3). This design was provided by the SCDOT and was intended to be generally representative of a worst case scenario based on current practices for the detailing of an exterior bent cap connection.

Hysteretic Behavior and Moment Capacity

Figures 7.2 through 7.5 detail the hysteretic behavior, with joint opening displacements considered to be positive. Positive displacements correspond to an axial tensile load applied to the pile. Conversely, pile displacements in the negative direction result in an axial compressive load applied to the pile.

Figures 7.2 through 7.5 detail the hysteretic behavior in the same manner that was presented for the behavior of the interior specimens. Figure 7.2 shows the moment versus displacement behavior of the specimen. The referenced displacement in this plot is taken as the measured pile displacement at 156 inches from the face of the connection. The moment is calculated at the face of the connection. This figure also shows results from the moment curvature analysis. Figure 7.3 details the behavior of the specimen in terms of lateral force versus displacement, Figure 7.4 shows the moment versus rotation behavior, and Figure 7.5 details the axial force versus displacement behavior.

From the plots in Figure 7.2 it can be seen that the full performance of the specimen did not achieve the behavior predicted by either of the two numerical models. This lack of satisfactory

performance is attributed to a prying failure of the bent cap that occurred during displacement in the closing direction. The three additional exterior specimens were created to improve the design of the exterior bent cap connection.

The remaining specimens were designed using one of two methods. The first method models the exterior pile as a hinge. This design is seen in specimen EB-2-1. The second method is to design the exterior piles to achieve significant moment capacity. As such, the pile must be developed by the bent cap connection. Two methods of accomplishing pile development are presented in specimens EB-26-1 and EB-22-1.

In Figures 7.3 and 7.5 the experimental behavior of specimen EB-18-1 is shown in terms of lateral and axial force versus displacement. From Figure 7.3 it can be seen that the specimen reaches levels of lateral load of 9.0 and 9.7 kips in the positive and negative directions respectively. These levels of applied load were reached by the specimen at pile displacements of 0.43 inches in the positive direction and 0.38 inches in the negative direction. The highest levels of applied axial load are seen at the same displacements in Figure 7.5. The levels of axial load achieved were 25.2 kips in tension and 27.4 kips in compression.

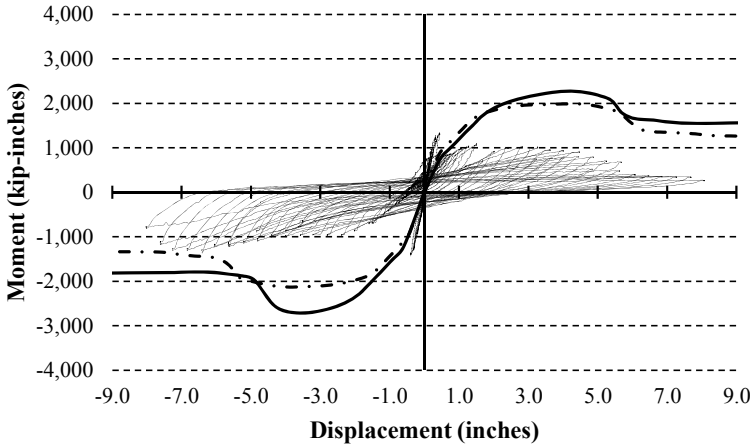

Figure 7.2 Moment versus Displacement - Specimen EB-18-1

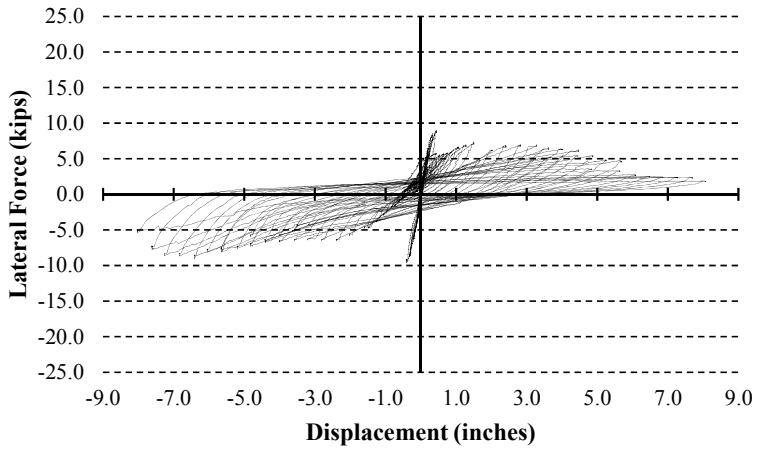

Figure 7.3 Lateral Force versus Displacement - Specimen EB-18-1

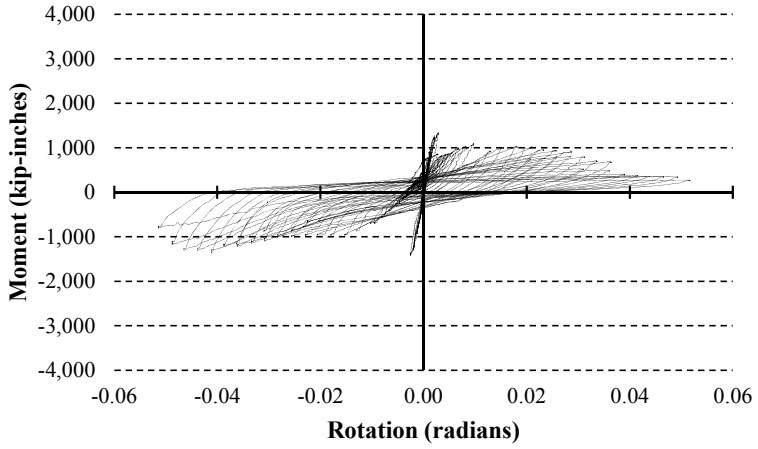

Figure 7.4 Moment versus Rotation - Specimen EB-18-1

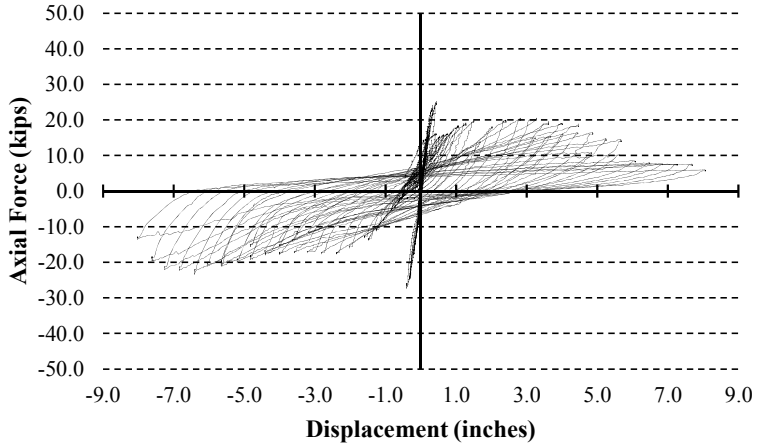

Figure 7.5 Axial Force versus Displacement - Specimen EB-18-1

Ductility capacity and % drift

Because this specimen failed prior to yielding, displacement ductility and drift are not calculated.

Plastic hinge mechanism and cracking pattern

This specimen was designed based on the current design practices used within the state of South Carolina. The intended behavior is that the development of a plastic hinge would occur along the length of the pile below the bent cap interface. Because the specimen failed due to prying action in the bent cap at a low level of displacement, a well developed plastic hinge did not form.

As a general statement, the behavior of the exterior specimens in the negative direction is similar to that of interior specimens. In the positive directions these specimens exhibit a reduction in moment capacity due to the application of an applied axial tensile load. The cracking pattern is shown in Figure 7.6.

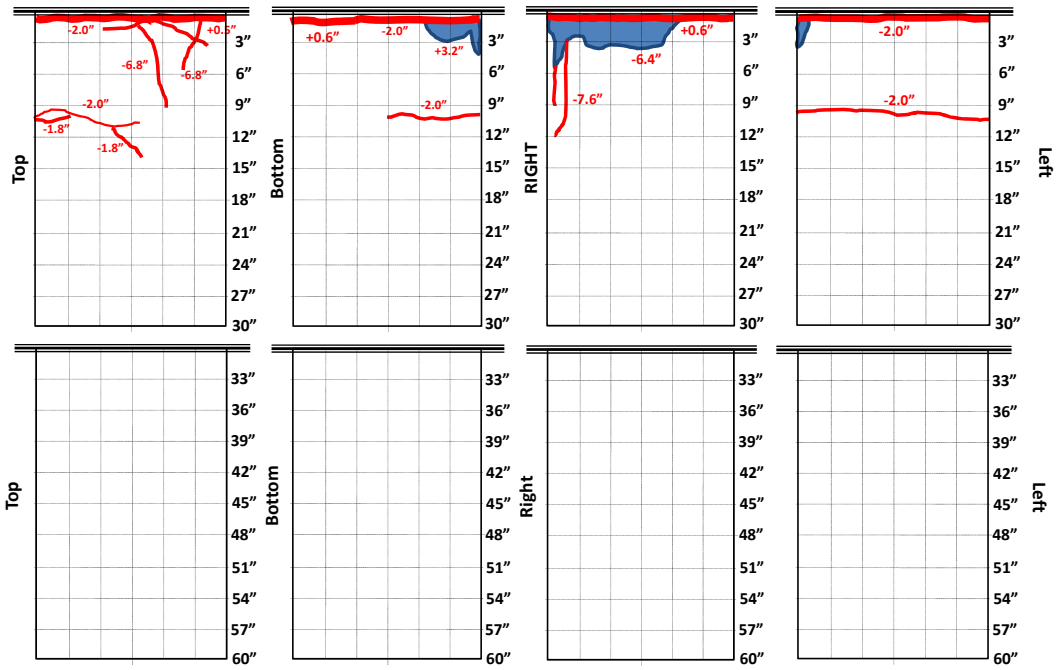

Figure 7.6 Crack Locations - Specimen EB-18-1

Joint shear stress, cap performance, and additional damage observations

The bent cap showed localized crushing failure in the area of the pile embedment that was precipitated by prying action in the closing direction. Figure 7.7 shows a photograph of the bent cap at the connection following the test. The damage to this specimen is dominated by a large crack about the perimeter of the pile just outside of the interface between pile and bent cap. This damage mechanism in the pile is similar to that of specimen IB-18-1. The stresses in the joint for this specimen were not calculated due to the early localized failure of the bent cap due to prying action. It is this failure mechanism of the bent cap that led to the design modifications of the remaining three exterior specimens.

Figure 7.7 Joint Region following Test Completion - Specimen EB-18-1

7.6 Specimen EB-2-1

General information

Specimen EB-2-1 was cast on December 16, 2009. This specimen was designed to simulate a hinged exterior pile connection. The embedment of the pile was only two inches and the perimeter of the embedded portion of the pile was surrounded by a compressible material. The remainder of the connection was completed with four No. 6 bars. These bars were embedded into the end of the pile to a depth of 24 inches. The remaining 12 inches was embedded into the bent cap. Each bar was terminated in a standard 90 degree. A photograph of this detail is shown in Figure 3.5. The specimen was tested on June 2, 2010.

Hysteretic Behavior and Moment Capacity

Although designed to perform as a hinge, some moment capacity was developed. This is shown in Figure 7.8 which details the moment versus displacement behavior. The specimen obtained maximum moment values of approximately 740 kip-inches and 970 kip-inches in the positive and negative directions, at displacements of 1.32 inches and 0.78 inches in these directions respectively. The specimen moment capacity is taken as 740 kip-inches. Because this specimen was designed to behave as a hinge the predictive relationships for moment capacity are not plotted for this specimen.

The maximum lateral and axial loads shown in Figures 7.9 and 7.11 correspond to the displacements at the maximum moment. In the positive direction, at a displacement of 1.3 inches, the specimen reached a maximum laterally applied force of 5.8 kips. A maximum axially applied load is found to be 15.9 kips. In the negative direction the maximum applied lateral and axial loads achieved were 5.7 kips and 16.4 kips, respectively. The hysteretic behavior of the specimen is shown in terms of moment versus rotation in Figure 7.10.

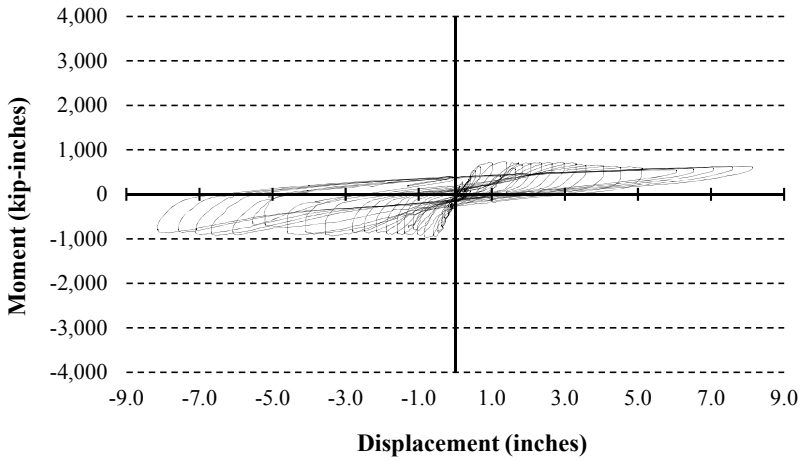

Figure 7.8 Moment versus Displacement - Specimen EB-2-1

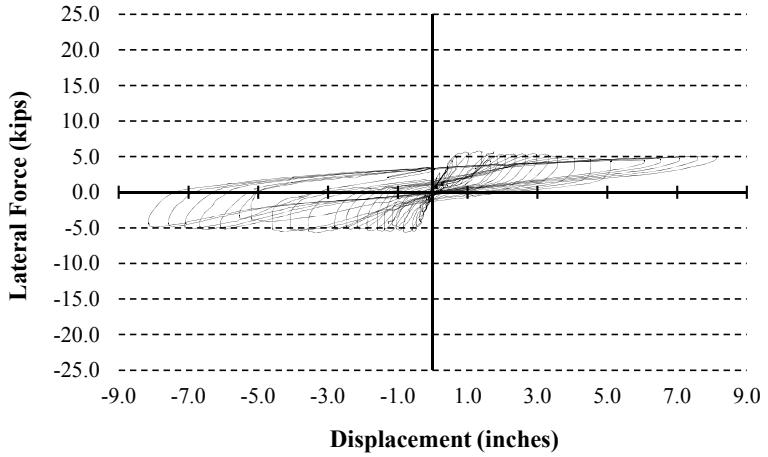

Figure 7.9 Lateral Force versus Displacement - Specimen EB-2-1

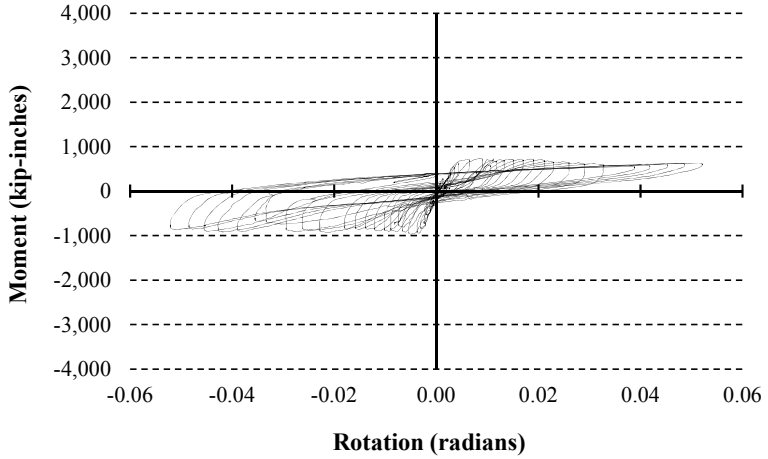

Figure 7.10 Moment versus Rotation - Specimen EB-2-1

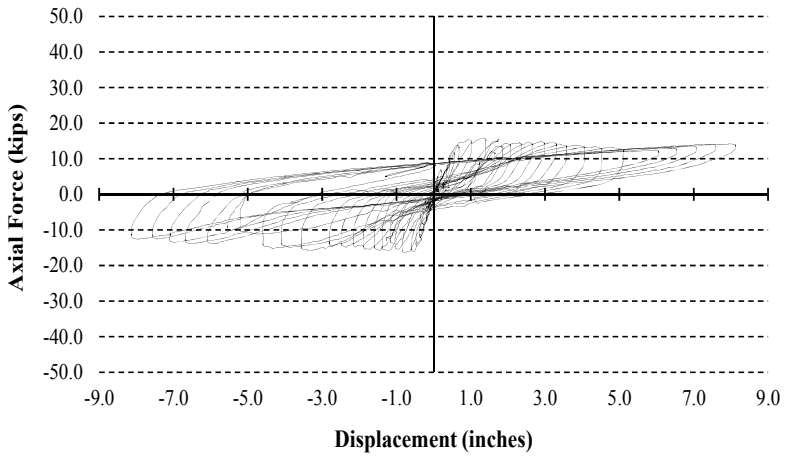

Figure 7.11 Axial Force versus Displacement - Specimen EB-2-1

Ductility Capacity and % Drift

Figure 7.8 is presented again in Figure 7.12 with axes of ductility and percent drift added. Points used to calculate the ductility capacity of the specimen have also been added. These points are again presented with black outlined and black circles representing the points at which the specimen is determined to yield and reach its displacement capacity.

The specimen yielded at displacements of 0.6 inches in both the positive and negative directions. The displacement capacity (determined at the point at which the moment degrades to 80 percent of its ultimate value) is found at displacements of 8.0 inches in both the positive and negative directions. These displacements are used to calculate a displacement ductility of 13.3. While presented here for completeness, it is noted that this calculation is not meaningful because the connection behaves essentially as a hinge.

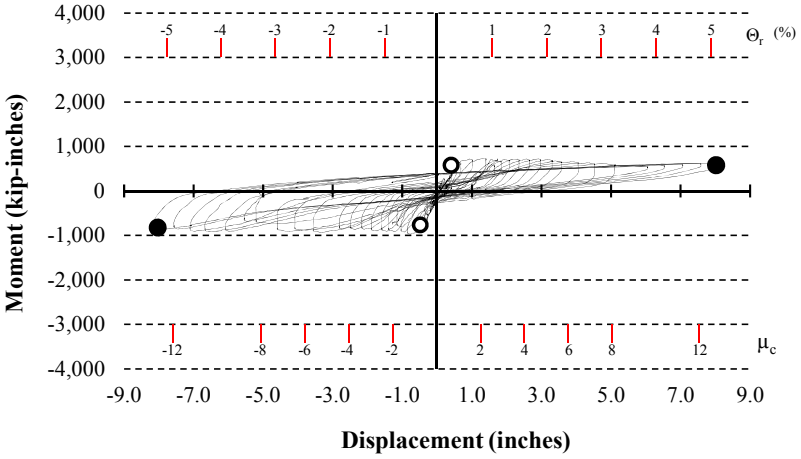

Figure 7.12 Displacement Ductility - Specimen EB-2-1

Plastic Hinge Mechanism and Cracking Pattern

Because this specimen was intentionally designed to behave as a hinge the development of a plastic hinge within the pile did not develop and no visible damage occurred to the pile. Figure 7.13 shows a photograph of the pile after testing.

As no damage occurred to the pile during the test the plots detailing the moment versus curvature behavior of the specimen are not presented. Energy dissipation occurred within the embedment region itself.

Figure 7.13 Pile Damage - Specimen EB-2-1

Joint Shear Stress, Cap Performance, and Additional Damage Observations

The design of the specimen was such that the damage was contained within the bars which made the connection. Figure 7.13, which shows the pile after testing, also shows the bent cap. Damage was not observed within the bent cap.

Strain was recorded in each of the five gages placed prior to casting of the bent cap. Results are shown in Figure 7.14 for the gage in location one. These strain results (plotted black) are plotted against time with moment (plotted grey) versus time being displayed on the same plot. As seen from the plots strain oscillates with displacement. The maximum strain range seen in the figure is approximately 30 micro-strain corresponding to 1% of the yield strain.

Additional strain measurements were taken from strain gages attached to the bars which made the connection (Figure 7.16). Strain is plotted in black and pile displacement is plotted in grey. This figure shows both interior and exterior gages from bars number three and four. The numbering of these bars is shown in the schematic of Figure 7.15. Interior gages are gages which were placed onto a portion of the bar which was embedded into the pile. These gages were placed at the midpoint of the embedded portion of the bar. Exterior gages were placed on the bars at the midpoint of the embedment into the bent cap. Comparing the gages on bar four, it is seen that the bar yields at the location of the interior gage at a pile displacement of 5.0 inches. The exterior gage is seen not to yield prior to this point. However, at a displacement of 5.0 inches the exterior gage is out of range. Both of the gages on bar three are also seen to go out of

range during testing. The exterior gage on bar three is lost early during the test, though up to the point of failure the gage behaves in much the same manner as the exterior gage on bar four. The interior gage on bar three failed at a pile displacement of 3.5 inches. Prior to failure, the gage does record a strain value of approximately 2,200 micro-strain, indicating that the gage failed just after yielding.

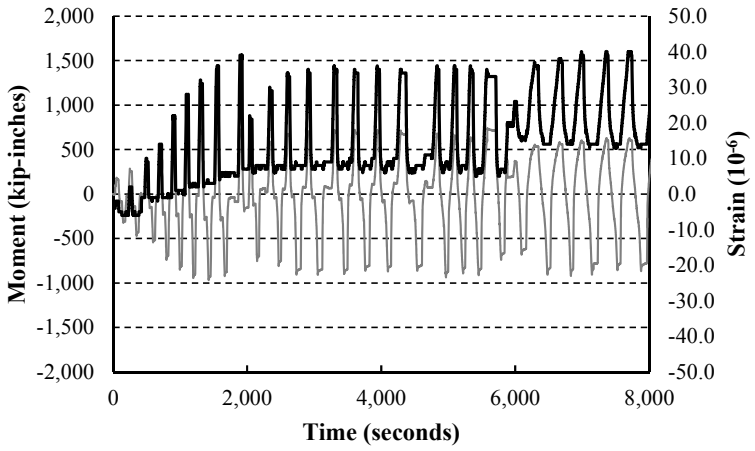

Figure 7.14 Bent Cap Strain - Specimen EB-2-1

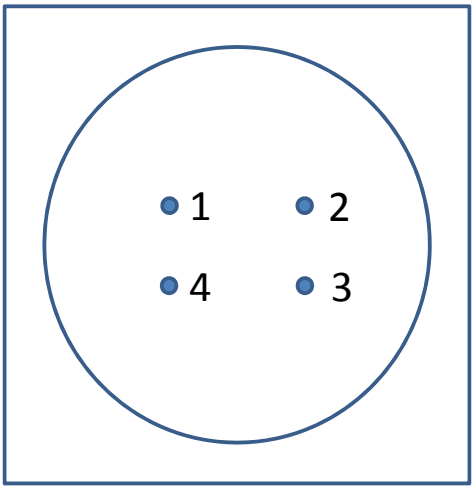

Figure 7.15 Dowel Bar Designation Schematic - Specimen EB-2-1

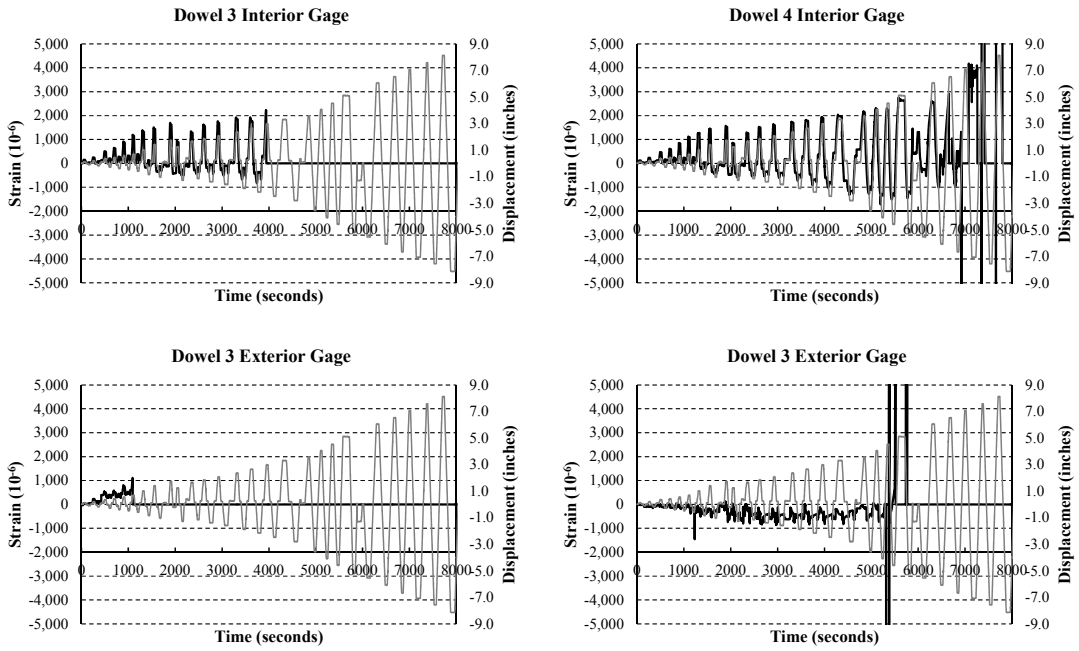

Figure 7.16 Dowel Bar Strain - Specimen EB-2-1

7.7 Specimen EB-26-1

General Information

Specimen EB-26-1 was designed to provide confinement to the pile and thus develop a significant moment capacity. The specimen was created with a heavily reinforced bent cap. The details of the reinforcement design are shown in Chapter 3. Figures 3.6 and 3.7 show a schematic and photograph of the reinforcement. The reinforcement was designed by Dr. David Sanders with use of a free downloadable Strut and Tie program (Fachwerk).

This specimen was cast on May 26, 2010, and tested 42 days later on July 7, 2010. The bent cap reached a 56 day compressive strength of 5,100 psi. The 26 inch embedment was the deepest used in the four exterior specimens.

Hysteretic Behavior and Moment Capacity

The hysteretic behavior is shown in Figures 7.17 through 7.20. These figures are presented in the same manner as those presented previously.

The moment versus displacement behavior is shown in Figure 7.17. The maximum moment in the positive direction was found to be 1,790 kip-inches at a displacement of approximately 1.0 inch. In the negative direction, corresponding to axial compression, the maximum moment was found to be 2,730 kip-inches at a displacement of 1.75 inches. Given the significant discrepancy between maximum moments in the positive and negative directions the smaller of the two moments (1,790 kip-inches) is taken as the moment capacity of the specimen.

Figure 7.17 also shows the results of the two numerical models. From the figure as well as the results of directional maximum moment it is clear that the applied axial load has a significant effect on the behavior. In the positive direction the specimen shows behavior greater than that predicted by either of the two models prior to displacements of approximately 1.7 inches. At larger displacements the performance drops below that of the predictive models.

In the negative direction the specimen performance exceeds the predictive models at early displacements. In the negative direction, the performance is greater than that of the models through displacements of 2.6 inches. Following displacements larger than 2.6 inches, the specimen performs comparatively well with the results of the numerical models through displacements of 4.5 inches at which point the specimen again performs better than expected from the model developed assuming full pile capacity. Through the displacement cycles between 2.6 and 4.5 inches the specimen performance is close to that of the second model.

The moment versus rotation behavior is shown in Figure 7.19. Figures 7.18 and 7.20 detail the lateral and axial applied force versus displacement behavior. From these figures the maximum forces applied to the pile are found along with the corresponding displacements. The displacements at the points of maximum applied load, both laterally and axially, correspond to the displacements at which the maximum moments are reached. The maximum lateral force applied to the pile in this specimen was 12.1 kips in the positive direction and 18.3 kips in the negative direction. At these points the applied axial force was also at a maximum. The applied axial load is a function of the performance of the specimen. The specimen achieved axial load of 50.4 kips in compression and 34.4 kips in tension.

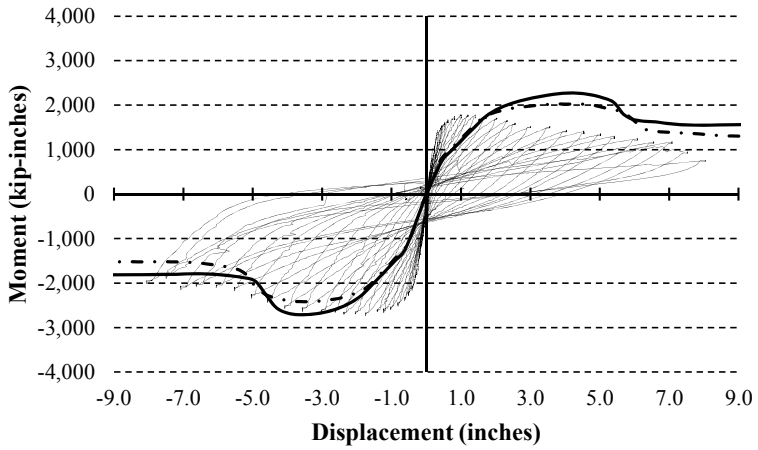

Figure 7.17 Moment versus Displacement - Specimen EB-26-1

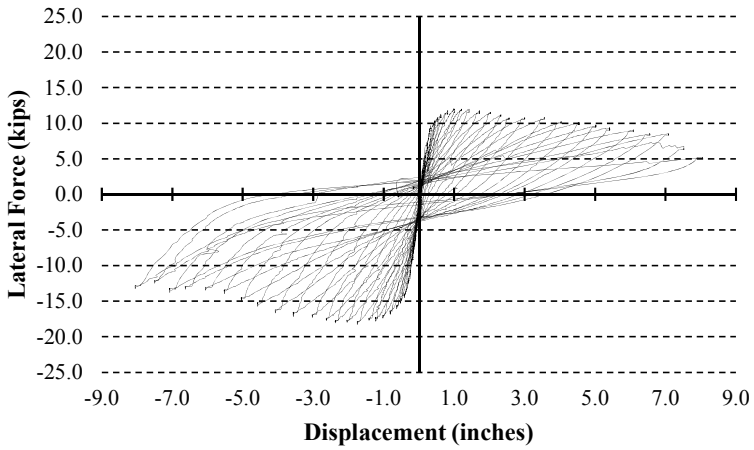

Figure 7.18 Lateral Force versus Displacement - Specimen EB-26-1

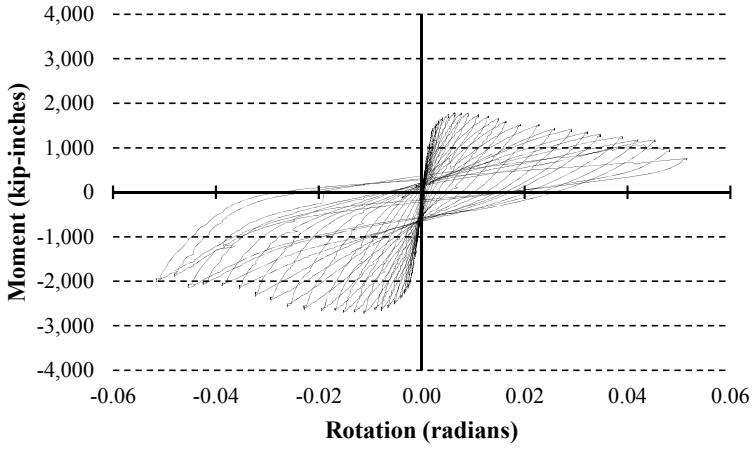

Figure 7.19 Moment versus Rotation - Specimen EB-26-1

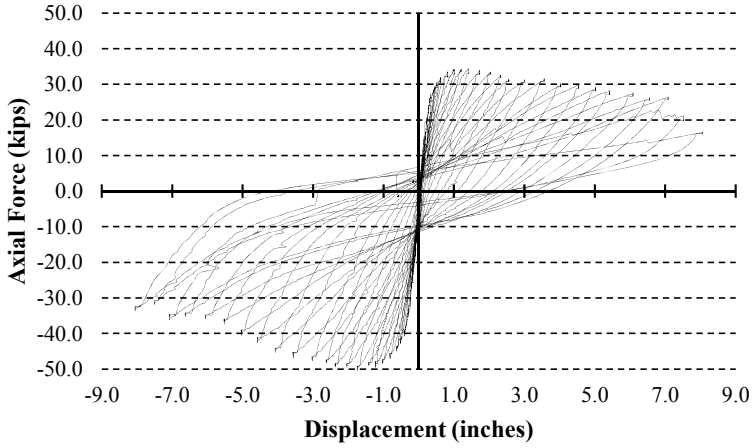

Figure 7.20 Axial Force versus Displacement - Specimen EB-26-1

Ductility Capacity and % Drift

The moment versus displacement behavior of the specimen is plotted again in Figure 7.21 with axes of ductility and percent drift added to the figure. The black outlined circles representing the points at yield are found at displacements of 0.31 and 0.41 inches in the positive and negative directions respectively. The black circles representing displacement capacity are found at displacements of 4.5 inches in the positive direction and 5.5 inches in the negative direction. The directional ductility for this specimen was calculated as 14.5 in the positive direction and 13.4 in the negative direction. An average of the two directional ductility capacities of 14.0 is taken for the specimen ductility capacity.

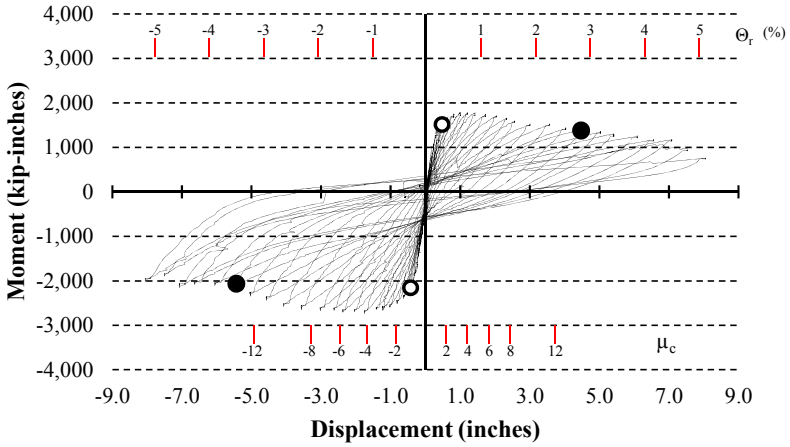

Figure 7.21 Displacement Ductility - Specimen EB-26-1

Plastic Hinge Mechanism and Cracking Pattern

As this specimen was designed to develop the full pile capacity, a plastic hinge mechanism was expected to develop within the region of the pile just outside the connection between the pile and bent cap. The length of the plastic hinge was estimated based on observed damage and the results of curvature recorded along the length of the pile.

The observed damage is presented in Figures 7.22 and 7.23. Figure 7.22 details the location of the observed cracks along the length of the pile. This schematic includes all cracks which developed during testing. Cracks are observed to develop along the perimeter of the pile to a distance of 41 inches from the face of the bent cap. The developing cracks are also shown in Figure 7.23 which shows a photograph of the pile taken between displacement cycles of 7.5 and 8.0 inches. The pile is marked in a red grid with grid lines separated by three inches. Cracks have been marked in blue. This figure also shows the gages which were used to measure curvature.

The results of the curvature gages are shown in Figure 7.24. These plots detail the amount of energy dissipation occurring at the points of measurement along the length of the expected plastic hinge zone. From these plots, energy dissipation may be seen at all points of measurement though it is predominant through the first two points.

Given the results of both the developed cracking pattern and the curvature measurements, the plastic hinge for this specimen is estimated to be 18 inches in length. This length is equal to that expected from the SCDOT SDS and may be conservative given the development of cracks along the length of the pile.

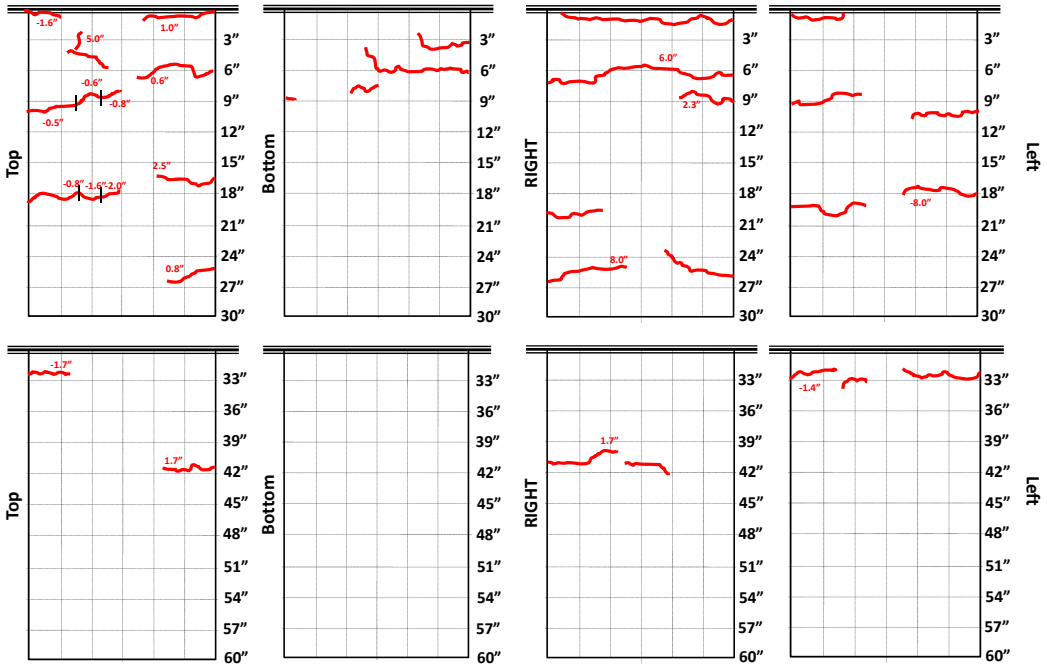

Figure 7.22 Crack Locations - Specimen EB-26-1

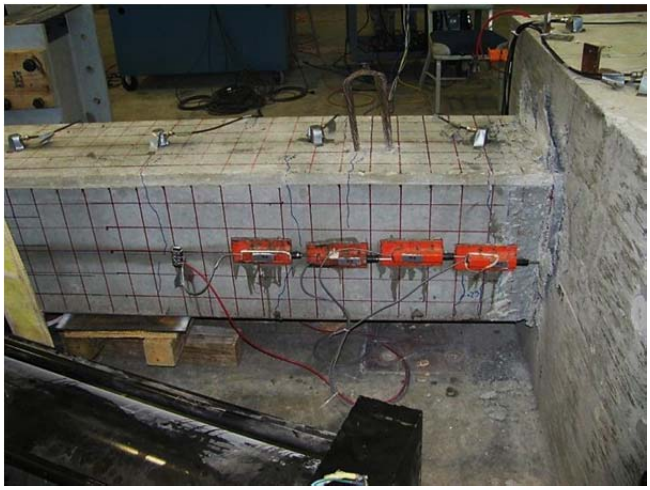

Figure 7.23 Observed Pile Damage - Specimen EB-26-1

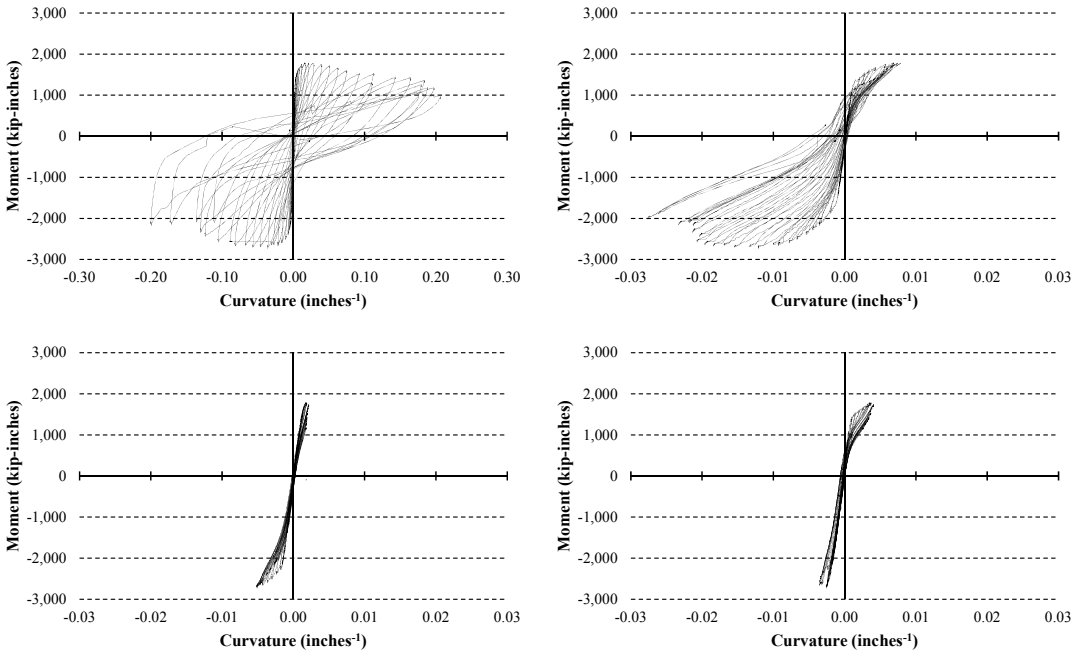

Figure 7.24 Moment versus Curvature - Specimen EB-26-1

Joint Shear Stress, Cap Performance, and Additional Damage Observations

Photographs of the joint region and bent cap following testing are shown in Figure 7.25. A significant amount of damage to the bent cap may be seen. This damage includes spalling of the bent cap concrete about the perimeter of the pile connection as well as cracks extending from the connection into the bent cap.

The spalling extended around the perimeter of the connection and exposed a significant crack in the pile which had developed just inside the interface. Cracking is seen to extend from the connection into the bent cap at the joint. This crack extension into the bent cap is seen in Figure 7.25. The crack extended from the top of the pile at the center of the connection into the bent cap and between the two string potentiometers attached to the bent cap at this location. Additional cracks were observed to develop at the top corners of the connection and to extend into the face of the cap to distances of less than six inches.

The stresses in the joint were calculated according to Figure 7.1 and are shown in Table 7.5. These stresses, including shear stress at the connection and principle tensile and compressive stresses, were below the allowable values established by the SCDOT.

Cap strain gages one and five were placed onto the longitudinal reinforcement closest to the connection. These gages recorded the highest values of 270 and 199 micro-strain. Results from gage one are shown in Figure 7.26.

This specimen was also instrumented with linear potentiometers to determine the point and magnitude at which strands slipped during testing. Although the gage located toward the interior side of the specimen was not active during the time of testing, the gage located on the strand

toward the exterior side of the specimen was able to record slipping of the strand. The results of this gage are shown in Figure 7.27. This figure plots the amount of strand slip versus moment. It can be seen that the exterior strand begins to slip at a moment of approximately 1,440 kip-inches. The strand is observed to slip to a distance of 0.66 inches.

Figure 7.25 Joint Region following Test Completion - Specimen EB-26-1

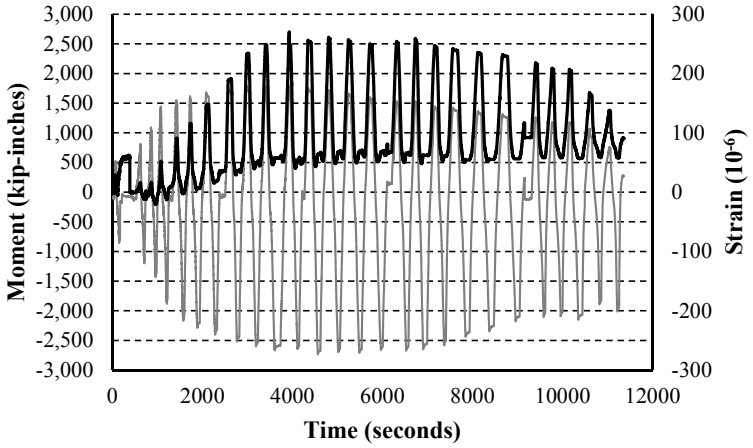

Figure 7.26 Bent Cap Strain - Specimen EB-26-1

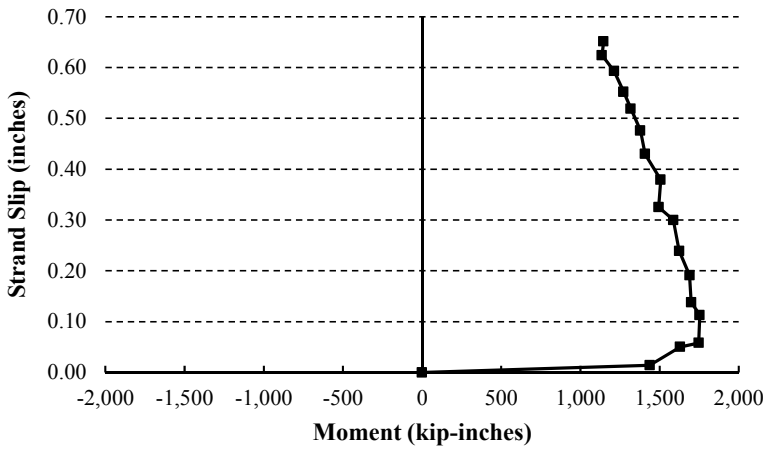

Figure 7.27 Strand Slip versus Moment - Specimen EB-26-1

7.8 Specimen EB-22-1

General Information

Specimen EB-22-1 was the second specimen designed to develop the moment capacity of the pile. This specimen was created with an extension at the exterior end of the bent cap. This extension allowed for additional confinement and associated shrinkage. The design provides a more economical option to develop exterior piles as compared with the heavily reinforced cap of EB-26-1. The specimen also featured a reduced cap depth of two feet six inches as seen previously for specimen IB-22-1.

The bent cap was cast on July 30, 2010. The pile used was taken from the second set of piles cast, and was instrumented with a number of strain gages as well as two vibrating wire strain gages within the embedment region of the pile. The specimen was tested on August 25, 2010, 26 days after casting of the bent cap.

Hysteretic Behavior and Moment Capacity

Figures 7.28 through 7.31 detail the hysteretic behavior including plots of moment versus displacement, moment versus rotation, and both lateral and axial force versus displacement.

Figure 7.28 shows the moment versus displacement results as well as the results of the two numerical models created for this specimen. The specimen is seen to reach a maximum moment in the positive direction of 2,050 kip-inches at a displacement of 3.5 inches. Positive displacements correspond to opening of the joint and axial tensile loads applied to the pile. In the negative direction, corresponding to axial compression, the specimen achieved a maximum moment of 2,830 kip-inches at a displacement of 3.5 inches. Similar to specimen EB-26-1, there is a large difference between moment capacities. Therefore the moment capacity of the specimen is taken as 2,050 kip-inches at approximately 3.5 inches.

In comparison with the numerical models shown in Figure 7.28 the specimen is seen to perform well as compared with either model. In the negative direction the specimen is seen to perform better than either of the predictions. Between displacements of 2.6 and 6.0 inches the experimental behavior matches that of the model which assumes full pile development. The remaining displacement cycles follow the second model.

In the positive direction the specimen again performs better than expected through displacements of 1.8 inch. The remaining displacement cycles of the test match well with the second model. Although the full moment capacity of the pile is not developed in this direction the model nicely predicts specimen behavior.

Applied lateral force versus displacement is shown in Figure 7.29 and applied axial force versus displacement is shown in Figure 7.31. At the 3.5 inch displacement cycles both axial force and lateral force reach maximum values. The applied lateral force reaches 13.9 kips in the positive direction and 18.8 kips in the negative direction. A maximum value of applied axial tension reaches 41.3 kips while a value of 50.3 kips is achieved in axial compression.

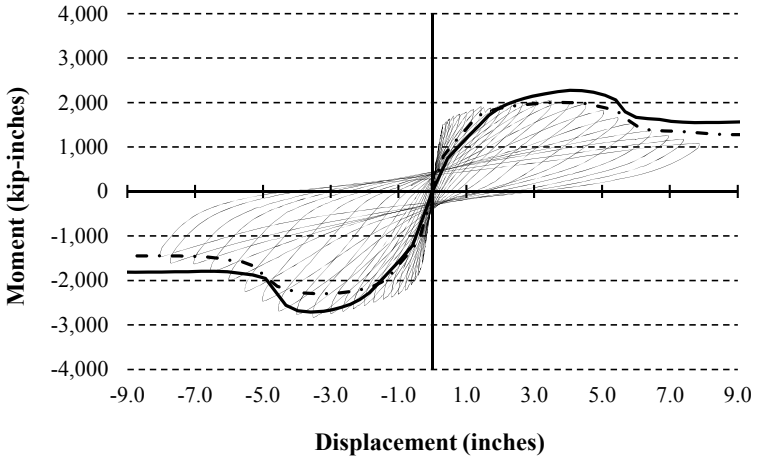

Figure 7.28 Moment versus Displacement - Specimen EB-22-1

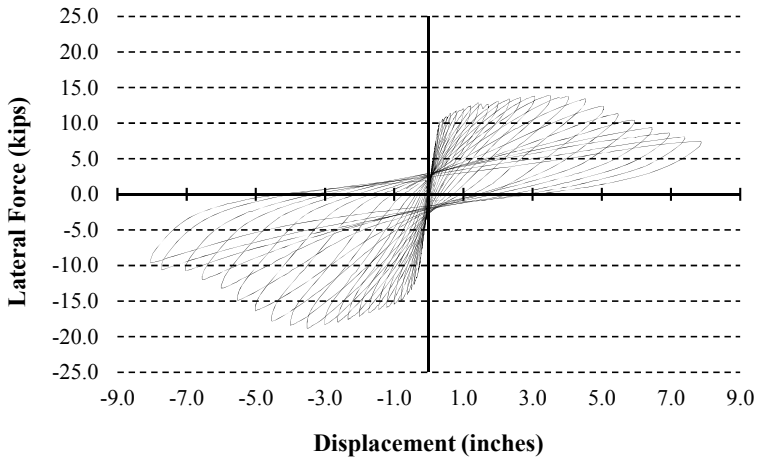

Figure 7.29 Lateral Force versus Displacement - Specimen EB-22-1

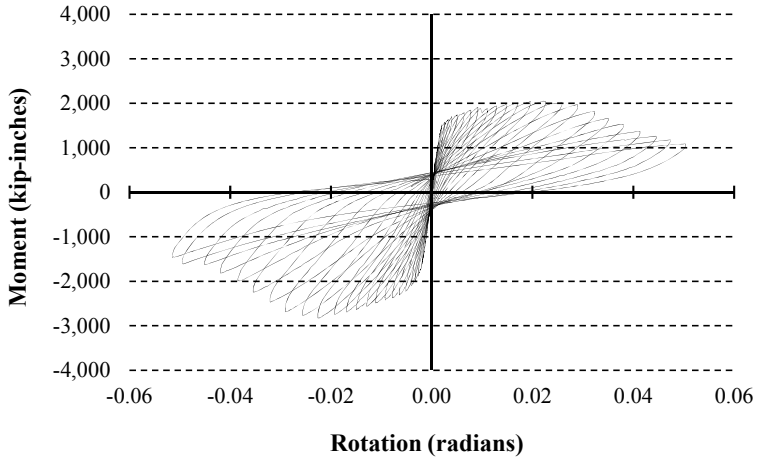

Figure 7.30 Moment versus Rotation - Specimen EB-22-1

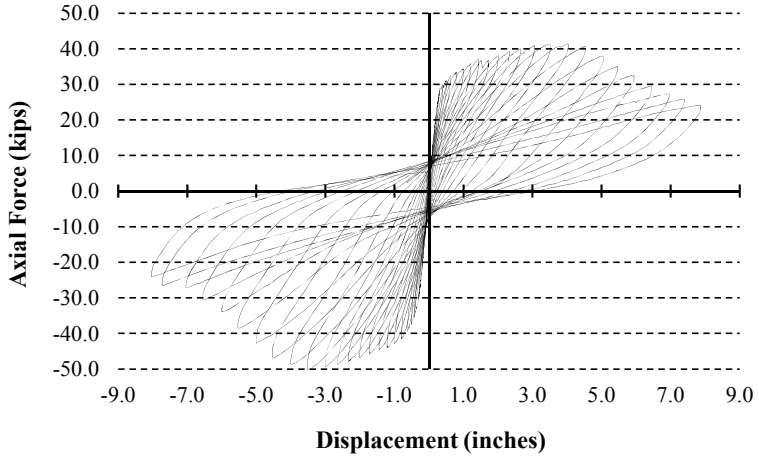

Figure 7.31 Axial Force versus Displacement - Specimen EB-22-1

Ductility Capacity and % Drift

Moment versus displacement behavior is shown again in Figure 7.32. From this plot the ductility capacity is calculated. The black outlined circles on this plot, representing the points at which the specimen is determined to yield, are found at displacements of 0.40 inches in the positive direction and 0.62 inches in the negative direction. The displacement capacities of the specimen seen in the figure with black circles are found at displacements of 6.0 and 5.5 inches in the positive and negative directions, respectively. The directional ductility capacities of the specimen are then found as the directional displacement capacity divided by the corresponding directional yield displacement. In the positive direction the displacement ductility capacity is found to be 15. In the negative direction this value is calculated as 8.8. Again, a large discrepancy is seen in behavior due to the axial loading. Therefore, the ductility capacity is taken as 8.8, which is significantly larger than required.

The large ductility capacity as calculated in the positive direction of displacement is the result of the low amount of degradation in moment capacity through larger displacement cycles. The consistency of developed moment is seen by comparing the behavior in both the positive and negative directions. In the negative direction following the achievement of maximum moment the moment capacity rapidly declines whereas in the positive direction the moment capacity gently drops following the point of maximum moment.

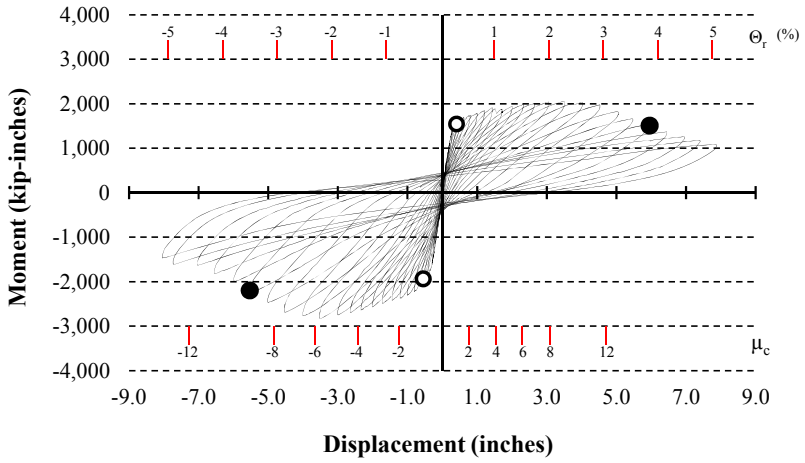

Figure 7.32 Displacement Ductility - Specimen EB-22-1

Plastic Hinge Mechanism and Cracking Pattern

The development of a plastic hinge was expected to occur in the pile extending away from the face of the bent cap. The length of the plastic hinge is estimated based on the observed cracking pattern which developed in the pile as well as the pile curvature data.

Figure 7.33 shows the location of the developed cracks along the length of the pile. From this figure as well as Figure 7.34, which shows a photograph of these cracks, it can be seen that cracks were well distributed along the length of the pile to a distance of 45 inches from the face of the bent cap.

Figure 7.35 shows plots of moment versus curvature at each of the four points of measured curvature. The hysteretic behavior of these plots shows the energy dissipation occurring across the points of measured curvature. From these plots it may be seen that energy dissipation occurred in this specimen through each of the four points of measurement.

Given the distribution of cracking along with the length along the pile to which these cracks developed, as well as the information gathered through the moment versus curvature plots shown in Figure 7.35, a plastic hinge length of 22 inches is estimated.

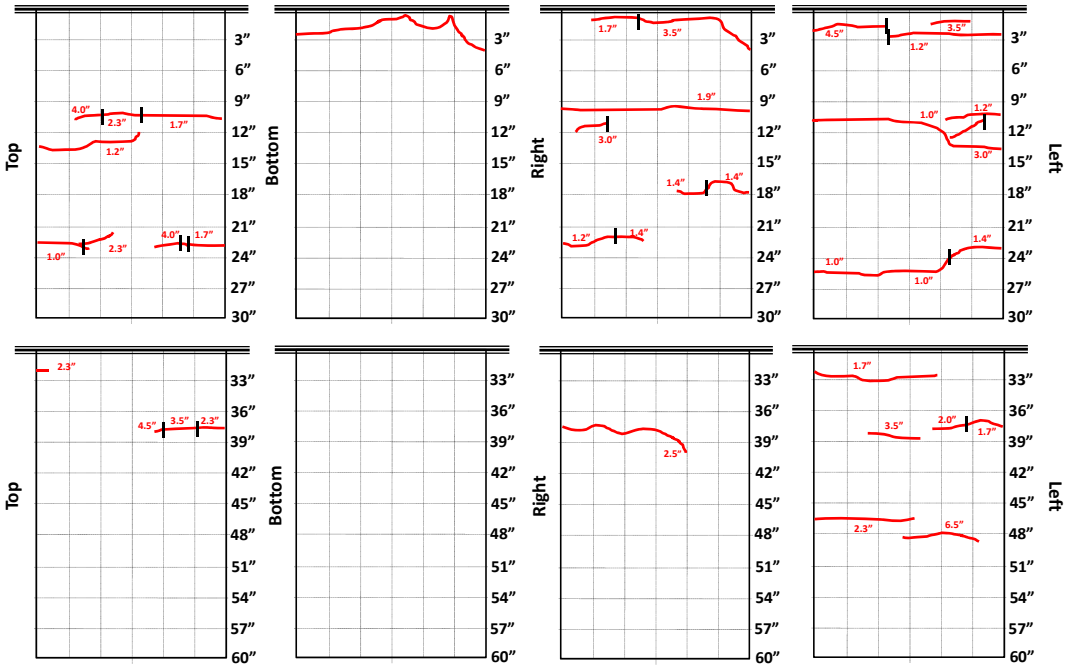

Figure 7.33 Crack Locations - Specimen EB-22-1

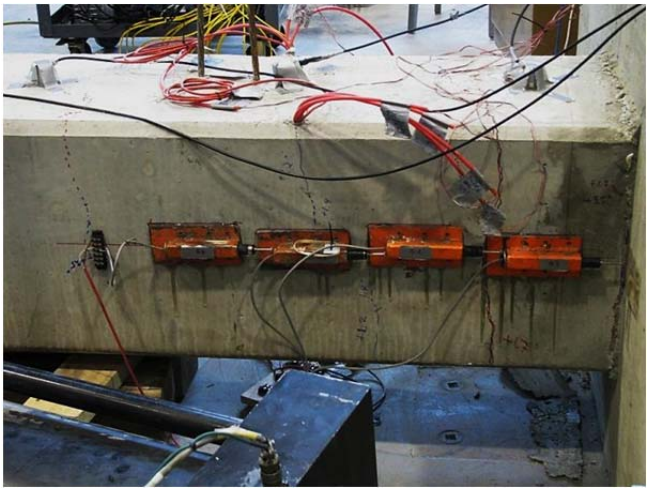

Figure 7.34 Pile Damage - Specimen EB-22-1

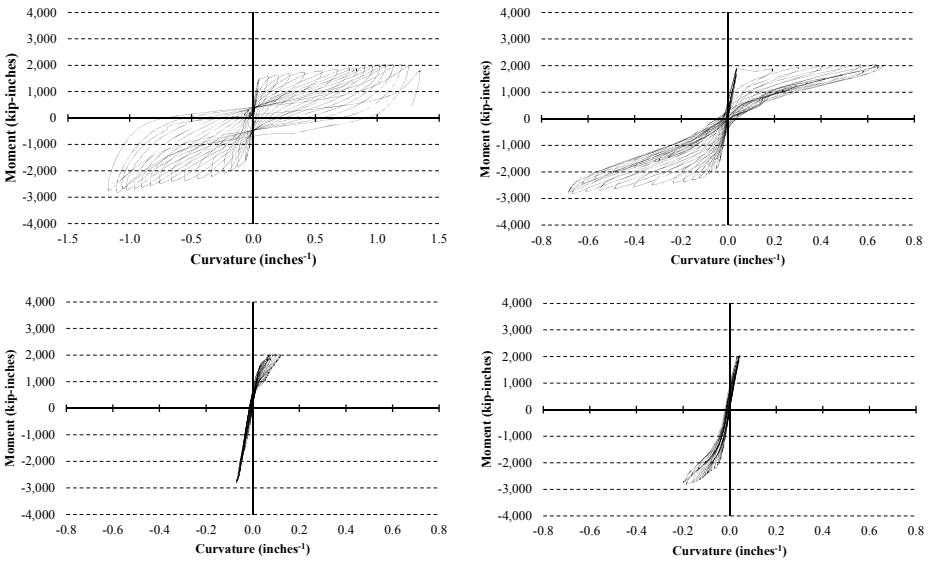

Figure 7.35 Moment versus Curvature - Specimen EB-22-1

Joint Shear Stress, Cap Performance, and Additional Damage Observations

Figure 7.36 shows the soffit following the conclusion of the test. Spalling occurred at the connection about the perimeter of the pile. This photograph also shows a large crack which developed at the connection. Figure 7.37 shows a photograph of cracking which occurred within the bent cap. It may be seen that three cracks developed in the bent cap. Two of these cracks began at the top corners of the connection to the pile and have extended into the bent cap. The third crack, seen on the top face of the bent cap, is near the center of the connection to the pile. Each of these cracks extended into the bent cap to distances greater than 10 inches.

The stresses in the joint region of this bent cap were again calculated using the equations presented in Figure 7.1, and results of these calculations are shown in Table 7.5. Similar to specimen EB-26-1 each of the calculated stresses is less than allowed by design.

As an additional check to the stresses in the joint, the results of the strain gages placed on reinforcement within the bent cap are checked. The maximum strain recorded through testing is found in cap gage two (Figure 7.38). This gage is located at the center of the joint on the longitudinal reinforcement above the joint at the location of the developed cracks. This gage recorded a maximum strain of 500 micro-strain corresponding to 24 percent of the yield strain of the bar.

Figure 7.36 Joint Region following Test Completion - Specimen EB-22-1

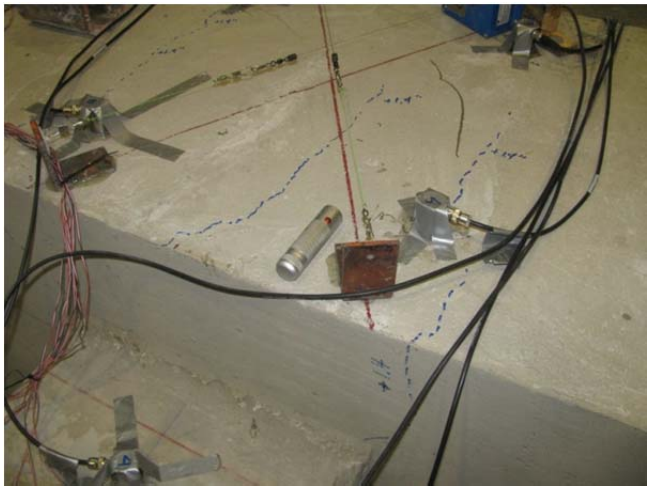

Figure 7.37 Joint Region following Test Completion - Specimen EB-22-1

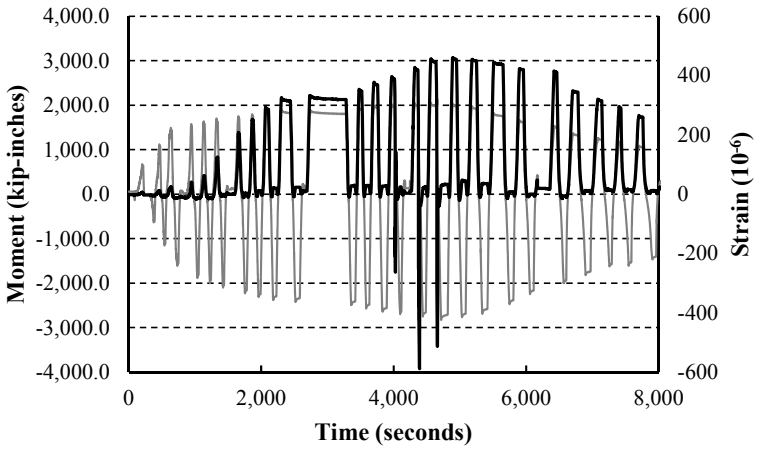

Figure 7.38 Bent Cap Strain - Specimen EB-22-1

This specimen was instrumented with two gages which monitored strand slipping. These gages were mounted to exposed strands on the pile nearest to the plane of displacement. The results of the exterior side gage are shown in Figure 7.39. From this figure the strand to which the gage is instrumented is seen to begin slipping at a moment of 1,700 kip-inches. By the termination of the test the strand had slipped to a level of 0.09 inches.

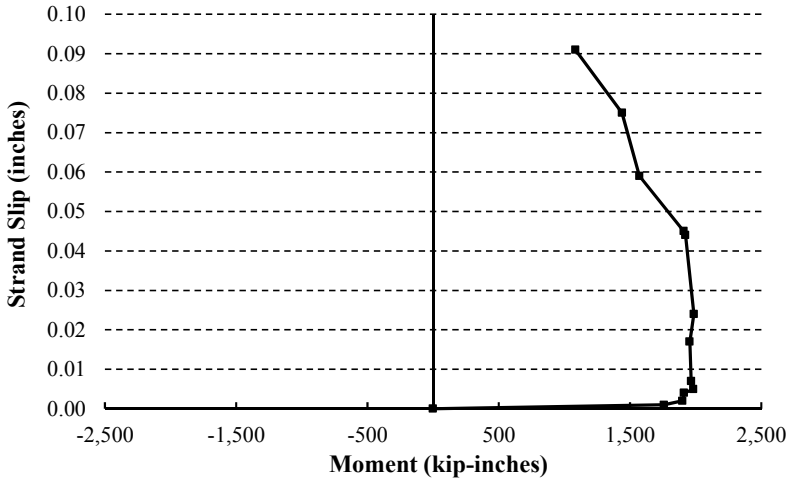

Figure 7.39 Strand Slip versus Moment - Specimen EB-22-1

Table 7.5 Joint Stress Calculation Results

	Direction	Principle Tensile Stress (ksi)	Principle Tensile Allowable (ksi)	Principle Compressive Stress (ksi)	Principle Compressive Allowable (ksi)	Shear Stress (ksi)
Specimen						
EB-18-1	**Opening**	-	-	-	-	-
	Closing	-	-	-	-	-
EB-2-1	**Opening**	0.039	0.250	0.028	1.275	0.033
	Closing	0.043	0.250	0.046	1.275	0.042
EB-26-1	**Opening**	0.093	0.237	0.069	1.15	0.077
	Closing	0.121	0.237	0.131	1.15	0.117
EB-22-1	**Opening**	0.127	0.235	0.094	1.125	0.105
	Closing	0.152	0.235	0.161	1.125	0.146

Chapter 8 - Three Pile Specimen

Contributed by Dr. David Sanders and Mark Cukrov

8.1 Introduction

The fabrication, instrumentation, test setup, loading protocol, and results for the three pile specimen are discussed in this chapter. This specimen was designed, constructed, and tested in collaboration with the University of Nevada-Reno.

8.2 Specimen fabrication

Pile fabrication and instrumentation

Three piles were fabricated for the specimen at Florence Concrete Products of Sumter, South Carolina. The piles were designed and constructed similar to piles used for the single pile specimens previously described. Piles were cast with a length of 17 feet 6 inches. This distance was determined based on constructability of the specimen along with the desire to maintain an inflection point similar to that used for the single pile specimens. Piles were constructed with nine ½ inch diameter prestressing strands, each stressed to 75 percent of the ultimate tensile strength. The strand orientation is shown in Figure 8.1. A W6 wire spiral with 13 inch interior diameter encased the strands. The W6 spiral was placed with 5 turns at a 1 inch pitch at each pile end. A 1½ inch cover remained between the pile end and the beginning of the spiral. The spiral maintained a 3 inch pitch throughout the remaining length of the pile. In addition to the W6 spiral spanning the length of each pile, a spiral created of No. 3 standard reinforcement (0.375 inch diameter) was used to prevent failure of the pile in the vicinity of the footing. This spiral was placed into each pile at the location that would be connected to the footing in the assembly of the test specimen. The spiral fit directly over the W6 spiral with a 14 inch inside diameter. One and one-half turns of the spiral along with an butt weld were used at either end for closure. In between each end, this spiral was turned eight times at a 3 inch pitch. With this configuration the spiral extended from the base of each pile to a distance of 27 inches. A photograph of a pile during construction is shown in Figure 8.2.

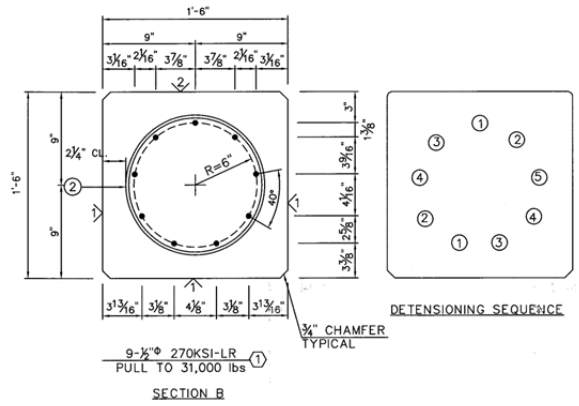

Figure 8.1 Pile Strand Pattern and De-tensioning Sequence - Three Pile Specimen

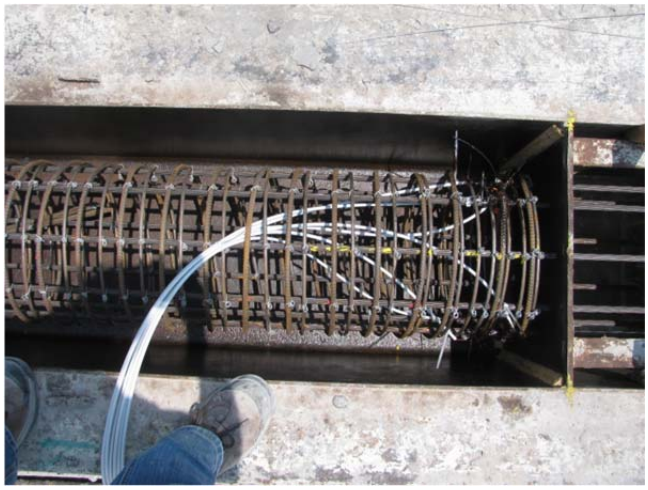

Figure 8.2 No. 3 Spiral - Three Pile Specimen

As stated previously, pile length was determined in an effort to maintain an inflection point similar to that used in the testing of single pile specimens. This length was determined from the results of moment capacity taken from specimens IB-22-1 and EB-2-1. Using the moment capacities of each of these specimens in both the opening and closing directions an estimation of the inflection point with respect to clear pile length was determined. The results and methodology of these calculations are shown in Figure 8.3. Pile lengths were determined based on the calculations performed, embedment depths at either end of the pile, and constructability of the three pile specimen.

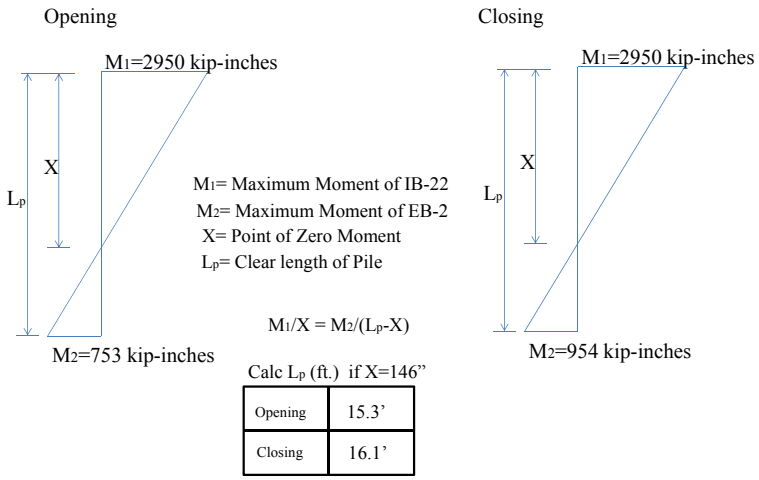

Figure 8.3 Pile Length Calculations - Three Pile Specimen

The piles were designed with a 28-day design compressive strength of 5,000 psi. The concrete mix design used is a proprietary mix of Florence Concrete Products created in accordance with specifications of the SCDOT. Table 8.2 shows the mix design ticket information as provided by Florence Concrete Products. Representatives of the University of South Carolina project team were present at Florence Concrete Products on June 4, 2011, the date piles and test cylinders were cast. Additional onsite quality tests were performed by representatives of Florence Concrete Products. These tests included bulk unit weight, concrete temperature, and air content as reported in Table 8.1.

Table 8.1 Fresh Properties of Piles - Three Pile Specimen

Fresh Properties	
Slump	7.75 inches
% Air	2.7 percent
Concrete temp.	91 °F
Ambient temp.	89 °F
Unit Weight	148 pcf

Table 8.2 Pile Mix Ticket Information - Three Pile Specimen

12:20	**7/14/2011**		**208 FCP**		**Ticket # 18**				
Bed #	**---**								
10A	**440'18" Pile**								
Yards	**Meters**	**Product Description**			**WTR ADJ**		**WTR ADJ(M)**		
5	3.82	0. SC-51309.0E			-5	gal.	-18.93	L	
Bin	**Material**	%	Target	M-	Actual1	M-1	Actual2	M-2	SSD
AG1	**67 Stone**	1.4	9278	4295	9190	lb.	4254.9		1830
Ag2	**Sand**	4.6	6402	2964	6370	lb.	2949.3		1224
Cm1	**Cement**	0	3525	1632	3500	lb.	1620.4		705
Wt1	**Water**	0	95	323	95	gal.	323		34.2
AX3	**Plastiment**	100	150	75	150	oz.	75		30
AX5	**Sikament2100**	100	200	100	200	oz.	100		40
End Load @	12:17		AZ=-40	CZ=-6		95	+	21	116
W/C Ratio:	1391.11/3500	0.397							

The connection between the piles and the footing was designed to behave as a hinge, as for specimen EB-2-1 as described in Chapter 3. The hinge was constructed with four No. 6 (0.75 inch diameter) bars (Figures 8.4 and 8.5). The placement of these dowel bars was completed with a Hilti 150 Max two part high strength epoxy. Two bars in each hinge assembly were instrumented with two 120 ohm resistance strain gages. Upon completion of construction and instrumentation the piles were shipped to the University of Nevada Reno for specimen assembly.

Figure 8.4 Pile Hinge Construction - Three Pile Specimen

Figure 8.5 Pile Hinge Construction - Three Pile Specimen

Bent cap

The bent cap was designed as a combination of single pile test specimens as described in previous chapters. The reinforcement cage used was constructed at the University of South Carolina and shipped along with the piles to the University of Nevada-Reno for assembly.

Based on positive results of certain exterior single pile specimens, two differing designs were chosen for exterior portions of the three pile specimen. The designs were taken from specimens EB-22-1 and EB-26-1. These specimens displayed significantly improved behavior when compared to the standard SCDOT specimen design of EB-18-1. The interior portion of the three pile specimen was held constant with that of the single pile interior specimens. The cap of this specimen was designed with the reduced cap depth of two feet six inches as described for specimens IB-22-1 and EB-22-1. Based on the parametric study, a seven foot center to center distance between piles was maintained. Overhang dimensions of the exterior portions of the bent cap were taken from the single pile specimens of one foot 10 inches and three feet from the

center of the pile for the heavily reinforced and cantilevered exterior specimens, respectively (EB-26-1 and EB-22-1). The overall length of the bent cap was 19 feet 10 inches. The width of the bent cap was maintained from the single pile specimens as three feet. Pertinent dimensions are shown in Figure 8.6.

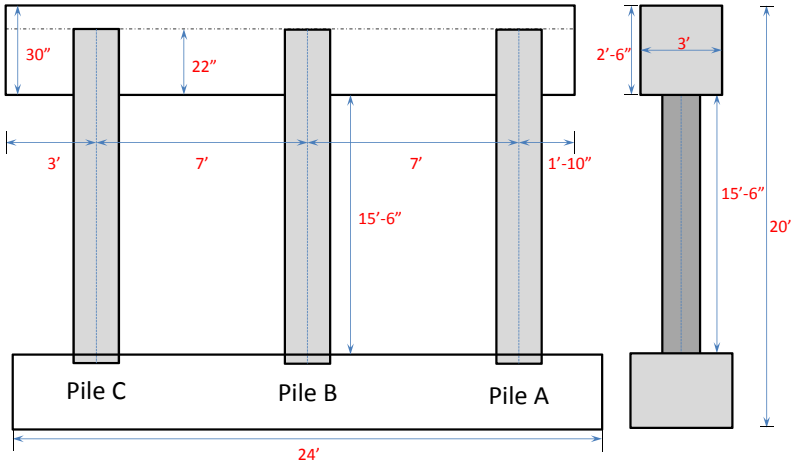

Figure 8.6 Pertinent Dimensions - Three Pile Specimen

Minor changes were made to the reinforcement design at the exterior portions of the bent cap. The reinforcement design is shown in Figures 8.7 through 8.9. The schematic shown in Figure 8.9 details these changes. Among the changes incorporated for the three pile specimen is the use of additional U-bars shown as bold in the schematic. These bars were used to provide further confinement to the pile, and to alleviate cracking of the bent cap seen in the tests of the single pile specimens. These additional bars were bundled to the longitudinal reinforcement.

Photographs of the reinforcement cage prior to shipment are shown in Figures 8.10 through 8.12. Upon arrival at the University of Nevada-Reno, the reinforcement cage was fit with 1.5 inch diameter PVC piping at the locations of applied axial load. These pipes were cast into the bent cap such that axial load could be applied through 5/8 inch diameter threaded steel rods which were later passed through the voids created by the pipes. These pipes were cast into the bent cap at eight locations.

The specimen was tested such that the longitudinal axes of the three piles were parallel to the laboratory floor. Two pipes were cast approximately six inches from the interior face of either exterior pile. The remaining four pipes were cast around the center pile at an offset of approximately six inches. A schematic of these locations is shown in Figure 8.13.

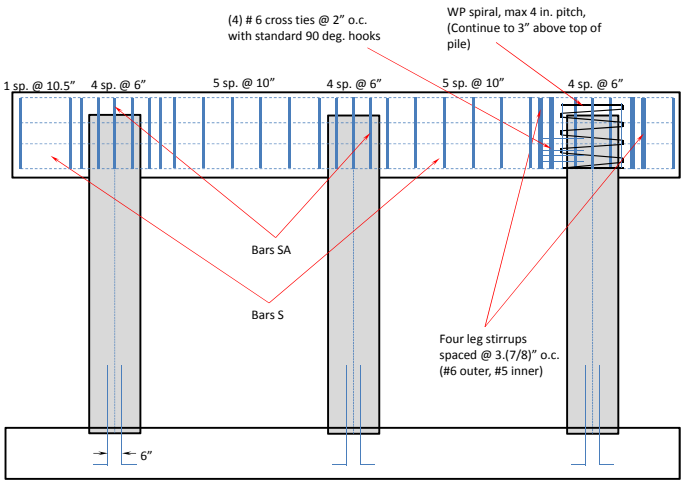

Figure 8.7 Bent Cap Shear Reinforcement - Three Pile Specimen

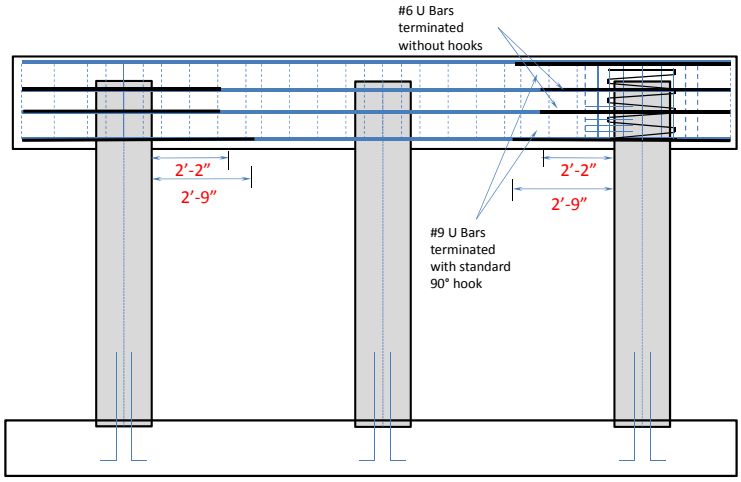

Figure 8.8 Longitudinal Reinforcement - Three Pile Specimen

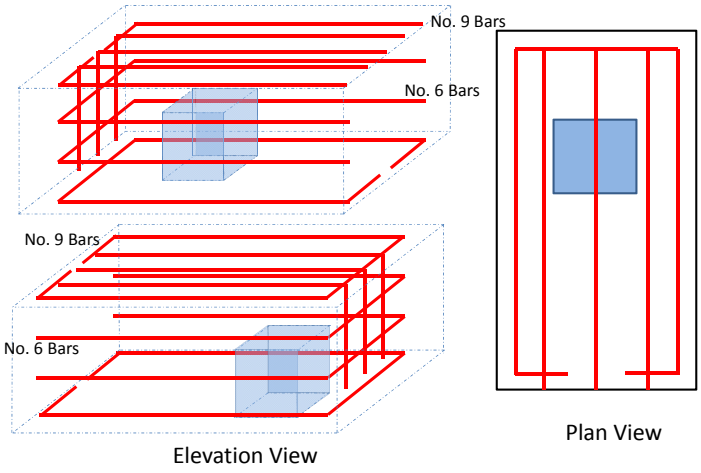

Figure 8.9 Reinforcement Modifications - Three Pile Specimen

Figure 8.10 Reinforcement Cage, Cantilevered End

Figure 8.11 Reinforcement Cage, Interior Portion

Figure 8.12 Reinforcement Cage, Heavily Reinforced End

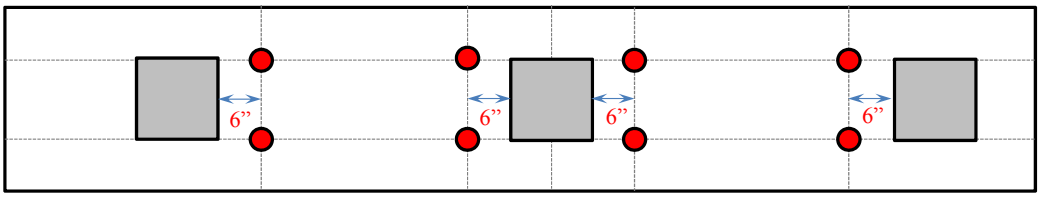

Pipes are shown enlarged for clarity

Figure 8.13 Axial Load Piping Locations - Three Pile Specimen

Footing

The footing was designed at the University of Nevada-Reno. This element was designed to accommodate the bottom of each of the three piles and the threaded rods for the application of axial load. The footing was also designed such that it could be anchored to the University's strong floor using post-tensioning rods. The footing was created with dimensions of 24 feet in length, two feet in width and four feet in height. The reinforcement of the footing (Figure 8.14) was designed conservatively such that all damage in the specimen would be confined to the piles and bent cap.

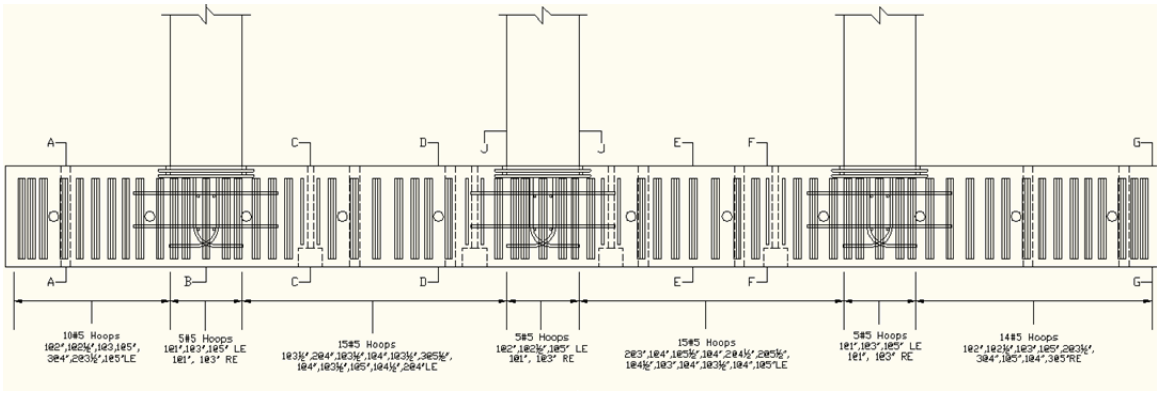

Figure 8.14 Footing Reinforcement - Three Pile Specimen

Assembly

Once the piles and the bent cap reinforcement cage arrived at the University of Nevada-Reno assembly of the specimen began. Pile elevations were maintained with wood cribbing. It was determined that using a high-strength ball bearing pack placed between two abrasion resistant AR500 steel plates was the closest representation of true boundary conditions. This assembly provided free movement and rotation to the bent cap in the two necessary planar directions. Two of these devices were placed beneath the cap for stability. The lower steel plates were placed on the strong floor using Hydro-Stone® while the upper plates were fitted with No. 3 steel dowel bars for anchorage to the bent cap. The bent cap reinforcement cage was then placed in position and instrumented with the piles fitting in their appropriate openings.

Figure 8.15 Bent Cap Prior to Casting - Three Pile Specimen

The reinforcement cage of the footing was built in between the reaction blocks, and cast-in-place when completed. A W21 x 48 steel beam was attached to the top of the bent cap to transfer load from the actuator into the bent cap. The purpose of this beam was to produce an even load transfer into the bent cap which would be more representative of true earthquake loading. Once the transfer beam was attached, eight 24 foot long, 5/8 inch nominal diameter threaded rods were placed through the bent cap and attached to the footing. These rods were used to apply axial load to the system representing the bridge superstructure weight.

8.3 Internal instrumentation

Reinforcement in both the bent cap and piles was instrumented with strain gages at selected locations. The purpose of these gages varied between elements and locations. A total of 18 gages were placed into each of the three piles. The bent cap was instrumented with a total of 15 strain gages. Six additional strain gages were placed on the dowel bars forming the hinge elements within the footings.

Bent cap internal instrumentation

The reinforcement of the bent cap was instrumented with a total of 15 strain gages (model C2A-06-062LW-120, 120 ohm resistance strain gages manufactured by Vishay Micro-Measurements). Within the bent cap five gages were placed on the longitudinal reinforcement at the center of each of the pile embedment regions. Figure 8.16 shows the location of these gages within the bent cap. Figure 8.17 shows a photograph of these gages following placement.

Figure 8.16 Bent Cap Strain Gage Locations - Three Pile Specimen

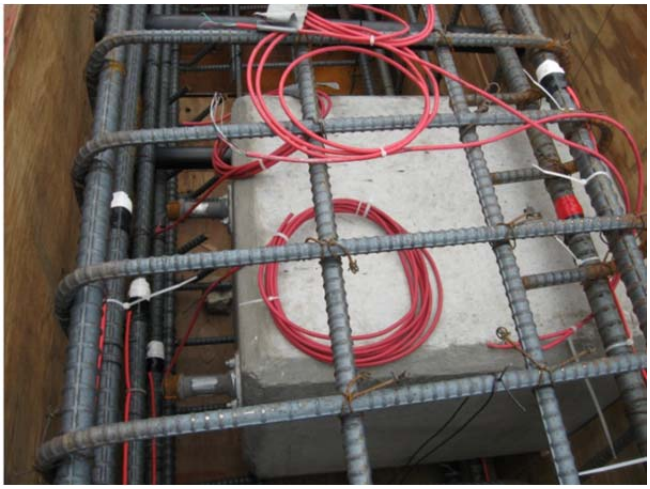

Figure 8.17 Bent Cap Strain Gage Placement - Three Pile Specimen

Pile internal instrumentation

Each pile was instrumented with 18 strain gages of the same type used in the bent cap. The location of these gages can be seen in the schematic of Figure 8.18. In addition to these gages, piles were also instrumented with two Geokon model 4200 vibrating wire strain gages. These gages were oriented both parallel and perpendicular to the eventual direction of displacement. A photograph of these gages prior to casting of the piles is shown in Figure 8.19. Following casting of the piles, two BEI Duncan 9615 linear potentiometers were placed on exposed strands. These gages were used in addition to the strain gages to determine the point and magnitude to which strands slipped during testing. A photograph of the placement of these gages is shown in Figure 8.20.

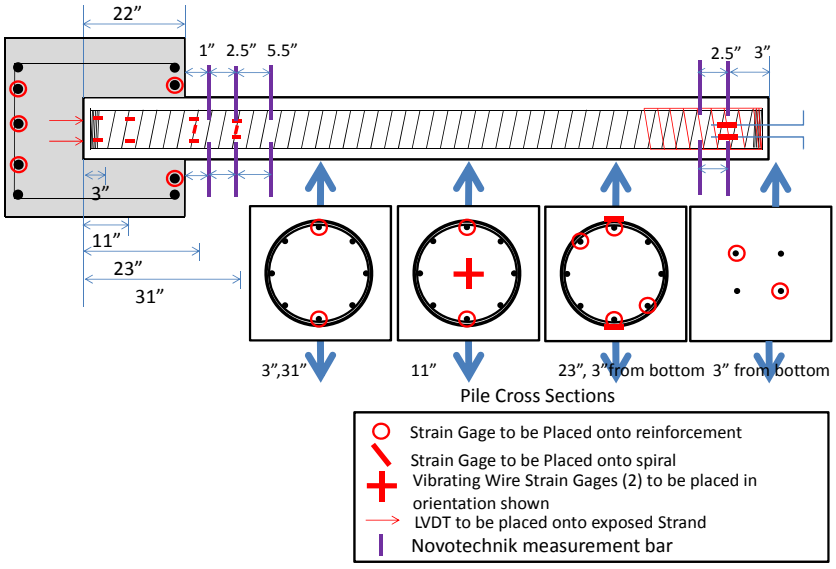

Figure 8.18 Pile Strain Gage Layout - Three Pile Specimen

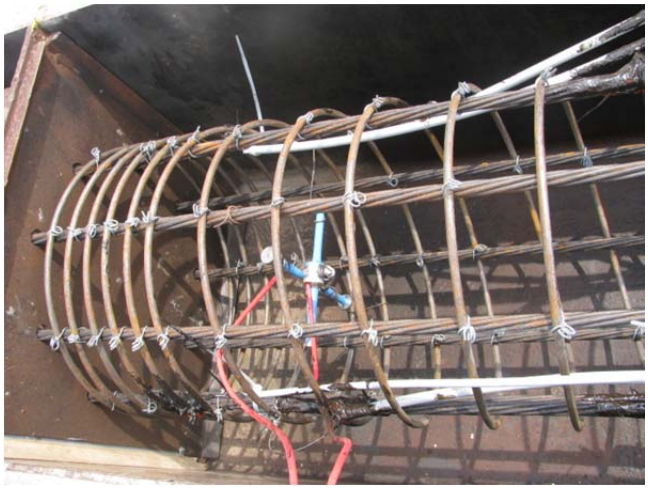

Figure 8.19 Vibrating Wire Strain Gage Placement - Three Pile Specimen

Figure 8.20 Linear Potentiometer Placement - Three Pile Specimen

8.4 Experimental setup

The bent cap and footing were cast in the position in which the specimen was tested. The test was located on a strong floor recently constructed near the current University of Nevada-Reno structures laboratory. In the testing configuration the longitudinal axis of the piles was parallel to the strong floor. This orientation was similar to that used in the experimental setup of the single pile exterior specimens. Figure 8.21 shows the specimen orientation and location. The specimen footing was connected to the strong floor and held in place with a number of high strength steel rods. This connection is shown in Figure 8.22

Figure 8.21 Testing Orientation - Three Pile Specimen

, 

Figure 8.22 Footing Connections - Three Pile Specimen

The specimen bent cap rested on a pair of steel plate and roller sandwich assemblies as previously described. The steel plates in the assembly were 48 inches in length, 0.5 inches in height, and 30 inches in width. These assemblies provided an allowable 24 inches of displacement of the bent cap in either direction. Figures 8.23 and 8.24 show the assembly.

Figure 8.23 Roller Sandwich Assembly - Three Pile Specimen

Figure 8.24 Roller Sandwich Assembly - Three Pile Specimen

Constant axial load was applied to the specimen representing typical dead loads found in South Carolina. The dead load was representative of that imposed by a superstructure as well as the self-weight of the bent cap. Each of the rods was loaded to 18 kips with individual 26 kip capacity Enerpac hollow core rams. The rams were loaded simultaneously ensuring an equal level of pressure was applied to each. Photographs of the axial loading system are shown in Figures 8.25 and 8.26.

Figure 8.25 Axial Loading Setup - Three Pile Specimen

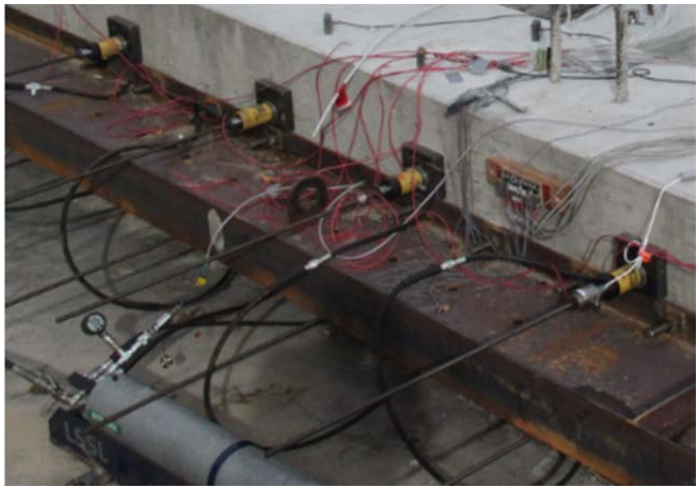

Figure 8.26 Axial Loading Setup - Three Pile Specimen

Transverse load was applied to the specimen through an MTS hydraulic actuator connected to a modified steel W-shape. The actuator was capable of applying 200 kips in tension and compression as well as displacements of ± 15 inches. The W-shape used to transfer the load from the actuator to the bent cap was a W21 x 48 modified for enhanced shear strength. This beam was connected to the bent cap through 1.0 inch diameter ASTM A193 B7 steel rods embedded 22 inches into the cap. Photographs of the loading assembly are shown in Figures 8.27, 8.28, and 8.29.

Figure 8.27 Loading Assembly - Three Pile Specimen

Figure 8.28 Transfer Beam Connection - Three Pile Specimen

Figure 8.29 Loading Assembly - Three Pile Specimen

8.5 External instrumentation

In addition to the instrumentation within the individual elements of the specimen, several additional sensors were applied to the specimen externally to monitor different aspects of behavior.

Thirty six Novetecknic curvature gages were installed at expected plastic hinge regions along the length of each pile and at the connection of each pile to the footing. These gages extended away from each connection at either side of the pile similar to the linear transducers described in Chapter 4. Photographs of these gages are shown in Figures 8.30 and 8.31.

Figure 8.30 Novetecknic Gages - Three Pile Specimen

Figure 8.31 Novetecknic Gages - Three Pile Specimen

Six string potentiometers, placed at various locations on the specimen, were also used during testing. Figure 8.32 provides a schematic of the location of these gages. For the purpose of this report these gages will be referred to as S.P. 1 - 6 (String Potentiometer 1 - 6). S.P. 1 was placed on the actuator piston and was used to measure actuator displacement. S.P. 2 was placed between the bent cap and the footing at the exterior end of the heavily reinforced exterior pile to monitor the relative displacement between the two points. S.P. 3 was used in comparison with S.P. 2 and was placed at the exterior end of the cantilevered exterior pile. S.P. 4 and S.P. 5 were both placed on the end of the bent cap at the cantilevered end. These two gages were then connected to a reference point outside of the lab floor. These gages were used as redundant measurements of displacement as well as any rotation of the bent cap at this end. S.P. 6 was placed in the same manner as S.P. 4 and S.P. 5, this sensor was however connected to the end of the transfer beam. This sensor placement allowed detection of any relative movement between the transfer beam and the bent cap.

The hydraulic actuator was equipped with an internal load cell used to measure transverse loading. Additionally a pressure transducer was used to monitor the axial load applied to the specimen.

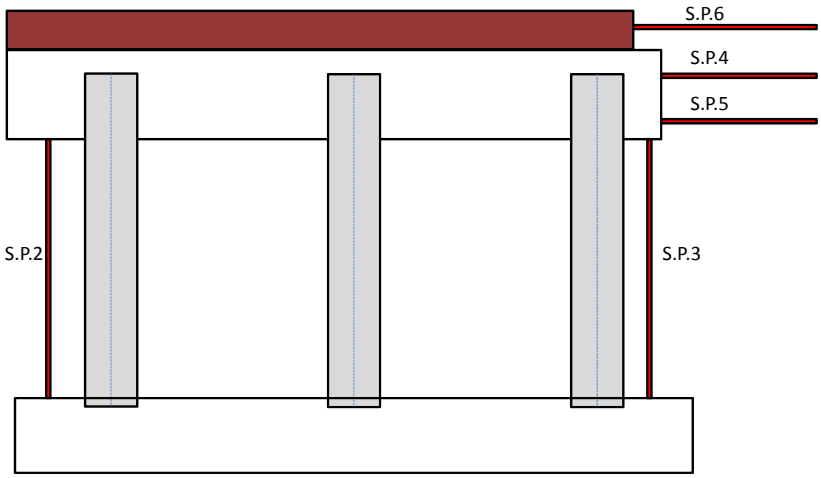

Figure 8.32 String Potentiometer Locations - Three Pile Specimen

8.6 SAP model

A numerical model using SAP2000 was created to determine the ground excitation response of the three pile specimen. Due to the use of an actuator attached to the bent cap as a means of force and displacement application, the response of the three pile specimen was determined with this model. Once the force-displacement response motions were found, they were transferred to the actuator and used as the excitation motion for the three pile system.

A frame model was created using SAP 2000 v.12-15. This model was created using the appropriate material and system properties, as described in Chapter 5. The model was constructed with a set of frame elements used to simulate the bent cap. An additional set of nonlinear links were used to simulate the piles, and a set of rigid links to simulate the portion of the pile embedded in the pile cap as seen in Figure 8.33.

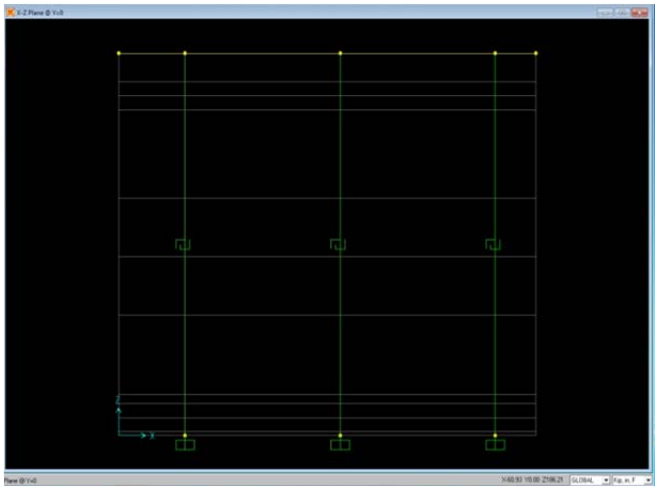

Figure 8.33 Sap Model Construction - Three Pile Specimen

Along with SAP2000, XTRACT was used to determine the moment-curvature relationships along the plastic hinge lengths for each pile. These moment-curvature relationships were used to determine a shear-deformation relationship. The moment outputs were divided by the distance from either the top or the bottom of the pile, depending on the portion of the pile being analyzed, to the inflection point of the moment diagram determined from a pushover analysis. Curvature outputs were used to determine the deformation values in the shear-deformation relationships. The yield curvature was multiplied by the distance previously used producing the yield displacement of that specific portion of the pile. The plastic curvature, defined as the yield curvature subtracted from the ultimate curvature, was multiplied by the plastic hinge length which produced the plastic displacement of a specific portion of the pile. A total pile displacement value is determined through addition. This procedure was performed for multiple points along each moment-curvature diagram. These shear-deformation relationships were defined in the SAP2000 model using nonlinear link elements which were inserted as a representation of the piles in order to complete the model.

An initial set of eight earthquake acceleration time histories were provided by the SCDOT. The three pile model was subjected to each of these time histories to determine the motion to be used for the full-scale experiment. Of the eight motions, the Josh-T motion produced the most deformation in the piles as determined by the SAP2000 model and was therefore selected as the motion for the full-scale test.

8.7 Loading procedure

Once the Josh-T motion was determined to be the testing motion, the acceleration time history was applied to the three pile specimen with increasing amplitude starting at ten percent of the full time history amplitude. The Josh-T motion amplitudes to which the specimen was subjected are shown in Table 8.3. Figure 8.34 shows the displacement versus time response given by Josh-T at amplitude of 1.0. This figure is presented as an aid to the interpretation of hysteretic behavior presented later. Following the completion of each motion a visual inspection of the piles and bent cap was performed.

Table 8.3 Loading Protocol - Three Pile Specimen

Testing Protocol	
Run Number	**Amplitude Josh-T**
1	0.10
2	0.20
3	0.50
4	0.75
5	1.0
6	1.5
7	2.0
8	2.5
9	3.0

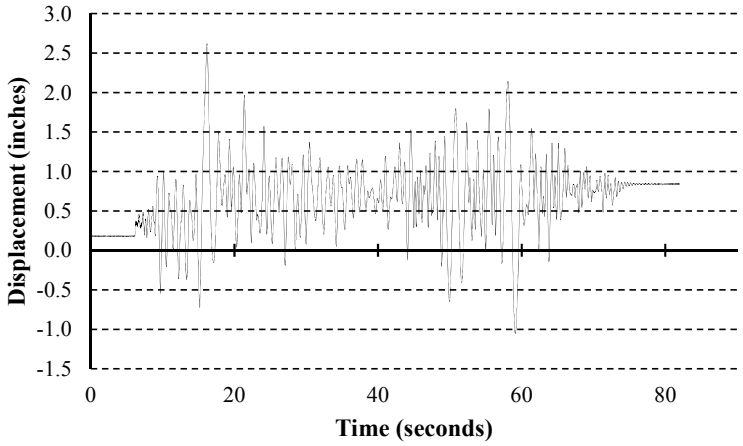

Figure 8.34 Displacement versus Time - 1.0 Josh-T

8.8 Material performance

Piles were cast at Florence Concrete Products of Sumter, South Carolina on July 14, 2011. De-tensioning of the strands took place 24 hours after casting. At the time the strands were released the piles had reached a compressive strength of 5,000 psi. Compressive strength tests were performed at the University of South Carolina at 3, 7, 14, 28, and 56 days. Tests were also performed for split tensile strength and elastic modulus at 28 and 56 days. The results of these tests are shown in Table 8.4. The piles reached a compressive strength of 8,400 psi at 56 days.

The bent cap was cast at the University of Nevada-Reno on October 14, 2011. Similar tests of compressive strength, split tensile strength, and elastic modulus were performed at the University

of Nevada-Reno. Compressive strength tests were performed at 7, 14, and 28 days following casting of the bent cap. Tests of tensile strength and elastic modulus were conducted at 28 and 56 days. Compressive testing was also performed on the day the specimen was tested. The results of these tests are shown in Table 8.5. The bent cap achieved compressive strength of 4,500 psi on the day of testing.

Table 8.4 Material Testing Results - Piles

Date	Day	Sample	Compressive Strength (psi)	Elastic Modulus (ksi)	Split Tensile Strength (psi)
7/15/2011	1	1	5,200		
		2	4,700		
		3	-		
		4			
		Average	4,900		
7/18/2011	3	1	6,500		
		2	6,300		
		3	5,800		
		4			
		Average	6,200		
7/21/2011	7	1	5,700		
		2	6,000		
		3	6,800		
		4			
		Average	6,200		
7/28/2011	14	1	7,500		
		2	7,200		
		3	6,600		
		4			
		Average	7,100		
8/11/2011	28	1	7,200	4,700	630
		2	8,200	5,750	550
		3	7,300	5,570	
		4			
		Average	7,600	5,340	590
9/8/2011	56	1	9,300		560
		2	8,100		600
		3	7,600		510
		4			
		Average	8,400		560

Table 8.5 Material Testing Results - Bent Cap and Footing

Date	Day	Sample	Bent Cap Compressive Strength (psi)	Footing Compressive Strength (psi)
10/21/2011	7	1	3,600	5,300
		2	3,500	5,400
		3	3,400	5,500
		4		
		Average	3,500	5,400
10/28/2011	14	1	4,400	6,200
		2	4,300	6,300
		3	4,000	6,400
		4		
		Average	4,200	6,300
11/11/2011	28	1	4,400	6,400
		2	4,500	6,300
		3	4,500	6,600
		4		
		Average	4,500	6,400
12/8/2011	56	1	4,400	6,600
		2	4,700	6,700
		3	4,500	6,400
		4		
		Average	4,500	6,600

As discussed previously, the piles were fit with two vibrating wire strain gages placed in the eventual embedment region of the pile, one parallel to and the other perpendicular to the direction of displacement. These gages were used to calculate the effective confining stress due to shrinkage. Pertinent data from these gages is shown in Table 8.6.

Table 8.6 Confining Stress Results - Three Pile Specimen

	Pile A (Heavily Reinforced)				Pile B (Interior)				Pile C (Cantilevered End)			
	Gage 1		Gage 2		Gage 3		Gage 4		Gage 5		Gage 6	
	Strain (10^{-6})	σ (psi)	Strain (10^{-6})	σ (psi)	Strain (10^{-6})	σ (psi)	Strain (10^{-6})	σ (psi)	Strain (10^{-6})	σ (psi)	Strain (10^{-6})	σ (psi)
10/15/2011	2,591	-	2,697	-	2,771	-	2,722	-	2,470	-	2,526	-
11/21/2011	2,790	-	2,659	-	2,819	-	2,866	-	2,661	-	2,543	-
Difference	92.6	484	67.6	353	97.0	508	94.6	494	126.8	662	72.8	380
Avg. Stress (psi)	418				500				521			

8.9 Specimen performance

The specimen was subjected to nine earthquake motions. Results from these motions are discussed below.

Hysteretic behavior

The hysteretic behavior was recorded during the application of each earthquake motion. Figures 8.35 through 8.39 detail the hysteretic behavior of the odd numbered runs.

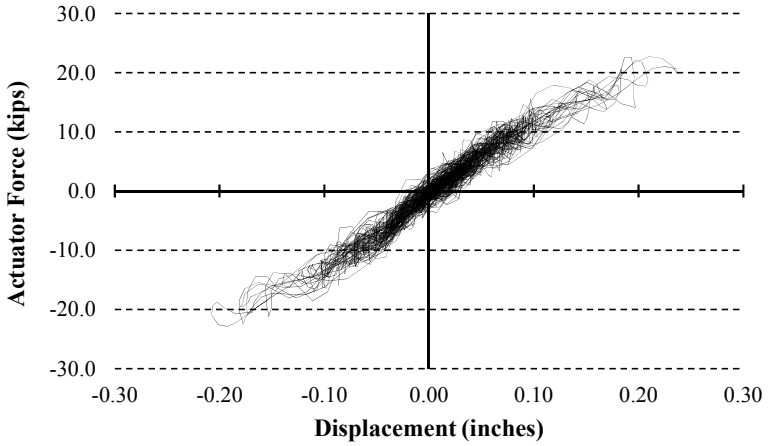

Figure 8.35 Force versus Displacement - 0.1 Josh-T

The first motion applied was 0.10 times the amplitude of the full Josh-T earthquake. As shown in Figure 8.35, the specimen remained elastic during the entire motion which was expected due to the very low displacements in the input motion. It can be seen that deviation from linearity occurs during the application of 1.0 Josh-T.

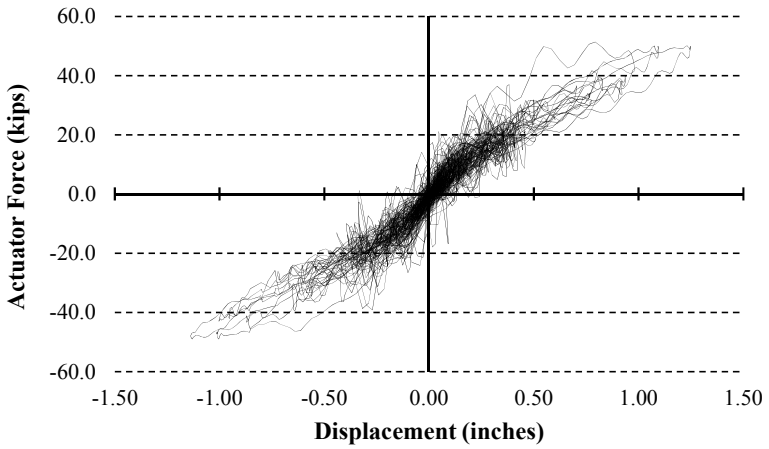

Figure 8.36 Force versus Displacement - 0.5 Josh-T

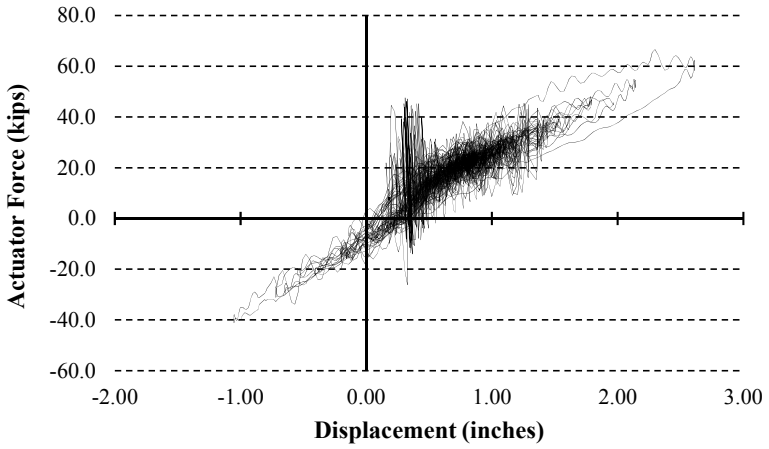

Figure 8.37 Force versus Displacement - 1.0 Josh-T

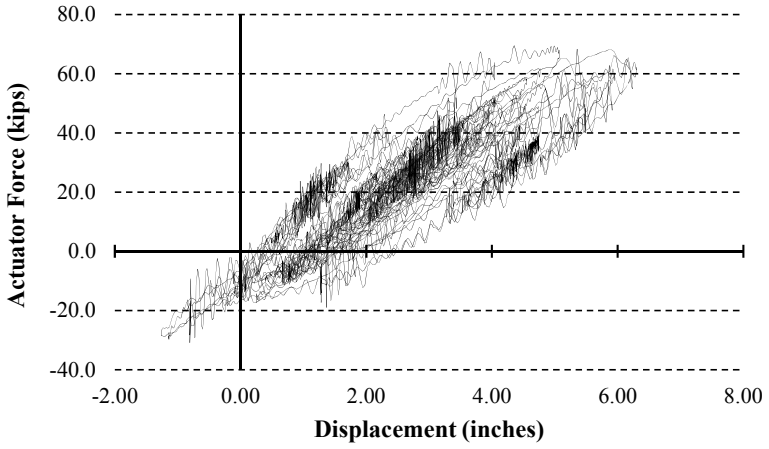

Figure 8.38 Force versus Displacement - 2.0 Josh-T

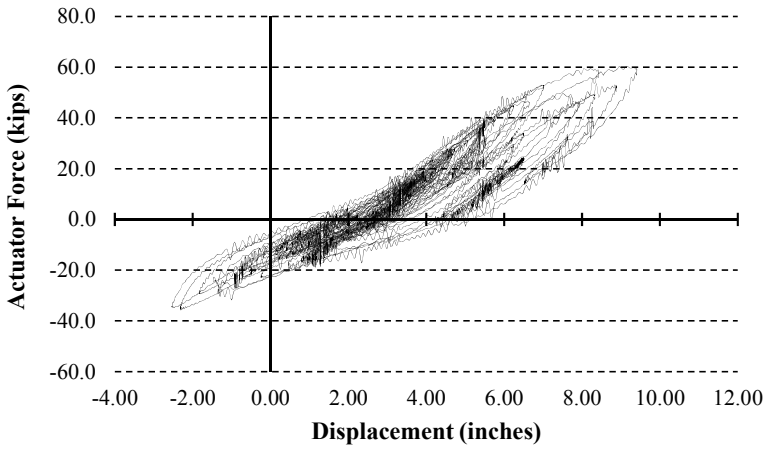

Figure 8.39 Force versus Displacement - 3.0 Josh-T

The final motion to which the specimen was subjected was amplitude 3.0 Josh-T (Figure 8.39). A significant amount of plastic deformation is seen during the application of this motion. Although a significant amount of plastic deformation occurred, the force capacity was not significantly diminished. To establish deterioration in response and establish a maximum capacity the specimen was subjected to displacements of ±12.0 inches.

Pile curvature/plastic hinge mechanism

The force versus curvature relationship is used similar to the moment versus curvature relationships presented in Chapters 6 and 7. This relationship aids in the estimation of the plastic hinge length. Given the nature of the loading protocol used in the test of this specimen, these results may also be used to determine the point at which a plastic hinge begins to develop.

Figures 8.40 and 8.41 detail the force versus curvature relationship as calculated at piles B and C through the first subjected motion of amplitude 0.1 Josh-T. There is little to be seen in terms of energy dissipation at the points of calculated curvature. Through the duration of this motion it can be determined that a significant amount of damage has not occurred within the piles. This is verified in Figure 8.35 which shows linearity of the specimen through the first applied motion in terms of force versus displacement.

Figures 8.42 and 8.43 illustrate the force versus curvature relationship during the application of amplitude 3.0 Josh-T. A significant amount of energy dissipation is observed as determined by the area inside the hysteretic loops. These figures show that the development of a plastic hinge has begun in each of the three piles. A clear difference in terms of magnitude of energy dissipation can be seen in comparing the figures presented for piles B and C. The difference in the curvature relationships indicate a difference in the extent of damage occurring to each of the two piles.

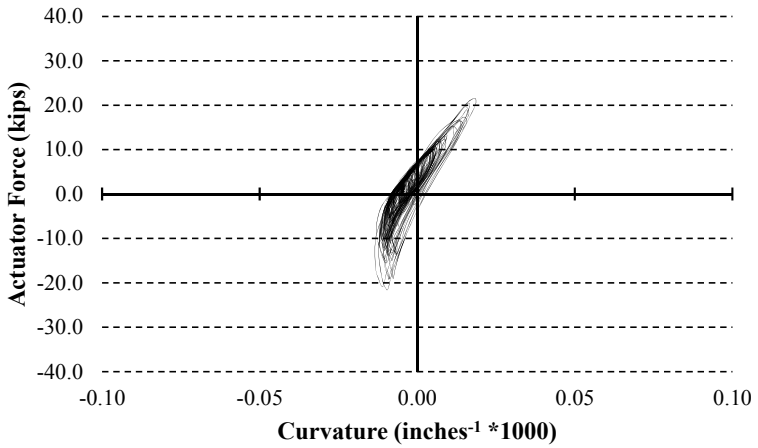

Figure 8.40 Force versus Curvature at Bent Cap Connection - 0.1 Josh-T, Pile B

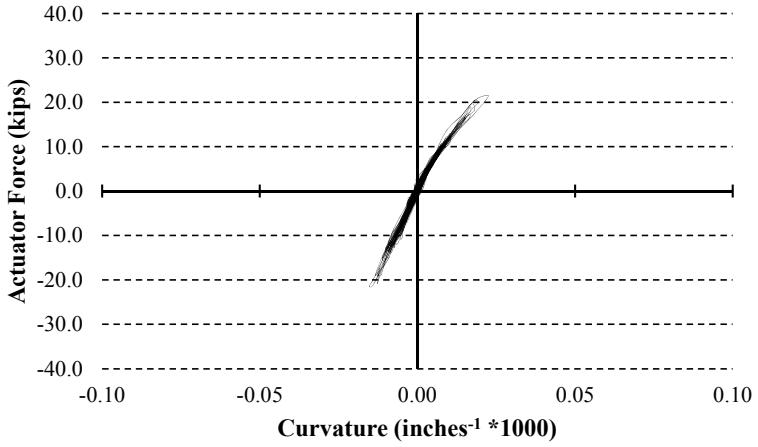

Figure 8.41 Force versus Curvature at Bent Cap Connection - 0.1 Josh-T, Pile C

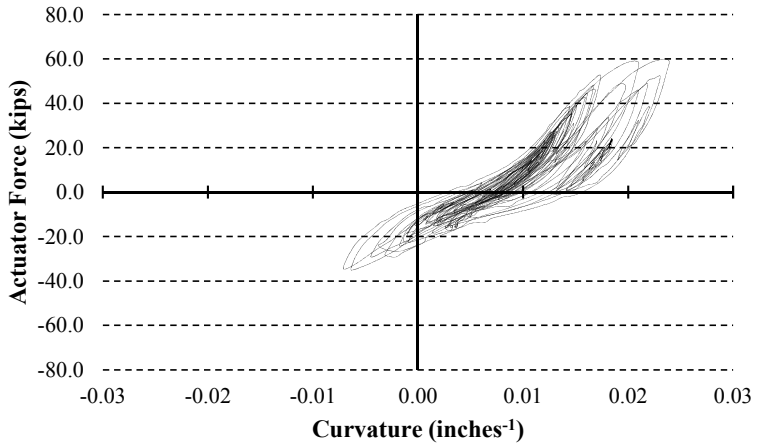

Figure 8.42 Force versus Curvature at Bent Cap Connection - 3.0 Josh-T, Pile B

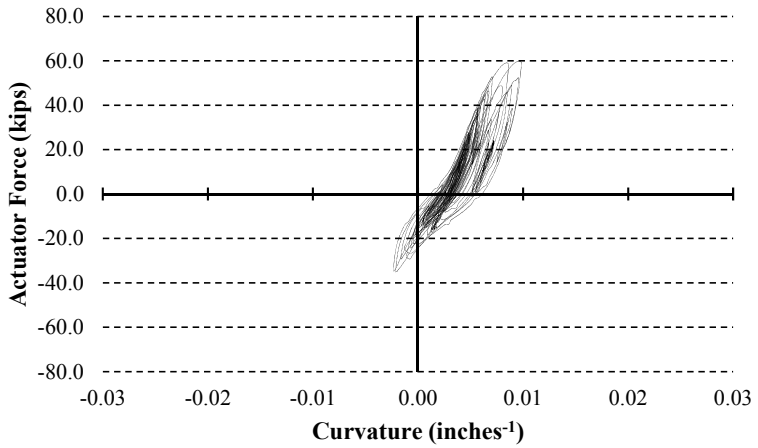

Figure 8.43 Force versus Curvature at Bent Cap Connection - 3.0 Josh-T, Pile C

The curvature data from the 3.0 amplitude of the Josh-T motion shows that the motion displacements were mainly in the positive direction. As the motions increased in amplitude, the residual displacements in the system increased. These displacements were carried over to the motion programmed to the actuator, which produced a response that rarely crossed over into a negative displacement region. Due to the onset of residual displacements, the measured curvature of pile B remains positive during most of the motion.

The curvature of pile B is shown in Figure 8.42. It can be seen that pile C reaches a much smaller magnitude of curvature. This is attributed to the geometry of the three pile specimen.

Strain in bent cap

Strain in the bent cap reinforcement during the application of amplitude 3.0 Josh-T is presented in Figures 8.44 and 8.45. These plots detail the strain versus time recorded at pile A. Figure 8.44 presents the data collected from the strain gage which was placed on the longitudinal reinforcement at the bottom of the bent cap in the center of the connection. Figure 8.45 presents the recorded strain during the same load step, as taken from the gage placed on the longitudinal reinforcement at the top of the bent cap at pile A. As expected, a much larger magnitude of strain is recorded at the bent cap bottom face. At this location strain reached values of approximately 200 micro-strain. This value corresponds to approximately 10 percent of the yield stress.

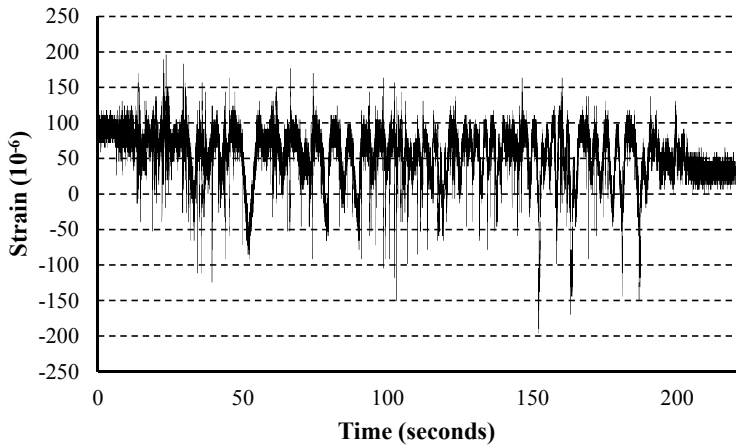

Figure 8.44 Bent Cap Reinforcement Strain - Pile A, Location 1

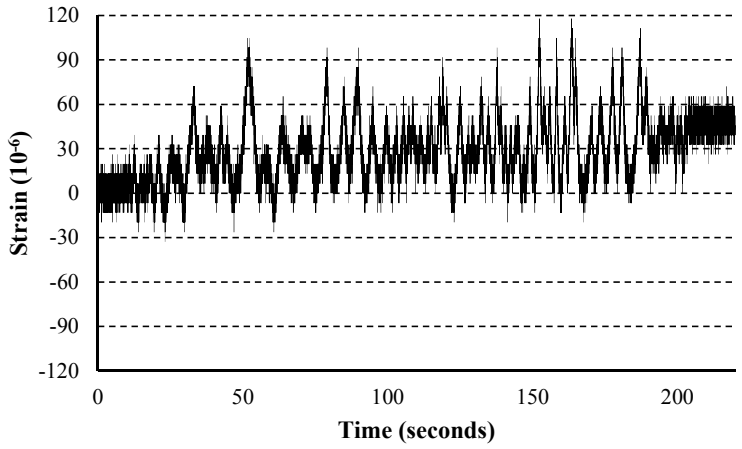

Figure 8.45 Bent Cap Reinforcement Strain - Pile A, Location 3

General observations

The full-scale three pile specimen was subjected to nine earthquake motions with increasing amplitude from 0.10 to 3.0 Josh-T. The specimen exhibited ductile behavior with little damage. Cracking did form at the pile to bent cap connection, though a sudden loss of strength was not observed. Similar to the bent cap, each of the piles of the specimen were observed to perform well.

Bent cap damage

Figures 8.48 through 8.50 show photographs of the bent cap at the connection to each of the three piles. From these photographs it can be seen that the amount of damage differed drastically between connections. The connection to pile A is seen to exhibit spalling about the perimeter of the connection. This connection is also seen to have developed a crack extending from the center of the connection at the top of the pile through the face of the bent cap. This crack is the only crack observed to occur in the bent cap. This spalling and cracking behavior is similar to that

exhibited by specimen EB-26-1 as reported in Chapter 7. This is the single pile specimen which served as the basis for the design of the connection at pile A.

Spalling to a lesser extent was observed about the perimeter of the connection at pile B. The spalling at this location is concentrated at the corners of the connection. This damage can be seen in Figure 8.49. The bent cap at the connection to pile C was observed to be undamaged following the application of the testing protocol. Figure 8.50 shows a photograph of the bent cap at this location.

Figure 8.46 Bent Cap Damage - Following 1.0 Josh-T, Pile A

Figure 8.47 Bent Cap Damage - Following 1.0 Josh-T, Pile A

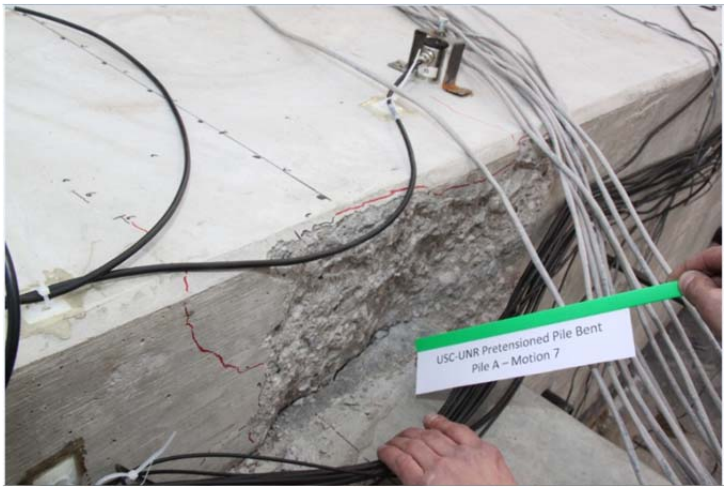

Figure 8.48 Bent Cap Damage - Following 2.0 Josh-T, Pile A

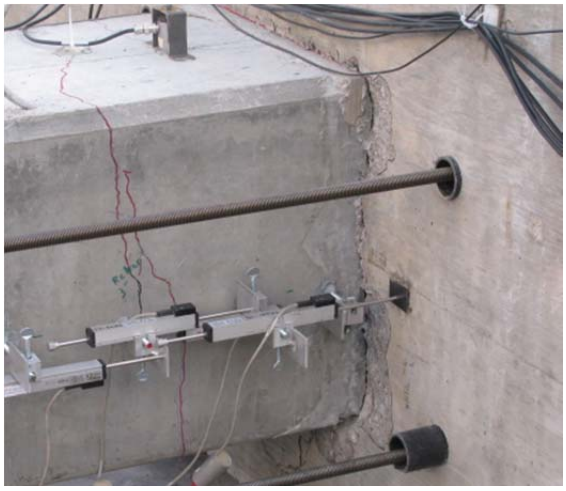

Figure 8.49 Bent Cap Damage - Following 2.0 Josh-T, Pile B

Figure 8.50 Bent Cap Damage - Following 2.0 Josh-T, Pile C

Pile damage

Photographs of each of the piles near the connection are shown in Figures 8.51 through 8.53. Most of the damage in the piles was concentrated at the pile to bent cap connection. Each of the three piles formed cracks within three inches of the bent cap face. Piles A and B had distributed damage along the length of the pile through the expected plastic hinge length in which curvature measurements were recorded. The damage to pile C was concentrated more closely to the connection between the pile and bent cap.

Figure 8.51 Damage to Pile - Following 2.0 Josh-T, Pile A

Figure 8.52 Damage to Pile - Following 2.0 Josh-T, Pile B

Figure 8.53 Damage to Pile - Following 2.0 Josh-T, Pile C

Chapter 9 - Design Guide and Example

Contributed by Drs. Timothy Mays and Jeff Mulliken

9.1 Introduction

This design guide has been developed as an aid to structural engineers, geotechnical engineers, and SCDOT bridge engineers when designing bridges supported on prestressed concrete piles embedded in cast-in-place bent caps in South Carolina. The material presented in this guide is focused on precast prestressed pile bent bridges with cast-in-place bent caps and flat slab superstructures. Similar procedures such as the modeling of the bridge bent and detailing considerations are appropriate for similar bents used for structures such as prestressed girder bridges. The guide uses a practical design analysis example to illustrate the application of research results. Because the research project involves the performance of the pile-to-bent cap connections and the cast-in-place bent cap, the design example focuses on these elements. However, design aids and recommendations related to hinge lengths, soil spring modeling, hysteretic behavior, pile embedment, cap detailing, pile detailing, and superstructure modeling are also provided. In addition, the complete pushover analysis of an example bridge is presented using SAP2000. The soil structure interaction models (i.e., p-y springs) were developed by S&ME, Inc. using LPILE Version 6.0. The design philosophies presented in this design guide are intended to adhere to and/or complement the SCDOT SDS.

9.2 Applicable research results

From the test results of the single pile specimens and the three pile specimen the following recommendations are addressed:

- Piles should be embedded to a depth equal to 1.3 times the pile dimension. A construction tolerance of ±3.0 inches should be allowed.

  Research results show clearly that the previous requirement of 1.0 times the pile dimension (± 6 inches) may result in excessive strand slip and significant reduction in moment capacity, particularly when the -6 inch construction tolerance occurs. Research results also indicate that as the embedment depth increases, moment capacity increases until the pile is fully developed with no measureable strand slip.

- For pile framing into bent cap, $L_p = 0.08L' \geq D^*$

  Research results suggest that the actual hinge length, L_p, for pile-to-bent cap connections is at least one pile dimension (D). Equation 6-2 from SCDOT SDS (SCDOT, 2008) appears to be reasonable and no modification is recommended. In the equation above, L' is the distance from the point of contra-flexure in the pile to the underside of the bent cap.*

- Typical SCDOT bent cap reinforcement details for interior pile-to-bent cap connections are adequate.

Research results manifest that without special reinforcement added to the bent cap, reliable and significant ductile pile behavior can occur in the interior piles with little to no damage to the bent cap.

- Typical SCDOT details for exterior pile-to-bent cap connections are inadequate.

  Research results manifest that without special reinforcement added to the bent cap or significant geometric modifications, pile hinging does not occur without significant damage to the bent cap. Although three design options are presented in the research, two options are presented in this design guide for end piles: (a) pinned connections and (b) specially reinforced cap detailing at the end of the bent caps.

  Note: Chapter 7 and 8 present research conducted in which an extended bent cap may be used to confine piles and develop the hinging mechanism discussed above.

One of the concerns of the experimental results for the pile-to-bent cap connections is that as the embedment of the pile into the bent cap is reduced, only partial pile moment capacity is achieved due to measureable strand slip. The strand slip mechanism also results in slightly more pinched hysteretic loops. On the surface, this pinching of the hysteretic loops this may seem significant. However, experimental testing at the University of South Carolina and previous research on weak interface pile connections has shown that so long as the hysteretic loops are stable the mechanism is reliable and can achieve significant energy dissipation.

9.3 Moment curvature analysis of pile to bent-cap connections

Table 9.1 presents moment versus curvature results obtained using the Section Designer application within SAP2000 for typical pile sections used for flat slab bridges in South Carolina. The table should be considered a design aid for structural and geotechnical engineers and can be used to select trial sizes and strand configurations for piles prior to performing pushover analysis. Other pile configurations and material properties may be used so long as the design adheres to the SCDOT SDS.

Table 9.1 Recommended Preliminary Design Assumptions for Flat Slab Bridges

Pile Dimension	Strands	M_p (kip-inches)	ϕ_y	ϕ_u	ϕ_u/ϕ_y
24 inch x 24 inch	20 - 0.5 inch	7,022	0.000199	0.00131	6.58
24 inch x 24 inch	20 - 0.5 inch (S)	7,407	0.000199	0.00126	6.33
20 inch x 20 inch	10 - 0.6 inch	4,015	0.000237	0.00162	6.83
20 inch x 20 inch	10 - 0.5 inch (S)	3,431	0.000234	0.00182	7.78
20 inch x 20 inch	9 - 9/16 inch	3,490	0.000182	0.00175	9.61
20 inch x 20 inch	11 - 0.5 inch	3,428	0.000128	0.00173	13.5
18 inch x 18 inch	9 - 1/2 inch	2,504	0.000290	0.00205	7.07
18 inch x 18 inch	8 - 1/2 inch	2,336	0.000254	0.00213	8.39
18 inch x 18 inch	8 - 1/2 inch (S)	2,460	0.000255	0.00206	8.03

Note: (a) Values assume f'_{ce} = 6,500 psi, f_y spiral = 65-70 ksi, W6 spiral @ 2 inches on center, 175 ksi in strand after losses

(b) Values assume axial load for seismic load case is 50 kips

(c) Elasto-plastic moment curvature values adequate only for preliminary design

9.4 Load path from superstructure to bent cap

Although not specific to the research discussed previously, it is worthwhile to discuss modeling issues specific to flat slab bridges. The actual demand on a pile to bent cap connection is directly related to the accuracy of the load path captured by the finite element model used to analyze the global structure. Traditionally, this bridge type is detailed with deflection joints at the abutments and as continuous over most supports. Expansion/deflection joints are also detailed as necessary at other supports. Joint detailing is dependent on the overall bridge length. Typical details used on SCDOT flat slab bridges are shown in Figure 9.1.

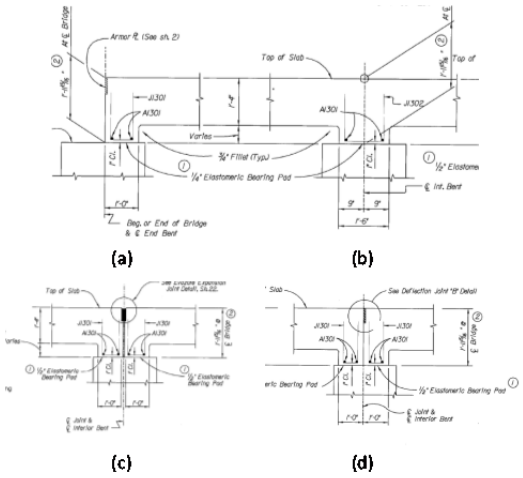

Figure 9.1 Typical Slab Details Used in Flat Slab Bridges

(a) deflection joint at abutment
(b) continuous slab over interior support
(c) expansion joint at interior support, and
(d) deflection joint at interior support

For both flat slab and prestressed concrete girder bridges supported on prestressed piles, the general dynamic behavior is typically governed by the superstructure acting as a rigid diaphragm. This results in fundamental modes primarily in the longitudinal and transverse directions, with some minor contribution by rotational modes about the vertical axis. Therefore, both structure types have similar load paths in which the superstructure modal mass forces are transmitted through bearing pads and anchor bolts or dowels into the bent caps. The end bent caps, along with end diaphragms, in turn transfer load into the abutment fills and piles. Interior bent caps transfer load directly to the piles. As these mechanisms are similar between the bridge types, the example contained in the guide is focused on the flat slab bridge type for simplicity. The approach can be easily modified to address differences, such as bearing type and anchor bolt behavior.

It should be noted that in all cases, the SCDOT Bridge Design Manual (SCDOT, 2006) requires plain elastomeric pads (PEPs) between slabs and bent caps. The SCDOT requires all pads to be neoprene with assumed shear modulus of G = 0.095 to 0.200 ksi. The pads used on South Carolina bridges are typically 0.25 to 0.50 inches thick. The larger thickness is usually used at movement joints where the required service deflection is larger. For seismic design, Section 21.2.2.7 of the Bridge Design Manual limits the maximum load transferred to the cap to 0.4 times the compression force (i.e., dead load) supported by the bearing pad. This is considered an upper bound above which the slab is ideally assumed to slide over the cap under constant shear resistance.

Typical dead load of flat slab bridges supported by an interior bearing pad is 1,500 to 2,500 psf. Hence, during a seismic event, the maximum shear stress in the elastomeric pad prior to sliding is 600 to 1,000 psf. These stresses occur at displacements less than 0.25 inches. Considering the typical pile strengths used for South Carolina bridges, it is clear that in much of the state, the demand transferred to the bent cap exceeds this limit, and positive anchorage for shear is

required. Some engineers detail special connections to transfer the lateral forces between the slab and the bent cap. This practice is encouraged where necessary. However, many bridge engineers use only the standard SCDOT No. 8 dowel bar detail shown in Figure 9.2 and a shear key detail similar to that shown in Figure 9.3 as additional load path elements.

The No. 8 dowel bar detail allows the slab to move up to ¼ inch in any direction prior to load transfer. When load transfer does occur, the mechanism is a combined shear/bending mechanism. Prior to a steel shear failure occurring, either a plastic hinge mechanism within the dowel forms or concrete crushing becomes excessive.

A detailed nonlinear model of this connection has been created to determine which failure mechanism does occur and what magnitude of load transfer is expected when subjected to the design earthquake. The finite element program SAP2000 was used to model the connection. The dowel was modeled using frame elements. The surrounding concrete was modeled using nonlinear springs that capture the nonlinear material model and actual stiffness of the material. The springs were modeled as compression only springs to account for the appropriate response of the dowel once bending takes place. The model suggests that a reliable transfer of 10 kips minimum to 15 kips maximum per dowel can be expected.

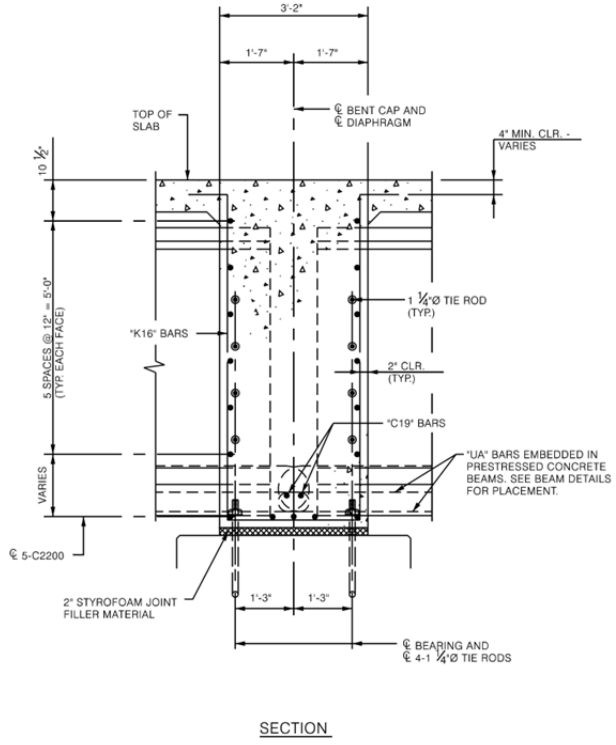

Figure 9.2 Girder Connection Detail

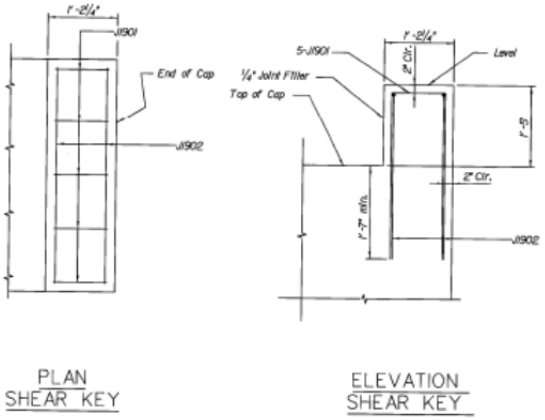

Figure 9.3 Typical Shear Key Detail

The shear key shown in Figure 9.3 is designed using standard shear friction calculations as discussed in Section 9.2 of the SCDOT SDS. No further discussion is provided here.

Finally, additional load transfer in the longitudinal direction is expected at the abutment where longitudinal movement of the abutment cap and back wall results in resisting passive pressure from the soil behind the cap. For short bridges in areas of the state with lower seismicity, the passive pressure resistance may be adequate to resist the entire seismic demand. In contrast, for longer bridges in areas of higher seismicity, the passive pressure resistance may only represent a small fraction of the seismic demand and neglecting its presence may be reasonable. Although not addressed in this design guide, some engineers are detailing more massive abutments for flat slab bridges in order to more effectively utilize the passive pressure at this location. This practice is encouraged where necessary or found to be more economical than traditional detailing.

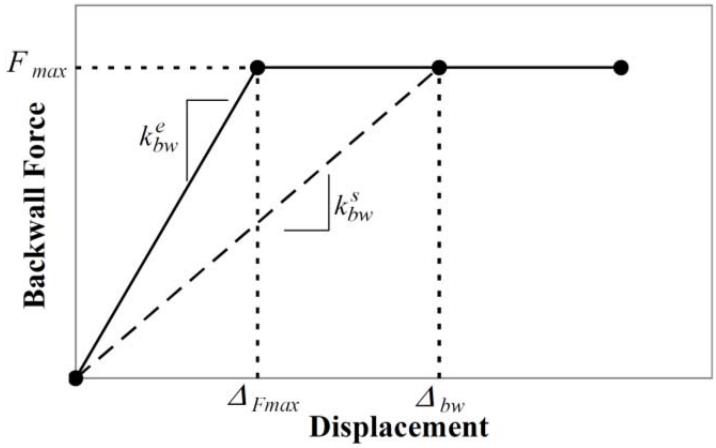

Figure 9.4 Backwall Force versus Displacement Behind Abutment of Flat Slab Bridges

9.5 Example bridge

The example bridge is shown in Figures 9.5 through 9.8. The following information is given:

- The superstructure is assumed to have adequate details to transfer lateral loads to all bent caps.
- The point of fixity for seismic is located 18 feet below ground and has been predetermined.
- f'_c = 4 ksi
- f_y = 60 ksi
- Superstructure weight = 20 kips per foot

For brevity, a 20 inch square pile is selected without detailing the iterative process needed for this selection. For design the iterative process mentioned is a necessity.

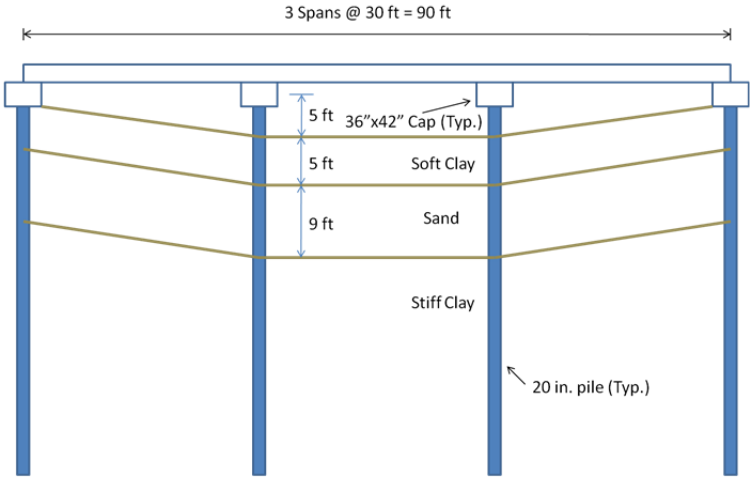

Figure 9.5 Example Bridge Elevation showing Three Span Continuous Slab

From Figure 9.5 and the listed assumptions, the dead load at interior and exterior caps can be calculated as:

Dead load at exterior cap = 240 kips (approximately 3.16 kips per foot acting on cap)

Dead load at interior cap = 660 kips (approximately 8.68 kips per foot acting on cap)

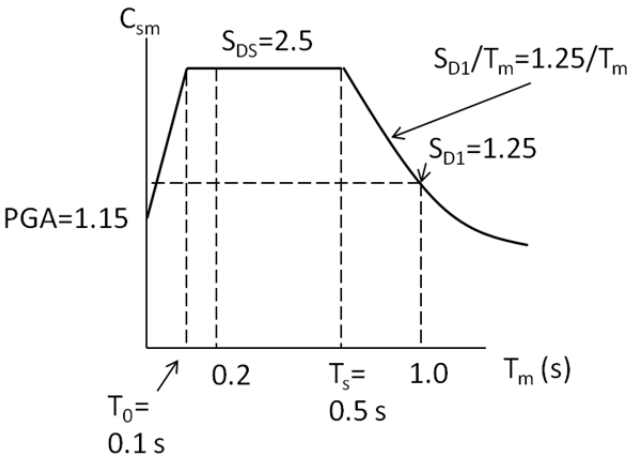

Figure 9.6 Design Response versus Period

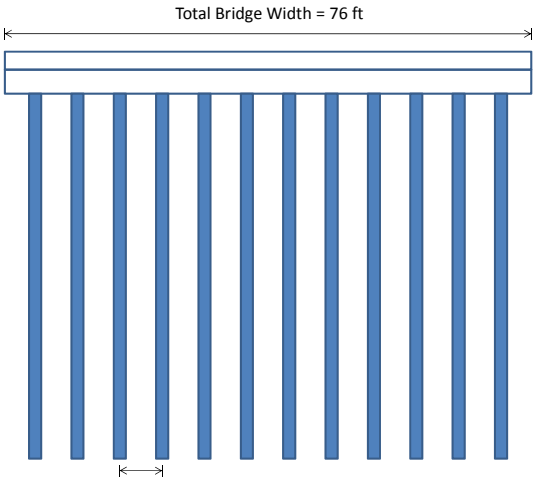

Figure 9.7 Example Bridge Elevation, 12 Piles per Bent
(Typical for Interior and End Bents)

For purposes of this design example it is assumed that the following geotechnical information has been provided:

Lateral load-transfer (p-y) curves were computed and output at seven depths.

Table 9.2 Interior Pile P-Y Curve Information

Depth No.	Depth Below Pile Head (feet)	Depth Below Ground Surface (feet)
1	5.00	0.00
2	10.0	5.00
3	15.0	10.0
4	20.0	15.0
5	25.0	20.0
6	30.0	25.0
7	40.0	35.0

Depth of ground surface below top of pile = 5.00 feet (Figure 9.5)
(See Appendix A for additional interior pile p-y curve information)

Table 9.3 Exterior Pile P-Y Curve Information

Depth No.	Depth Below Pile Head (feet)	Depth Below Ground Surface (feet)
1	1.00	1.00
2	5.00	5.00
3	10.0	10.0
4	15.0	15.0
5	20.0	20.0
6	25.0	25.0
7	35.0	35.0

Depth of ground surface below top of pile = 0.0 feet (Figure 9.5)
(See Appendix B for additional exterior pile p-y curve information)

The curve presented in Figure 9.8 was provided by the geotechnical engineer as the pressure behind the abutment for response in the longitudinal direction.

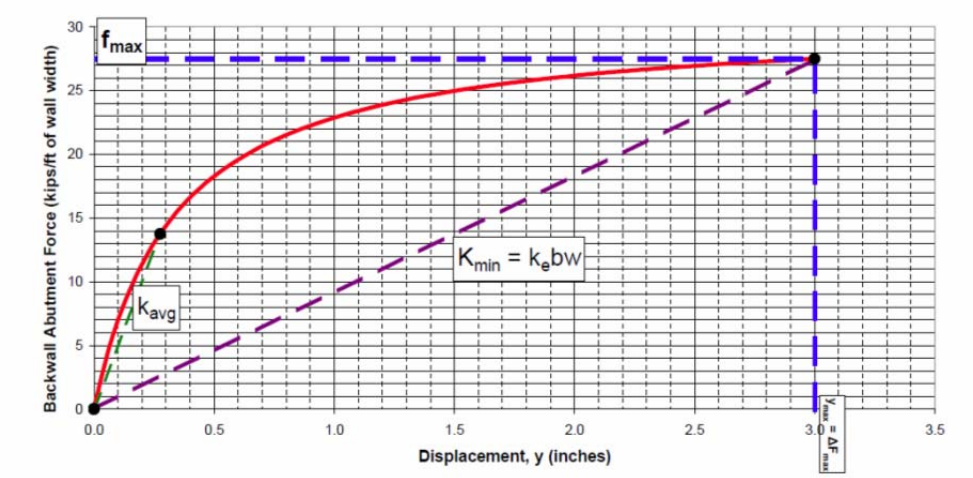

Figure 9.8 Abutment Force versus Displacement

STEP #1 - Convert P-Y data from geotechnical report to P-Y springs needed for structural model

It is important to note that in order to accurately capture the lateral stiffness of the structure using p-y springs, an appropriate number of springs must be used. These springs should be located near the middle of soil layers where possible. The following recommendations typically result in structural models that accurately match the response obtained by the geotechnical engineer using programs such as LPILE Version 6.0.

- Maximum recommended spacing of springs in upper 30 feet of soil is five feet
- Maximum recommended spacing of springs after top 30 feet of soil is ten feet
- Locate springs at least two feet from top or bottom of soil layers if possible

The third recommendation is based on the fact that programs such as LPILE provide p-y springs only for the type of soil present in the layer at the requested location. The spring stiffness is usually specified by the geotechnical engineer in units of pounds per inch per inch (lb/in./in.), thus the structural engineer must multiply the provided spring stiffness by the tributary depth of pile in order to obtain the desired spring stiffness in pounds per inch (lb/in.). When the provided stiffness of the p-y spring is at a soil boundary, the tributary depth is not correct. The depth above the spring is a different soil type than considered in the provided value. For this example, although spring spacing recommendations are adhered to, the locations of some springs are purposely placed near soil layer boundaries. Placement of springs in this example is intended to show error propagation when springs are provided at these locations.

Programs such as LPILE Version 6.0 are becoming so robust that they can now perform much of the nonlinear structural calculations. A general recommendation is to have the geotechnical engineer always simulate soil structure interaction models using elastic properties for the piles and with zero axial load. Although these values will not be used in the final structural models, they are key values needed to calibrate the structural models and to ensure that the inclusion of p-y springs by the structural engineer accurately captures the response of the structure to lateral

forces. The structural model used for pushover analysis (capacity) and modal analysis (demand) should include the appropriate stiffness of the piles and axial effects only after the model is appropriately created using the elastic input.

Spring depths for this example have been chosen at depths of 0, 5, 10, 15, 20, 25, and 35 feet below the ground surface (Figure 9.5). The tributary pile depth and generation of each of these springs is shown in Tables 9.4 and 9.6 for interior and exterior piles respectively. Springs are generated by modeling response to a specified displacement range seen in the tables.

Tables 9.5 and 9.7 show the spring forces developed by each of the springs for interior and exterior piles respectively. These forces are found as the product of the tributary pile length and the spring stiffness from Tables 9.4 and 9.6.

It should be noted that in Table 9.4, the tributary depths of the pile are not simply the tributary length of pile between springs. This would only be the case if all soil were the same type (i.e., one soil layer). Notice that the first soil spring is provided by the geotechnical engineer at the ground surface (depth z = 0 feet). The tributary depth assigned to this soil spring is 5 feet. This depth is assigned as this spring is the only spring located in the first soil layer (see Figure 9.5).

The tributary depth assigned to the soil spring located in the second soil layer is the 2.5 feet below this spring. The portion of soil above this spring is accounted for by the first soil spring located at depth z = 0 feet.

For the third soil spring at depth z = 15 feet the tributary pile length is taken to be 6.5 feet accounting for 2.5 feet of the second soil layer, which has not been accounted for by the second soil spring. The remaining four foot portion of the tributary length is assigned from the third soil layer below this spring. This must be done as the provided spring stiffness is for a given soil type as previously discussed. It should be noted that some accuracy is lost when tributary depths are assigned close to soil boundaries.

Table 9.4 Interior Pile P-Y Spring Generation

Depth (ft.)	0	Depth (ft.)	5	Depth (ft.)	10	Depth (ft.)	15	Depth (ft.)	20	Depth (ft.)	25	Depth (ft.)	35
Trib L (ft.)	5	Trib L (ft.)	2.5	Trib L (ft.)	6.5	Trib L (ft.)	3.5	Trib L (ft.)	5	Trib L (ft.)	7.5	Trib L (ft.)	5
Trib L (in.)	60	Trib L (in.)	30	Trib L (in.)	78	Trib L (in.)	42	Trib L (in.)	60	Trib L (in.)	90	Trib L (in.)	60
y (in.)	p (lb/ in.)	y (in.)	p (lb/ in.)	y (in.)	p (lb/ in.)	y (in.)	p (lb/ in.)	y (in.)	p (lb/ in.)	y (in.)	p (lb/ in.)	y (in.)	p (lb/ in.)
-50	-300	-50	-471	-50	-1262	-50	-2110	-50	-2684	-50	-3240	-50	-3240
-7.5	-300	-20.8	-471	-20.8	-1262	-4.5	-2110	-4.5	-2684	-4.5	-3240	-4.5	-3240
-4	-300	-0.750	-471	-0.750	-1262	-4	-2110	-4	-2684	-4	-3240	-4	-3240
-1.5	-216	-0.542	-369	-0.542	-990	-2	-1774	-2	-2257	-2	-2725	-2	-2725
-1.375	-210	-0.333	-268	-0.333	-717	-1	-1492	-1	-1898	-1	-2291	-1	-2291
-1.25	-204	-0.306	-254	-0.306	-680	-0.4	-1186	-0.4	-1509	-0.4	-1822	-0.4	-1822
-1.125	-197	-0.278	-239	-0.278	-642	-0.3	-1104	-0.3	-1405	-0.3	-1696	-0.3	-1696
-1	-189	-0.250	-225	-0.250	-602	-0.2	-998	-0.2	-1269	-0.2	-1532	-0.2	-1532
-0.875	-181	-0.222	-209	-0.222	-561	-0.1	-839	-0.1	-1067	-0.1	-1288	-0.1	-1288
-0.75	-172	-0.194	-193	-0.194	-517	-0.04	-667	-0.04	-849	-0.04	-1025	-0.04	-1025
-0.625	-162	-0.167	-176	-0.167	-471	-0.02	-561	-0.02	-714	-0.02	-862	-0.02	-862
-0.5	-150	-0.139	-157	-0.139	-421	4E-3	-375	4E-3	-477	4E-3	-576	4E-3	-576
-0.375	-136	-0.111	-137	-0.111	-368	2E-3	-316	2E-3	-401	2E-3	-484	2E-3	-484
-0.25	-119	-0.083	-115	-0.083	-309	4E-4	-211	4E-4	-268	4E-4	-324	4E-4	-324
-0.125	-94	-0.056	-90.0	-0.056	-241	2E-4	-177	2E-4	-226	2E-4	-272	2E-4	-272
-0.004	-30	-0.028	-59.0	-0.028	-158	4E-5	-119	4E-5	-151	4E-5	-182	4E-5	-182
0	0	0	0	0	0	0	0	0	0	0	0	0	0
0.004	30	0.028	59.0	0.028	158	4E-5	119	4E-5	151	4E-5	182	4E-5	182
0.125	94	0.056	90.0	0.056	241	2E-4	177	2E-4	226	2E-4	272	2E-4	272
0.25	119	0.083	115	0.083	309	4E-4	211	4E-4	268	4E-4	324	4E-4	324
0.375	136	0.111	137	0.111	368	2E-3	316	2E-3	401	2E-3	484	2E-3	484
0.5	150	0.139	157	0.139	421	4E-3	375	4E-3	477	4E-3	576	4E-3	576
0.625	162	0.167	176	0.167	471	0.02	561	0.02	714	0.02	862	0.02	862
0.75	172	0.194	193	0.194	517	0.04	667	0.04	849	0.04	1025	0.04	1025
0.875	181	0.222	209	0.222	561	0.1	839	0.1	1067	0.1	1288	0.1	1288
1	189	0.250	225	0.250	602	0.2	998	0.2	1269	0.2	1532	0.2	1532
1.125	197	0.278	239	0.278	642	0.3	1104	0.3	1405	0.3	1696	0.3	1696
1.25	204	0.306	254	0.306	680	0.4	1186	0.4	1509	0.4	1822	0.4	1822
1.375	210	0.333	268	0.333	717	1	1492	1	1898	1	2291	1	2291
1.5	216	0.542	369	0.542	990	2	1774	2	2257	2	2725	2	2725
4	300	0.75	471	0.75	1262	4	2110	4	2684	4	3240	4	3240
7.5	300	20.8	471	20.75	1262	4.5	2110	4.5	2684	4.5	3240	4.5	3240
50	300	50	471	50	1262	50	2110	50	2684	50	3240	50	3240

**** For depths of 15 ft., 20 ft., 25 ft., and 35 ft., y values less than .002 in. are represented with scientific notation.***

Table 9.5 P-Y Springs for Interior Piles

Depth (ft.)	0	Depth (ft.)	5	Depth (ft.)	10	Depth (ft.)	15	Depth (ft.)	20	Depth (ft.)	25	Depth (ft.)	35
Trib L (ft.)	5	Trib L (ft.)	2.5	Trib L (ft.)	6.5	Trib L (ft.)	3.5	Trib L (ft.)	5	Trib L (ft.)	7.5	Trib L (ft.)	5
Trib L (in.)	60	Trib L (in.)	30	Trib L (in.)	78	Trib L (in.)	42	Trib L (in.)	60	Trib L (in.)	90	Trib L (in.)	60
y (in.)	P (lb)	y (in.)	P (lb)	y (in.)	P (lb)	y (in.)	P (lb)	y (in.)	P (lb)	y (in.)	P (lb)	y (in.)	P (lb)
-50	-1.8E+4	-50	-1.4E+4	-50	-9.8E+4	-50	-8.9E+4	-50	-1.6E+5	-50	-2.9E+5	-50	-1.9E+5
-7.5	-1.8E+4	-20.8	-1.4E+4	-20.8	-9.8E+4	-4.5	-8.9E+4	-4.5	-1.6E+5	-4.5	-2.9E+5	-4.5	-1.9E+5
-4	-1.8E+4	-0.750	-1.4E+4	-0.750	-9.8E+4	-4	-8.9E+4	-4	-1.6E+5	-4	-2.9E+5	-4	-1.9E+5
-1.5	-1.3E+4	-0.542	-1.1E+4	-0.542	-7.7E+4	-2	-7.5E+4	-2	-1.4E+5	-2	-2.5E+5	-2	-1.6E+5
-1.375	-1.3E+4	-0.333	-8.0E+3	-0.333	-5.6E+4	-1	-6.3E+4	-1	-1.1E+5	-1	-2.1E+5	-1	-1.4E+5
-1.25	-1.2E+4	-0.306	-7.6E+3	-0.306	-5.3E+4	-0.4	-5.0E+4	-0.4	-9.1E+4	-0.4	-1.6E+5	-0.4	-1.1E+5
-1.125	-1.2E+4	-0.278	-7.2E+3	-0.278	-5.0E+4	-0.3	-4.6E+4	-0.3	-8.4E+4	-0.3	-1.5E+5	-0.3	-1.0E+5
-1	-1.1E+4	-0.250	-6.7E+3	-0.250	-4.7E+4	-0.2	-4.2E+4	-0.2	-7.6E+4	-0.2	-1.4E+5	-0.2	-9.2E+4
-0.875	-1.1E+4	-0.222	-6.3E+3	-0.222	-4.4E+4	-0.1	-3.5E+4	-0.1	-6.4E+4	-0.1	-1.2E+5	-0.1	-7.7E+4
-0.75	-1.0E+4	-0.194	-5.8E+3	-0.194	-4.0E+4	-0.04	-2.8E+4	-0.04	-5.1E+4	-0.04	-9.2E+4	-0.04	-6.1E+4
-0.625	-9.7E+3	-0.167	-5.3E+3	-0.167	-3.7E+4	-0.02	-2.4E+4	-0.02	-4.3E+4	-0.02	-7.8E+4	-0.02	-5.2E+4
-0.5	-9.0E+3	-0.139	-4.7E+3	-0.139	-3.3E+4	4E-3	-1.6E+4	4E-3	-2.9E+4	4E-3	-5.2E+4	4E-3	-3.5E+4
-0.375	-8.2E+3	-0.111	-4.1E+3	-0.111	-2.9E+4	2E-3	-1.3E+4	2E-3	-2.4E+4	2E-3	-4.4E+4	2E-3	-2.9E+4
-0.25	-7.1E+3	-0.083	-3.5E+3	-0.083	-2.4E+4	4E-4	-8.9E+3	4E-4	-1.6E+4	4E-4	-2.9E+4	4E-4	-1.9E+4
-0.125	-5.7E+3	-0.056	-2.7E+3	-0.056	-1.9E+4	2E-4	-7.5E+3	2E-4	-1.4E+4	2E-4	-2.5E+4	2E-4	-1.6E+4
-0.004	-1.8E+3	-0.028	-1.8E+3	-0.028	-1.2E+4	4E-5	-5.0E+3	4E-5	-9.1E+3	4E-5	-1.6E+4	4E-5	-1.1E+4
0	0	0	0	0	0	0	0	0	0	0	0	0	0
0.004	1.8E+3	0.028	1.8E+3	0.028	1.2E+4	4E-5	5.0E+3	4E-5	9.1E+3	4E-5	1.6E+4	4E-5	1.1E+4
0.125	5.7E+3	0.056	2.7E+3	0.056	1.9E+4	2E-4	7.5E+3	2E-4	1.4E+4	2E-4	2.5E+4	2E-4	1.6E+4
0.25	7.1E+3	0.083	3.5E+3	0.083	2.4E+4	4E-4	8.9E+3	4E-4	1.6E+4	4E-4	2.9E+4	4E-4	1.9E+4
0.375	8.2E+3	0.111	4.1E+3	0.111	2.9E+4	2E-3	1.3E+4	2E-3	2.4E+4	2E-3	4.4E+4	2E-3	2.9E+4
0.5	9.0E+3	0.139	4.7E+3	0.139	3.3E+4	4E-3	1.6E+4	4E-3	2.9E+4	4E-3	5.2E+4	4E-3	3.5E+4
0.625	9.7E+3	0.167	5.3E+3	0.167	3.7E+4	0.02	2.4E+4	0.02	4.3E+4	0.02	7.8E+4	0.02	5.2E+4
0.75	1.0E+4	0.194	5.8E+3	0.194	4.0E+4	0.04	2.8E+4	0.04	5.1E+4	0.04	9.2E+4	0.04	6.1E+4
0.875	1.1E+4	0.222	6.3E+3	0.222	4.4E+4	0.1	3.5E+4	0.1	6.4E+4	0.1	1.2E+5	0.1	7.7E+4
1	1.1E+4	0.250	6.7E+3	0.250	4.7E+4	0.2	4.2E+4	0.2	7.6E+4	0.2	1.4E+5	0.2	9.2E+4
1.125	1.2E+4	0.278	7.2E+3	0.278	5.0E+4	0.3	4.6E+4	0.3	8.4E+4	0.3	1.5E+5	0.3	1.0E+5
1.25	1.2E+4	0.306	7.6E+3	0.306	5.3E+4	0.4	5.0E+4	0.4	9.1E+4	0.4	1.6E+5	0.4	1.1E+5
1.375	1.3E+4	0.333	8.0E+3	0.333	5.6E+4	1	6.3E+4	1	1.1E+5	1	2.1E+5	1	1.4E+5
1.5	1.3E+4	0.542	1.1E+4	0.542	7.7E+4	2	7.5E+4	2	1.4E+5	2	2.5E+5	2	1.6E+5
4	1.8E+4	0.750	1.4E+4	0.750	9.8E+4	4	8.9E+4	4	1.6E+5	4	2.9E+5	4	1.9E+5
7.5	1.8E+4	20.8	1.4E+4	20.8	9.8E+4	4.5	8.9E+4	4.5	1.6E+5	4.5	2.9E+5	4.5	1.9E+5
50	1.8E+4	50	1.4E+4	50	9.8E+4	50	8.9E+4	50	1.6E+5	50	2.9E+5	50	1.9E+5

**** For depths of 15 ft., 20 ft., 25 ft., and 35 ft., y values less than .002 in. are represented with scientific notation.***

Table 9.6 Exterior Pile P-Y Spring Generation

Depth (ft.)	1	Depth (ft.)	5	Depth (ft.)	10	Depth (ft.)	15	Depth (ft.)	20	Depth (ft.)	25	Depth (ft.)	35
Trib L (ft.)	5	Trib L (ft.)	2.5	Trib L (ft.)	6.5	Trib L (ft.)	3.5	Trib L (ft.)	5	Trib L (ft.)	7.5	Trib L (ft.)	5
Trib L (in.)	60	Trib L (in.)	30	Trib L (in.)	78	Trib L (in.)	42	Trib L (in.)	60	Trib L (in.)	90	Trib L (in.)	60
y (in.)	p (lb/ in.)	y (in.)	p (lb/ in.)	y (in.)	p (lb/ in.)	y (in.)	p (lb/ in.)	y (in.)	p (lb/ in.)	y (in.)	p (lb/ in.)	y (in.)	p (lb/ in.)
-10	-335	-40.75	-493	-40.8	-1262	-5	-2120	-5	-2694	-5	-3240	-5	-3240
-7.5	-335	-20.75	-493	-20.8	-1262	-4.5	-2120	-4.5	-2694	-4.5	-3240	-4.5	-3240
-4	-335	-0.750	-493	-0.750	-1262	-4	-2120	-4	-2694	-4	-3240	-4	-3240
-1.5	-241	-0.542	-387	-0.542	-990	-2	-1783	-2	-2266	-2	-2725	-2	-2725
-1.375	-234	-0.333	-280	-0.333	-717	-1	-1499	-1	-1905	-1	-2291	-1	-2291
-1.25	-227	-0.306	-266	-0.306	-680	-0.4	-1192	-0.4	-1515	-0.4	-1822	-0.4	-1822
-1.125	-219	-0.278	-251	-0.278	-642	-0.3	-1109	-0.3	-1410	-0.3	-1696	-0.3	-1696
-1	-211	-0.250	-235	-0.250	-602	-0.2	-1002	-0.2	-1274	-0.2	-1532	-0.2	-1532
-0.875	-202	-0.222	-219	-0.222	-561	-0.1	-843	-0.1	-1071	-0.1	-1288	-0.1	-1288
-0.75	-191	-0.194	-202	-0.194	-517	-0.04	-670	-0.04	-852	-0.04	-1025	-0.04	-1025
-0.625	-180	-0.167	-184	-0.167	-471	-0.02	-564	-0.02	-716	-0.02	-862	-0.02	-862
-0.5	-167	-0.139	-165	-0.139	-421	4E-3	-377	4E-3	-479	4E-3	-576	4E-3	-576
-0.375	-152	-0.111	-144	-0.111	-368	2E-3	-317	2E-3	-403	2E-3	-484	2E-3	-484
-0.25	-133	-0.083	-121	-0.083	-309	4E-4	-212	4E-4	-269	4E-4	-324	4E-4	-324
-0.125	-105	-0.056	-94.3	-0.056	-241	2E-4	-178	2E-4	-227	2E-4	-272	2E-4	-272
-0.004	-33.5	-0.028	-61.9	-0.028	-158	4E-5	-119	4E-5	-152	4E-5	-182	4E-5	-182
0	0	0	0	0	0	0	0	0	0	0	0	0	0
0.004	33.5	0.028	61.9	0.028	158	4E-5	119	4E-5	152	4E-5	182	4E-5	182
0.125	105	0.056	94.3	0.056	241	2E-4	178	2E-4	227	2E-4	272	2E-4	272
0.25	133	0.083	121	0.083	309	4E-4	212	4E-4	269	4E-4	324	4E-4	324
0.375	152	0.111	144	0.111	368	2E-3	317	2E-3	403	2E-3	484	2E-3	484
0.5	167	0.139	165	0.139	421	4E-3	377	4E-3	479	4E-3	576	4E-3	576
0.625	180	0.167	184	0.167	471	0.02	564	0.02	716	0.02	862	0.02	862
0.75	191	0.194	202	0.194	517	0.04	670	0.04	852	0.04	1025	0.04	1025
0.875	202	0.222	219	0.222	561	0.1	843	0.1	1071	0.1	1288	0.1	1288
1	211	0.250	235	0.250	602	0.2	1002	0.2	1274	0.2	1532	0.2	1532
1.125	219	0.278	251	0.278	642	0.3	1109	0.3	1410	0.3	1696	0.3	1696
1.25	227	0.306	266	0.306	680	0.4	1192	0.4	1515	0.4	1822	0.4	1822
1.375	234	0.333	280	0.333	717	1	1499	1	1905	1	2291	1	2291
1.5	241	0.542	387	0.542	990	2	1783	2	2266	2	2725	2	2725
4	335	0.750	493	0.750	1262	4	2120	4	2694	4	3240	4	3240
7.5	335	20.8	493	20.8	1262	4.5	2120	4.5	2694	4.5	3240	4.5	3240
10	335	40.8	493	40.8	1262	5	2120	5	2694	5	3240	5	3240

**** For depths of 15 ft., 20 ft., 25 ft., and 35 ft., y values less than .002 in. are represented with scientific notation.***

Table 9.7 P-Y Springs for Exterior Piles

Depth (ft.)	1	Depth (ft.)	5	Depth (ft.)	10	Depth (ft.)	15	Depth (ft.)	20	Depth (ft.)	25	Depth (ft.)	35
Trib L (ft.)	5	Trib L (ft.)	2.5	Trib L (ft.)	6.5	Trib L (ft.)	3.5	Trib L (ft.)	5	Trib L (ft.)	7.5	Trib L (ft.)	5
Trib L (in.)	60	Trib L (in.)	30	Trib L (in.)	78	Trib L (in.)	42	Trib L (in.)	60	Trib L (in.)	90	Trib L (in.)	60
y (in.)	P (lb)	y (in.)	P (lb)	y (in.)	P (lb)	y (in.)	P (lb)	y (in.)	P (lb)	y (in.)	P (lb)	y (in.)	P (lb)
-10	-2.0E+4	-40.8	-1.5E+4	-40.8	-9.8E+4	-5	-8.9E+4	-5	-1.6E+5	-5	-2.9E+5	-5	-1.9E+5
-7.5	-2.0E+4	-20.8	-1.5E+4	-20.8	-9.8E+4	-4.5	-8.9E+4	-4.5	-1.6E+5	-4.5	-2.9E+5	-4.5	-1.9E+5
-4	-2.0E+4	-0.750	-1.5E+4	-0.750	-9.8E+4	-4	-8.9E+4	-4	-1.6E+5	-4	-2.9E+5	-4	-1.9E+5
-1.5	-1.4E+4	-0.542	-1.2E+4	-0.542	-7.7E+4	-2	-7.5E+4	-2	-1.4E+5	-2	-2.5E+5	-2	-1.6E+5
-1.375	-1.4E+4	-0.333	-8.4E+3	-0.333	-5.6E+4	-1	-6.3E+4	-1	-1.1E+5	-1	-2.1E+5	-1	-1.4E+5
-1.25	-1.4E+4	-0.306	-8.0E+3	-0.306	-5.3E+4	-0.4	-5.0E+4	-0.4	-9.1E+4	-0.4	-1.6E+5	-0.4	-1.1E+5
-1.125	-1.3E+4	-0.278	-7.5E+3	-0.278	-5.0E+4	-0.3	-4.7E+4	-0.3	-8.5E+4	-0.3	-1.5E+5	-0.3	-1.0E+5
-1	-1.3E+4	-0.250	-7.1E+3	-0.250	-4.7E+4	-0.2	-4.2E+4	-0.2	-7.6E+4	-0.2	-1.4E+5	-0.2	-9.2E+4
-0.875	-1.2E+4	-0.222	-6.6E+3	-0.222	-4.4E+4	-0.1	-3.5E+4	-0.1	-6.4E+4	-0.1	-1.2E+5	-0.1	-7.7E+4
-0.75	-1.1E+4	-0.194	-6.1E+3	-0.194	-4.0E+4	-0.04	-2.8E+4	-0.04	-5.1E+4	-0.04	-9.2E+4	-0.04	-6.1E+4
-0.625	-1.1E+4	-0.167	-5.5E+3	-0.167	-3.7E+4	-0.02	-2.4E+4	-0.02	-4.3E+4	-0.02	-7.8E+4	-0.02	-5.2E+4
-0.5	-1.0E+4	-0.139	-4.9E+3	-0.139	-3.3E+4	4E-3	-1.6E+4	4E-3	-2.9E+4	4E-3	-5.2E+4	4E-3	-3.5E+4
-0.375	-9.1E+3	-0.111	-4.3E+3	-0.111	-2.9E+4	2E-3	-1.3E+4	2E-3	-2.4E+4	2E-3	-4.4E+4	2E-3	-2.9E+4
-0.25	-8.0E+3	-0.083	-3.6E+3	-0.083	-2.4E+4	4E-4	-8.9E+3	4E-4	-1.6E+4	4E-4	-2.9E+4	4E-4	-1.9E+4
-0.125	-6.3E+3	-0.056	-2.8E+3	-0.056	-1.9E+4	2E-4	-7.5E+3	2E-4	-1.4E+4	2E-4	-2.5E+4	2E-4	-1.6E+4
-0.004	-2.0E+3	-0.028	-1.9E+3	-0.028	-1.2E+4	4E-5	-5.0E+3	4E-5	-9.1E+3	4E-5	-1.6E+4	4E-5	-1.1E+4
0	0	0	0	0	0	0	0	0	0	0	0	0	0
0.004	2.0E+3	0.028	1.9E+3	0.028	1.2E+4	4E-5	5.0E+3	4E-5	9.1E+3	4E-5	1.6E+4	4E-5	1.1E+4
0.125	6.3E+3	0.056	2.8E+3	0.056	1.9E+4	2E-4	7.5E+3	2E-4	1.4E+4	2E-4	2.5E+4	2E-4	1.6E+4
0.25	8.0E+3	0.083	3.6E+3	0.083	2.4E+4	4E-4	8.9E+3	4E-4	1.6E+4	4E-4	2.9E+4	4E-4	1.9E+4
0.375	9.1E+3	0.111	4.3E+3	0.111	2.9E+4	2E-3	1.3E+4	2E-3	2.4E+4	2E-3	4.4E+4	2E-3	2.9E+4
0.5	1.0E+4	0.139	4.9E+3	0.139	3.3E+4	4E-3	1.6E+4	4E-3	2.9E+4	4E-3	5.2E+4	4E-3	3.5E+4
0.625	1.1E+4	0.167	5.5E+3	0.167	3.7E+4	0.02	2.4E+4	0.02	4.3E+4	0.02	7.8E+4	0.02	5.2E+4
0.75	1.1E+4	0.194	6.1E+3	0.194	4.0E+4	0.04	2.8E+4	0.04	5.1E+4	0.04	9.2E+4	0.04	6.1E+4
0.875	1.2E+4	0.222	6.6E+3	0.222	4.4E+4	0.1	3.5E+4	0.1	6.4E+4	0.1	1.2E+5	0.1	7.7E+4
1	1.3E+4	0.250	7.1E+3	0.250	4.7E+4	0.2	4.2E+4	0.2	7.6E+4	0.2	1.4E+5	0.2	9.2E+4
1.125	1.3E+4	0.278	7.5E+3	0.278	5.0E+4	0.3	4.7E+4	0.3	8.5E+4	0.3	1.5E+5	0.3	1.0E+5
1.25	1.4E+4	0.306	8.0E+3	0.306	5.3E+4	0.4	5.0E+4	0.4	9.1E+4	0.4	1.6E+5	0.4	1.1E+5
1.375	1.4E+4	0.333	8.4E+3	0.333	5.6E+4	1	6.3E+4	1	1.1E+5	1	2.1E+5	1	1.4E+5
1.5	1.4E+4	0.542	1.2E+4	0.542	7.7E+4	2	7.5E+4	2	1.4E+5	2	2.5E+5	2	1.6E+5
4	2.0E+4	0.750	1.5E+4	0.750	9.8E+4	4	8.9E+4	4	1.6E+5	4	2.9E+5	4	1.9E+5
7.5	2.0E+4	20.8	1.5E+4	20.8	9.8E+4	4.5	8.9E+4	4.5	1.6E+5	4.5	2.9E+5	4.5	1.9E+5
10	2.0E+4	40.8	1.5E+4	40.8	9.8E+4	5	8.9E+4	5	1.6E+5	5	2.9E+5	5	1.9E+5

**** For depths of 15 ft., 20 ft., 25 ft., and 35 ft., y values less than .002 in. are represented with scientific notation.***

STEP #2 - Create finite element models of all bents and verify soil stiffness modeling

The geotechnical engineer typically performs free and fixed head analyses of the piles. For calibration of the structural model in this example, the geotechnical engineer is assumed to have utilized LPILE to develop shear, moment, and deflection curves for all typical conditions (i.e., fixed head, free head, interior pile, exterior pile).

Figures 9.9 through 9.20 detail plots of the geotechnical pile models. It should be noted that to generate these curves the piles were assumed to be elastic and without the presence of axial load. In this manner the piles will behave more rigidly than those used in the final structural models. The moment of inertia of the piles in these models was taken as the gross moment of inertia. Axial loads were neglected such that P-delta effects would not suggest more pile flexibility than really exists. P-delta effects are included in the final structural models presented in this example and should be considered in design.

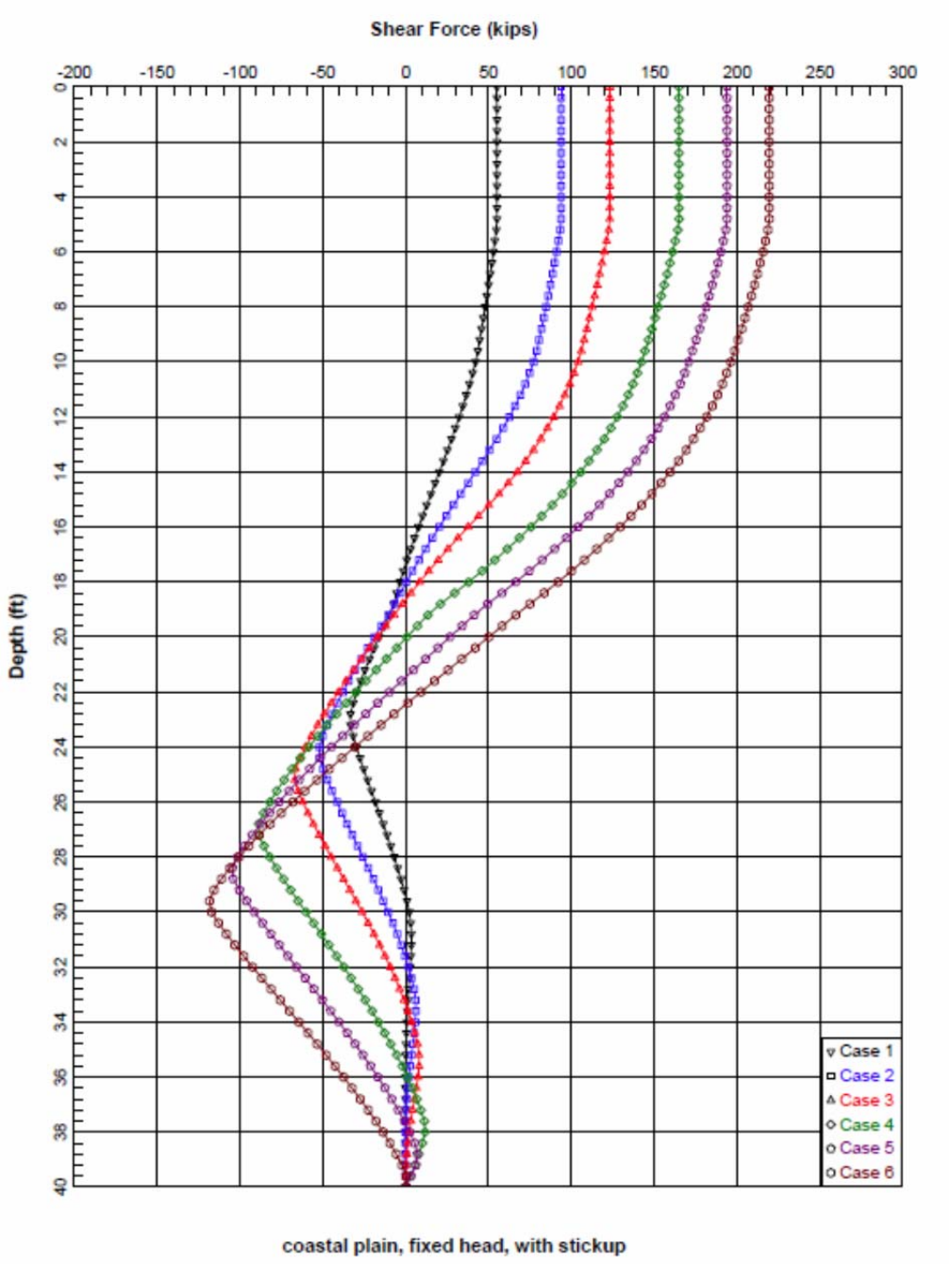

Figure 9.9 Shear Diagram for Example Bridge (Fixed Head, Interior Bent)

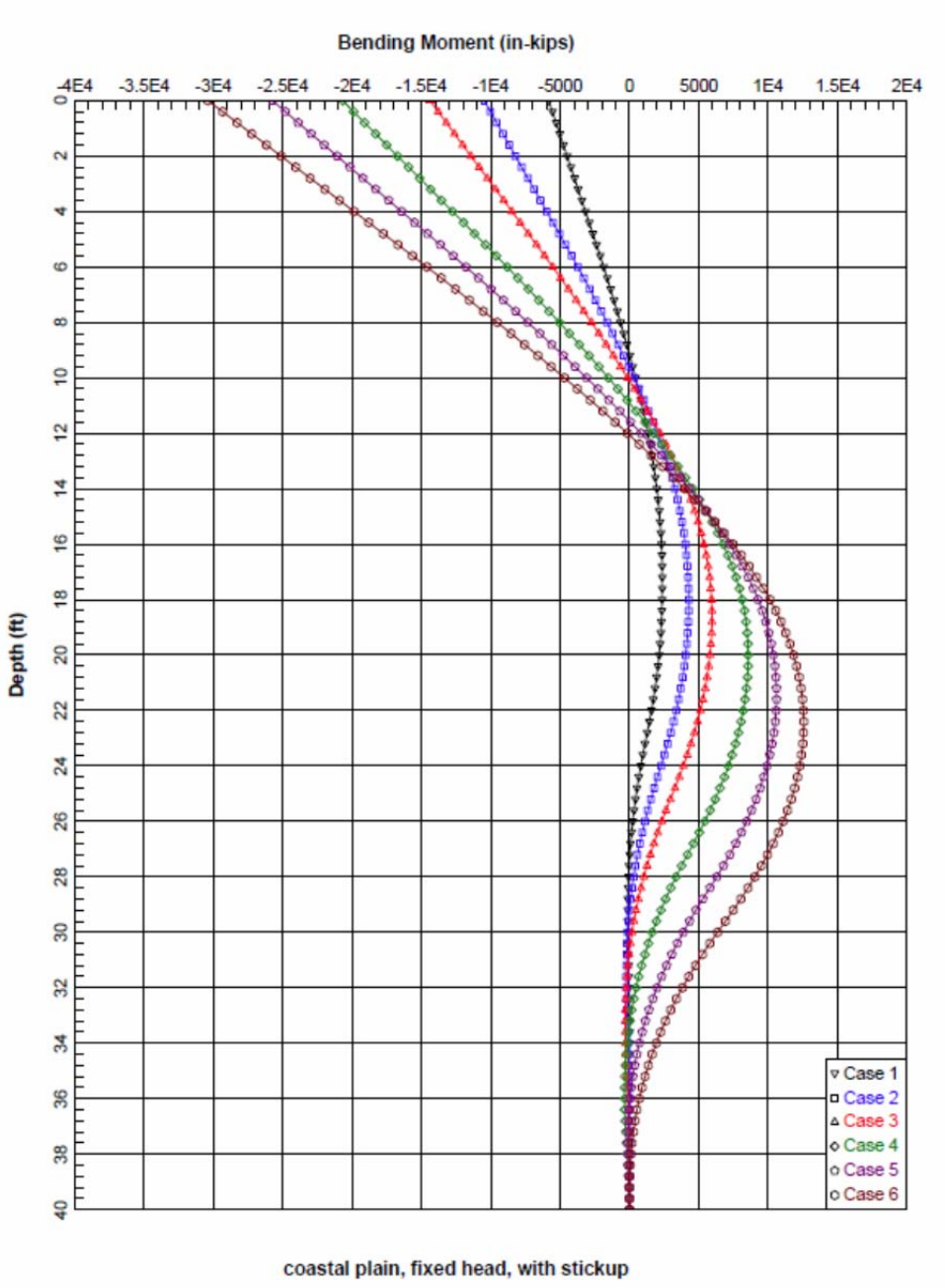

Figure 9.10 Moment Diagram for Example Bridge (Fixed Head, Interior Bent)

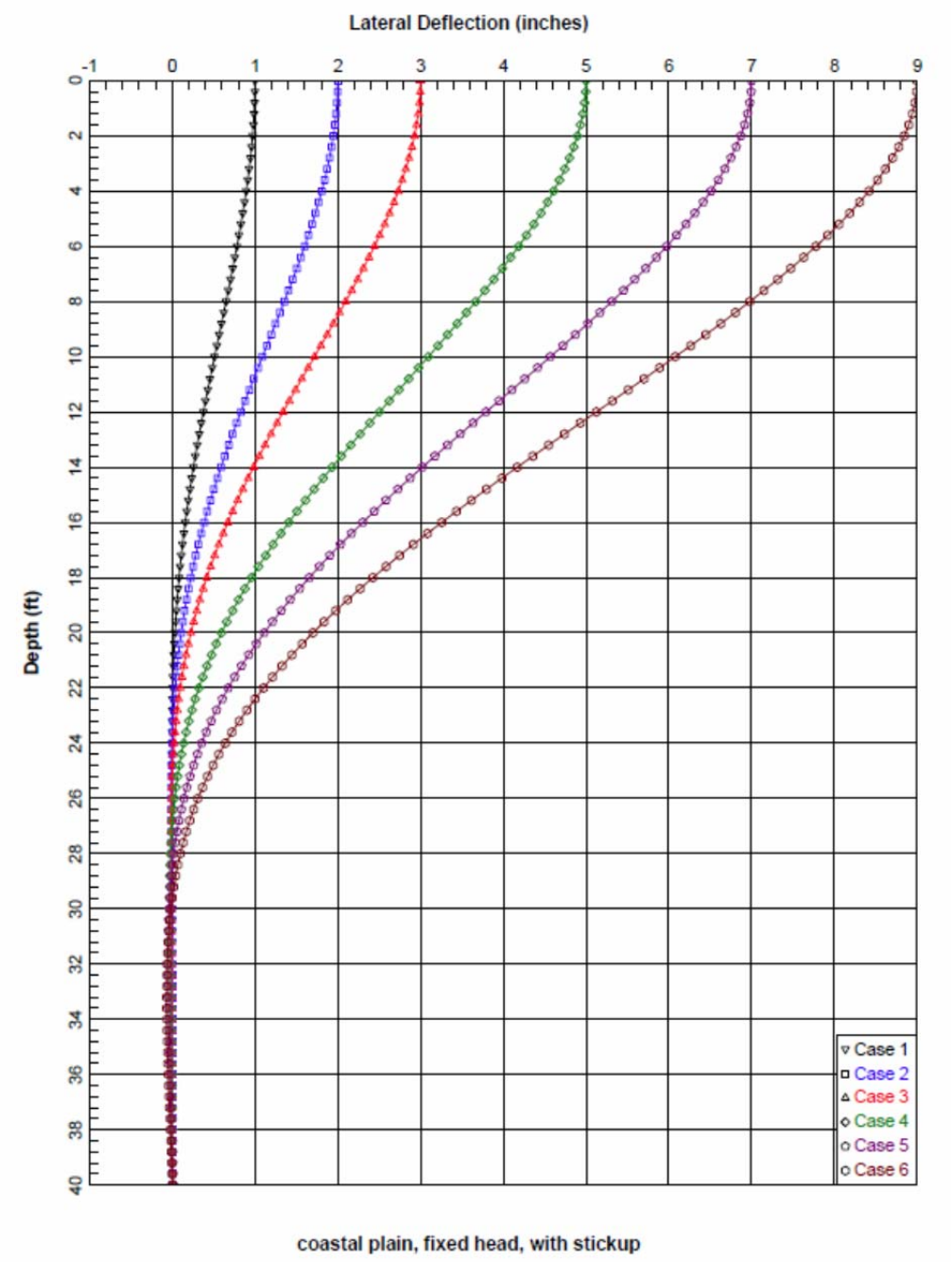

Figure 9.11 Deflection Diagram for Example Bridge (Fixed Head, Interior Bent)

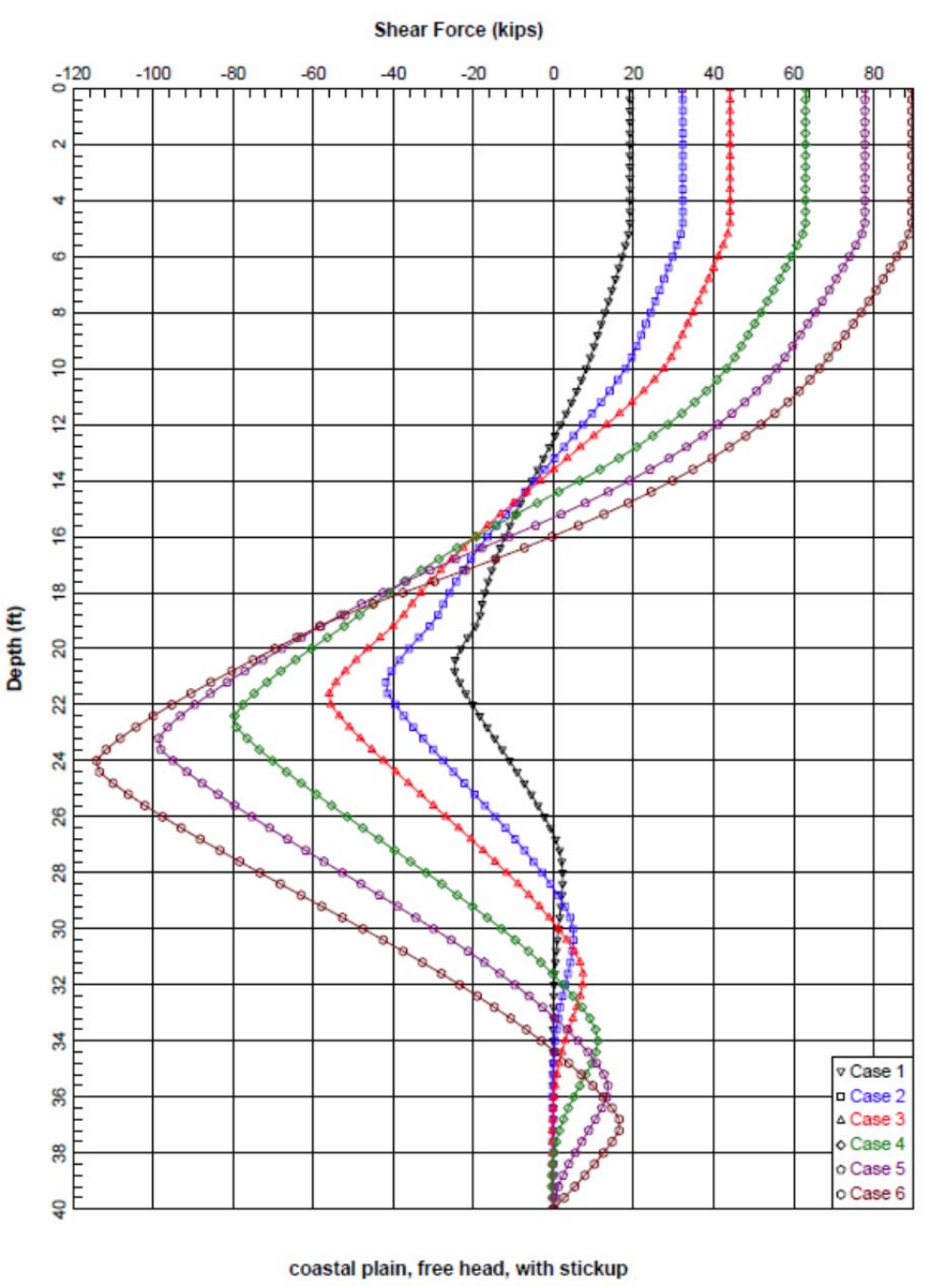

Figure 9.12 Shear Diagram for Example Bridge (Free Head, Interior Bent)

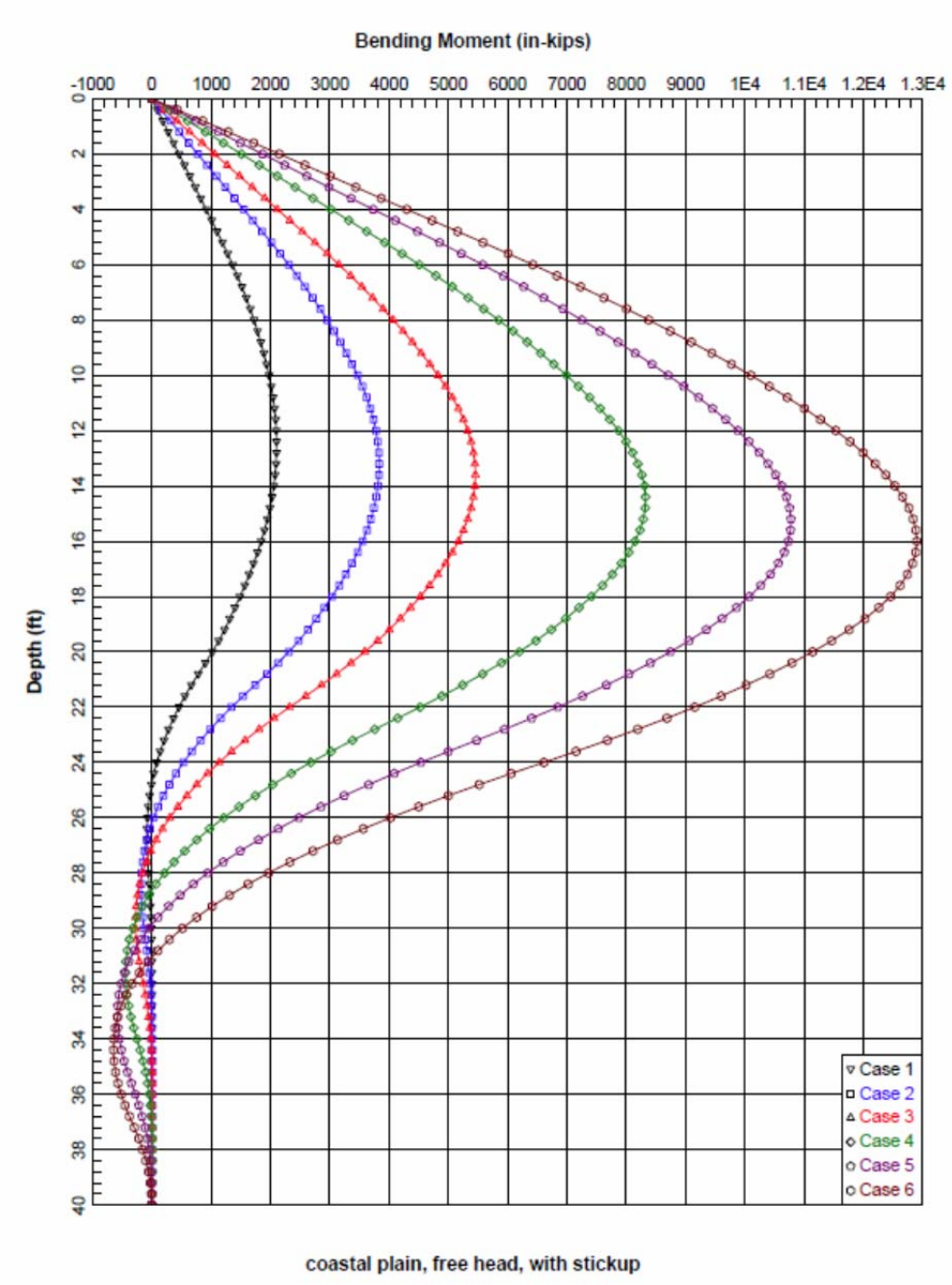

Figure 9.13 Moment Diagram for Example Bridge (Free Head, Interior Bent)

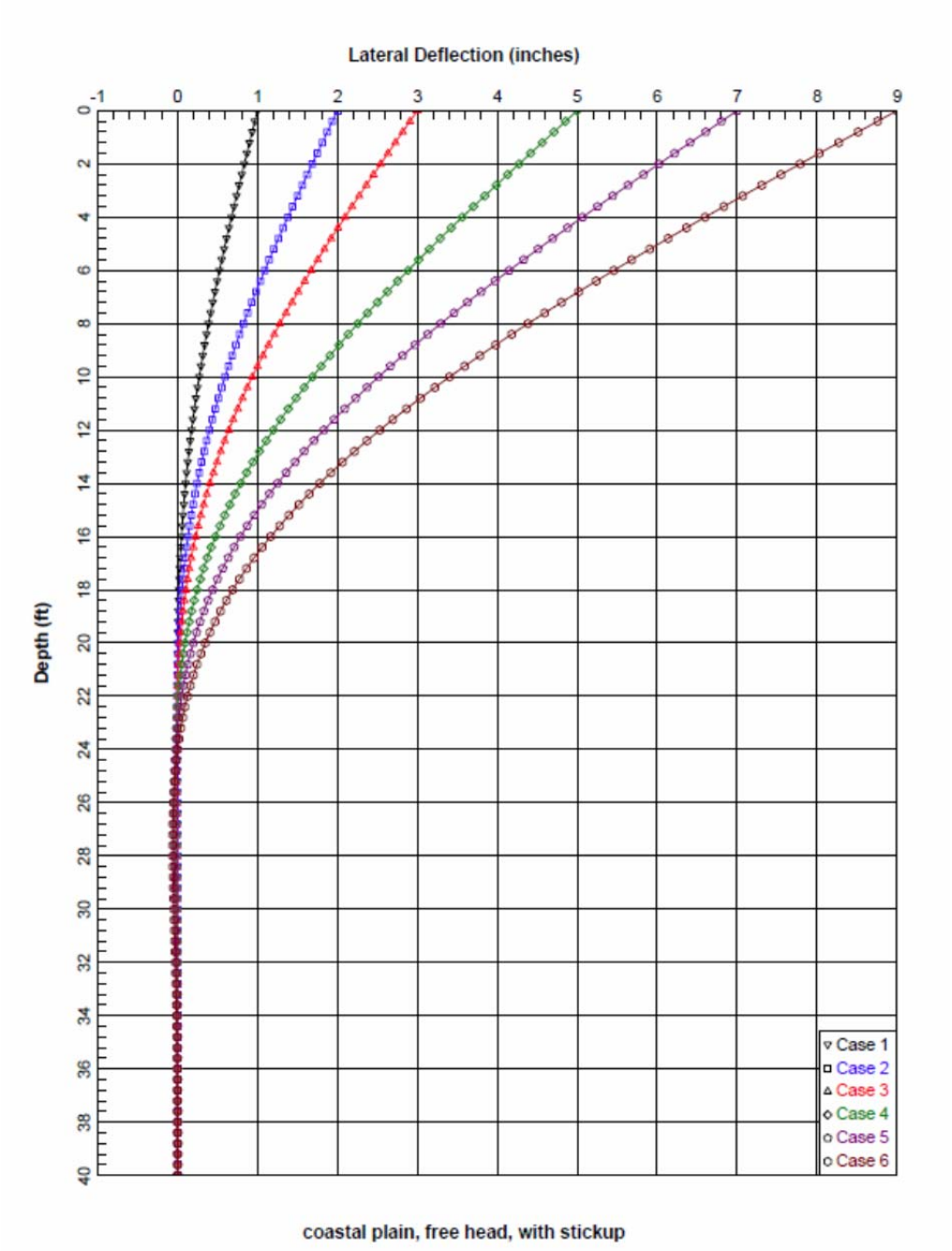

Figure 9.14 Deflection Diagram for Example Bridge (Free Head, Interior Bent)

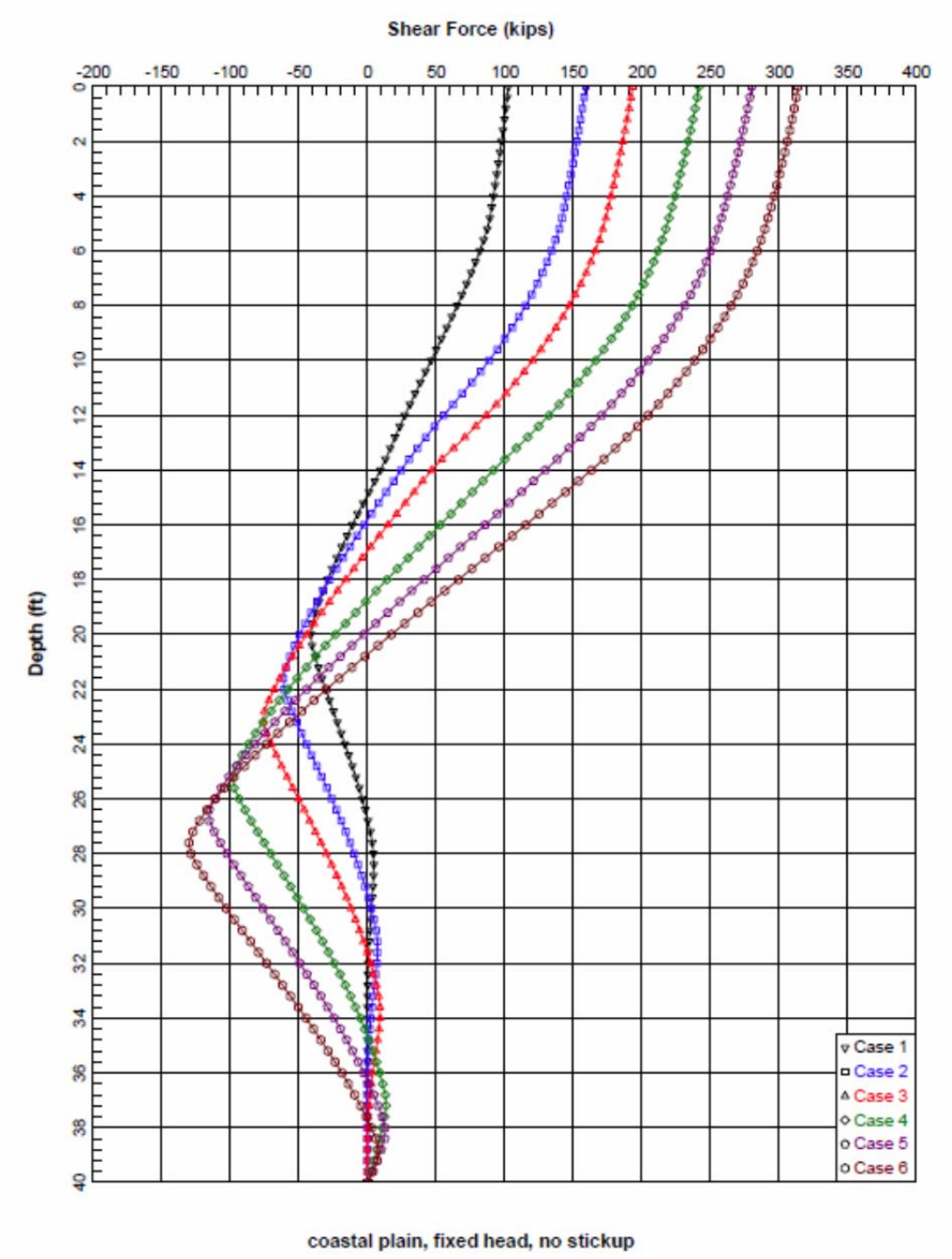

Figure 9.15 Shear Diagram for Example Bridge (Fixed Head, Exterior Bent)

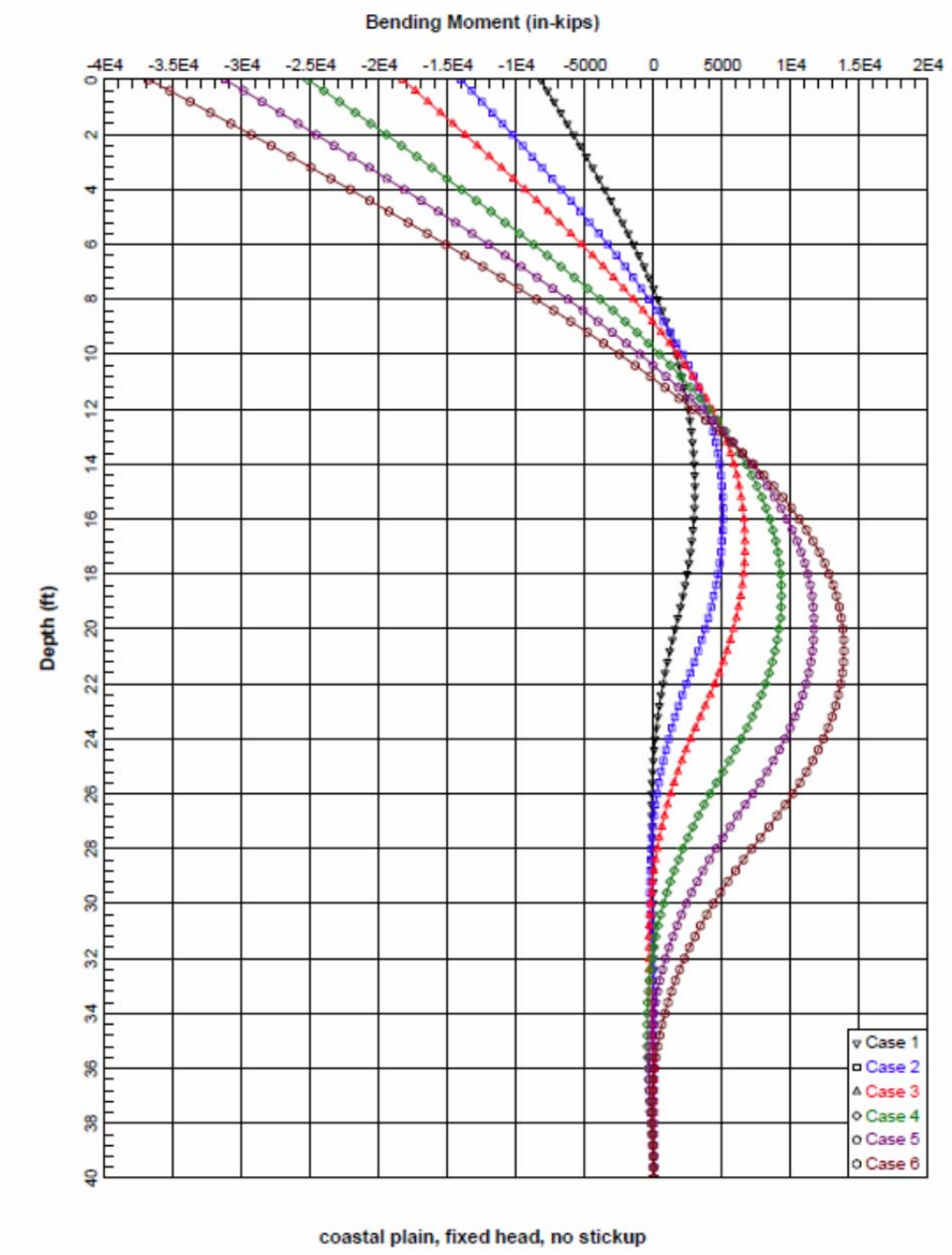

Figure 9.16 Moment Diagram for Example Bridge (Fixed Head, Exterior Bent)

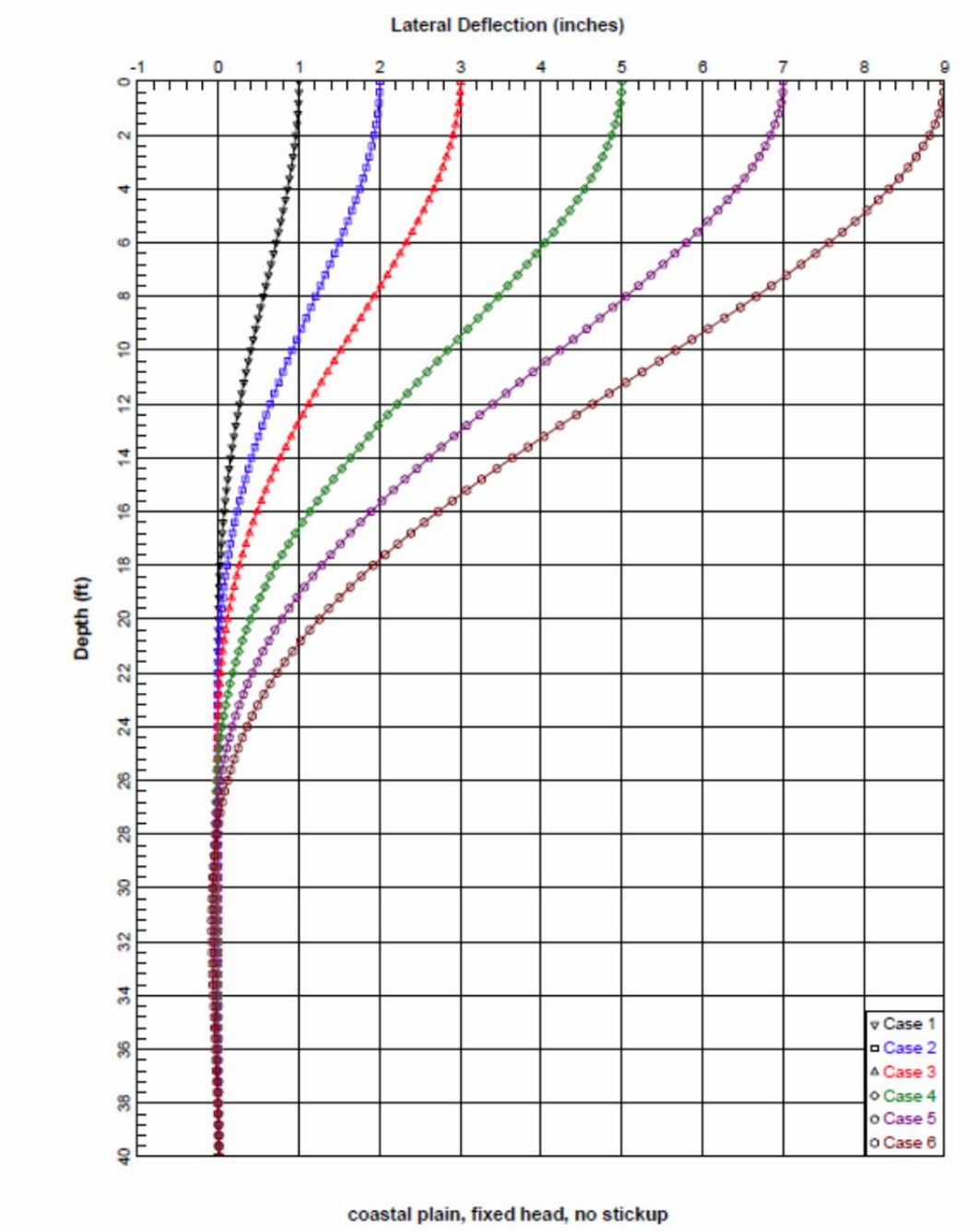

Figure 9.17 Deflection Diagram for Example Bridge (Fixed Head, Exterior Bent)

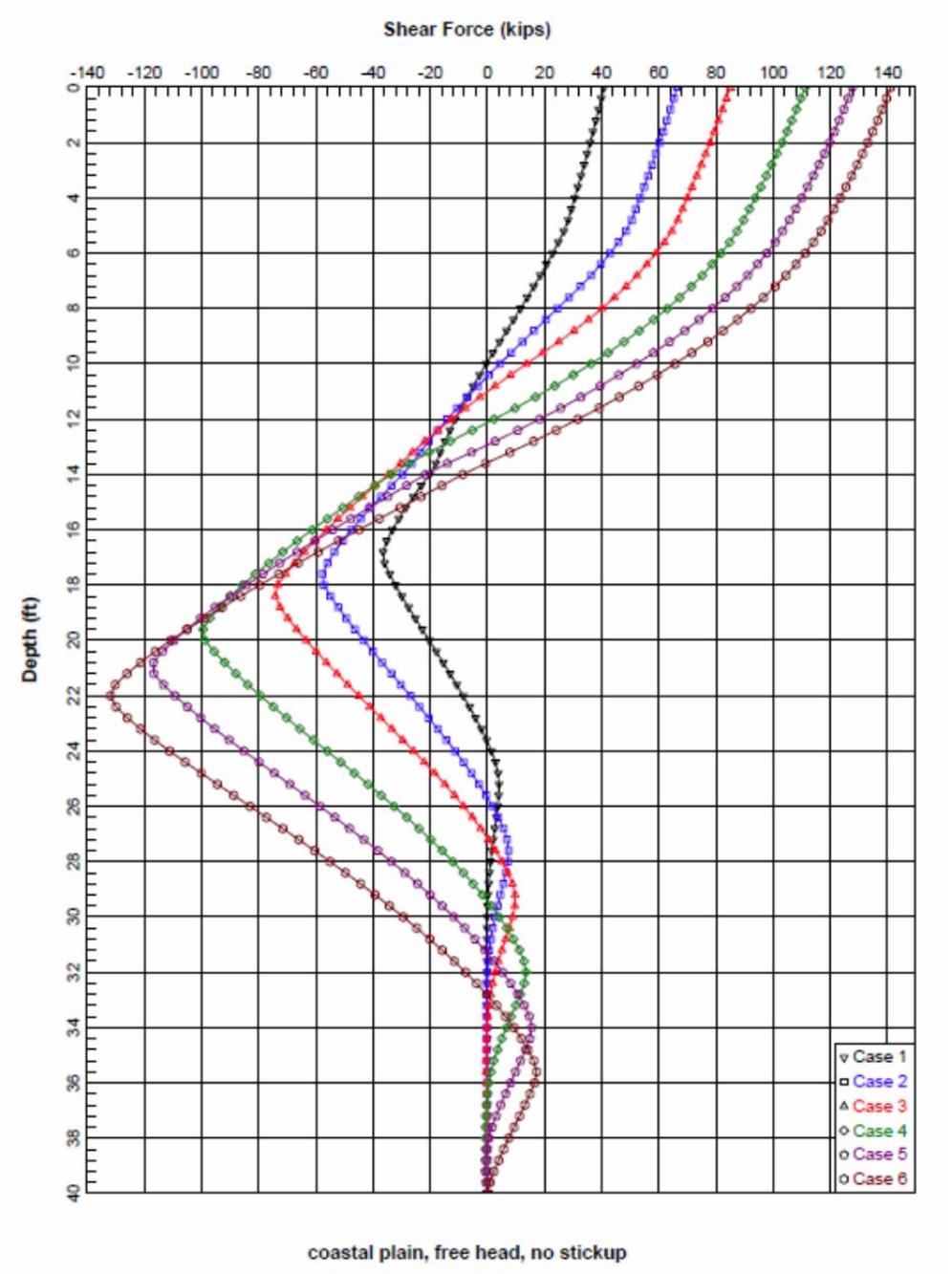

Figure 9.18 Shear Diagram for Example Bridge (Free Head, Exterior Bent)

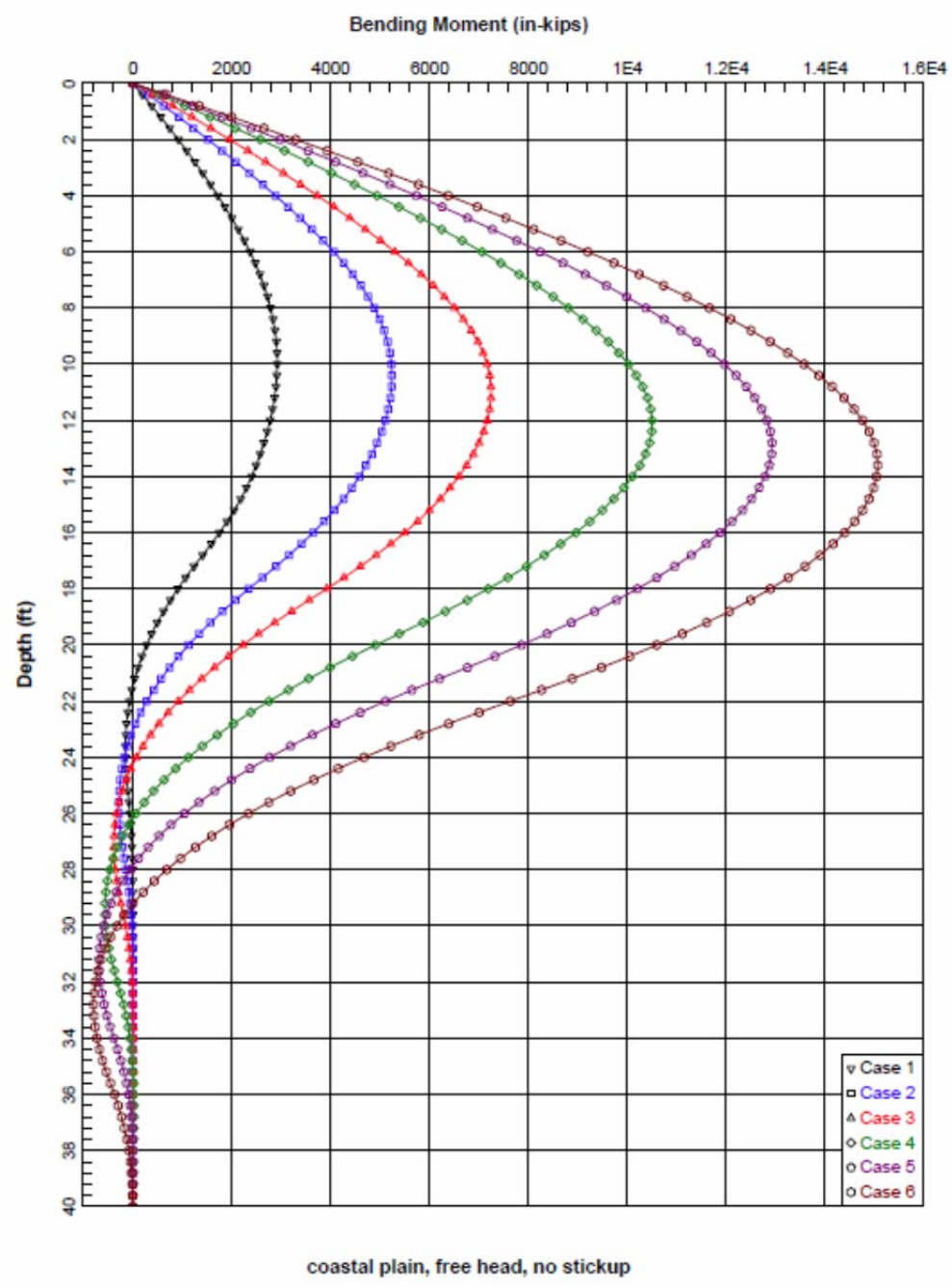

Figure 9.19 Moment Diagram for Example Bridge (Free Head, Exterior Bent)

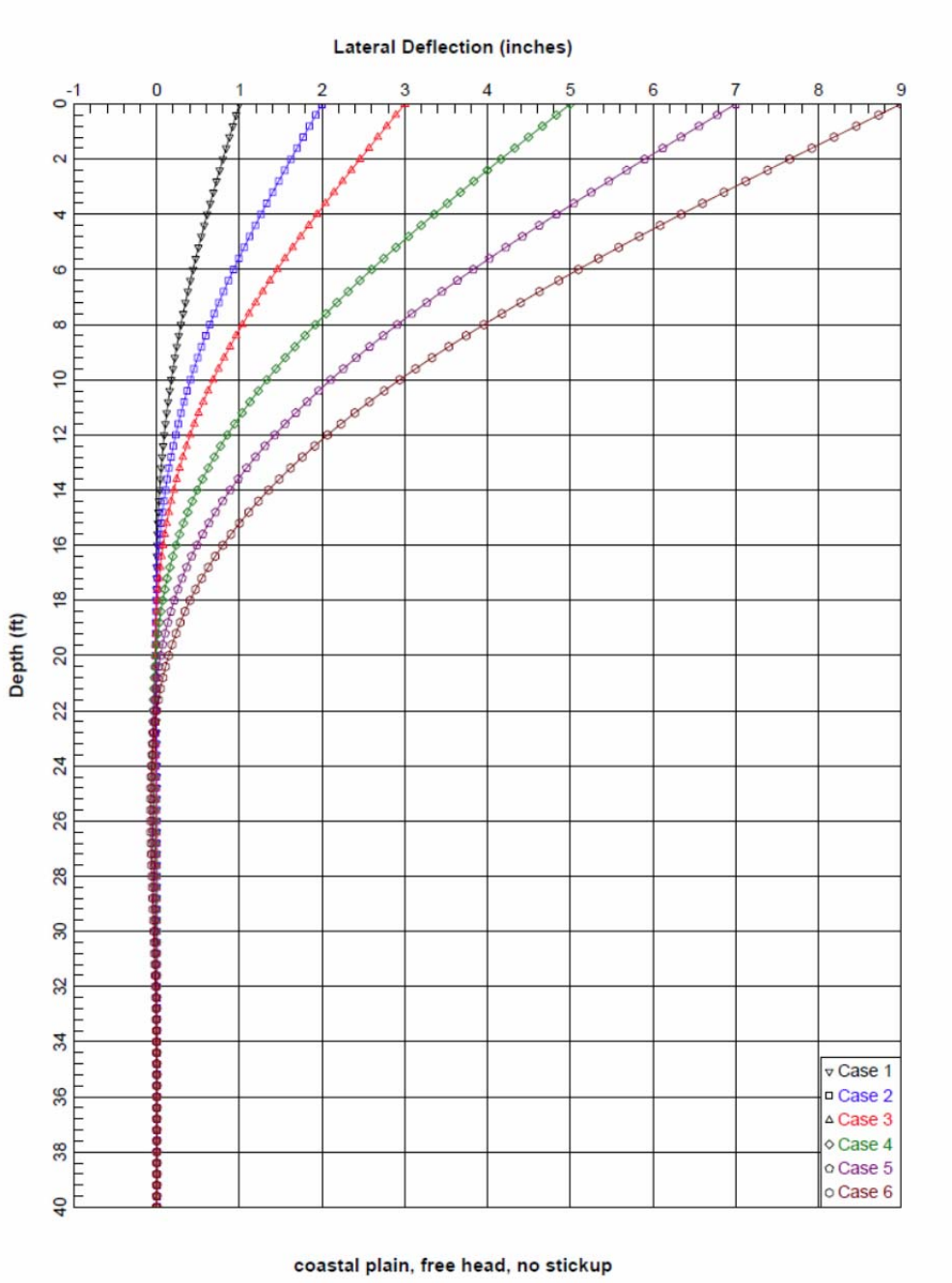

Figure 9.20 Deflection Diagram for Example Bridge (Free Head, Exterior Bent)

The finite element model of a typical interior bridge bent is shown in Figure 9.21. A similar model not presented here was created for the exterior bents. To ensure that the p-y curves as provided are adequate, test cases of the model shown in Figure 9.21 were analyzed. The results of these test cases are presented in Table 9.9. It should be noted that stiffness modifiers for the piles were taken as 1.0 and the pile cap stiffness modifier for the pile cap (I_x, I_y, and J) were all taken as 100 to represent a rigid cap as considered by LPILE. These stiffness modifiers are used for the purpose of spring calibration to the structural model.

Table 9.8 LPile Plot Output

Bent	Condition	Shear at Pile Head (kip)	Max Moment (kip-inches)	Max Deflection (inches)
Interior	**Fixed**	123	-14,300	3.00
Interior	**Free**	44	5,400	3.00
End	**Fixed**	192	-18,000	3.00
End	**Free**	85	7,200	3.00

Table 9.9 SAP Model Output with P-Y Springs

Bent	Condition	Shear at Pile Head (kip)	Max Moment (kip-inches)	Max Deflection (inches)
Interior	**Fixed**	123	-14,600	2.80
Interior	**Free**	44	6,200	2.95
End	**Fixed**	192	-18,100	2.86
End	**Free**	85	7,500	2.60

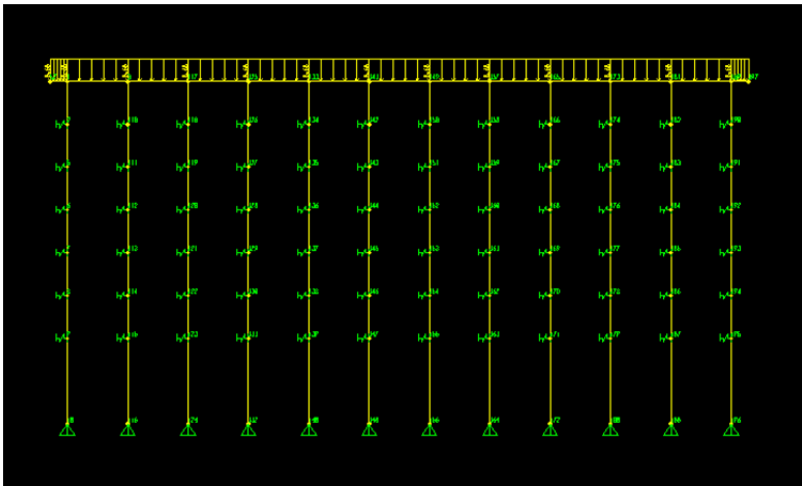

Figure 9.21 SAP Model of Interior Bent with Soil Springs Shown

It should be noted that agreement is found between the LPILE output and that of the SAP2000 model as shown in the comparison between Tables 9.8 and 9.9. Although not exact, the results are found to be within reason. The use of more springs or direct adherence to the previous recommendations regarding spring placement within layers would result in less error (less than 5% total error is typically considered good agreement).

STEP #3 - Modify finite element models of all bents to account for expected stiffness

The finite element model created in the previous step must at this point be modified using stiffness modification factors. These modification factors account for the effects of cracked concrete during the design earthquake. Recall that stiffness modification factors applied before were employed for the purpose of spring calibration. Section 5.5.7 of the SCDOT SDS recommends that expected section properties be used when modeling piles and bent caps. This document provides values of $I_g/2$ for piles and $I_g/3$ for bent caps when the expected properties are not known. Although $I_g/2$ for the piles may be reasonable (0.4 - 0.7 times I_g are commonly used values), experimental testing and anticipated demand in most cases suggests that for the bent cap $1.0I_g$ may be more applicable for flat slab bridges constructed with 18 to 20 inch precast prestressed piling. Research presented in preceding chapters shows that proper detailing of bent caps results in full displacement demands being reached without cracking of the bent cap. Therefore a full gross moment of inertia ($1.0I_g$) may be used. In this example, the approximate values of $I_g/2$ for the piles and $1.0I_g$ for the bent cap are used. The effective torsional moment of inertia is taken as 0.2J for both piles and bent cap as required by Section 5.5.7.

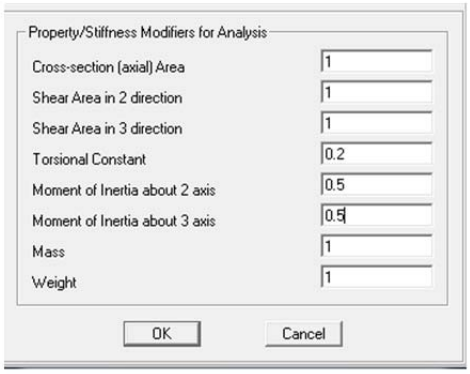

Pile Stiffness Modification Factors

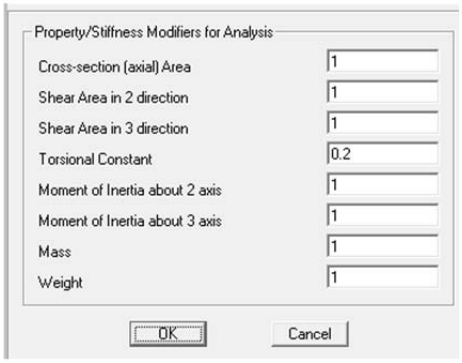

Bent Cap Stiffness Modification Factors

Figure 9.22 Elemental Modification Factors

STEP #4 - Determine demand based on multi-mode spectrum analysis

For this structure the displacement demand was determined using multi-mode spectrum analysis (MSA) in accordance with Section 5.5 of the SCDOT SDS. Figure 9.23 shows the three dimensional model used for analysis. Figure 5.9 of the SCDOT SDS was used to locate the point of fixity, which was found to be 18 feet below ground for both the interior and exterior pile bents. The location was found using rigid cap and elastic pile assumptions in order to match the LPILE results. After locating the point of fixity, the properties from Step #3 were included in the MSA model. Soil springs representing the passive pressure behind the abutment in the longitudinal direction were included directly as linear springs in accordance with Figure 5.7 from the SCDOT SDS. Initially, the elastic pile stiffness was used. Once displacements greater than three inches were achieved secant stiffness was calculated. The final stiffness used in the model is based on 6.7 inches of displacement in the longitudinal direction. Modal analysis revealed the three primary modes and natural periods shown in Figures 9.24 through 9.26.

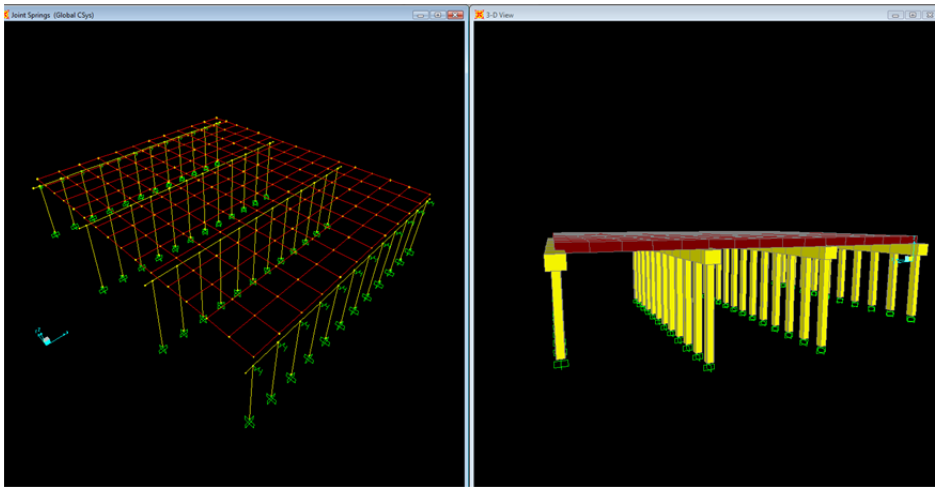

Figure 9.23 MSA Model for Bridge

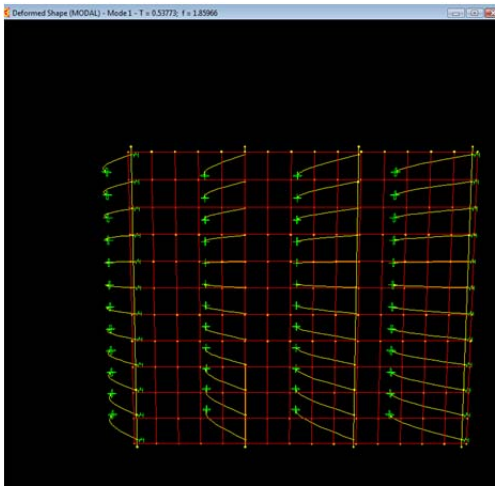

Figure 9.24 First Mode - Longitudinal Response, T = 0.54 seconds

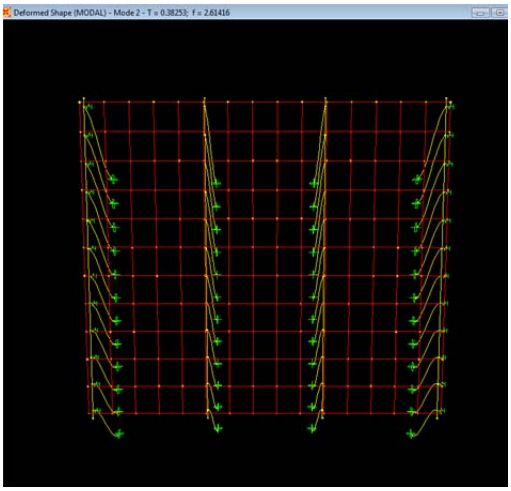

Figure 9.25 Second Mode - Transverse Response, T = 0.38 seconds

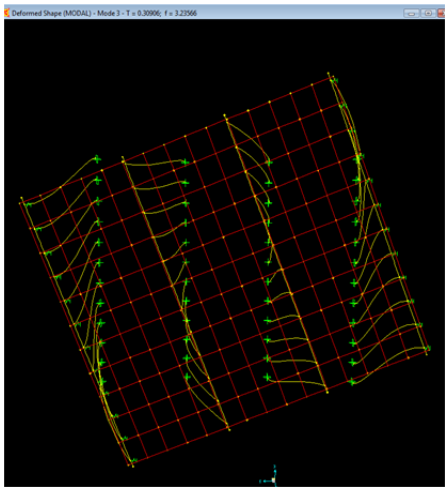

Figure 9.26 Third Mode - Torsional Response, T = 0.31 seconds

For this perfectly symmetrical structure (without interior joints), the torsional mode contributed negligibly to the response in the principal directions. The response spectrum method was used to obtain displacements as follows:

Table 9.10 Response Spectrum Method Displacements

Direction	X (inches)	Y (inches)
X (Transverse)	3.56	0.00
Y (Longitudinal)	0.00	6.70

In accordance with Section 5.2.4 of the SCDOT SDS displacement magnification is required for short period structures. The value of R_T used shall be taken based on the maximum value of R expected in the design of the subject bridge. This value is obtained by dividing the spectral force by the plastic capacity of the bridge component where plastic hinging is expected. This ratio is not known during this particular calculation. Hence a value is usually selected based on anticipated bridge damage and then checked at final design. For the bridge example in this chapter, R = 3 was assumed for illustrative purposes. The calculation of this magnification is presented below.

$$T^* = 1.25T_s = 1.25(0.5) = 0.625 \quad s$$

$$\frac{T^*}{T_L} = \frac{0.625}{0.54} = 1.157 > 1$$

$$R = 3 \quad (Assumed)$$

$$R_{T,L} = (1 - 1/R)(T^*/T) + 1/R = (1 - 1/3)(1.157) + 1/3 = 1.1 > 1 \quad (ok)$$

$$\frac{T^*}{T_T} = \frac{0.625}{0.38} = 1.645 > 1$$

$$R = 3 \quad (Assumed)$$

$$R_{T,T} = (1 - 1/R)(T^*/T) + 1/R = (1 - 1/3)(1.645) + 1/3 = 1.43 > 1 \quad (ok)$$

$U_{x,max} = 1.0R_{T,T}(X_{Transverse}) + 0.30R_{T,L}(X_{Longitudinal}) = 1.0(1.43)(3.56) + 0.3(1.1)(0) = 5.1$ inches

$U_{y,max} = 0.3R_{T,T}(Y_{Transverse}) + 1.0R_{T,L}(Y_{Longitudinal}) = 0.3(1.43)(0) + 1.0(1.1)(6.7) = 7.4$ inches

STEP #5 - Select trial pile section and insert trial plastic hinge details into finite element model

Seismic design is an iterative process where models are run and rerun to provide a safe and economical solution for the design earthquake. For brevity within this design guide a trial size of a 20 inch square pile dimension was initially selected to expedite this process. It should also be noted that the effects of axial loading should not be neglected at this point. These effects are included in the following sections. The results of the modal analysis of the developed model in terms of maximum cap moment demand without over-strength are as follows:

- Positive moment at end piles: 5,100 kip-inches
- Negative moment at end piles: 6,100 kip-inches
- Maximum positive moment at 1st interior pile: 4,100 kip-inches
- Maximum negative moment at 1st interior pile: 4,300 kip-inches
- All other locations (at all other interior piles): 3,000 kip-inches (positive and negative)
- Maximum shear in cap: 101 kips (at same load step as maximum moment)
- Maximum shear in pile: 101 kips
- Axial loads in piles: 50 kips (1 end pile - tension); -20 kips (interior piles-compression); -110 kips (1 end pile-compression)

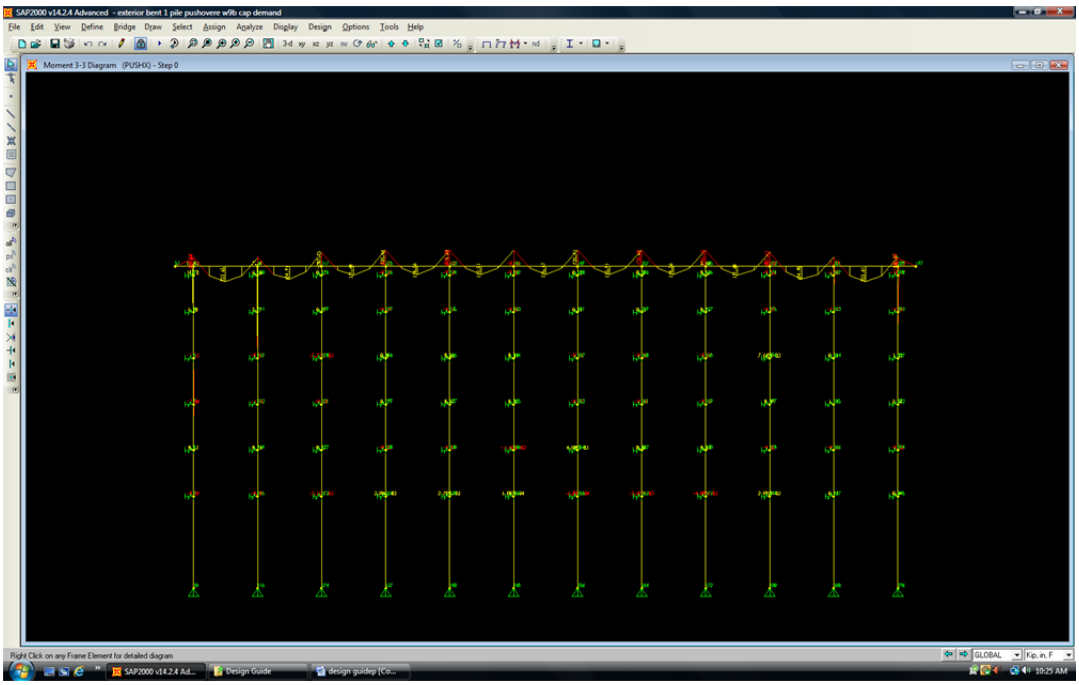

Figure 9.27 Moment Demand
Note: Load Step 0 (dead load only - note negative moment on top)

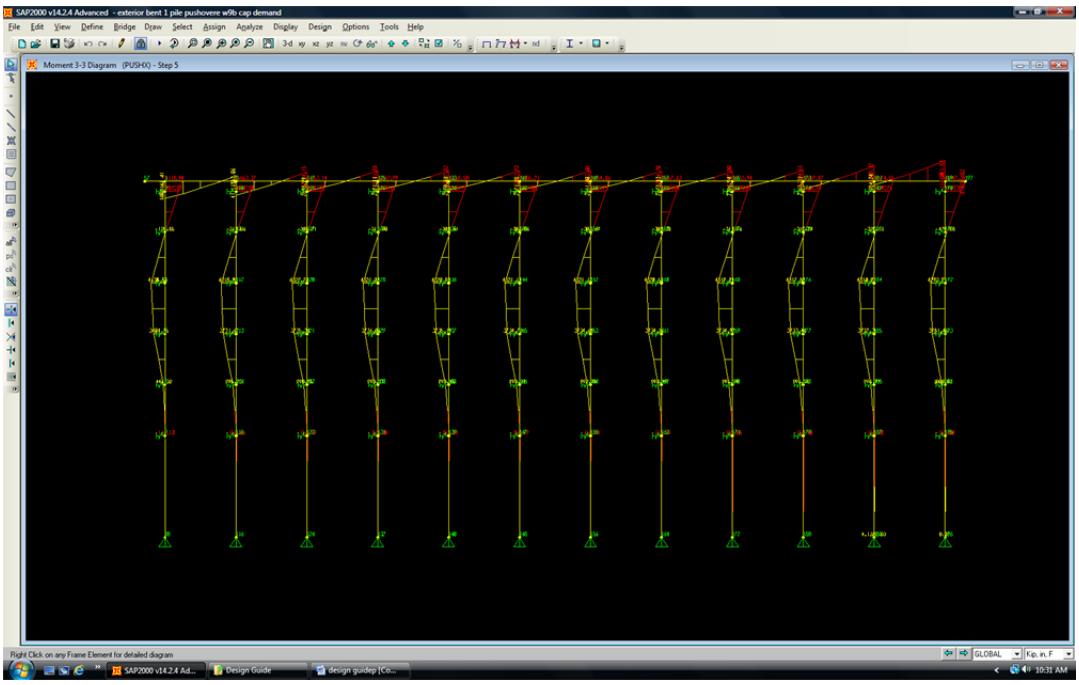

Figure 9.28 Critical Moment Demand

The critical moment demand is determined from the model to occur at an intermediate load step corresponding to 2.5 inches deflection. The moments used for design are taken directly from model outputs and modified to include over strength. This load step is highlighted in Figures

9.28 and 9.29. This is a unique feature of precast pile bents. As these systems shed a significant amount of load following the formation of a plastic hinge, the maximum demand is based on the maximum moment in the pile at the cap. This occurs early in the pushover analysis. It should be noted that when the maximum moment occurs in the bent cap the hinges below ground have yet to form.

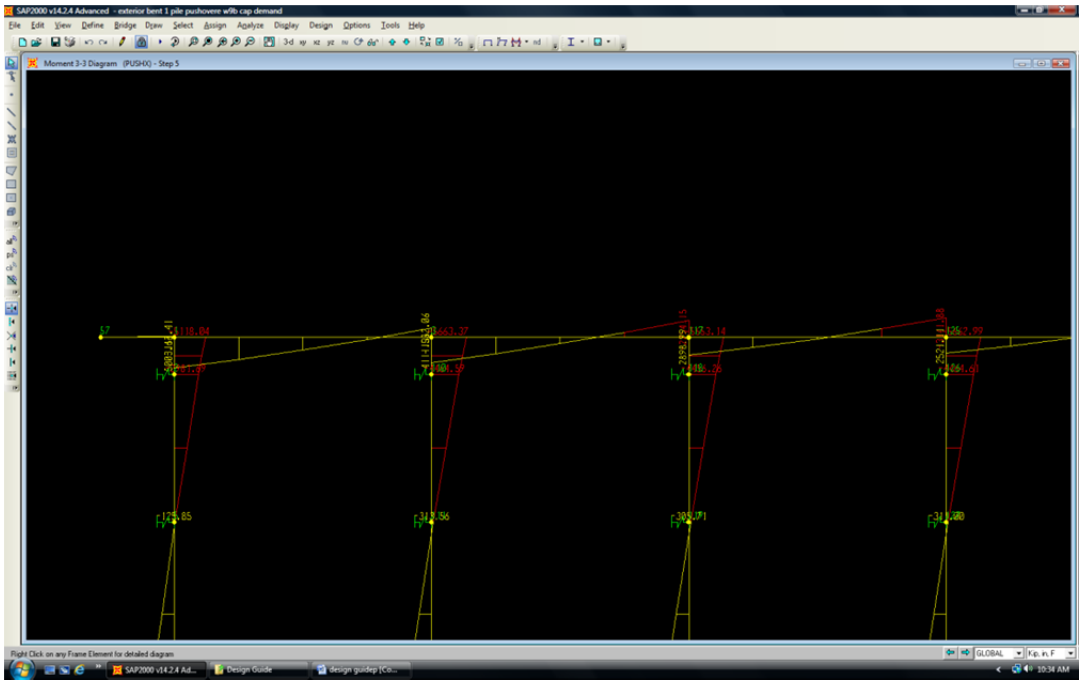

Figure 9.29 Critical Moment Demand (Figure Zoomed)

Figure 9.29 presents an enlarged portion of Figure 9.28 for clarity. When a fixed connection is made at the end pile the bent cap must be able to develop the pile with over-strength. Typically, at locations after the first interior pile, the cap is able to develop all other piles using both sides of the cap. As a result, additional longitudinal steel is usually required at the bottom face of the cap through the 2nd interior pile.

Once the moment demand has been determined through modal analysis, initial pile size and detailing may be selected and checked. Again it should be noted that for the purposes of this design guide an initial pile size has been chosen as 20 inches square. With the initial selection of size and detailing the design process is presented as follows:

- Try 20 inch x 20 inch prestressed pile constructed with W6 spiral encasement at a pitch of two inches on center.
- Try a strand pattern of 10 – ½ inch special (0.6 inches diameter).
- Assume 38 kips per strand after losses

These parameters along with the appropriate material models are input into the SAP 2000 section designer as shown in Figures 9.30 and 9.31 respectively. Discussion regarding the material models to be used are discussed in the SCDOT SDS Section 6.6 and briefly described in Chapter 5. Once completed, the designed section is subject to a moment curvature analysis with respect

to the critical axial loading as found through the initial results of the modal analysis. The axial loads considered in this example have been presented previously as 50 kips (axial tension) at one end exterior pile, -20 kips (axial compression) at interior piles, and -110 kips (axial compression) at the opposite exterior end pile. The results of these analyses are seen in Figures 9.32 through 9.34 respectively.

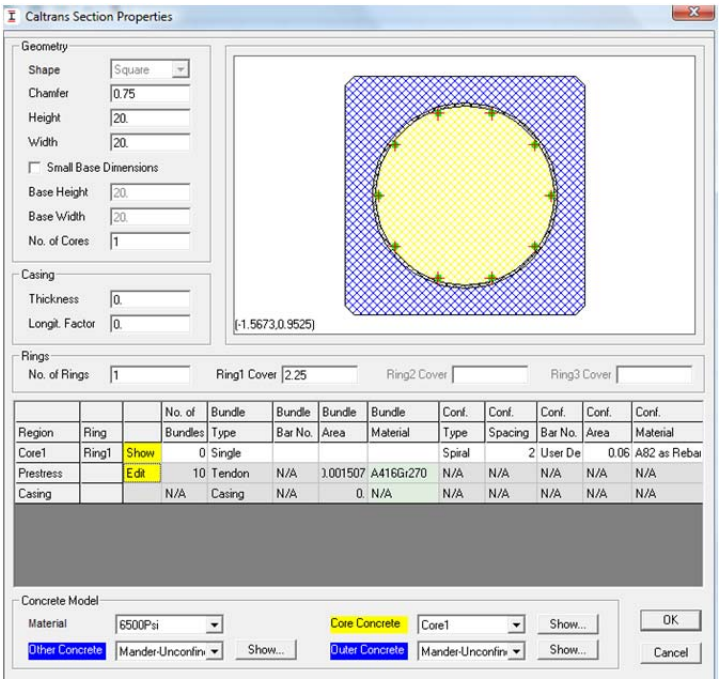

Figure 9.30 Section Designer Input for SAP2000

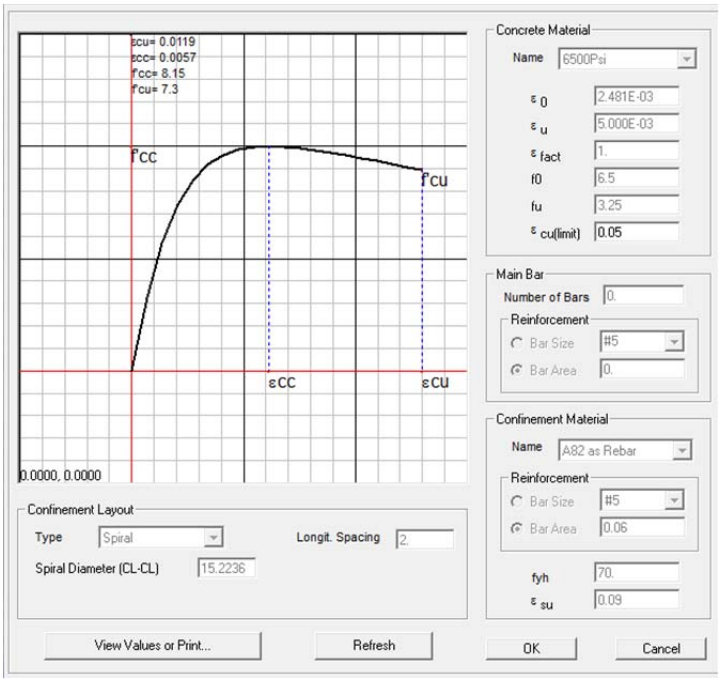

Figure 9.31 Confined Concrete Properties with Section Designer Using SAP2000

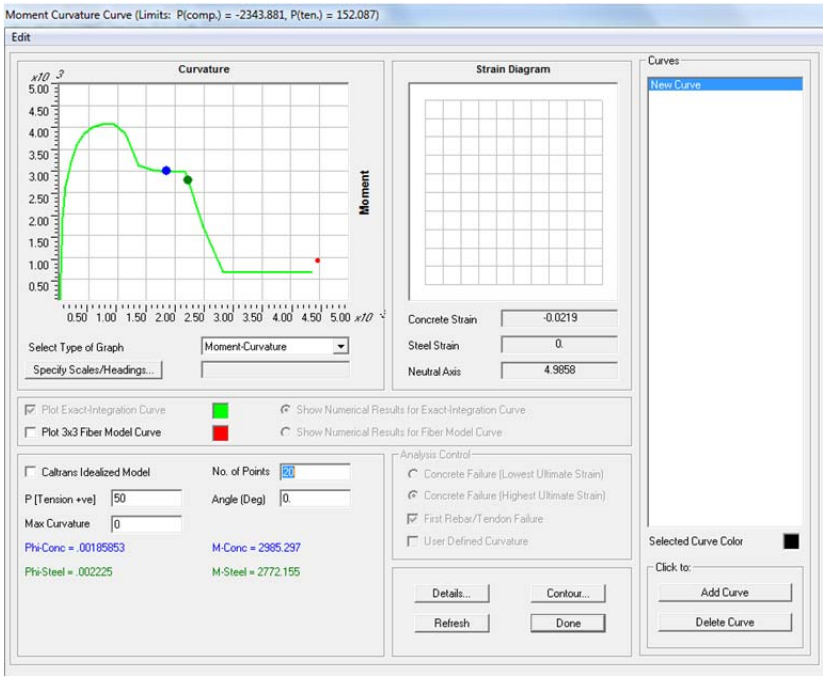

Figure 9.32 Moment Curvature Plot for Axial Force = 50 kips (Tension)

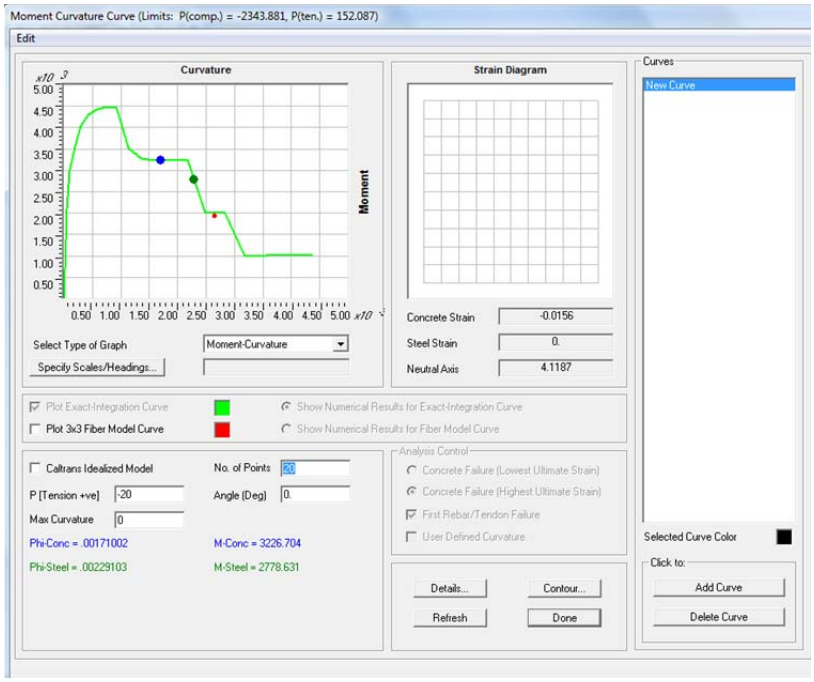

Figure 9.33 Moment Curvature Plot for Axial Force = -20 kips

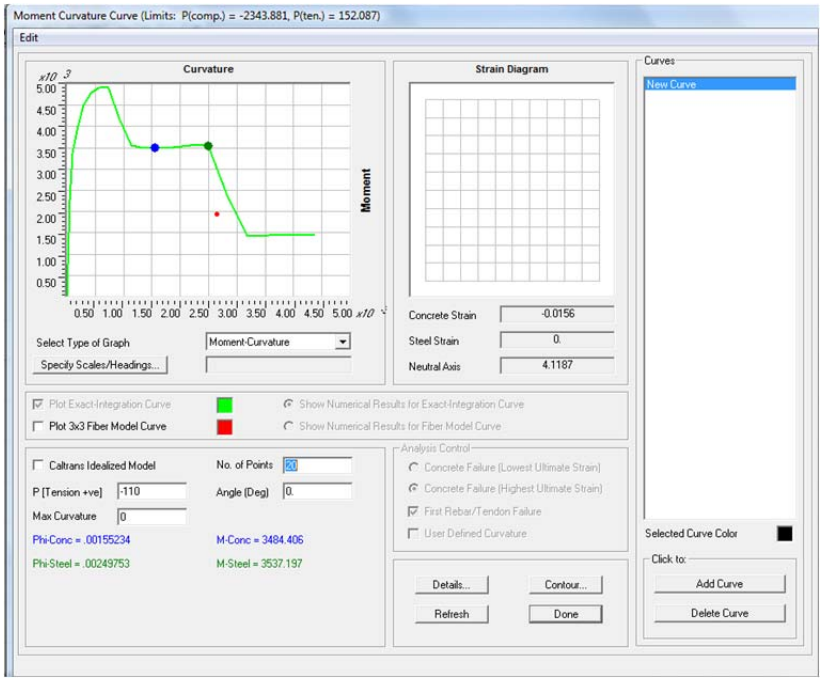

Figure 9.34 Moment Curvature Plot for Axial Force = -110 kips

Following the completion of the moment curvature analyses, the hinge mechanisms must be input into the finite element model. The expected hinges are input in terms of the length to which they are expected to develop. Hinge lengths should be calculated for both the resultant hinges

occurring at the cap and within the ground. These hinge lengths are calculated as maximum values given by the equations shown below according to Section 6.3 of the SCDOT SDS.

At cap:

$L_p = 0.08L' \geq D^*$

$D^* = 20$ inches = Pile cross sectional dimension

$L' = 9$ feet = Distance to point of contra-flexure

[9 feet is one half of the distance between the bent cap and point of fixity (18 feet)]

$L_p = 0.08(9)(12) = 8.64$ inches

$L_p = 20$ inches

In ground:

$L_p = D^* + 0.08H'$

$H' = 9$ feet = Distance to point of contra-flexure

$L_p = 20+0.08(9)(12) = 28.64$

Both the top and bottom hinge lengths are input into the model at each point of critical axial load (for this example +50 kips, -20 kips, and -110 kips). These inputs are presented here in Figures 9.35 through 9.40. These figures show top and bottom hinges for the cases of +50 kips, -20 kips, and -110 kips respectively. Following the analysis shown in these figures top hinges are checked for rotation as compared with that of the previous moment curvature analyses. The top hinges are also used for the calculation of maximum moment. Rotation is found both from the hinge analysis and as the product of maximum curvature and the respective axis length. Note that in this example square piles are modeled and thus the length is 20 inches, irrespective of the chosen axis. Bottom hinges are checked for rotational capacity. The rotational capacity is calculated as the rotation, as calculated by the hinge model, multiplied by the ratio between the in ground hinge length and pile cross sectional dimension. The results of these calculations are presented in the following pages.

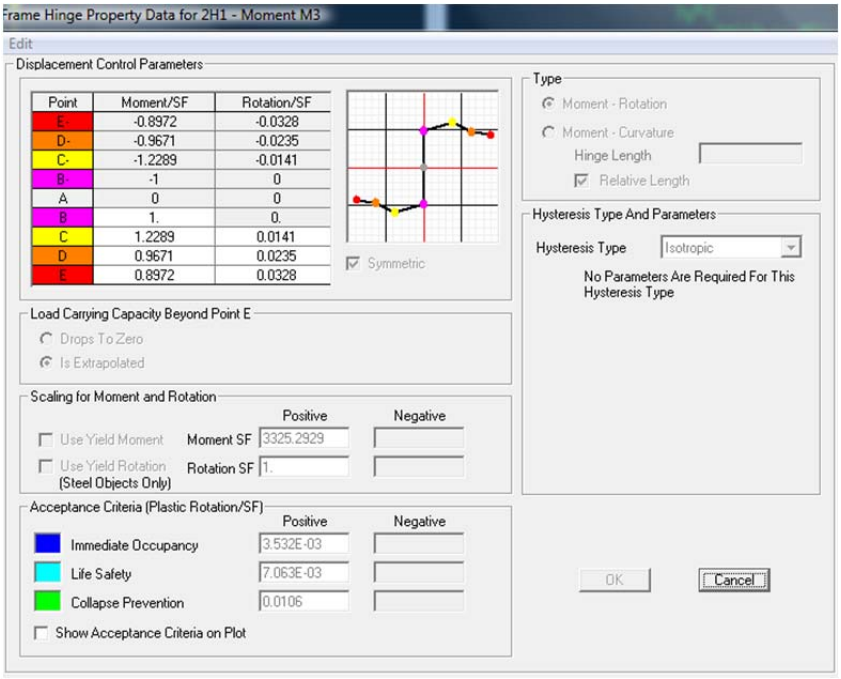

Figure 9.35 Typical Hinge Model (50 kips)

Rotation = 0.00185(20) = 0.037 radians > 0.328 radians

M_{max} = 3,325(1.23) = 4,090 kip-inches

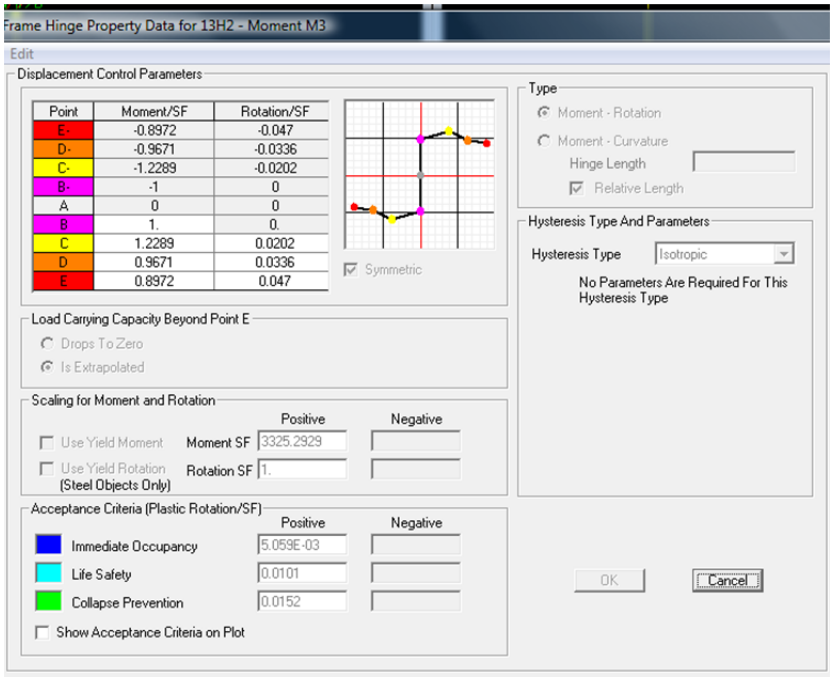

Figure 9.36 Rotational Capacity Bottom Hinge

Rotation Capacity = 28.64/20(0.0328) = 0.047 radians

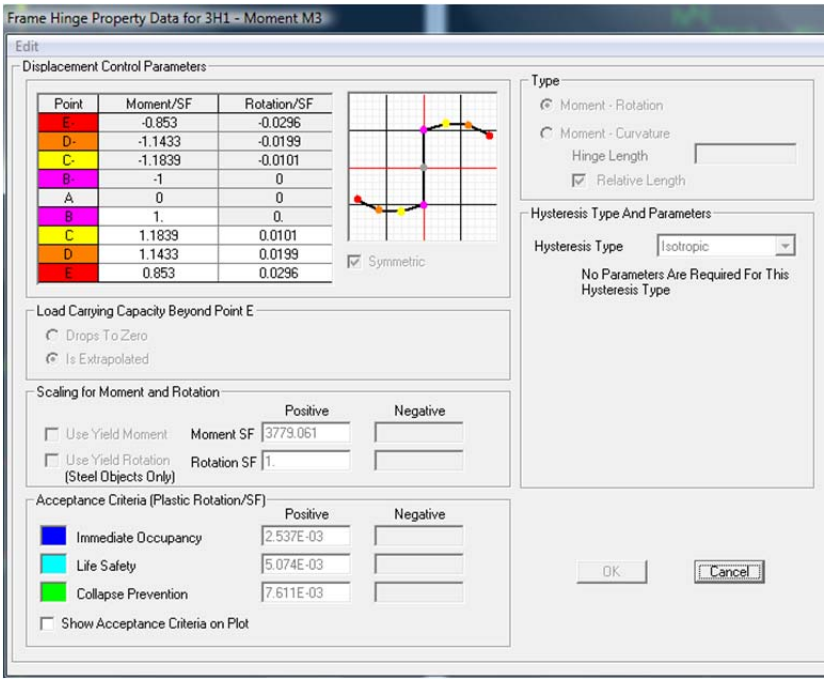

Figure 9.37 Typical Hinge Model (-20 kips)

Rotation = 0.00171(20) = 0.0342 radians > 0.0296 radians

M_{max} = 3,779(1.19) = 4,500 kip-inches

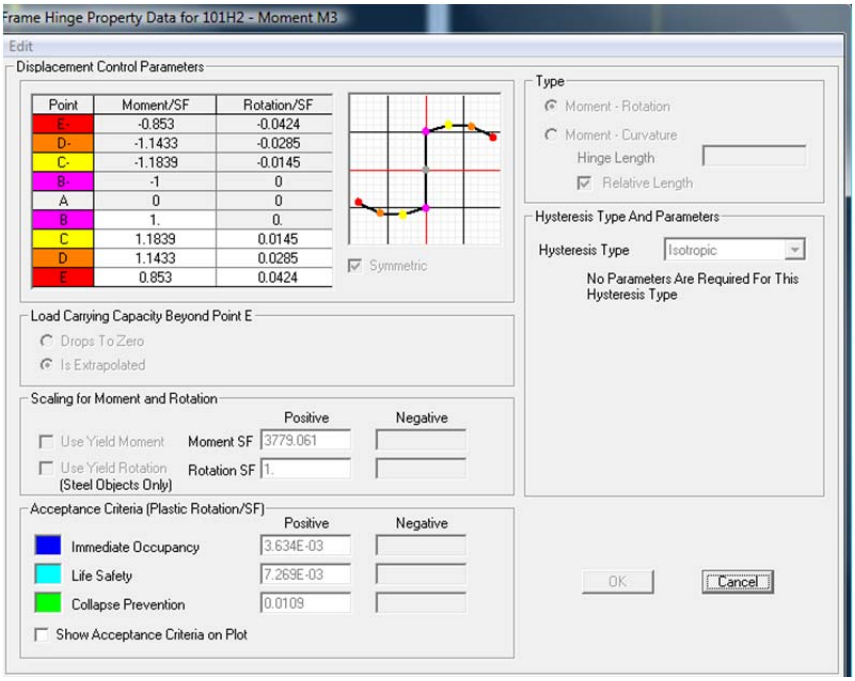

Figure 9.38 Rotational Capacity Bottom Hinge

Rotation Capacity = 28.64/20(0.0296) = 0.0424 radians

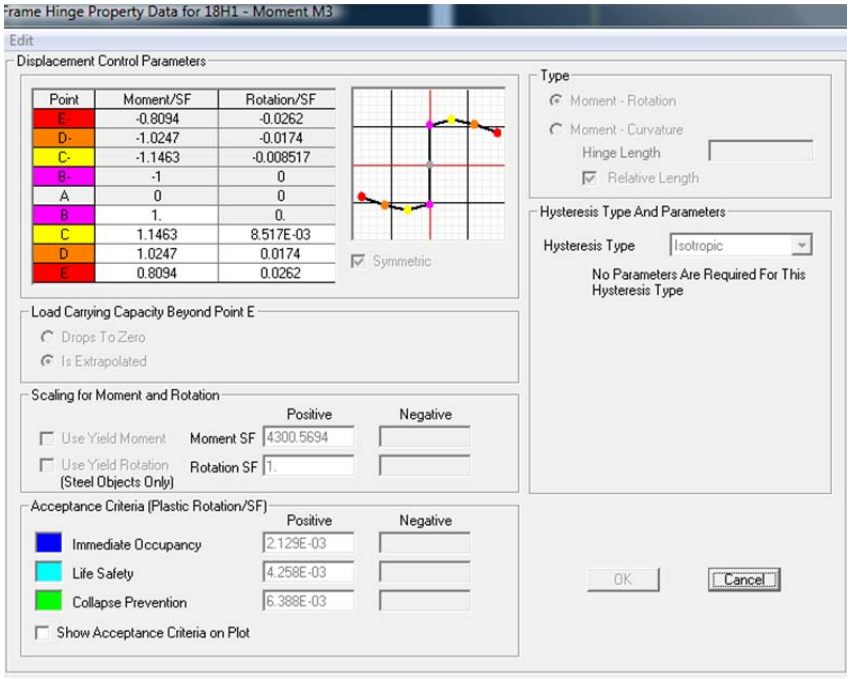

Figure 9.39 Typical Hinge Model (-110 kips)
Rotation = 0.00155(20) = 0.031 radians > 0.0262 radians
M_{max} = 4,300(1.15) = 4,950 kips-inches

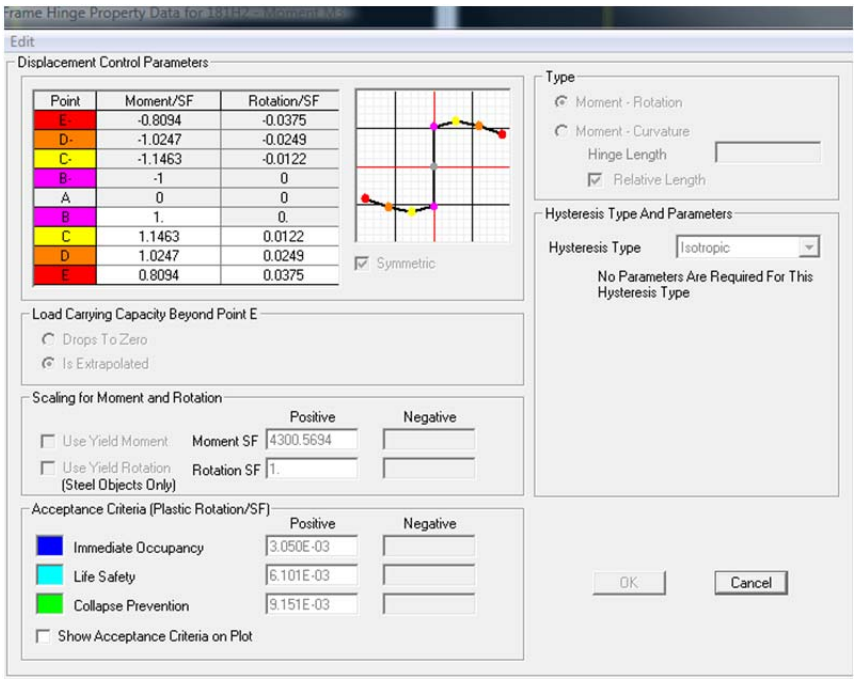

Figure 9.40 Rotational Capacity Bottom Hinge
Rotation Capacity = 28.64/20(0.0262) = 0.0375 radians

Following the input of the hinge length the model is complete. The model is then subjected to a pushover analysis. The results of this analysis including displacement capacity and yield

displacement are used for comparison with demand displacements (as given by modal analysis) and ductility per Section 7.3 of the SCDOT SDS. The results of the pushover analysis completed at this point in the example are seen in Figures 9.41 and 9.42. From these figures the displacement capacities of the system are found in the X and Y directions respectively. As seen below the selected pile detailing results in displacement capacity that is less than demand. As such, modified detailing must be selected with results recalculated and checked. It is noted that the pushover analysis stops at the point at which any increase in load will cause an unbounded displacement response, i.e. stiffness of the plastic hinge approaches zero. The model also provides the user with a yield displacement, in this case 0.8 inches. This displacement is used in the calculation of ductility as seen below.

For demand in the X direction (transverse):

$$\Delta_D = 5.1 \;\; in. > \Delta_C = 4.0 \;\; inches \;\; (ng)$$

For demand in the Y direction (longitudinal):

$$\Delta_D = 7.4 \;\; in. < \Delta_C = 7.5 \;\; inches \;\; (ok)$$

For ductility:

$\mu_c = \Delta_c / \Delta_y = 5.2/0.8 = 6.5 > 3.0$ (ok)

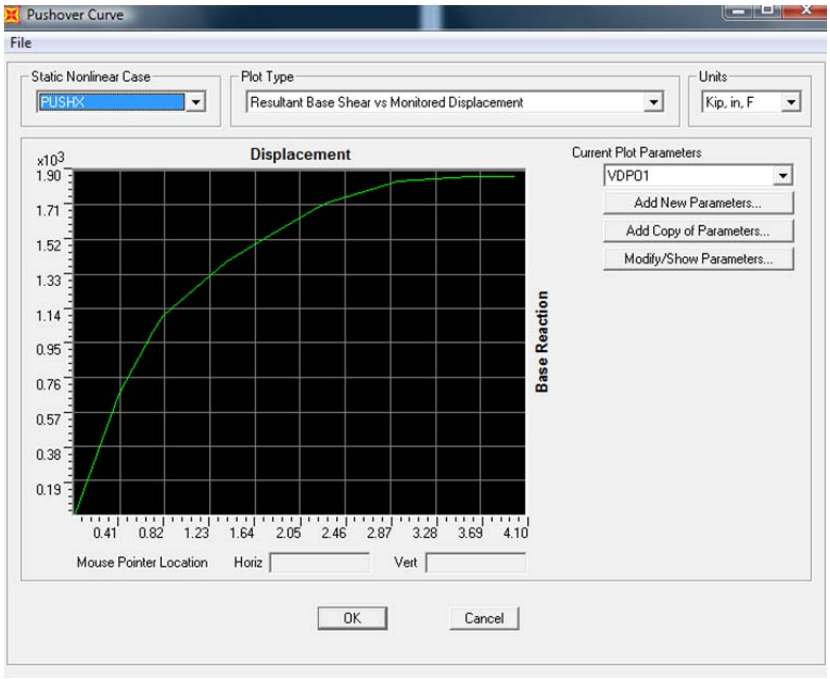

Figure 9.41 Results of Pushover Analysis
Note: P-delta effects are included in the model as a line load on the bent

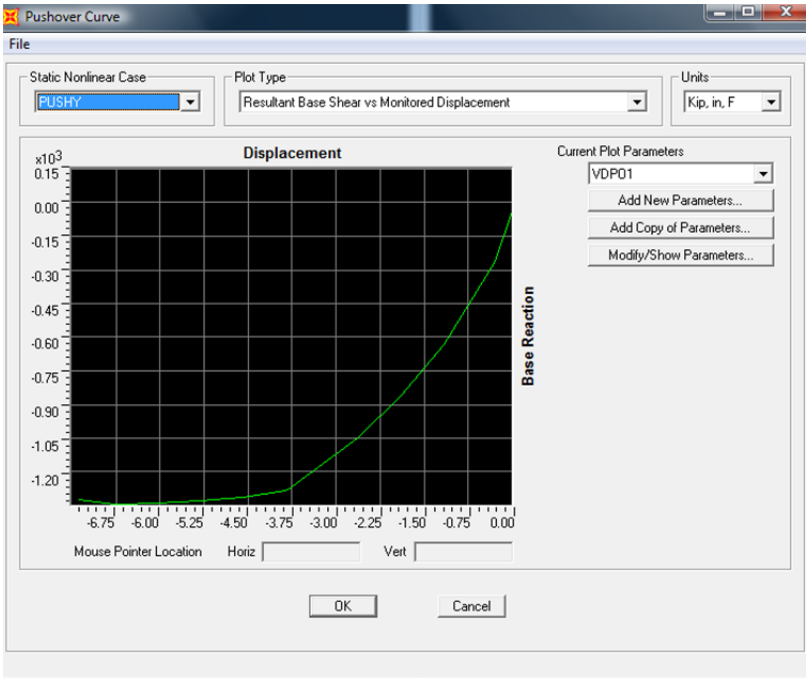

Figure 9.42 Results of Pushover Analysis

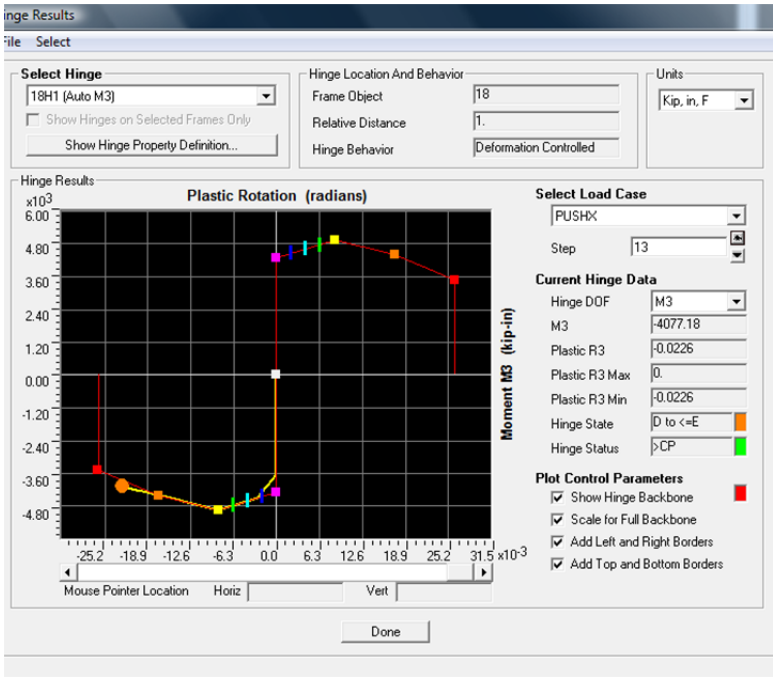

Figure 9.43 Critical Transverse Hinge Performance
Circle indicates plastic rotation just prior to hinge failure (top of pile - maximum compression)

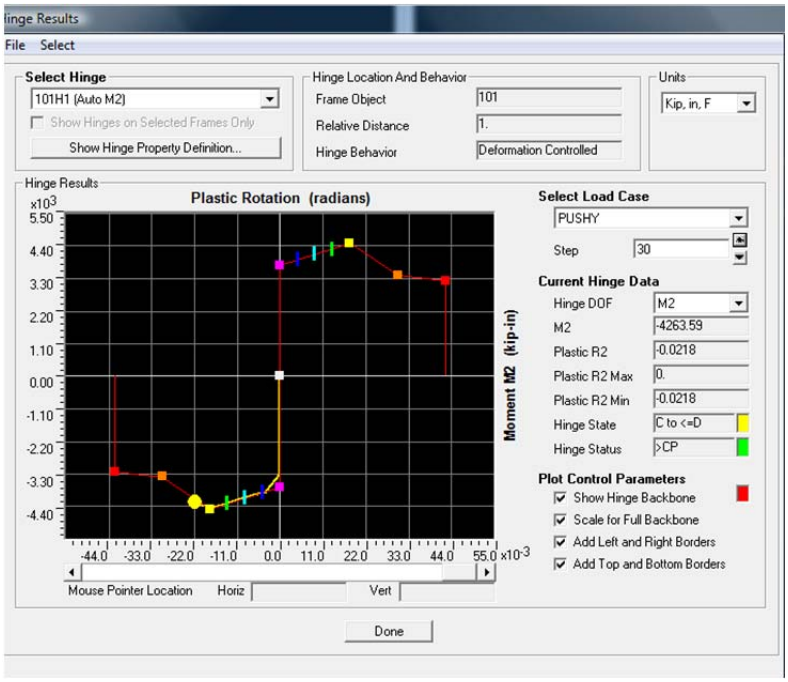

Figure 9.44 Typical Longitudinal Hinge Performance
Circle indicates plastic rotation of typical hinge just prior to reaching capacity

Given the results of the pushover analysis for the first selection of pile detailing it has been shown above that the strength was achieved. However, the displacement demand in the transverse direction was inadequate. Thus a modification to the pile detailing is selected with additional confinement. The W6 spiral modeled previously is changed to a W9 spiral with the same pitch.

- Try 20 inches x 20 inches prestressed pile constructed with W9 spiral encasement at a pitch of 2 inches on center
- Try a strand pattern of 10 – ½ inch special (0.6 inch diameter)
- Assume 38 kips per strand after losses

The same procedure previously presented is performed. Following the input of the modified pile detailing moment curvature analysis for each of the critical positions, hinge analyses, and pushover analyses are completed. The results of these analyses are seen in Figures 9.45 through 9.56.

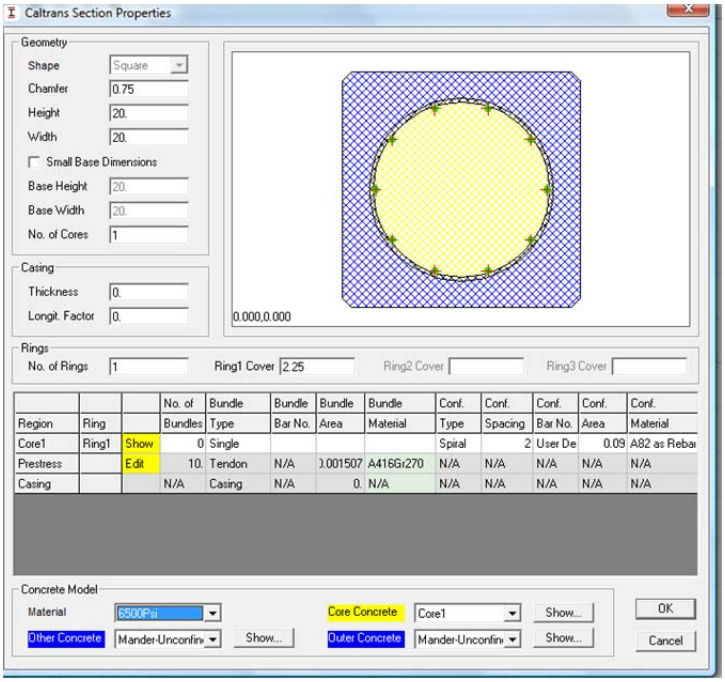

Figure 9.45 Section Designer Input for SAP2000

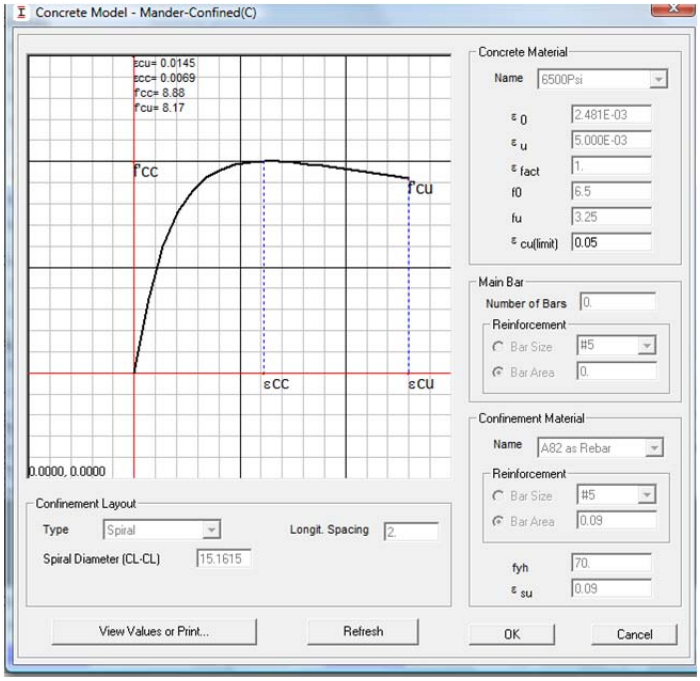

Figure 9.46 Confined Concrete Properties with Section Designer Using SAP2000

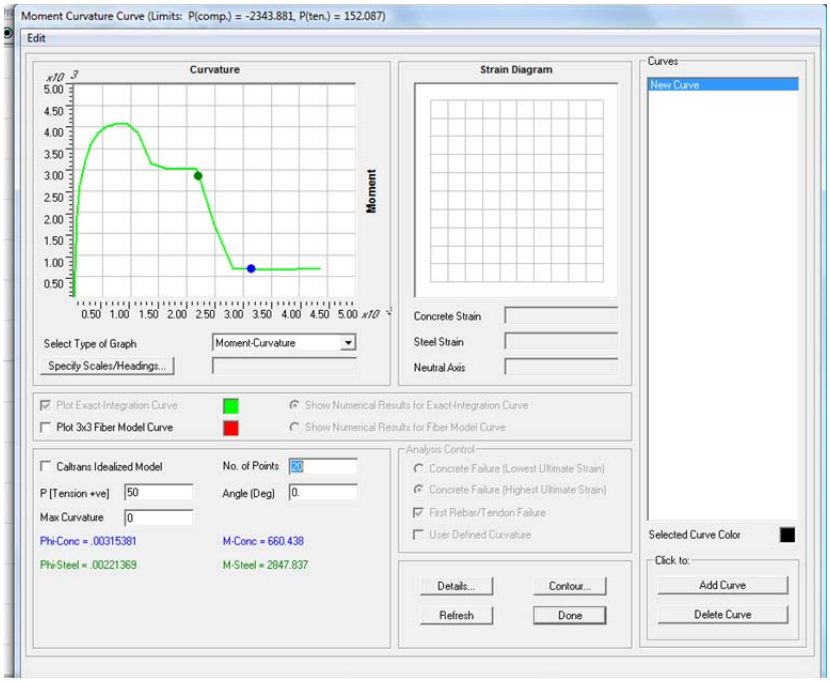

Figure 9.47 Moment Curvature Plot for Axial Force = 50 kips (Tension)

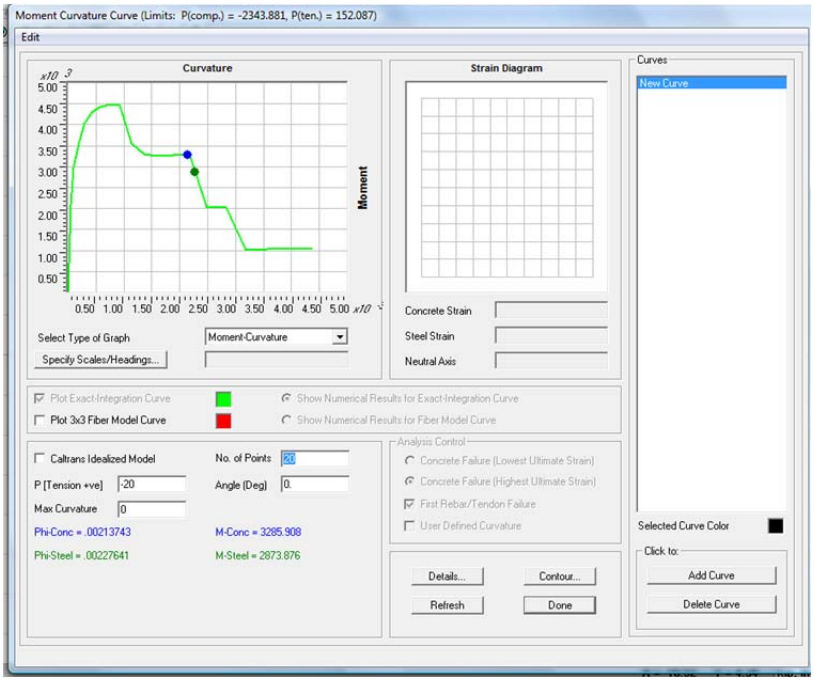

Figure 9.48 Moment Curvature Plot for Axial Force = -20 kips

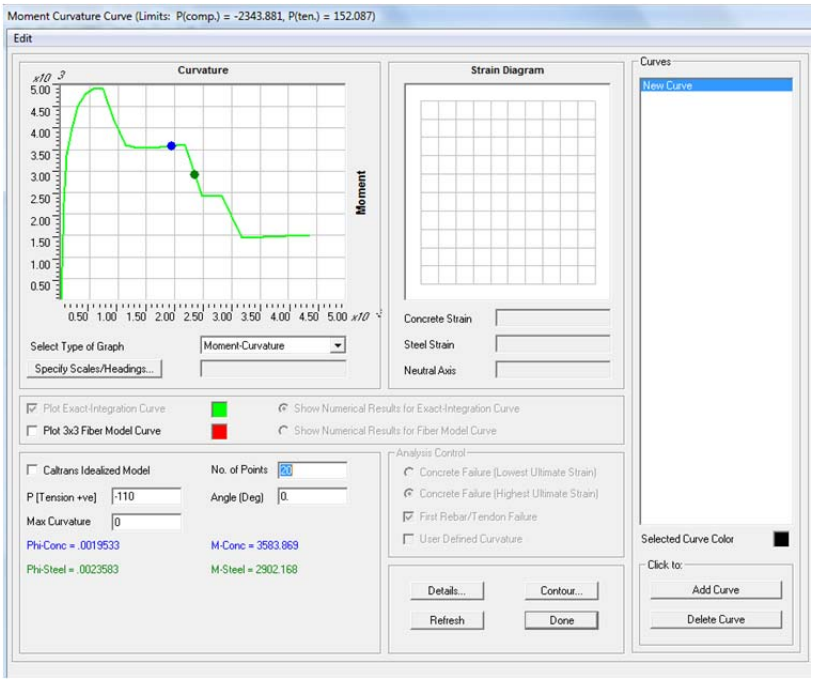

Figure 9.49 Moment Curvature Plot for Axial Force = -110 kips

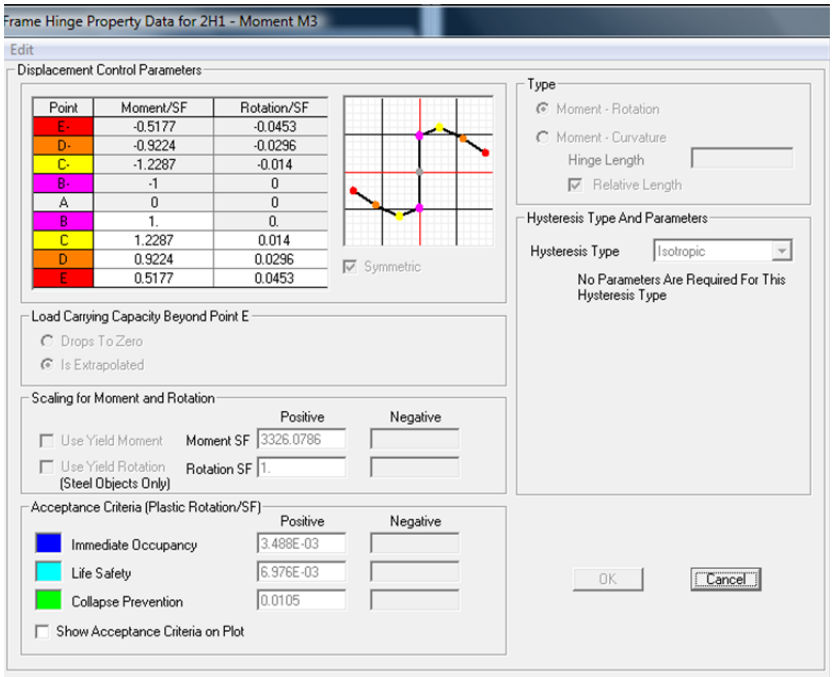

Figure 9.50 Typical Hinge Model (50 kips)

Rotation = 0.00221(20) = 0.0442 radians < 0.0453 radians

M_{max} = 3,326(1.23) = 4,090 kip-inches

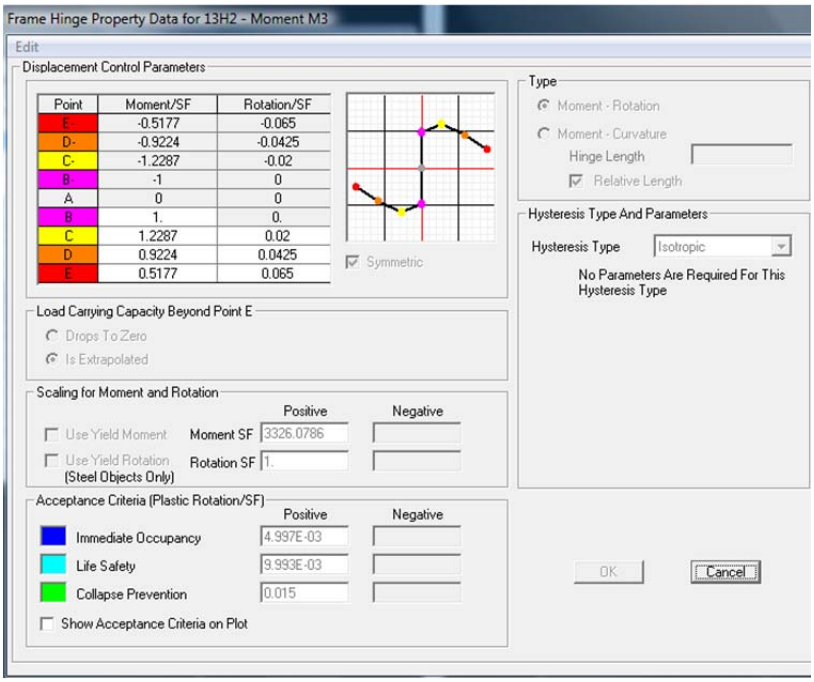

Figure 9.51 Rotational Capacity Bottom Hinge
Rotation Capacity = 28.64/20(0.0453) = 0.065 radians

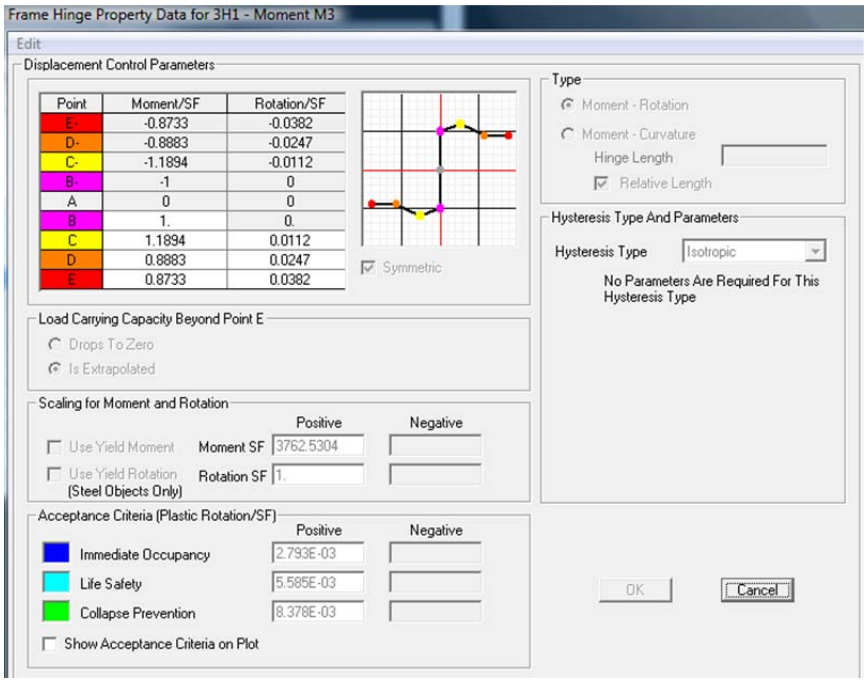

Figure 9. 52 Typical Hinge Model (-20 kips)
Rotation = 0.00213(20) = 0.043 radians > 0.0382 radians
M_{max} = 3,762(1.19) = 4,480 kip-inches

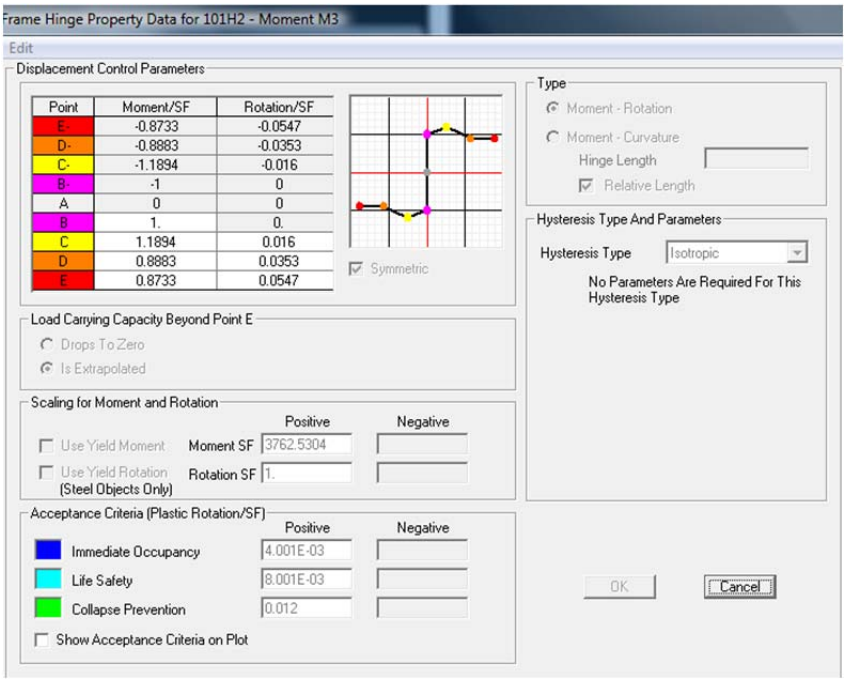

Figure 9.53 Rotational Capacity Bottom Hinge
Rotation Capacity = 28.64/20(0.0382) = 0.055 radians

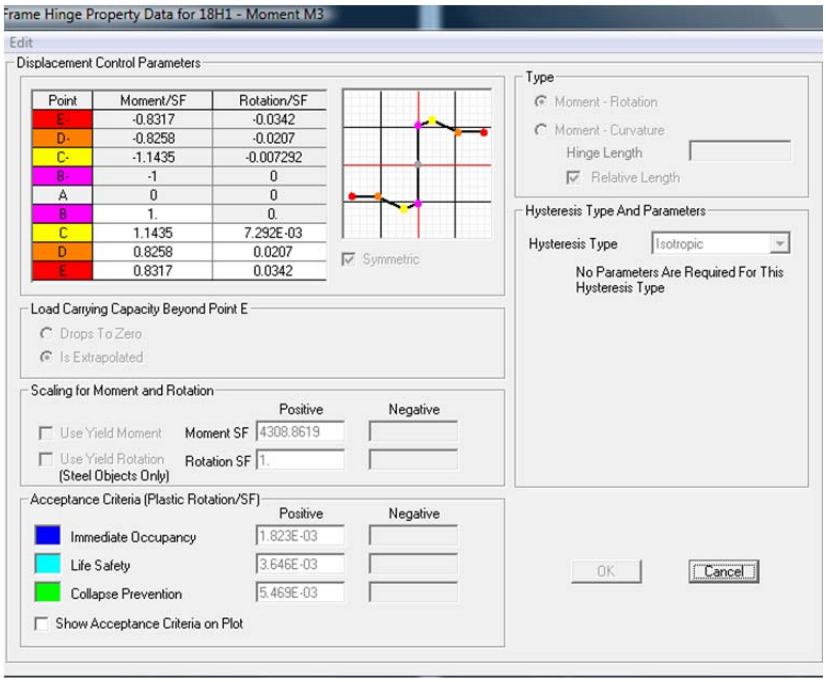

Figure 9.54 Typical Hinge Model (-110 kips)
Rotation = 0.00195(20) = 0.039 rad > 0.0342 radians
M_{max} = 4,308(1.14) = 4,910 kip-inches

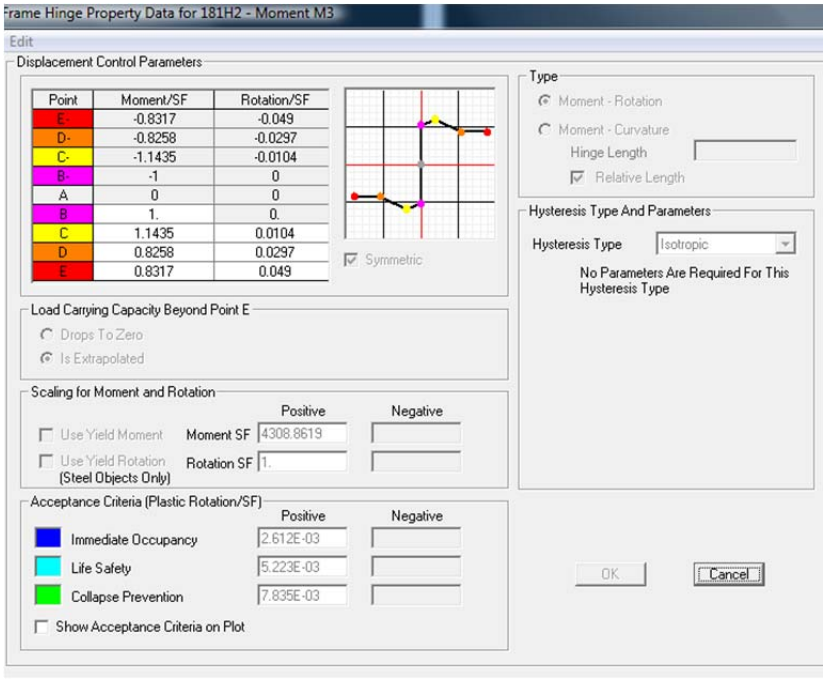

Figure 9.55 Rotational Capacity Bottom Hinge
Rotation Capacity = 28.64/20(0.0342) = 0.049 radians

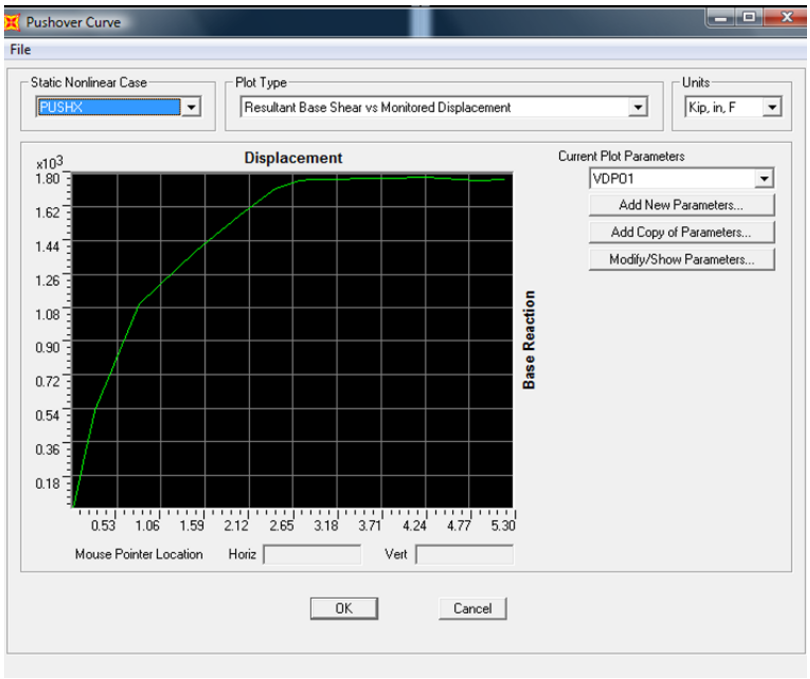

Figure 9.56 Results of Pushover Analysis
Note: P-delta effects are included in the model as a line load on the bent

Results of the pushover analysis indicate that the increased spiral size resulted in the additional confinement needed for design. The capacity in the X direction has increased to 5.2 inches, greater than the 5.1 inches demand.

For demand in the X direction (transverse):

$$\Delta_D = 5.1 \ \ inches < \Delta_C = 5.2 \ \ inches \ \ (ok)$$

For ductility:

$$\mu_c = \Delta_c / \Delta_y = 5.2/0.8 = 6.5 > 3.0 \text{ (ok)}$$

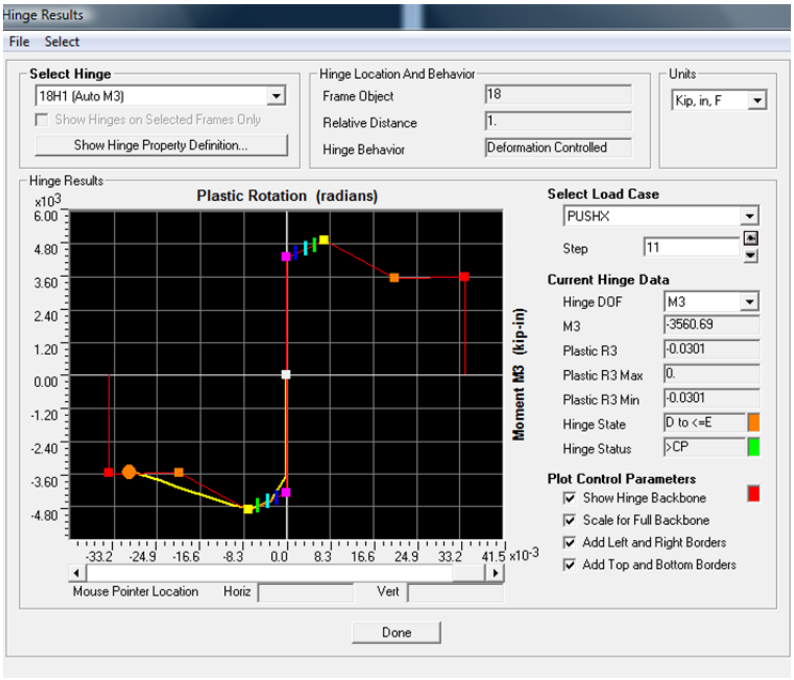

Figure 9.57 Critical Transverse Hinge Performance
Circle indicates plastic rotation just prior to hinge failure at bent capacity (top of pile - max compression)

Check shear strength of the pile:

According to Section 6.7.5 of the *SCDOT Seismic Design Specifications for Highway Bridges* (SCDOT, 2006), the maximum shear is calculated as:

$$V_{po} = \frac{2M_{po}}{L_1 + L_2} = \frac{2(1.2)(4{,}910/12)}{18} = 55 \ \ kips$$

This is non-conservative as the actual maximum shear in the pile at failure is 1.2(101) = 121 kips. It should be noted that Section 6.7.5 is a minimum value. If the pushover model indicates a higher shear demand, that value along with the factor 1.2 shall be applied to the model value.

Check shear capacity of the piles (Section 8.6.1):

In the following calculations $V_{c,-50}$ is the concrete shear capacity for the pile with an axial load of 50 kips (tension), $V_{c,-20}$ is the concrete shear capacity for the pile with an axial load of 20 kips (compression), and $V_{c,-110}$ is the concrete shear capacity for the pile with an axial load of 110 kips

(compression). It should be noted that the below calculations are performed conservatively with the assumption $V_c = 0$. This may be modified per ACI equation 11-8 (ACI, 2008).

$$\phi V_n = \phi V_c + \phi V_s$$

$$V_{c,50} = 0 \quad kips$$

$$\rho_s = \frac{4A_{sp}}{sD'} = \frac{4(0.09)}{2(15.5)} = 0.0116$$

$$f_s = \rho_s f_{yh} = 0.0116(65) = 0.755 \le 0.35 \quad (ng)$$

$$f_s = 0.35$$

$$\mu_d = 3.5 \quad (from \quad SAP2000)$$

$$0.3 \le \alpha' = \frac{f_s}{0.15} + 3.67 - \mu_d = \frac{0.35}{0.15} + 3.67 - 3.5 = 2.5 \le 3 \quad (ok)$$

$$\alpha' = 2.5$$

$$v_c = 0.032\alpha'\left(1 + \frac{P_u}{2A_g}\right)\sqrt{f_c'} \le \min\begin{vmatrix} 0.11\sqrt{f_c'} \\ 0.047\alpha'\sqrt{f_c'} \end{vmatrix}$$

$$v_{c,-20} = 0.032(2.5)\left(1 + \frac{20}{2(20)(20)}\right)\sqrt{4} = 0.164 \quad ksi \le \min\begin{vmatrix} 0.11\sqrt{4} = 0.22 \quad (ok) \\ 0.047(2.5)\sqrt{4} = 0.24 \quad (ok) \end{vmatrix}$$

$$V_{c,-20} = v_{c,-20}(0.8A_g) = 0.164(0.8)(20)(20) = 52.5 \quad kips$$

$$v_{c,-110} = 0.032(2.5)\left(1 + \frac{110}{2(20)(20)}\right)\sqrt{4} = 0.182 \quad ksi \le \min\begin{vmatrix} 0.11\sqrt{4} = 0.22 \quad (ok) \\ 0.047(2.5)\sqrt{4} = 0.24 (ok) \end{vmatrix}$$

$$V_{c,-120} = v_{c,-20}(0.8A_g) = 0.22(0.8)(20)(20) = 58.2 \quad kips$$

$$V_s = \frac{\pi A_v f_y D'}{2s} = \frac{\pi(0.09)(65)(15.5)}{2(2)} = 71$$

$$\phi V_{n,50} = \phi V_{c,50} + \phi V_{s,50} = 0.85(0 + 71) = 60 \quad kips \le V_u = 121 \quad kips \quad (ng)$$

$$\phi V_{n,-20} = \phi V_{c,-20} + \phi V_{s,-20} = 0.85(52.5 + 71) = 105 \quad kips \le V_u = 121 \quad kips \quad (ng)$$

$$\phi V_{n,-110} = \phi V_{c,-120} + \phi V_{s,-120} = 0.85(58.2 + 71) = 110 \quad kips \le V_u = 121 \quad kips \quad (ng)$$

Per the calculations presented the shear strength of the piles is less than the demand. In order to satisfy this higher shear, more spiral reinforcement must be added to all piles:

- Try 20 inch x 20 inch prestressed pile with W20 spiral at two inches on center
- Try ten 0.6 inch strands (38 kips per strand after losses)

Recalculating the nominal shear capacity using the modified spiral for the pile with axial tension of 50 kips, the calculations show that the pile can resist the acting shear forces.

$$\phi V_n = \phi V_c + \phi V_s$$

$$V_{c,50} = 0 \quad kips$$

$$V_s = \frac{\pi A_v f_y D'}{2s} = \frac{\pi(0.20)(65)(15.5)}{2(2)} = 158 \quad kips$$

$$\phi V_{n,50} = \phi V_{c,50} + \phi V_{s,50} = 0.85(0+158) = 134 \quad kips > V_u = 121 \quad kips \quad (ok)$$

Note that in accordance with the research findings, the end pile connections to the cap can be modeled and detailed as pin connections (Chapter 7). Although the complete results of the analysis with pinned end pile connections are not presented here, the analysis was performed and the results show that the axial tension in the end pile is all but eliminated, the maximum compression in the end pile is reduced significantly, shear in the end piles is reduced somewhat, while the shear in the interior piles is increased somewhat as expected based on relative stiffness among piles.

Check p-Δ effects:

P-Δ effects should be checked as per Equation 7.4 of the SCDOT SDS. In this equation P_{dl} is the dead load in the pile (kips), Δ_r is the relative lateral offset between the point of contra-flexure and the end of the plastic hinge (inches), and M_p is the plastic moment capacity of the pile (kip-inches). For purposes of this example P_{dl} is taken as the maximum axial compressive load experienced (110 kips).

$$P_{dl}\Delta_r \leq 0.25 \times M_p$$

$$110 \times 7.5 \ \leq \ 0.25 \times 4910 \qquad (ok)$$

SCDOT DETAILING CHECKS

According to Section 8.4.2 in the SCDOT SDS, the maximum axial load in a member where ductility is greater than one should be calculated using the following equation:

$$P_{max} = 0.2 \, f'_{ce} A_g$$

In the previous equation P_{max} is the maximum allowable axial load applied on the member (kips), f'_{ce} is the expected maximum concrete compressive strength (ksi), and A_g is the gross area of the member.

$$P_{\max} = 0.2 f'_{ce} A_g = 0.2(6.5)(20)(20) = 520 \quad kips > P_u = 110 \quad kips \quad (ok)$$

CAP DESIGN AND DETAILING

It is recommended to use the equations provided in Section 8.7 in the SCDOT SDS for the joint shear design. In the referenced section it is specified that the bent caps and the moment resisting connection with the column should be able to resist seismic forces combined with dead load. The design of the beam-column joints can be either single directional, resisting moments generated from seismic forces acting along the centerline of pile or bent, or multi-directional, where special detailing allows moment to be transferred to the superstructure (SCDOT, 2008).

The principal stresses in any vertical plane within the pile to bent cap connection can be calculated using the following equations; where P_t is principal tensile stress (ksi), P_c is principal compressive stress (ksi), f_h is average axial horizontal stress (ksi), f_v is average axial vertical stress (ksi), and v_{jh} is average joint shear stress (ksi).

$$P_t = \frac{f_h + f_v}{2} - \sqrt{\left(\frac{f_h - f_v}{2}\right)^2 + v_{jh}^2}$$

$$P_c = \frac{f_h + f_v}{2} + \sqrt{\left(\frac{f_h - f_v}{2}\right)^2 + v_{jh}^2}$$

The following equation can be used to determine the effective width of the joint depending on the rectangular shape of the pile framing into the joint. In this equation b_{fe} is the effective joint width (inches), D_c is the maximum cross sectional dimension of pile (inches), and h_c is the width of the pile (inches).

$$b_{fe} = D_c + h_c$$

The average joint shear stress can be estimated using the following equation. In this equation h_b is the distance from the center of gravity of the tensile force to the center of gravity of the compressive force on the section (inches), and M_{po} is the over-strength plastic hinge moment (kip-inches).

$$v_{jh} = \frac{M_{po}}{h_b D_c b_{fe}}$$

The average axial stress in the joint is provided by the axial force in the column P_{col} (kips). An average stress at mid-height of the cap can be calculated using the following equation by assuming a 45˚ spread away from the pile in all directions.

$$f_v = \frac{P_{col}}{b_{fe}(D_c + h_b)}$$

The horizontal axial stress, f_h (ksi), is based on the mean axial force at the center of the joint where: P_b is the axial force in the cap including prestress (kips), h_b is cap depth (inches), and b_b is the cap width (inches).

$$f_h = \frac{P_b}{b_b h_b}$$

Assuming the following values for the design examples the principal stresses can be calculated as follows:

$D_c = 20 \quad inches$

$h_c = 20 \quad inches$

$b_b = 42 \quad inches$

$h_b = 36 \quad inches$

$P_{col} = 110 \quad kips$

$b_{je} = D_c + h_c = 40 \quad inches$

$M_{po} = 1.2(4{,}910) = 5{,}892 \quad kip - inches$

$$v_{jh} = \frac{M_{po}}{h_b D_c b_{je}} = \frac{5{,}892}{36(20)(40)} = 0.204 \quad ksi$$

$$f_v = \frac{P_{col}}{b_{je}(D_c + h_b)} = \frac{110}{40(20+36)} = 0.049 \quad ksi$$

$$p_t = \frac{f_h + f_v}{2} - \sqrt{\left(\frac{f_h - f_v}{2}\right)^2 + v_{jh}^2}$$

$$= \frac{0 + 0.049}{2} - \sqrt{\left(\frac{0 - 0.049}{2}\right)^2 + 0.204^2} = -0.181 \quad ksi$$

$$p_c = \frac{f_h + f_v}{2} + \sqrt{\left(\frac{f_h - f_v}{2}\right)^2 + v_{jh}^2}$$

$$= \frac{0 + 0.049}{2} + \sqrt{\left(\frac{0 - 0.049}{2}\right)^2 + 0.204^2} = 0.230 \quad ksi$$

Maximum Allowable Principal Stress

The principal stresses calculated should be limited to the values given by this section. The following equations give the maximum allowable tensile stress $P_{t,max}$, and the maximum allowable compressive stress $P_{c,max}$. The principal tensile and compressive stresses shall not exceed the allowable maximum tensile and compressive stresses, respectively. In the following equations f'_c is the expected maximum concrete compressive strength (ksi).

$$P_t \leq 0.379\sqrt{f'_c}$$

$$P_c \leq 0.25\sqrt{f'_c}$$

Maximum

$$p_t = 0.179 \quad \text{ksi} \leq p_{t,max} = 0.379\sqrt{f'_c} = 0.379\sqrt{5} = 0.847 \quad \text{ksi} \quad (\text{ok})$$

$$p_c = 0.232 \quad \text{ksi} \leq p_{t,max} = 0.25 f'_c = 0.25(5) = 1.25 \quad \text{ksi} \quad (\text{ok})$$

Per Section 8.7.4 the maximum tensile stress is sufficiently low such that the design need not satisfy Sections 8.7.5 through 8.7.7. This is typical for all bents in flat slab bridges. However, the designer shall verify that Section 8.7.4 is satisfied for each bent of all bridges.

However, stirrups in the bent cap must be designed for shear and longitudinal steel must be designed for positive and negative bending. Additional steel such as skin reinforcement and end cap steel is not discussed here but is required.

Try six No. 8 bars top and bottom:

$$a = \frac{A_s F_y}{0.85 f_c^{'} b} = \frac{6(0.79)(60)}{0.85(4)(42)} = 1.99 \quad inches$$

$$d \approx 32 \quad inches$$

$$\phi M_n = 0.9(6)(0.79)(60)(32 - 1.99/2) = 7{,}940 > 1.2(6{,}100) = 7{,}320 \quad kip - inches(ok)$$

At the second interior pile from each end (third pile from each end), reduce to four No. 8 bars top and bottom:

$$a = \frac{A_s F_y}{0.85 f_c^{'} b} = \frac{4(0.79)(60)}{0.85(4)(42)} = 1.33 \quad inches$$

$$d \approx 32 \quad inches$$

$$\phi M_n = 0.9(4)(0.79)(60)(32 - 1.33/2) = 5{,}347 > 1.2(3{,}000) = 3{,}600 \quad kip - inches(ok)$$

Note: a minimum longitudinal reinforcement of five No. 9 bars or equivalent is required per SCDOT BDM (SCDOT, 2006).

Maximum shear in the cap is 101 kips, try No. 5 hoops at 6 inches on center. The strength of the concrete is conservatively neglected. A 1.2 over-strength magnifier is used.

$$\phi V_n = \phi V_c + \phi V_s$$

$$V_s = \frac{A_v f_y d_e^{'}}{s} = \frac{2(0.31)(60)(0.8)(32)}{6} = 159 \quad \text{kips}$$

$$\phi V_n = 0.85(159) = 135 \quad \text{kips} > 121 \quad \text{kips} \quad \text{(ok)}$$

Chapter 10 - Recommendations and Conclusions

10.1 Literature review

Chapter 2 presents a literature review of related work. The connection details investigated through this project are common throughout the state of South Carolina. The behavior of these types of connections and the ability to predict the associated behavior are of interest. The literature review shows the connection to be viable. Although most of the connection types described in the existing literature are not identical to those used in South Carolina, the related studies are nonetheless important. An understanding of the conclusions drawn from the investigations described in Chapter 2 aided in the successful completion of this investigation. The number of investigations similar to this one shows an interest in the behavior of similar connection types and underlines the need to better explain and predict the behavior of such connections.

The connections reported encompass a number of different types including plain pile embedment. As seen in the literature review connections are often made through doweling action with reinforcement being developed both within the bent cap as well as the connected pile. Additionally, the literature review has shown the recent classification system adopted by the American Society of Civil Engineers (ASCE). ASCE's Seismic Design of Piers and Wharfs provides a basis for classification of the connection type investigated in this research.

10.2 Connection detail

This investigation was undertaken to better understand and evaluate the current construction detail employed within the state of South Carolina and recommended by the South Carolina Department of Transportation (SCDOT). This portion of the work concerns specimens IB-18-1, IB-18-2, EB-18-1 and related finite element model simulations. The connection investigated is that of a precast prestressed pile embedded into a cast-in-place bent cap without additional anchorage, referred to as plain pile embedment. The depth of this embedment was held at a depth equal to a pile cross sectional dimension, as recommended by the SCDOT. In addition to physical specimens tested with a recommended embedment depth, numerical models are presented to evaluate the construction tolerances of ± 6.0 inches in the current recommendation.

Each of the three single pile specimens as well as the numerical models created within the construction tolerances were designed based on current practices employed in the design of these connections. Included in the construction of these specimens was a reinforcement design of bent caps taken as a realistic worst case scenario based on current construction practices. The testing of these specimens included both axial compressive and tensile loading. Although this loading case occurs in practice it had not been previously investigated in a laboratory setting.

In addition to evaluation of current connection details the investigation proposes modifications. The modifications are represented by specimens IB-26-1, IB-22-1, EB-2-1, EB-26-1, and EB-22-1 as well as the three-pile specimen described in Chapter 8. Related finite element models are also presented.

10.3 Development of computer models

Both finite element models and moment curvature models were developed and utilized. Two moment curvature models (XTRACT) were created for each of the single pile specimens. The results of these models are used for comparison with the experimental results.

The first of the two moment curvature models assumes that the full capacity of the pile is developed. The second of the models considers the relative shrinkage between the pile and the bent cap in terms of time and the resulting force exerted onto the embedded portion of the pile as a result of shrinkage (ElBatanouny et al., 2012).

The results of these two models are shown in the plots of hysteretic behavior for the single pile specimens (Chapters 6 and 7). The numerical models are able to predict the behavior of the specimens with relative accuracy and are relatively simple to create. The second of the two models, which accounts for the clamping force exerted due to shrinkage, provides an improved fit to the measured hysteretic behavior. This model also improves upon predicted behavior in comparison to models based on the current ACI code equation (equation 12.4; ACI, 2008) for development of prestressing strands (ElBatanouny et al., 2012).

In addition to the moment curvature models, ABAQUS was used to create finite element models of a number of specimens (Table 10.1). Model calibration and verification was performed through comparison between results of the finite element models and the experimental results of single pile specimens. Following the model calibration additional models were created, taking into account a number of parameters including specimen type (interior or exterior), embedment length, pile dimension, dimensions of the corresponding bent cap, and reinforcement within the bent cap. The finite element models were utilized for investigation of the bent cap behavior with respect to these variables. Although the behavior of the bent cap is the focus of these models it is noted that the model provides reasonable comparisons between the simulations and measured results for the pile behavior as well.

The models were evaluated in terms of moment versus displacement behavior and bent cap performance. The bent cap element of each model is evaluated in terms of several parameters. The first of the evaluation parameters is the initiation of cracking within the bent cap and the global characteristics of the model at the onset of cracking. The extent to which the developed cracks extend into the bent cap and the predicted strain in the reinforcement is also evaluated.

Table 10.1 Description of Modeled Specimens

	Interior Specimen		**Exterior Specimen**	
Pile Dimension	**Embedment Depth (inches)**			
18 inches	22	12	22	12
24 inches	30	18	30	18

10.4 Full-Scale laboratory testing - Interior specimens

Four full-scale single pile specimens representing interior portions of a typical bent cap were tested at the University of South Carolina. The pile portions of these specimens were cast at Florence Concrete Products of Sumter, South Carolina and the bent caps were fabricated and cast at the University of South Carolina Structures Laboratory (Chapter 6). These specimens were constructed with a pile orientation such that the 'top bar' effect was minimized for bending in the transverse direction. This practice is recommended for detailing at all connections. Two of the four specimens represented current construction practice while the remaining two specimens were intended to further evaluate and improve the connection.

Material performance

All pile elements reached 28-day strength of 5,000 psi and all bent cap elements reached a 28-day compressive strength of 4,000 psi. Piles used in the construction of the interior specimens were cast in two sets. The first set of piles reached 28-day strength of 8,300 psi and the second pile set reached a 28-day compressive strength of 7,300 psi. The bent cap of specimen IB-22-1 was not tested for 28-day strength, however it is inferred from the 56-day strength of 5,500 psi that the 28-day strength requirement was met. Based on the results of core sampling this bent cap achieved compressive strength of 6,100 psi at the time of testing.

Moment capacity

Table 10.2 summarizes the directional moments achieved and the corresponding displacements. Specimens IB-18-1 and IB-18-2, both constructed with an embedment depth equal to that currently recommended, developed moment capacities less than predicted assuming no strand slippage. The moment capacities and corresponding displacements of these specimens were also significantly less than that of the other two specimens. Additionally, referring to Figure 6.13 it can be seen that the experimental behavior of specimen IB-18-2 did not reach the level of the model with strand slippage considered.

Specimens IB-26-1 and IB-22-1 both met or exceeded the predicted behavior considering no strand slip. The behavior of these specimens corresponded to this model up to the point of ultimate moment and exceeded the prediction thereafter.

Table 10.2 Maximum Moment and Related Displacement - Interior Specimens

Specimen	Maximum moment, + direction (kip-inches)	Related displacement (inches)	Maximum moment, - direction (kip-inches)	Related displacement (inches)	Averaged moment (kip-inches)	Averaged displacement (inches)
IB-18-1	2,350	2.8	2,330	2.8	2,340	2.8
IB-18-2	2,100	1.7	2,050	1.0	2,075	1.4
IB-26-1	2,780	3.5	2,640	3.0	2,710	3.3
IB-22-1	2,940	4.4	2,920	3.9	2,930	4.2

Ductility capacity

Displacement ductility is calculated per Equation 6.1, with the displacement capacity taken as the point at which the moment capacity degrades to 80% of its ultimate value. Table 10.3 summarizes the ductility calculations for the interior specimens. Each of the four specimens performed well in terms of ductility. Each specimen attained a ductility capacity significantly larger than the value of 3.0 required by the SCDOT Seismic Design Specifications with the minimum calculated ductility capacity of 10.8 occurring in specimen IB-26-1. In the positive direction the moment capacity of specimen IB-22-1 did not degrade to the 80% value, therefore the final displacement of this specimen is used for calculation.

Table 10.3 Displacement Ductility - Interior Specimens

Specimen	Yield, + direction (inches)	Displacement capacity, + direction (inches)	Ductility	Yield, - direction (inches)	Displacement capacity - direction (inches)	Ductility	Averaged ductility
IB-18-1	0.40	5.9	14.8	0.40	5.9	14.8	14.8
IB-18-2	0.53	7.4	14.0	0.56	5.4	10.0	12.0
IB-26-1	0.56	7.0	12.5	0.78	7.0	9.00	10.8
IB-22-1	0.80	8.0	10.0	0.60	8.0	13.0	11.5

Plastic hinge mechanism

A plastic hinge developed within the pile for each specimen. The length of the plastic hinge is expected to reach one pile cross sectional dimension (18 inches). Plastic hinge lengths are estimated based on observed damage along the length of the pile as well as energy dissipation based on curvature measured along the expected plastic hinge zone. For each of the four specimens, figures are presented to estimate the length of the developed plastic hinge (Chapter 6).

Table 10.4 summarizes the estimated length of the plastic hinge which developed in each of the four specimens tested. An embedment length of 18 inches did not develop the desired length of the plastic hinge. Specimens with embedment lengths of 22 and 26 inches developed a plastic hinge length greater than one pile cross sectional dimension.

Table 10.4 Plastic Hinge Length - Interior Specimens

Specimen	Plastic hinge length (inches)
IB-18-1	15
IB-18-2	15
IB-26-1	25
IB-22-1	25

Joint shear and bent cap performance

Specimens were designed such that the bent caps remain elastic without significant damage. To evaluate the performance of the bent caps damage observations were recorded and stresses in the joint region were calculated according to the SCDOT SDS. The results of the joint stress calculations are presented in Table 6.5. As discussed in Chapter 6 these values are significantly less than the allowable values. Observed damage to each of the bent caps is summarized in Table 10.5. Although spalling is seen about the perimeter of the connection for all specimens, only in specimen IB-26-1 was cracking of the bent cap observed. This cracking extended from the lower right corner of the connection (Figure 6.30). Strain in the longitudinal reinforcement of IB-26-1 reached of maximum value of 95 micro-strain.

Table 10.5 Observed Damage - Interior Specimens

Specimen	Observed Damage	Damage Locations
IB-18-1	Spalling	Soffit perimeter
IB-18-2	Minor spalling	Top surface of connection
IB-26-1	Spalling Cracking of bent cap	Top surface of connection Lower corner of connection extending into bent cap
IB-22-1	Minor spalling	Corners of connection

10.5 Full-Scale laboratory testing - Exterior specimens

In addition to the four interior specimens, four specimens representative of an exterior portion of a bent cap were also tested at the University of South Carolina Structures Laboratory. Similar to the interior specimens the pile elements were cast at Florence Concrete Products, while the bent cap elements were fabricated and cast at the University of South Carolina. For these specimens the 'top bar' effect was also mitigated with proper pile orientation during the embedment process. The test setup for these specimens imposed axial tensile and compressive loading. Though important to the behavior of the connection, the application of axial tensile loading had not been considered in previous investigations.

Specimens EB-18-1 and EB-2-1 were designed to be representative of current construction practice, with pile embedment depths of 18 and 2 inches respectively. These specimens as well as specimen EB-22-1 were constructed with what was deemed a realistic worst case scenario in terms of bent cap reinforcement design.

Based on the results of specimen EB-18-1 specimens EB-26-1 and EB-22-1 were designed. The design of the remaining two specimens was completed in an effort to develop a significant moment capacity while conforming to the evaluation criteria set forth by the SCDOT SDS. The method of moment capacity development differed significantly between the two specimens. Specimen EB-26-1 was designed such that the pile was developed through the inclusion of significant additional reinforcement. Specimen EB-22-1 was designed such that the pile was

developed through additional overhang of the bent cap. Shear reinforcement of the extended cap specimen was modified to accommodate the additional length.

Material performance

The material conformance of the exterior specimens was identical to that of the interior specimens (bent caps attaining 4,000 psi and piles 5,000 psi for 28-day compressive strength). The piles used for these specimens were cast along with those for the interior specimens (compressive strengths of 8,300 and 7,300 psi). This is also true for the bent cap of specimen EB-22-1 which was cast from the same batch of concrete for specimen IB-22-1. The bent caps for remaining specimens each reached the required 4,000 psi prior to testing (Table 7.1).

Moment capacity

Table 10.6 details the moment capacity of each specimen along with the directional moment capacities of the specimens and corresponding displacements. Specimen moment capacity is not given for specimen EB-18-1 and further discussion is presented in Chapter 7. Referring to Figure 7.3, the moment capacity of this specimen was significantly less than that corresponding to the full capacity of the pile. Specimen EB-2-1 was designed to perform as a hinge and developed a moment capacity of 740 kip-inches at a displacement of approximately one inch.

Specimens EB-26-1 and EB-22-1 were each designed to develop the capacity of the pile. In the negative direction corresponding to axial compression each specimen performed well in comparison with the full pile capacity model. In the positive direction the moment capacity of each is less than the same model, though the behavior of specimen EB-22-1 approaches the prediction of the second numerical model.

Table 10.6 Maximum Moment and Related Displacement - Exterior Specimens

Specimen	Maximum moment (kip-inches)	Displacement at Maximum Moment (inches)	Minimum Moment (kip-inches)	Displacement Min Moment (inches)	Moment Capacity (kip-inches)	Moment Capacity Displacement (inches)
EB-18-1	N/A	N/A	N/A	N/A	N/A	N/A
EB-2-1	740	1.32	970	0.78	740	1.05
EB-26-1	1,790	1.00	2,730	1.75	1,790	1.00
EB-22-1	2,050	3.50	2,830	3.50	2,050	3.50

Ductility capacity

Displacement ductility is summarized in Table 10.7. The calculation of this parameter is taken from Equation 6.1. Similar to moment capacity this value is not presented for specimen EB-18-1. Each of the remaining specimens performed well in terms of ductility capacity with a minimum calculated value determined from specimen EB-22-1 of 8.8. This value is considerably larger than the required value of 3.0.

Table 10.7 Displacement Ductility - Exterior Specimens

Specimen	Yield, + direction (inches)	Displacement capacity, + direction (inches)	Ductility	Yield, - direction (inches)	Displacement capacity, - direction (inches)	Ductility	Averaged Ductility
EB-18-1	N/A	N/A	N/A	N/A	N/A	N/A	N/A
EB-2-1	0.60	8.0	13.3	0.60	8.0	13.3	13.3
EB-26-1	0.31	4.5	14.5	0.41	5.5	13.4	14.0
EB-22-1	0.40	6.0	15.0	0.62	5.5	8.8	8.8

Plastic hinge mechanism

Plastic hinge lengths are shown in Table 10.8. Because specimen EB-2-1 was designed to perform as a true hinge a plastic hinge in the pile was not developed during testing. Both EB-26-1 and EB-22-1 did develop a plastic hinge of sufficient length. An estimation of plastic hinge length is also not provided for specimen EB-18-1 because this specimen failed at a very low level of displacement.

Table 10.8 Plastic Hinge Length - Exterior Specimens

Specimen	Plastic hinge length (inches)
EB-18-1	N/A
EB-2-1	N/A
EB-26-1	18
EB-22-1	22

Joint shear and bent cap performance

The bent cap performance of the exterior specimens was similar to that of the interior specimens. Specimen EB-18-1 developed a large crack about the perimeter of the pile along with minor spalling occurring at both the interior and exterior faces of the soffit. Specimens EB-26-1 and EB-22-1 both exhibited spalling about the perimeter of the connection though this was slightly more pronounced in specimen EB-22-1. The bent caps of these specimens were observed to crack along the top of the interface, with the cracks extending into the depths of the bent cap. This cracking was also more pronounced in specimen EB-22-1. Strain in the vicinity of these cracks was measured and found to be far less than yield. The bent cap of specimen EB-2-1 was undamaged. Table 7.5 summarizes the results of the joint stress calculations and the results are less than allowable values.

Table 10.9 Observed Damage - Exterior Specimens

Specimen	Observed Damage	Damage Locations
EB-18-1	Minor spalling	Soffit corners
EB-2-1	No damage	-
EB-26-1	Spalling Cracking of bent cap	Soffit perimeter Extending from middle of soffit into top of bent cap
EB-22-1	Spalling Cracking of bent cap	Soffit perimeter Extending from two corners and center of soffit into top of bent cap

10.6 Full-Scale laboratory testing - Three pile specimen

The three pile test specimen was assembled and tested at the University of Nevada-Reno. The piles and bent cap reinforcement were shipped to the University of Nevada-Reno and the bent cap and footing were cast-in-place. This specimen was designed with multiple components of the single piles tests conducted at the University of South Carolina including cap designs taken from specimens EB-26-1 and EB-22-1 and a reduced cap depth as seen in specimens IB-22-1 and EB-22-1. The specimen was subjected to multiple amplitudes of the Josh-T time history as described in Chapter 8.

Material performance

The material performance of the three pile specimen also required that the bent cap and piles reach 28-day compressive strengths of 4,000 and 5,000 psi and this was achieved. Compression testing was performed following specimen testing and the results showed the piles reached compressive strength of 8,300 psi while the bent cap reached compressive strength of 4,600 psi. The footing of the specimen was also tested for compressive strength following testing and reached compressive strength of 6,600 psi.

Hysteretic behavior

From the figures shown in Chapter 8 it can be seen that the specimen remains linear elastic through the majority of the motion of JOSH-T 1.0. Deviation from linearity begins in this motion which reached a maximum displacement greater than 2.5 inches. From the figures detailing the hysteretic behavior it can also be seen that the specimen does not significantly degrade in terms of lateral force capacity through the duration of the testing protocol. The specimen was subjected to displacements of ± 12.0 inches to acquire the specimen response following a degradation of lateral force capacity.

Bent cap performance

Photographs detailing the damage to the bent cap are shown in Chapter 8. These photographs detail the damage occurring to the bent cap at each of the pile connections. Damage outside of

these photographs between the pile connections was not observed during testing. The majority of the damage was concentrated at the connection to pile A. The design of this portion of the bent cap was based on the design of specimen EB-26-1 and is referred to as the heavily reinforced portion of the bent cap. It should be noted that the damage occurring to the bent cap at this location was limited to spalling about the perimeter of the connection and a single crack extending from the top of the pile into the bent cap. Additional damage of the bent cap was observed at the connection to pile B, though this damage was limited to minor spalling concentrated at the corners of the soffit. Damage to the bent cap at the connection to pile C was not observed.

10.7 Design guide

Chapter 9 of this report provides guidance related to methods for design of the investigated connections. This guide is intended to aid readers in the process by which bridges employing the detail found in this report may be designed according to the SCDOT Bridge Design Manual, SCDOT SDS, and the findings of this report.

Table 10.10 presented previously as Table 9.1 provides engineers the results of moment curvature analyses as performed in SAP2000 for common pile and strand configurations used in flat slab bridges. This table is again presented here for convenience.

Table 10.10 Recommended Preliminary Design Assumptions for Flat Slab Bridges

Pile Dimension	Strands	M_p (kip-inches)	ϕ_y	ϕ_u	ϕ_u/ϕ_y
24 inch x 24 inch	20 - 0.5 inch	7,022	0.000199	0.00131	6.58
24 inch x 24 inch	20 - 0.5 inch (S)	7,407	0.000199	0.00126	6.33
20 inch x 20 inch	10 - 0.6 inch	4,015	0.000237	0.00162	6.83
20 inch x 20 inch	10 - 0.5 inch (S)	3,431	0.000234	0.00182	7.78
20 inch x 20 inch	9 - 9/16 inch	3,490	0.000182	0.00175	9.61
20 inch x 20 inch	11 - 0.5 inch	3,428	0.000128	0.00173	13.5
18 inch x 18 inch	9 - 1/2 inch	2,504	0.000290	0.00205	7.07
18 inch x 18 inch	8 - 1/2 inch	2,336	0.000254	0.00213	8.39
18 inch x 18 inch	8 - 1/2 inch (S)	2,460	0.000255	0.00206	8.03

10.8 Conclusions and recommendations

The results of this investigation emphasize the need for careful evaluation of connections between prestressed piles and cast-in-place bent caps. The early portion of the investigation involving the evaluation of the typical SCDOT design and detailing practices shows that the interior connection is capable of developing sufficient ductility while maintaining reasonable bent cap performance. However, the interior connection was incapable of developing the capacity of the pile and this was reflected in plastic hinge lengths that were less than expected.

For the exterior connection detail premature failure of the bent cap occurred due to prying action. Simulations presented in Chapter 5 provide further evaluation of the current details.

Additional single pile specimens and simulations demonstrate improved performance for pile embedments deeper than a single pile diameter. The laboratory investigations resulted in full pile development in both interior and exterior specimens with an embedment depth equal to 22 inches (for piles with 18 inch cross sectional dimension). Specimens constructed with deeper embedment show similar improvements in the development of moment capacity. Additionally, specimens constructed with embedment depths greater than one pile diameter sufficiently develop the desired plastic hinge mechanism. Deeper pile embedments distribute damage further along the length of the pile and minimize the damage at or just inside the interface between the pile and bent cap. Improved performance is seen without an appreciable decay in ductility capacity.

Further testing and simulations indicate that while maintaining limited damage to the bent cap, sufficient pile embedment in exterior specimens is able to develop the pile near its full capacity when sufficient confinement is provided. This is shown for either of the two methods for pile confinement as seen in specimens EB-26-1 and EB-22-1.

As seen in specimen EB-26-1, providing confinement to the pile is possible while maintaining minimal cap dimensions. The confinement in this specimen is provided through the use of additional reinforcement (Chapter 7). Although this design enhanced the behavior of the connection, some damage to the bent cap was evident. Modifications to the design to improve cap behavior by limiting damage are discussed in Chapter 8. Through the results discussed in Chapter 8 it can be seen that the modifications are able to reduce damage in the bent cap. Therefore, this reinforcement design with modifications as described in Chapter 8 is recommended as one method to develop the moment capacity of exterior piles.

In specimen EB-22-1, additional confinement to the pile is provided through extending the exterior portion of the bent cap (extended from one foot ten inches from the center of the pile to three feet). It is recommended that the extension given for larger pile dimensions (up to 24 inches by 24 inches in cross section) be proportional to the relationship between cap width and extension provided for specimen EB-22-1. It has also been shown that damage to the bent cap observed in specimen EB-22-1 was significantly reduced with the addition of a minimal amount of additional reinforcement as provided in the construction of the three pile specimen. Therefore, it is recommended that similar additional reinforcement be provided in the event that this detail is utilized. Of the two methods described above for developing the moment capacity of exterior piles, providing additional bent cap overhang appears to be more economical.

It has also been shown that exterior piles may be designed to behave as a true hinge as for specimen EB-2-1. Given the behavior of this design additional bent cap reinforcement is not needed.

For piles of typical cross sectional geometry (18 to 24 inches), results indicate that a plain pile embedment is able to meet the criteria outlined by the SCDOT provided that proper bent cap detailing and sufficient pile embedment length are provided. To achieve sufficient performance, piles should be embedded to depth of 1.3 times the pile cross sectional dimension, with a

construction tolerance of ± 3.0 inches. It has also been shown that a properly designed reinforcement scheme at both interior and exterior portions of the bent is able to minimize damage to the bent cap. Appropriate detailing is shown in the reinforcement design of the three pile specimen presented in Chapter 8.

Table 10.11 details the difference between the recommended embedment depth presented here and the current embedment depth recommendation. The table shows embedment depths of 18, 20 and 24 inch piles at the minimum and maximum depths based on current and proposed construction tolerances. It is further recommended that cap depths be based on the current South Carolina Bridge Design Manual section 20.2.7.1. As such a minimum cap depth of 30 inches should be used for 18 inch piles. The embedment depth of larger piles dictates the minimum cap depth needed. Static punching shear of the bent cap should be investigated, particularly for cases with minimal cover above the pile.

Table 10.11 Current versus Proposed Embedment Depths

18 inch pile		
	1.0*D	1.3*D
Maximum	24	26.4
Minimum	12	20.4
20 inch pile		
	1.0*D	1.3*D
Maximum	26	29.0
Minimum	14	23.0
24 inch pile		
	1.0*D	1.3*D
Maximum	30	34.2
Minimum	18	28.2

It should be noted that the investigations were primarily focused on horizontal loading. In the case of the exterior specimens and the three pile specimen tensile and compressive axial loading was also involved. The case of potential vertical ground movement should also be investigated, with particular emphasis on potential punch through of the piles and related shear reinforcement requirements for the bent cap.

References Cited

AASHTO, "Bridge Design Specifications, 3rd Edition", *American Association of State Highway and Transportation Officials*, Washington, DC, 2004.

ACI Committee 318, "Building Code Requirements for Structural Concrete (ACI 318-08)," *American Concrete Institute*, Farmington Hills, MI, 2008.

ACI Committee 209, "Prediction of Creep, Shrinkage, and Temperature Effects in Concrete Structures (ACI 209R-92) (Re-approved 1997)," *American Concrete Institute*, Farmington Hills, MI, pp. 48, 1992.

ASCE, "Seismic Design of Piers and Wharfs", Unpublished National Standard (draft).

"Dassault Systèmes, Abaqus Analysis User's Manual V. 6.9.", ABAQUS Inc., *Dassault Systèmes*, RI, USA, 2009.

ElBatanouny, M.K., "Determining Slipping Stress of Prestressing Strands in Piles Embedded in CIP Caps", *Thesis Submitted in Partial Fulfillment of the Master of Science Degree*. University of South Carolina, Columbia, SC, 2010.

ElBatanouny, M.K., Ziehl, P.H., Larosche, A., Mays, T., and Caicedo, J.M., "Bent-cap Confining Stress Effect on the Slip of Prestressing Strands," *ACI Structural Journal,* V.109, No. 4, July-August 2012.

ElBatanouny, M. K., and Ziehl, P. H., "Determining Slipping Stress of Prestressing Strands in Confined Sections", *ACI Structural Journal,* in press, May, 2012.

Harries, K.A., and Petrou, M.F., "Behavior of Precast, Prestressed Concrete Pile to Cast-In-Place Pile Cap Connections", *PCI Journal*, V.46, No. 4, 82-93, 2001.

Joen, Pam H., and Park, R., "Simulated Seismic Load Tests on Prestressed Concrete Piles and Pile-Pile Cap Connections", *PCI Journal*, V.35, No. 6, pp. 42-61, 1990.

Mander, J.B., Priestley, M.J.N., and Park, R., "Theoretical Stress-Strain Model for Confined Concrete", *Journal of Structural Engineering*, V.114, Issue 8, pp. 1804-1826, 1988.

Marcakis, K., and Mitchell, D., "Precast Concrete Connections with Embedded Steel Members", *PCI Journal*, V.25, No. 4, July-August, pp. 88-116, 1980.

Mattock, A.H., and Gaafar, G.H., "Strength of Embedded Steel Sections as Brackets", *ACI Journal*, V.79, No. 2, March-April, pp. 83-93, 1982.

Mays, T.W., and Mulliken, J., "Task 1b: Computer Modeling of Selected South Carolina Bridges", *Final Report submitted to the SCDOT*, 2008.

"PCI Design Handbook: Precast and Prestressed Concrete", 6th Edition, MNL-120-4, *Precast/Prestressed Concrete Institute*, Chicago, IL, 2004.

Pizzano, B.A., "Behavior of Prestressed Concrete Piles Under Seismic Loading", *Thesis Submitted in Partial Fulfillment of the Master of Science in Civil Engineering*, University of Washington, Seattle, WA. 1984.

Priestley, M.J.N., Sieble, F., and Calvi, G.M.," Seismic Design and Retrofit of Bridges", *John Wiley & Sons, Inc.,* New York, NY, 2006.

Reese, L.C., and Wang, S.T., "LPILE 6.0 User Manual", *Ensoft, Inc*. Austin, TX, 2011.

Roeder, C.W., Graff, R., Soderstrom, J.L., and Yoo, J.H., "Seismic Performance of Pile–Wharf Connections", *Pacific Earthquake Engineering Research Center*, College of Engineering, University of California, Berkeley, December 2001.

SAP2000, "Structural Analysis Program, Nonlinear Version 12.15", *Computer and Structures, Inc.* Berkeley, CA, USA; 2000.

SCDOT Bridge Design Manual, *South Carolina Department of Transportation,* Columbia, SC, 2006.

SCDOT Seismic Design Specifications for Highway Bridges, Version 2.0, *South Carolina Department of Transportation*, Columbia, SC, 2008.

Shahawy, M., Issa, M., and Polodna, M., "Development Length of Prestressed Concrete Piles", Report No. SSR-01-90, Florida Department of Transportation, Tallahassee, FL, 1990.

Shahawy, M.A., and Issa, M., "Effect of Pile Embedment on the Development Length of Prestressing Strands", *PCI Journal*, V.37, No. 6, pp. 44-59, 1992.

Sheppard, D.A., "Seismic Design of Prestressed Concrete Piling", *PCI Journal*, V.28, No. 2, pp. 20-49, 1983.

Steunenberg, M., Sexsmith, R., and Stiemer, S., "Seismic Behavior of Steel Pile to Precast Concrete Cap Beam Connections", *ASCE Journal of Bridge Engineering*, V.3, No. 4, pp.177–185, 1998.

South Carolina Geological Survey, Recent Earthquakes. http://www.dnr.sc.gov/geology/RecentEarthquakes.htm. March 25, 2011.

Swiegart, S.,"Seismic Performance of Prestressed Concrete Piles in CIP Reinforced Concrete Pile Caps", *Thesis Submitted in Partial Fulfillment of the Master of Science Degree,* University of South Carolina, Columbia, SC, 2010.

Teguh, M., Duffield, C., Mendis, P., and Hutchinson, G., "Seismic Performance of Pile-to-Pile Cap Connections: An Investigation of Design Issues", *Electronic Journal of Structural Engineering*, V.6, pp. 8-18, 2006.

USGS, South Carolina Earthquake History. http://earthquake.usgs.gov/earthquakes/states/south_carolina/history.php. March 25, 2011.

USGS, Top Earthquake States. http://earthquake.usgs.gov/regional/states/top_states.php. January 30 2009.

Xiao, Y., "Experimental Studies on Precast Prestressed Concrete Pile to CIP Concrete Pile- Cap Connections", *PCI Journal*, V. 48, No.6, pp. 82-91. 2003.

XTRACT "Cross Section Analysis of Components", *TRC Software*, Rancho Cordova, CA, USA; 2011.

Appendix - A

P-Y Curve Data for Interior Bents - Example 1

```
------------------------------------------------------------------------
------
                    p-y Curves Reported for Specified Depths
------------------------------------------------------------------------
------


p-y Curve Computed Using the Soft Clay Criteria for Static Loading
Conditions

Soil Layer Number           =            1
Depth below pile head       =       60.000 in
Depth below ground surface  =        0.000 in
Equivalent Depth            =        0.000 in
Pile Diameter               =       20.000 in
Cohesion, c                 =        5.000 lbs/in**2
Avg Eff Unit Weight         =      0.01900 lbs/in**3
Epsilon50 parameter         =      0.01000
Default J parameter         =        0.500
Y50                         =      0.50000 in
p-multiplier                =      1.00000
y-multiplier                =      1.00000

        y, in            p, lbs/in
---------------    -----------------
         0.0000           0.0000
        0.00400         30.00000
        0.12500         94.49408
        0.25000        119.05508
        0.37500        136.28404
        0.50000        150.00000
        0.62500        161.58260
        0.75000        171.70714
        0.87500        180.76067
        1.00000        188.98816
        1.12500        196.55561
        1.25000        203.58132
        1.37500        210.15295
        1.50000        216.33744
        4.00000        300.00001
        7.50000        300.00000
       10.00000        300.00000
```

p-y Curve in Sand Computed Using Reese Criteria for Static Loading Conditions

Soil Layer Number	=	2	
Depth below pile head	=	120.000	in
Depth below ground surface	=	60.000	in
Ground Slope	=	0.000	degrees
Pile Batter	=	0.000	degrees
Effective Slope	=	0.000	degrees
Equivalent Depth (see note)	=	113.217	in
Pile Diameter b	=	20.000	in
Angle of Friction	=	29.000	deg.
Avg. Eff. Unit Weight	=	0.01900	pcf
kpy	=	40.000	pcf
K active	=	0.347	
K passive	=	2.882	
K0	=	0.400	
Pst	=	535.040	lbs/in
Psd	=	579.893	lbs/in
Ps = Pst (shallow controls)	=	535.040	lbs/in
A (static)	=	0.8800	
B (static)	=	0.5000	
C = pm/(ym^(1/n))	=	521.7297	
n = pm/(m ym)	=	1.6447	
m = (pu-pm)/(yu-ym)	=	487.9560	
yk = [c/(kx)]^(n/(n-1))	=	0.0040	in
pk	=	18.271	lbs/in
ym = b/60	=	0.3333	in
pm = B ps	=	267.520	lbs/in
yu = 3b/80	=	0.7500	in
pu = A ps	=	470.835	lbs/in
Es,lim	=	4528.683	lbs/in/in
p-multiplier	=	1.00000	
y-multiplier	=	1.00000	

This p-y curve is computed using the equivalent depth.

y, in	p, lbs/in
0.0000	0.0000
0.02778	59.04915
0.05556	89.99946
0.08333	115.16046
0.11111	137.17221
0.13889	157.10407
0.16667	175.52122
0.19444	192.76726
0.22222	209.07032
0.25000	224.59139
0.27778	239.44935
0.30556	253.73502
0.33333	267.51976
0.54167	369.17726
0.75000	470.83477
20.75000	470.83477
40.75000	470.83477

p-y Curve in Sand Computed Using Reese Criteria for Static Loading Conditions

Soil Layer Number	=	2
Depth below pile head	=	180.000 in
Depth below ground surface	=	120.000 in
Ground Slope	=	0.000 degrees
Pile Batter	=	0.000 degrees
Effective Slope	=	0.000 degrees
Equivalent Depth (see note)	=	173.217 in
Pile Diameter b	=	20.000 in
Angle of Friction	=	29.000 deg.
Avg. Eff. Unit Weight	=	0.02350 pcf
kpy	=	40.000 pcf
K active	=	0.347
K passive	=	2.882
K0	=	0.400
Pst	=	1439.647 lbs/in
Psd	=	1434.472 lbs/in
Ps = Psd (deep controls)	=	1434.472 lbs/in
A (static)	=	0.8800
B (static)	=	0.5000

C = pm/(ym^(1/n)) = 1398.7872
n = pm/(m ym) = 1.6447
m = (pu-pm)/(yu-ym) = 1308.2380
yk = [c/(kx)]^(n/(n-1)) = 0.0169 in
pk = 116.936
lbs/in
ym = b/60 = 0.3333 in
pm = B ps = 717.236
lbs/in
yu = 3b/80 = 0.7500 in
pu = A ps = 1262.335
lbs/in
Es,lim = 6928.683
lbs/in/in
p-multiplier = 1.00000
y-multiplier = 1.00000
This p-y curve is computed using the equivalent depth.

y, in	p, lbs/in
0.0000	0.0000
0.02778	158.31415
0.05556	241.29370
0.08333	308.75177
0.11111	367.76654
0.13889	421.20498
0.16667	470.58242
0.19444	516.82004
0.22222	560.52947
0.25000	602.14236
0.27778	641.97739
0.30556	680.27810
0.33333	717.23576
0.54167	989.78534
0.75000	1262.33492
20.75000	1262.33492
40.75000	1262.33492

p-y Curve Computed Using Static Criteria for Stiff Clay without Free Water

Soil Layer Number = 3
Depth below pile head = 240.000 in
Depth below ground surface = 180.000 in
Ground Slope Angle = 0.000
degrees
Pile Batter Angle = 0.000
degrees
Effective Slope = 0.000
degrees
Equivalent Depth = 108.382 in
Diameter = 20.000 in

Undrained cohesion, c = 18.00000
lbs/in**2
Average Eff. Unit Weight = 0.02513
lbs/in**3
Epsilon-50 = 0.00500
Pct = 2109.916
lbs/in
Pcd = 3240.000
lbs/in
Pu = 2109.916
lbs/in
y50 = 0.250 in
p-multiplier = 1.00000
y-multiplier = 1.00000

y, in	p, lbs/in
0.0000	0.0000
0.0000400	118.64928
0.0002000	177.42205
0.0004000	210.99156
0.00200	315.50599
0.00400	375.20196
0.02000	561.05779
0.04000	667.21391
0.10000	838.97709
0.20000	997.71752
0.30000	1104.15595
0.40000	1186.49277
1.00000	1491.93567
2.00000	1774.22052
4.00000	2109.91566
4.50000	2109.91566
5.00000	2109.91566

p-y Curve Computed Using Static Criteria for Stiff Clay without Free Water

Soil Layer Number = 3
Depth below pile head = 300.000 in
Depth below ground surface = 240.000 in
Ground Slope Angle = 0.000
degrees
Pile Batter Angle = 0.000
degrees
Effective Slope = 0.000
degrees
Equivalent Depth = 168.382 in
Diameter = 20.000 in
Undrained cohesion, c = 18.00000
lbs/in**2

Average Eff. Unit Weight = 0.02635 lbs/in**3
Epsilon-50 = 0.00500
Pct = 2684.173 lbs/in
Pcd = 3240.000 lbs/in
Pu = 2684.173 lbs/in
y50 = 0.250 in
p-multiplier = 1.00000
y-multiplier = 1.00000

y, in	p, lbs/in
0.0000	0.0000
0.0000400	150.94214
0.0002000	225.71114
0.0004000	268.41729
0.00200	401.37748
0.00400	477.32096
0.02000	713.76130
0.04000	848.81001
0.10000	1067.32209
0.20000	1269.26703
0.30000	1404.67488
0.40000	1509.42138
1.00000	1897.99690
2.00000	2257.11141
4.00000	2684.17295
4.50000	2684.17295
5.00000	2684.17295

p-y Curve Computed Using Static Criteria for Stiff Clay without Free Water

Soil Layer Number = 3
Depth below pile head = 360.000 in
Depth below ground surface = 300.000 in
Ground Slope Angle = 0.000 degrees
Pile Batter Angle = 0.000 degrees
Effective Slope = 0.000 degrees
Equivalent Depth = 228.382 in
Diameter = 20.000 in
Undrained cohesion, c = 18.00000 lbs/in**2
Average Eff. Unit Weight = 0.02708 lbs/in**3
Epsilon-50 = 0.00500

Pct = 3259.127 lbs/in
Pcd = 3240.000 lbs/in
Pu = 3240.000 lbs/in
y50 = 0.250 in
p-multiplier = 1.00000
y-multiplier = 1.00000

y, in	p, lbs/in
0.0000	0.0000
0.0000400	182.19859
0.0002000	272.45044
0.0004000	324.00000
0.00200	484.49301
0.00400	576.16254
0.02000	861.56393
0.04000	1024.57796
0.10000	1288.33859
0.20000	1532.10141
0.30000	1695.54894
0.40000	1821.98590
1.00000	2291.02597
2.00000	2724.50439
4.00000	3240.00000
4.50000	3240.00000
5.00000	3240.00000

p-y Curve Computed Using Static Criteria for Stiff Clay without Free Water

Soil Layer Number = 3
Depth below pile head = 480.000 in
Depth below ground surface = 420.000 in
Ground Slope Angle = 0.000 degrees
Pile Batter Angle = 0.000 degrees
Effective Slope = 0.000 degrees
Equivalent Depth = 348.382 in
Diameter = 20.000 in
Undrained cohesion, c = 18.00000 lbs/in**2
Average Eff. Unit Weight = 0.02791 lbs/in**3
Epsilon-50 = 0.00500

Pct = 4409.932 lbs/in
Pcd = 3240.000 lbs/in
Pu = 3240.000 lbs/in
y50 = 0.250 in
p-multiplier = 1.00000
y-multiplier = 1.00000

y, in	p, lbs/in
0.0000	0.0000
0.0000400	182.19859
0.0002000	272.45044
0.0004000	324.00000
0.00200	484.49301
0.00400	576.16254
0.02000	861.56393
0.04000	1024.57796
0.10000	1288.33859
0.20000	1532.10141
0.30000	1695.54894
0.40000	1821.98590
1.00000	2291.02597
2.00000	2724.50439
4.00000	3240.00000
4.50000	3240.00000
5.00000	3240.00000

Appendix - B

P-Y Curve Data for Exterior Bents - Example 1

```
------------------------------------------------------------------------
------
                    p-y Curves Reported for Specified Depths
------------------------------------------------------------------------
------


p-y Curve Computed Using the Soft Clay Criteria for Static Loading
Conditions

Soil Layer Number           =            1
Depth below pile head       =       12.000 in
Depth below ground surface  =       12.000 in
Equivalent Depth            =       12.000 in
Pile Diameter               =       20.000 in
Cohesion, c                 =        5.000 lbs/in**2
Avg Eff Unit Weight         =      0.01900 lbs/in**3
Epsilon50 parameter         =      0.01000
Default J parameter         =        0.500
Y50                         =      0.50000 in
p-multiplier                =      1.00000
y-multiplier                =      1.00000

        y, in            p, lbs/in
---------------    -----------------
         0.0000           0.0000
        0.00400         33.45600
        0.12500        105.37980
        0.25000        132.77022
        0.37500        151.98397
        0.50000        167.28000
        0.62500        180.19692
        0.75000        191.48780
        0.87500        201.58430
        1.00000        210.75959
        1.12500        219.19881
        1.25000        227.03389
        1.37500        234.36257
        1.50000        241.25951
        4.00000        334.56001
        7.50000        334.56000
       10.00000        334.56000
```

p-y Curve in Sand Computed Using Reese Criteria for Static Loading Conditions

Soil Layer Number	=	2	
Depth below pile head	=	60.000	in
Depth below ground surface	=	60.000	in
Ground Slope	=	0.000	degrees
Pile Batter	=	0.000	degrees
Effective Slope	=	0.000	degrees
Equivalent Depth (see note)	=	116.197	in
Pile Diameter b	=	20.000	in
Angle of Friction	=	29.000	deg.
Avg. Eff. Unit Weight	=	0.01900	pcf
kpy	=	40.000	pcf
K active	=	0.347	
K passive	=	2.882	
K0	=	0.400	
Pst	=	560.632	lbs/in
Psd	=	579.893	lbs/in
Ps = Pst (shallow controls)	=	560.632	lbs/in
A (static)	=	0.8800	
B (static)	=	0.5000	
C = pm/(ym^(1/n))	=	546.6860	
n = pm/(m ym)	=	1.6447	
m = (pu-pm)/(yu-ym)	=	511.2968	
yk = [c/(kx)]^(n/(n-1))	=	0.0043	in
pk	=	19.771	lbs/in
ym = b/60	=	0.3333	in
pm = B ps	=	280.316	lbs/in
yu = 3b/80	=	0.7500	in
pu = A ps	=	493.357	lbs/in
Es,lim	=	4647.896	lbs/in/in
p-multiplier	=	1.00000	
y-multiplier	=	1.00000	

This p-y curve is computed using the equivalent depth.

y, in	p, lbs/in
0.0000	0.0000
0.02778	61.87370
0.05556	94.30448
0.08333	120.66902
0.11111	143.73368
0.13889	164.61895
0.16667	183.91707
0.19444	201.98805
0.22222	219.07095
0.25000	235.33446
0.27778	250.90313
0.30556	265.87214
0.33333	280.31625
0.54167	386.83642
0.75000	493.35659
20.75000	493.35659
40.75000	493.35659

p-y Curve in Sand Computed Using Reese Criteria for Static Loading Conditions

Soil Layer Number	=	2
Depth below pile head	=	120.000 in
Depth below ground surface	=	120.000 in
Ground Slope	=	0.000 degrees
Pile Batter	=	0.000 degrees
Effective Slope	=	0.000 degrees
Equivalent Depth (see note)	=	176.197 in
Pile Diameter b	=	20.000 in
Angle of Friction	=	29.000 deg.
Avg. Eff. Unit Weight	=	0.02350 pcf
kpy	=	40.000 pcf
K active	=	0.347
K passive	=	2.882
K0	=	0.400
Pst	=	1486.001 lbs/in
Psd	=	1434.472 lbs/in
Ps = Psd (deep controls)	=	1434.472 lbs/in
A (static)	=	0.8800
B (static)	=	0.5000

C = pm/(ym^(1/n)) = 1398.7872
n = pm/(m ym) = 1.6447
m = (pu-pm)/(yu-ym) = 1308.2380
yk = [c/(kx)]^(n/(n-1)) = 0.0162 in
pk = 113.883
lbs/in
ym = b/60 = 0.3333 in
pm = B ps = 717.236
lbs/in
yu = 3b/80 = 0.7500 in
pu = A ps = 1262.335
lbs/in
Es,lim = 7047.896
lbs/in/in
p-multiplier = 1.00000
y-multiplier = 1.00000

This p-y curve is computed using the equivalent depth.

y, in	p, lbs/in
0.0000	0.0000
0.02778	158.31415
0.05556	241.29370
0.08333	308.75177
0.11111	367.76654
0.13889	421.20498
0.16667	470.58242
0.19444	516.82004
0.22222	560.52947
0.25000	602.14236
0.27778	641.97739
0.30556	680.27810
0.33333	717.23576
0.54167	989.78534
0.75000	1262.33492
20.75000	1262.33492
40.75000	1262.33492

p-y Curve Computed Using Static Criteria for Stiff Clay without Free Water

Soil Layer Number = 3
Depth below pile head = 180.000 in
Depth below ground surface = 180.000 in
Ground Slope Angle = 0.000
degrees
Pile Batter Angle = 0.000
degrees
Effective Slope = 0.000
degrees
Equivalent Depth = 109.441 in
Diameter = 20.000 in

Undrained cohesion, c = 18.00000 lbs/in**2
Average Eff. Unit Weight = 0.02513 lbs/in**3
Epsilon-50 = 0.00500
Pct = 2119.978 lbs/in
Pcd = 3240.000 lbs/in
Pu = 2119.978 lbs/in
y50 = 0.250 in
p-multiplier = 1.00000
y-multiplier = 1.00000

y, in	p, lbs/in
0.0000	0.0000
0.0000400	119.21512
0.0002000	178.26818
0.0004000	211.99779
0.00200	317.01064
0.00400	376.99131
0.02000	563.73349
0.04000	670.39588
0.10000	842.97819
0.20000	1002.47566
0.30000	1109.42170
0.40000	1192.15119
1.00000	1499.05076
2.00000	1782.68183
4.00000	2119.97791
4.50000	2119.97791
5.00000	2119.97791

p-y Curve Computed Using Static Criteria for Stiff Clay without Free Water

Soil Layer Number = 3
Depth below pile head = 240.000 in
Depth below ground surface = 240.000 in
Ground Slope Angle = 0.000 degrees
Pile Batter Angle = 0.000 degrees
Effective Slope = 0.000 degrees
Equivalent Depth = 169.441 in
Diameter = 20.000 in
Undrained cohesion, c = 18.00000 lbs/in**2
Average Eff. Unit Weight = 0.02635 lbs/in**3

Epsilon-50 = 0.00500
Pct = 2694.261 lbs/in
Pcd = 3240.000 lbs/in
Pu = 2694.261 lbs/in
y50 = 0.250 in
p-multiplier = 1.00000
y-multiplier = 1.00000

y, in	p, lbs/in
0.0000	0.0000
0.0000400	151.50943
0.0002000	226.55944
0.0004000	269.42610
0.00200	402.88599
0.00400	479.11489
0.02000	716.44385
0.04000	852.00012
0.10000	1071.33345
0.20000	1274.03736
0.30000	1409.95412
0.40000	1515.09429
1.00000	1905.13020
2.00000	2265.59439
4.00000	2694.26097
4.50000	2694.26097
5.00000	2694.26097

p-y Curve Computed Using Static Criteria for Stiff Clay without Free Water

Soil Layer Number = 3
Depth below pile head = 300.000 in
Depth below ground surface = 300.000 in
Ground Slope Angle = 0.000 degrees
Pile Batter Angle = 0.000 degrees
Effective Slope = 0.000 degrees
Equivalent Depth = 229.441 in
Diameter = 20.000 in
Undrained cohesion, c = 18.00000 lbs/in**2
Average Eff. Unit Weight = 0.02708 lbs/in**3
Epsilon-50 = 0.00500
Pct = 3269.231 lbs/in

Pcd = 3240.000 lbs/in
Pu = 3240.000 lbs/in
y50 = 0.250 in
p-multiplier = 1.00000
y-multiplier = 1.00000

y, in	p, lbs/in
0.0000	0.0000
0.0000400	182.19859
0.0002000	272.45044
0.0004000	324.00000
0.00200	484.49301
0.00400	576.16254
0.02000	861.56393
0.04000	1024.57796
0.10000	1288.33859
0.20000	1532.10141
0.30000	1695.54894
0.40000	1821.98590
1.00000	2291.02597
2.00000	2724.50439
4.00000	3240.00000
4.50000	3240.00000
5.00000	3240.00000

p-y Curve Computed Using Static Criteria for Stiff Clay without Free Water

Soil Layer Number = 3
Depth below pile head = 420.000 in
Depth below ground surface = 420.000 in
Ground Slope Angle = 0.000 degrees
Pile Batter Angle = 0.000 degrees
Effective Slope = 0.000 degrees
Equivalent Depth = 349.441 in
Diameter = 20.000 in
Undrained cohesion, c = 18.00000 lbs/in**2
Average Eff. Unit Weight = 0.02791 lbs/in**3
Epsilon-50 = 0.00500
Pct = 4420.053 lbs/in
Pcd = 3240.000 lbs/in
Pu = 3240.000 lbs/in

y50 = 0.250 in
p-multiplier = 1.00000
y-multiplier = 1.00000

y, in	p, lbs/in
0.0000	0.0000
0.0000400	182.19859
0.0002000	272.45044
0.0004000	324.00000
0.00200	484.49301
0.00400	576.16254
0.02000	861.56393
0.04000	1024.57796
0.10000	1288.33859
0.20000	1532.10141
0.30000	1695.54894
0.40000	1821.98590
1.00000	2291.02597
2.00000	2724.50439
4.00000	3240.00000
4.50000	3240.00000
5.00000	3240.00000

BEHAVIOR OF PILE TO BENT CAP CONNECTIONS SUBJECTED TO SEISMIC FORCES

ADDENDUM NO. 1 - September 25, 2012

This addendum is issued to address the “top bar” effect (for the case of prestressed piles referred to as the “top strand” effect) as it pertains to the connection behavior between precast prestressed piles and cast in place bent caps.

Research has shown that placement of reinforcement during casting of prestressed members can significantly affect bond. Strands cast near the top of formwork generate less bond strength as a result of aggregate settlement during the casting process and thus require a longer development length (Wan et al., 2002).

Strands within piles may achieve full development provided that adequate confining stress is present. For the majority of the specimens investigated, the prestressed piles were intentionally oriented such that the “top strand” remained out of the plane of displacement. It is reasonable to expect that should the “top strand” be oriented such that it remained in the plane of displacement results would differ. It is therefore recommended that piles be oriented such that the “top strand” is placed closest to the longitudinal face of bent caps.

Reference:

Wan, B., Petrou, M.F., Harries, K.A., Husein, A.A., “Top Bar Effects in Prestressed Concrete Piles”, *ACI Structural Journal*, V.99, No. 2, pp. 208-214, 2002.